Feasibility Study of Centrifuge Modeling of SAGD Caprock Integrity

by

Jingyu Wu

A thesis submitted in partial fulfillment of the requirements for the degree of

Master of Science

in

Geotechnical Engineering

Department of Civil and Environmental Engineering

University of Alberta

Abstract

The Joslyn steam release incident in 2006 has significantly influenced the approval process for steam assisted gravity drainage (SAGD) projects, which now require rigorous caprock integrity assessment to be conducted. In the past, most of the research efforts have been devoted to reservoir geomechanical simulation studies of caprock integrity. Physical modeling is conducted to a lesser extent, as it is difficult to carry out physical modeling of prototypes at such a scale as SAGD projects. Within the **Geo**technical **C**entrifuge **E**xperimental **R**esearch **F**acility (GeoCERF) at University of Alberta, research is ongoing to utilize the newly built 50g-ton beam centrifuge for physical modeling study of caprock failure mechanisms at high gravitational fields. The centrifuge model will be spun at 100g. According to the scaling law, a 20m thick caprock formation can be simulated using only 20cm thick test material, which makes scaled physical modeling of caprock failure possible.

Prototype, reservoir geomechanical simulation and centrifuge modeling are closely integrated in this research. Caprock is deemed as homogeneous material without any pre-existing faults or weak planes. Thus, shear failure and tensile failure are the two major failure modes of caprock to be explored. In reservoir geomechanical simulations, caprock behaviour is described using the elasto-perfectly plastic model with Mohr-Coulomb failure criterion. The development of shearing zones in caprock is analyzed along with displacement profile evolutions at the base of caprock. According to parametric analysis, caprock shearing failure is commonly observed for caprock with different mechanical properties and the shearing patterns of caprock at failure are the same with the vertical displacement at the base of caprock being the main driving force regardless of material property differences. In addition, the vertical displacement profiles at caprock shearing failure also share the same characteristics.

A custom-designed electromechanical device named **Geo**mechanical **C**aprock **D**eflection **M**echanism (GeoCDM) was successfully built and commissioned within GeoCERF to fail the caprock at 100g. In this research, over-consolidated Speswhite kaolin with consistent properties is employed to mimic the caprock in the centrifuge models for the purpose of eliminating the influences of property variability of in-situ materials. Consolidated-drained triaxial tests are conducted on samples cored from the kaolin block and the test results reveal that there are significant property differences between the caprock shale and the over-consolidated Speswhite kaolin in terms of material stiffness, strength and dilation behaviour after shearing. This research is focused on the feasibility study of centrifuge modeling of caprock integrity; however, for future studies, creating synthetic materials with close properties to caprock shale should be a research focus.

Through an image-based displacement measurement technique of particle image velocimetry (PIV), the deformation of the kaolin block can be directly captured. Two Kulite miniature pore pressure transducers are installed inside the overconsolidated Speswhite kaolin block for observation of the internal pore pressure changes and an external pore pressure transducer is connected to the base of the kaolin block. Mariotte Bottle is employed to maintain the hydrostatic pressure inside the centrifuge model. Two preliminary tests were conducted to test the GeoCDM setup. Pore pressure transducers are proven to be working well within the GeoCDM setup and the PIV system can effectively track the soil deformation during centrifuge spinning. However, the PIV analysis results had been compromised due to the faulty hydro-mechanical sealing at the base of the kaolin block, which are now being modified for future tests. For future studies, the results of the centrifuge testing should be compared to those of numerical simulations to verify and modify the numerical tools for SAGD caprock integrity study.

Acknowledgement

I would like to express my sincere gratitude to my supervisor, Dr. Rick Chalatumyk for his immeasurable amount of guidance and support during this research. I greatly appreciate his exceptional patience and encouragement. His directions, advice, and expertise were instrumental in accomplishing this research.

I am also grateful to my co-supervisor, Dr. Gonzalo Zambrano-Narvaez, for his invaluable guidance, suggestions, and encouragement throughout these years of research, which is a great asset to my life.

I would like to thank Jakob Brandl and Steve Gamble for their untiring professional assistance through all the design and commissioning work in this research. I also like to thank Gilbert Wong and Keivan Khaleghi for their help and guidance during my experimental work at Geomechanical Reservoir Experimental Facility (GeoREF).

I acknowledge the help and advice from Dr. Jonathan Black for good PIV setups within GeoCERF and appreciate the permission granted by Dr. David White and Dr. Andy Take to use the GeoPIV software for this research.

I appreciate the financial support from the Foundation CMG Industrial Research Consortia on Reservoir Geomechanics for Unconventional Resources.

I would like to thank numerous friends and colleagues, in particular Lang Liu, Meng Li and Yazhao Wang for their support, help and discussions during this research.

The love and support of my parents have always been a source of strength during my life. I am deeply grateful to them.

TABLE OF CONTENTS

List of Figures

List of Tables

Chapter 1 : Introduction

1.1 Problem Statement

The vast oilsands reserves in Western Canada is a major source of the world's heavy oil reserves and play an important role in supplementing conventional crude oil supply and securing our energy future. Of all the oilsands reserves, only 20% can be extracted using surface mining techniques. The majority of the remaining resources can be accessed using in-situ thermal recovery methods; among which the steam assisted gravity drainage (SAGD) has become the commercial technology of choice. SAGD operates at a relatively low pressure compared to another commercial in-situ thermal recovery technology of cyclic steam stimulation (CSS) and the importance of caprock integrity for safe SAGD operation was highlighted with the occurrence of the Joslyn steam release incident in May 2006. The Joslyn incident significantly influenced the approval process for SAGD projects which now require rigorous caprock integrity assessment to be conducted.

In the past, most of the research efforts have been devoted to reservoir geomechanical simulation studies of caprock integrity. Samples are cored from the caprock formation and then triaxial tests are conducted to obtain the mechanical properties of the caprock for input to numerical models. Presently, there are many well established numerical simulation tools for caprock integrity analysis; however, these numerical tools require verifications by experimental data or field data. Comparing to field tests, physical modeling has the advantages of less cost and faster completion. However, physical modeling study of caprock integrity has been conducted to a lesser extent, as it is difficult to carry out physical modeling of prototypes at such a scale as SAGD projects. The establishment of the Geotechnical Centrifuge Experimental Research Facility (GeoCERF)

at University of Alberta, the first of its kind in Western Canada, provides the unique opportunities to physically study the caprock behaviour as a whole in SAGD process.

1.2 Objective, Scope and Methodology

The overall objectives of this research are to explore the failure modes of caprock suitable for centrifuge modeling and develop a testing program for studying caprock failure mechanism at high gravitational field using the newly-built 50 g-ton beam centrifuge at GeoCERF. This research will set the stage for physical modeling studies of SAGD caprock integrity, which will serve as the verification cases for numerical tools.

The scope of this thesis is focused on shallow caprock, which is homogenous without any pre-existing faults or weak planes. Thus no failures triggered along the faults or weak planes are considered. Shearing failure and tensile failure are the two major failure modes to be explored. No in-situ caprock materials are used in this research; instead, commonly used Speswhite kaolin is used to make overconsolidated kaolin block to mimic the caprock in the centrifuge models.

The methodology of this research is first conducting reservoir geomechanical simulations of SAGD caprock integrity to find the suitable failure modes for centrifuge modeling and then developing a displacement controlled mechanism to fail the caprock at 100g based on the numerical findings (Figure 1-1). Decoupled reservoir geomechanical simulations of caprock integrity are conducted using the CMG STARS (reservoir simulator) and ITASCA FLAC (geomechanical simulator). Caprock behaviour is described using the elasto-perfectly plastic model with Mohr-Coulomb failure criterion. The development of shearing zones in caprock is analyzed along with displacement profile evolutions at the base of caprock. Based on the simulation results, an electromechanical device named Geomechanical Caprock Deflection Mechanism (GeoCDM) is designed and

manufactured to uplift/shear the caprock during centrifuge spinning, during which the deformation of caprock can be captured using the technique of particle image velocimetry (PIV).

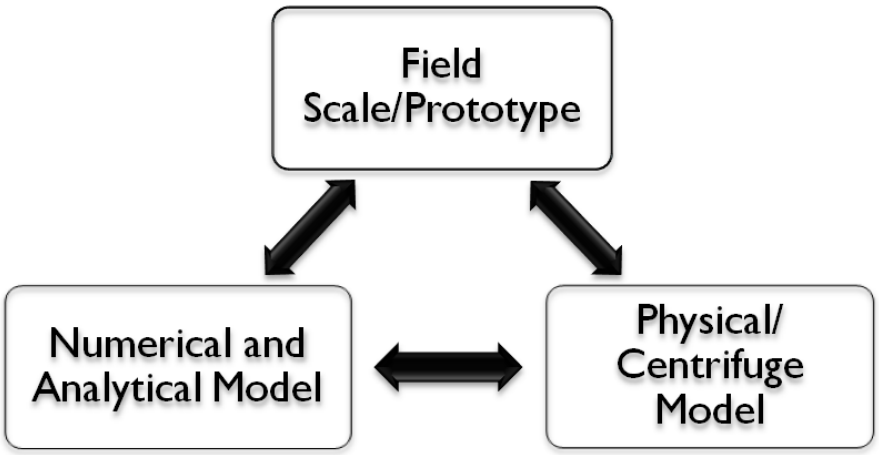

Figure 1-1 Research methodology.

1.3 Organization of Thesis

Chapter 2 gives a brief introduction to the concept of steam assisted gravity drainage (SAGD) for developing Alberta's oilsands reserves. The geomechanical processes involved in the SAGD process are described and discussed as well as the geomechanical properties of oilsands and caprock shale. Also, the principles of centrifuge modeling are explained and the literature review of experimental devices, which could possibly serve as the reference case for this research, is presented.

Chapter 3 briefly introduces the Geotechnical Centrifuge Experimental Research Facility (GeoCERF) at University of Alberta. The Speswhite kaolin is used for making overconsolidated kaolin block to mimic the caprock in the centrifuge models. The preparation procedure of overconsolidated Speswhite kaolin block and consolidated-drained triaxial test results on this material are presented. The installation procedure of

Kulite miniature pore pressure transducer and the particle image velocimetry (PIV) system for deformation measurement are also described in details.

Chapter 4 focuses on the numerical study of SAGD caprock integrity. Decoupled reservoir geomechanical simulations are conducted on a synthetic one well-pair SAGD project based on the geology of the Joslyn SAGD project to explore suitable failure modes to simulate in centrifuge modeling. A parametric analysis is conducted to study the influences of material stiffness, strength and dilation on the behaviour of caprock in the SAGD process. The feasibility of using a simplified displacement profile at the base of caprock to study caprock failure mechanism in centrifuge modeling is also studied.

Chapter 5 provides a detailed description of the custom designed electromechanical device named Geomechanical Caprock Deflection Mechanism (GeoCDM) as well as the commissioning work on the this device. Chapter 6 establishes a comprehensive GeoCDM centrifuge testing procedure and the results of two preliminary tests are presented and discussed.

Chapter 7 summarizes the conclusions obtained in the previous chapters and provides recommendations and suggestions for the next stage of this research.

Chapter 2 : Literature Review

2.1 Steam Assisted Gravity Drainage

2.1.1 Oilsands Resource in Canada

In the past few decades, significant efforts have been devoted to the development of heavy oil deposits as the conventional oil reserves greatly declined. Among all countries with oil reserves, Canada ranks third after Saudi Arabia and Venezuela with an estimated 175 billion barrels reserves, of which 170 billion barrels are oilsands reserves. Oilsands are a major source of the world's heavy oil reserves and are generally viewed as a strategic natural resource that can supplement conventional crude oil supply and secure the energy future.

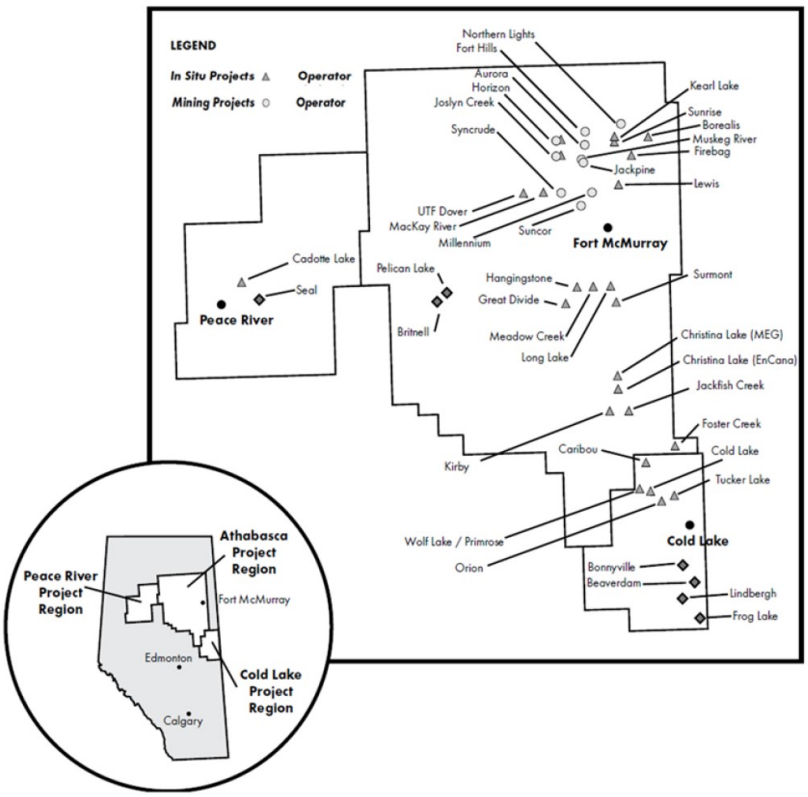

Figure 2-1 Distribution of SAGD projects (modified after National Energy Board, 2006).

Most of the oilsands reserves are deposited in three regions of Northern Alberta: Athabasca River, Peace River and Cold Lake (Figure 2-1). Only 20% of the oilsands reverses could be extracted using surface mining technology; the rest are too deep to develop by the same method. To extract those more deeply buried oilsands reserves, in-situ recovery methods are developed, among which steam assisted gravity drainage (SAGD) is generally considered as a promising technology for unlocking the vast oilsands reserves.

2.1.2 Concept of Steam Assisted Gravity Drainage

The fundamental principle of SAGD is to reduce the viscosity of bitumen by injecting high pressure and high temperature steam into the reservoir. The viscosity of bitumen drops significantly to that of water at temperatures of approximately 250°C, allowing bitumen to be pumped to the surface. To heat the reservoir and pump oil to the surface, two horizontal wells are drilled near the bottom of the oilsands pay zone, which are typically 5m apart in the vertical direction. The upper well performs as injector well and the lower one is producer well.

SAGD process can be divided into three phases: circulation, semi-SAGD and full SAGD. Initially, steam is being circulated within both injector and producer wells using concentric tubing during circulation phase (Figure 2-2). The circulation phase typically lasts for three to four months until clear communication between injector and producer wells is established. Then it comes to the semi-SAGD phase, when steam is injected through both strings of the injector well while the producer well is kept on circulation. During semi-SAGD phase, the heating of reservoir is less uniform, but much faster. Finally, it comes to the full SAGD phase. At this phase, no steam is injected to the

producer well and the mixture of bitumen and water flows through the tubing to surface (Total E&P, 2007).

During SAGD process, steam moves upward and sideways because of the lower density of steam and gradually, an area saturated with steam is formed known as the steam chamber. The mobilized bitumen is driven by gravity and flows parallel to the surface of the steam chamber down to the producer well as indicated in Figure 2-3. Initially, the vertical growth of steam chamber outweighs the sideways growth until the steam chamber hits the base of caprock. After the steam chamber reaches the base of caprock, its vertical growth is significantly restricted by the caprock layer with extremely low permeability and then lateral expansion of the steam chamber dominates. After some time, a single steam layer forms at the top of the oilsands pay zone and continuous heating maintains bitumen flow under gravity to the producer well, which will allow almost complete coverage of the reservoir volume and represents a fantastic aspect of SAGD (Mohsen, 2012).

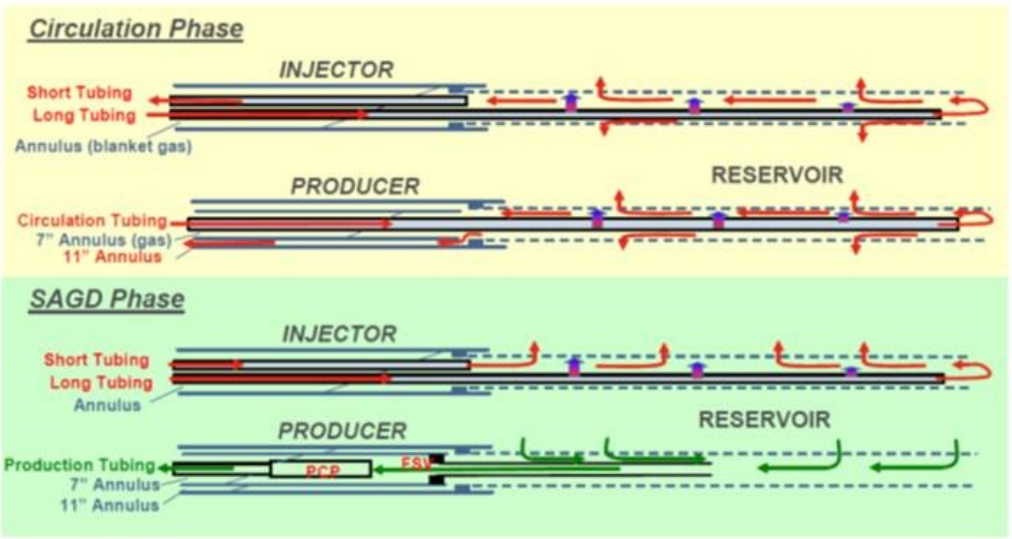

Figure 2-2 Well architecture during Circulation and SAGD phases (Total E&P, 2007).

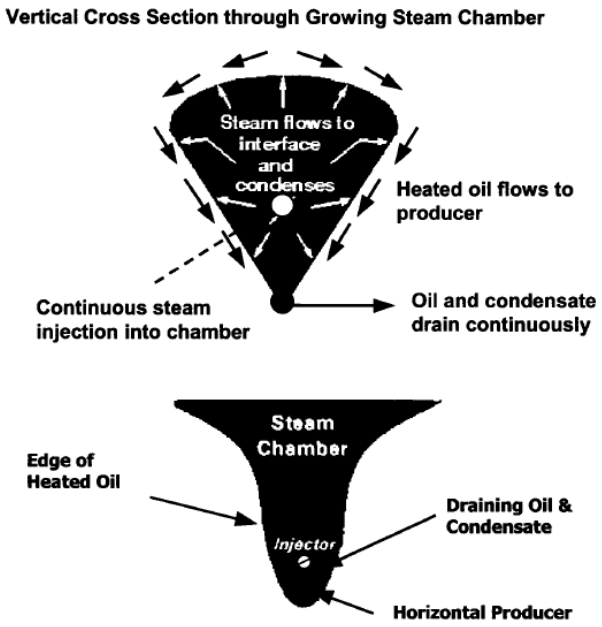

Figure 2-3 Concept of steam chamber (modified after Butler, 1980; Li, 2006).

2.2 Geomechanics Involved in SAGD Process

The geology of a typical SAGD site can be simplified into four layers: overburden, caprock (shale), oilsands reservoir and underburden (limestone) as shown in Figure 2-4. With continuous injection of high temperature and high pressure steam into the reservoir, initial stress and temperature fields within both caprock and reservoir layers will be altered. As the steam chamber grows, the influenced areas of pore pressure and temperature will also expand at the same time. Due to different propagation mechanisms, the pore pressure front grows faster than the temperature front as shown in Figure 2-5. The pore pressure front is approximately four to five meters in front of the temperature front (Li et al., 2006).

The geomechanical processes involved in SAGD is complex. In this research, the stress and strain field alteration in caprock formation is the focus. However, deformation of caprock mainly results from reservoir expansion. Therefore it is also important to

understand the geomechanical behaviours of oilsands reservoir during SAGD process to study the deformation of caprock over the lifetime of SAGD process.

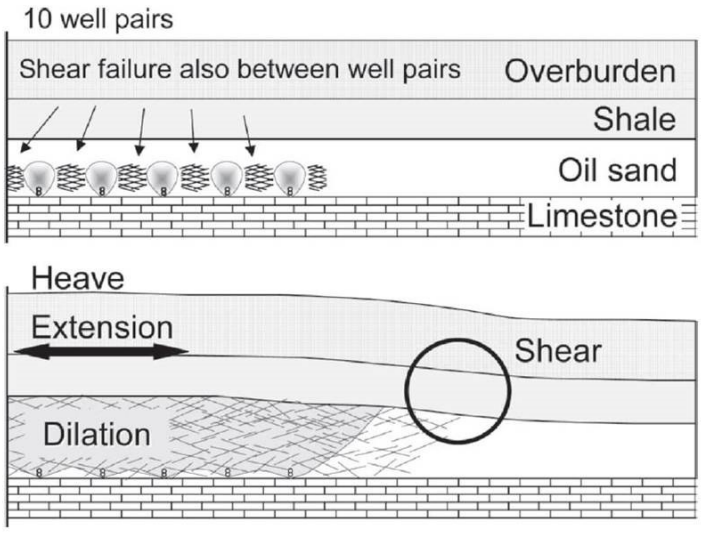

Figure 2-4 Shear, dilation and heave associated with SAGD (Collins et al., 2007).

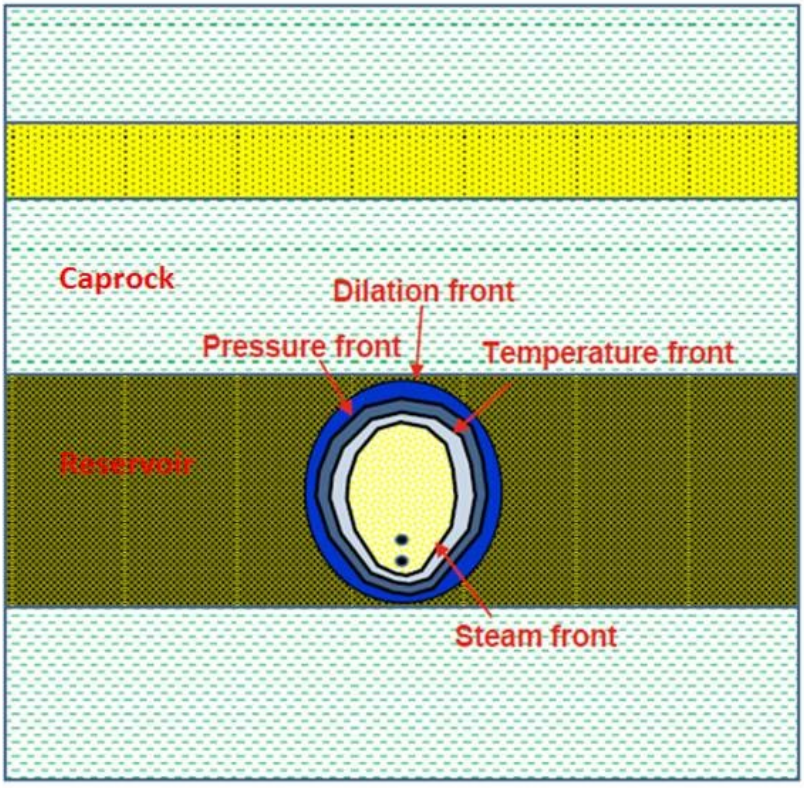

Figure 2-5 Different fronts developing ahead of a steam chamber (modified after Total E&P, 2007).

2.2.1 Geomechanical Properties of Oilsands and Clearwater Shale

2.2.1.1 Geomechanical Properties of Oilsands

Mechanical properties of oilsands have been extensively studied since 1970s. The test results show, in general, similar behavior and the stress-strain curves from Samieh and Wong (1997) are presented here to demonstrate the oilsands behaviour (Figure 2-6). It has been revealed that oilsands demonstrate a strain-softening behaviour. Also, Athabasca oilsands have almost zero cohesion and a high peak friction angle because of the interlocking fabric. During shearing, oilsands will undergo significant dilation under relatively low mean effective stresses (Total E&P, 2007).

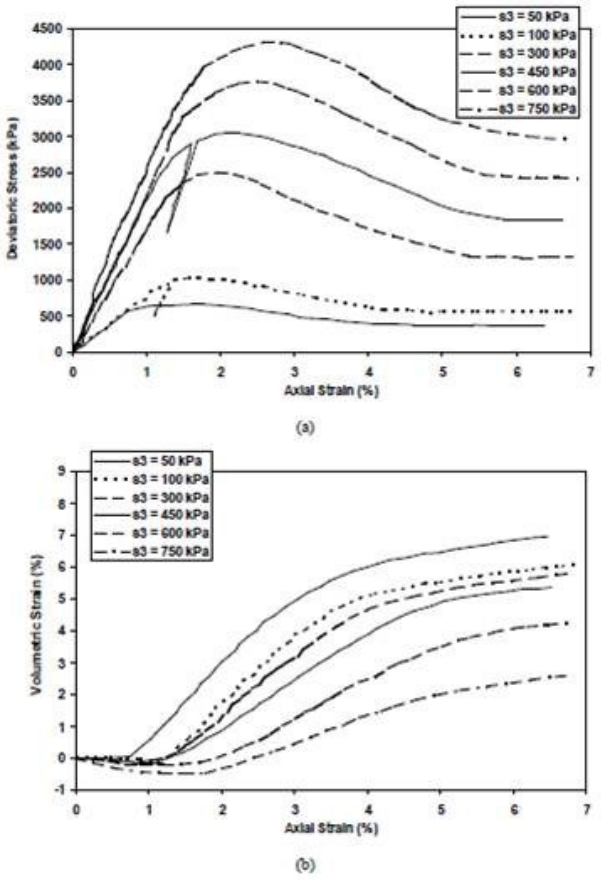

Figure 2-6 Deviatoric stress and volumetric strain versus axial strain results for oilsands (Samieh and Wong, 1997; Li, 2006).

2.2.1.2 Geomechanical Properties of Clearwater shale

Similar to oilsands in terms of stress-strain behaviors, caprock shale also demonstrates a strongly dilative behaviour after shear failure. Figure 2-7 shows triaxial test results on Clearwater shale samples taken from the Joslyn SAGD project (Total E&P, 2007).

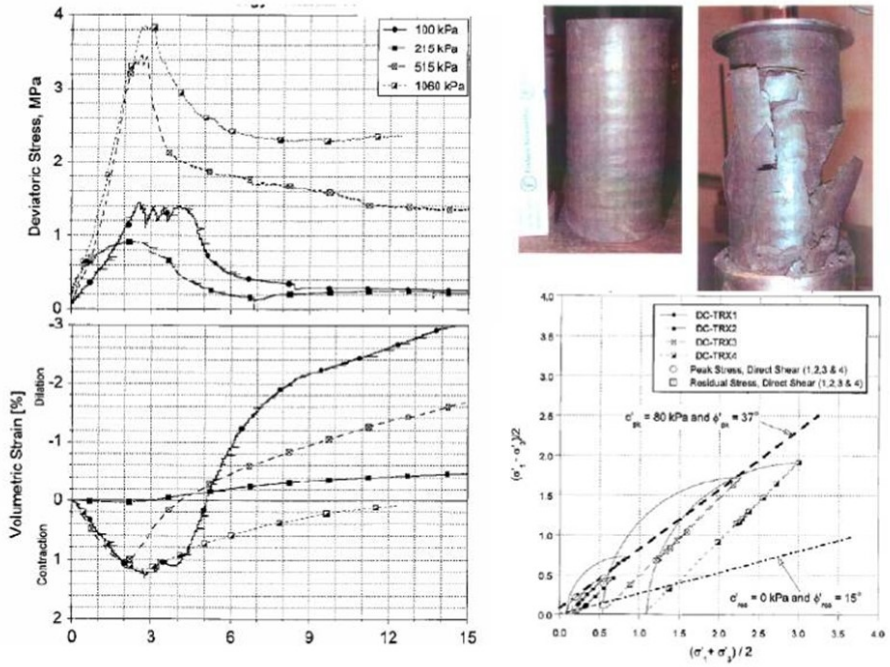

Figure 2-7 Triaxial test results on Clearwater shale (Total E&P, 2007).

2.2.2 Oilsands and Caprock Behaviors during SAGD Process

During SAGD process, the oilsands reservoir will undergo isotropic unloading due to pore pressure increase, thermal expansion caused by temperature increase and stress anisotropy induced shear dilation, which all contribute to the reservoir expansion and significantly alter the stress and strain fields in both caprock and oilsands reservoir.

2.2.2.1 Oilsands Behaviors during SAGD Process

1) Isotropic unloading

With continuous injection of steam at a steady bottom hole pressure (BHP), pore pressures within the pressure front are maintained at a constant value and the pore

pressures beyond the pressure front drop gradually until reaching the initial reservoir pressure at far field (Li et al., 2006). At regions with higher pore pressures than the initial value, oilsands undergo isotropic unloading given that the total stresses remain the same. Herein, it is necessary to clarify that isotropic unloading means the same reduction in effective confining stresses at all directions (Li et al., 2006). As shown in Figure 2-8, $(\sigma_1' + 2\sigma_3')/3$ represents the mean effective stress and the $(\sigma_1' - \sigma_3')/2$ represents the shear stress. The total stresses of σ_1 and σ_3 remain constant while the pore pressure increases; thus the effective mean stress decreases with the shear stress being constant. As the effective confining stress decreases, the oilsands porosity will increase (Figure 2-9) (Chalaturnyk, 1996; Li, 2004).

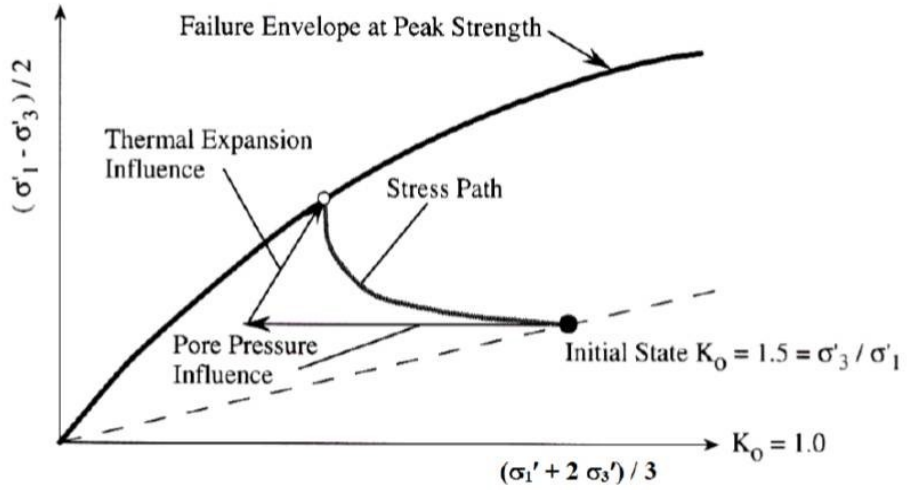

Figure 2-8 Stress path of oilsands during SAGD process (Chalaturnyk, 1996).

The isotropic unloading induced expansion can be expresses as:

$$\Delta\varepsilon_{ij} = -\delta_{ij}\frac{(1-2\nu)}{E}\Delta u \quad \text{..... (1)}$$

where δ_{ij} is the Kronecker Delta and E is the Young's Modulus.

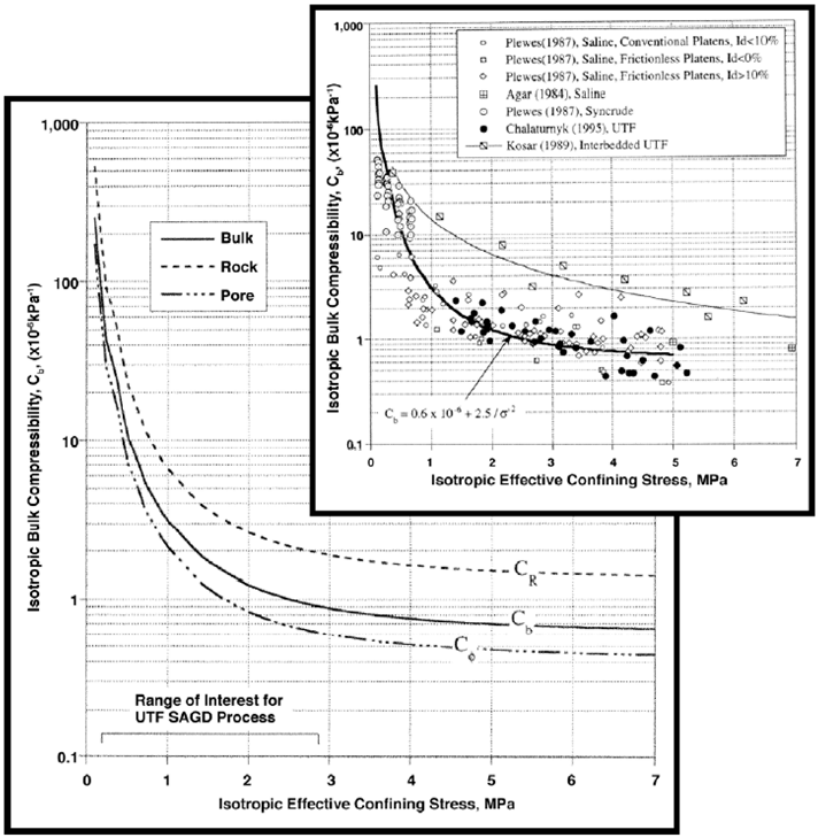

Figure 2-9 Compressibility vs. effective stress (Chalaturnyk, 1996; Li, 2004).

2) Thermal expansion

The thermal expansion of the reservoir region within the temperature front creates a large thermal stress normal to the front surface. The volumetric expansion coefficient α is defined by:

$$\alpha = -\frac{1}{\rho}\left(\frac{d\rho}{dT}\right)_P = \frac{1}{V}\left(\frac{\partial V}{\partial T}\right)_P \quad \ldots\ldots (2)$$

The volumetric thermal expansion coefficient α is related to linear thermal expansion coefficient β by

$$\alpha = 3\beta \quad \ldots\ldots (3)$$

Thermal stress due to the volumetric expansion can be calculated by:

$$\Delta\sigma_T = -E\alpha\Delta T \quad \text{..... (4)}$$

Thermal expansion induced strain in different directions can be calculated by:

$$\Delta\varepsilon_{ij} = -\delta_{ij}\beta\Delta T \quad \text{..... (5)}$$

3) Shear dilation

The stress anisotropy will increase under the influences of isotropic unloading and thermal expansion, and when the stress path reaches the failure envelope, shear failure will occur (Figure 2-8) and for oilsands, results in dilative volume changes. Shearing induced dilation is most likely to happen within and near the steam chamber where both isotropic unloading and thermal expansion are happening.

2.2.2.2 Stress and Strain Fields in SAGD Process

1) Stress Field

Figure 2-10 demonstrates the changes of horizontal and vertical stresses at the top of and beside the steam chamber qualitatively. Along line A–A', vertical stresses increase due to the reservoir vertical expansion, while horizontal stresses drop because of extensional strain. Along line B–B', the horizontal stress has a large increase caused by the reservoir horizontal expansion, but vertical stresses have dropped because of extensional strain. As a result, stress anisotropy will be created around the steam chamber (Dusseault et al., 2007). This anisotropy is visualized by Dusseault et al. (2007) in two dimensions using stress trajectories and small arrows for principal stresses and the locations of maximum shear stress along the overburden interface are indicated by shear symbols (Figure 2-11).

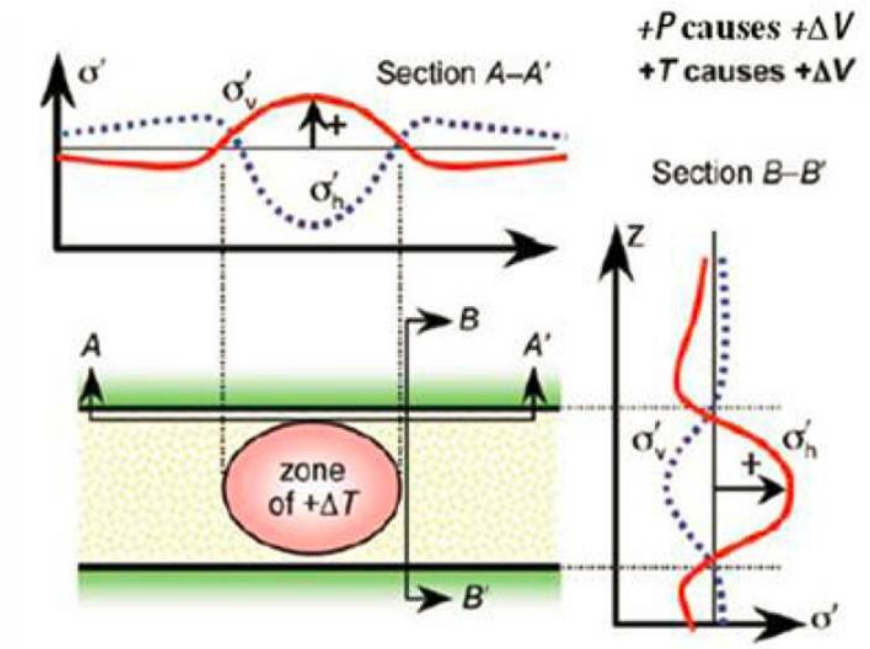

Figure 2-10 In-situ stresses variation due to pressure and temperature increase in reservoir (modified after Dusseault, 2007; Han et al., 2012).

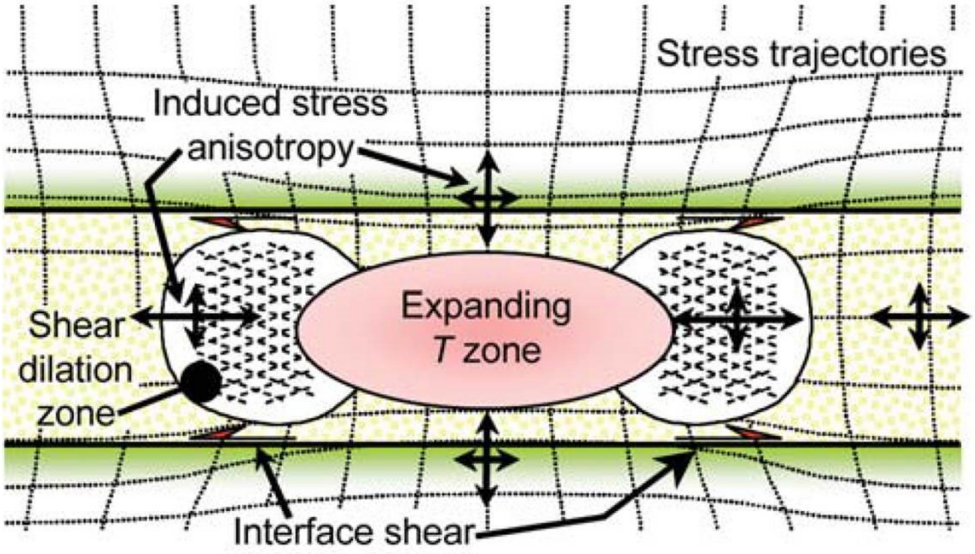

Figure 2-11 Stress trajectories and shearing effects (Dusseault et al., 2007).

2) Strain Field

At SAGD projects (especially shallow ones), there is limited restraint on the vertical deformation. Due to the horizontal continuity of reservoir, the horizontal expansion is

significantly constrained. As a consequence the steam injection induced vertical deformation is larger than the horizontal deformation.

Figure 2-12 demonstrates the typical strain field during a SAGD process (Azad and Chalaturnyk, 2011). Green vectors represent the deformation field and the white arrows show the general trend of the deformation in reservoir and above the reservoir.

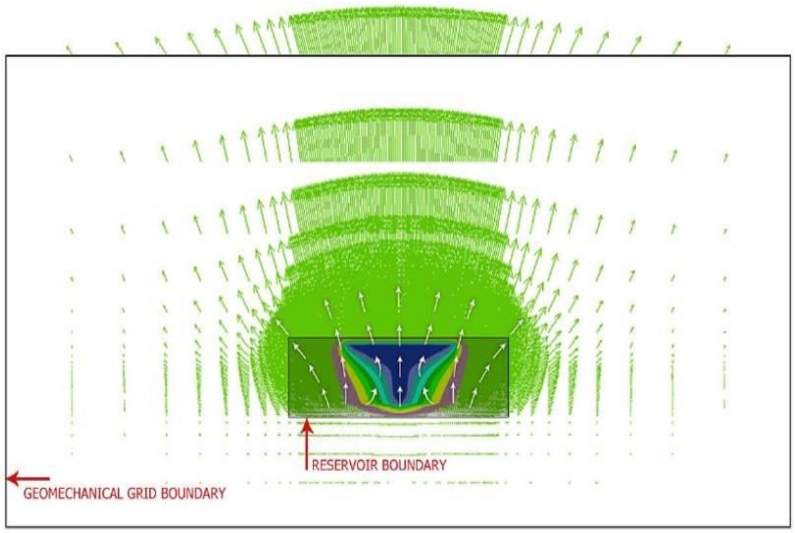

Figure 2-12 Typical reservoir deformation during a SAGD process (Azad and Chalaturnyk, 2011).

2.2.2.3 Possible Caprock Failure Mechanism

Under the influences of reservoir expansion, there will be significant stress and strain changes in the caprock formation which might cause caprock failures. For geotechnical materials, there are two major failure modes: one is the tensile failure and another is the shearing failure.

1） Tensile Failure

For conservative analysis, it is assumed that if the minimum effective stress goes below zero, tensile failure will occur. The fracture pressure (minimum total stress) can be

measured in-situ using mini-frac test and a fraction of this pressure (currently chosen as 0.8) is generally adopted as the upper limit for steam injection pressure.

2） Shear Failure

Compared to tensile failure, shear failure is more difficult to predict as it requires the knowledge of constitutive behaviours of in-situ materials and the in-situ stress conditions. Mohr-Coulomb failure criterion is commonly used to examine whether or not the shear failure is reached under a certain stress condition. The failure criterion can be expressed using Eqn (6):

$$\tau_{max} = c' + \sigma_n tan\varphi' \quad \text{..... (6)}$$

As indicated in Figure 2-13, there are mainly two ways of Mohr circles approaching the failure envelope: the increase of pore pressures or the increase of the deviator effective stress $(\sigma_1' - \sigma_3')$, where σ_1' denotes the maximum principal stress and σ_3' denotes the minimum principal stress. Obviously, these two phenomena could happen at the same time.

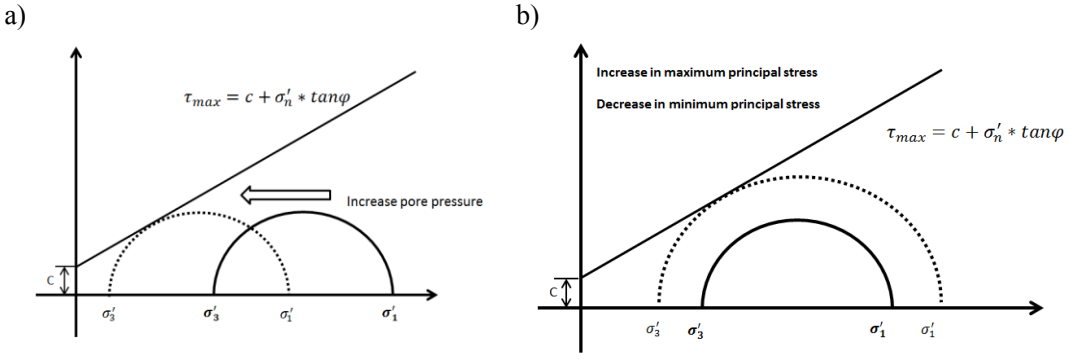

Figure 2-13 Two situations where the Mohr circles approach the failure envelope (modified after Han et al., 2012).

2.3 Geotechnical Centrifuge Modeling

2.3.1 Principles of Geotechnical Centrifuge Modeling

Geo-materials have stress dependent behaviour, which makes stress level an important factor in geotechnical physical modeling. For physical modeling conducted at Earth's gravity (1g), the model typically has the problem of low stress level or different stress profile compared to that in prototypes. The geotechnical centrifuge provides an ideal solution to this problem. Scaled models placed at the end of a centrifuge arm can be accelerated so that they are subjected to an inertial radial acceleration field, which is similar to a gravitational acceleration field but many times stronger than Earth's gravity (Taylor, 1995). This high inertial radial acceleration field will generate similar stress profile in the model as that in prototype.

Scaling laws

It is essential to determine the right scaling relations to extrapolate the model measurements to the prototype. These relations can be obtained by dimensional analysis or analysis of the field equations describing the physical phenomenon like consolidation. In Table 2-1, some scaling relations commonly used in centrifuge modeling are listed. If the model is constructed using the same material as that of prototype, then these scaling relations can be used to transfer the model measurements to describe prototype behaviour.

Table 2-1 Scaling relations in centrifuge models (modified after Ko, 1988)

Quantity	Prototype	Model
Length	N	1
Area	N^2	1
Volume	N^3	1
Velocity	1	1
Acceleration	1	N
Mass	N^3	1
Force	N^2	1
Energy	N^3	1

Stress	1	1
Strain	1	1
Mass density	1	1
Energy density	1	1
Time(dynamic)	N	1
Time(diffusion)	N^2	1
Time(creep)	1	1
Frequency	1	N

Modeling of models

All these scaling relations are obtained through theoretical derivation; however, in real situations, some conditions assumed in the derivations may become invalid. Also, the boundary effects exerted by the container will induce other unpredictable changes to model behaviour. Thus these scaling relations should be verified.

The verification can be best done by comparison with the prototype. However, conducting 1:1 model is often too costly and time-consuming. Besides, some prototypes cannot be repeated, like the steam release incident at Total's Joslyn project. To overcome these constraints, the technique of modeling of models was developed to verify the scaling laws.

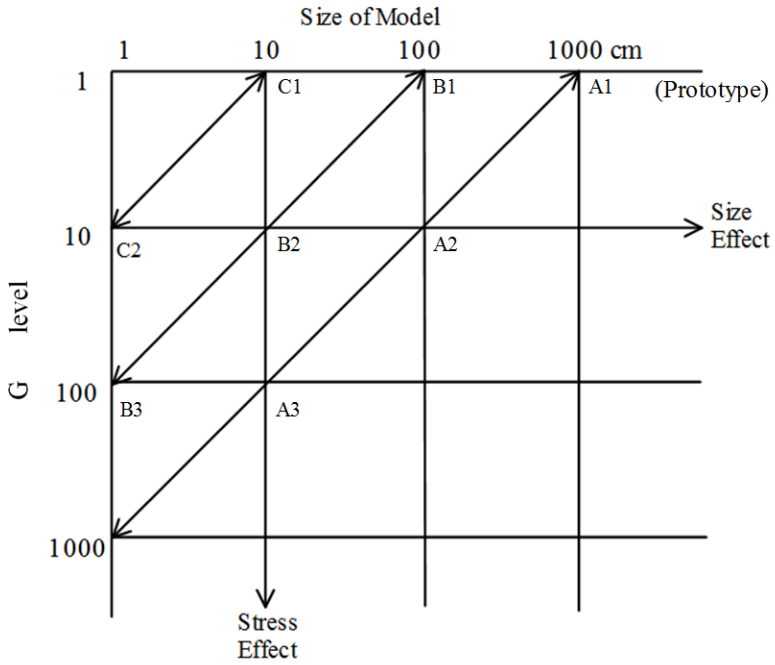

Figure 2-14 Principles of modeling of models (modified after Ko, 1988).

The primary duty of geotechnical centrifuge is to ensure stress similarity between the scaled model and the corresponding prototype. Although the stress level is fixed for a certain prototype, the model size could vary according to different centrifuge acceleration level as indicated in the following equation. This relationship can be reflected in Fig 2-14.

$$\sigma_{p,H} = N * \sigma_{m,h}$$

where, $\sigma_{p,H}$ = vertical stress at a depth of H in the prototype,

N = scale factor,

$\sigma_{m,h}$ = vertical stress at a depth of h in the scaled model.

As shown in Figure 2-14, A1 (1g) represents the prototype which cannot be modeled. A2 (10g) and A3 (100g) are not only scaled models of the same prototype (A1), but they are also the models of each other. The technique of modeling of models is conducted by comparing A2 with A3 and transferring both model measurements to the prototype using

the same scaling relations. If the scaling relations are correct, then behaviours of A2 and A3 should both predict the same corresponding prototype behaviour. Any suitable models along the line A1-A2-A3 can be selected to conduct modeling of model technique and by this way, the verification of the scaling relations can be achieved.

As seen in Table 2-1, there are various scaling relations for the same parameter of "time" for different phenomena, which may occur in the same model test. The scaling relation for dynamic events is N: 1 (prototype to model), while the time for diffusion scales by N^2. For such circumstance, it is significant to find the threshold centrifuge acceleration at which the scaling relation conflict becomes negligible. And to determine the threshold, two models of different values of N such as A2 and A3 should be carried out. Thus when actually conducting the tests, the centrifuge should be spinning under the threshold acceleration to get a unified scaling relation for the conflicting phenomena.

As the model becomes smaller, the boundary effects are thought to exert more and more influences on model behaviour. These influences can again be deduced by conducting modeling of models technique.

Validation of numerical methods

Numerical modeling and centrifuge modeling can be linked together to enhance both techniques. Since the stress level is the same as that in prototype, the centrifuge modelling results could largely represent the prototype behaviour if carefully prepared. Then the centrifuge test is analyzed with numerical methods which duplicate every aspect of the test: boundary conditions, loadings, material properties of the test. Comparison between the centrifuge test results and the analytical results will then pinpoint any discrepancy in the modeling approach. Since the centrifuge results can be verified to be

accurate through modelling of model technique, the numerical procedure can be refined until an acceptable match is obtained.

2.3.2 Similar Centrifuge Setups

As discussed in previous sections, caprock deformation is mainly caused by the reservoir expansion. Thus in centrifuge models, it is essential to find the appropriate test setups for mimicking the influences of the oilsands reservoir expansion at the base of caprock. Herein, the literature review of experimental devices that could possibly accomplish such requirement is presented.

2.3.2.1 Tunneling Stability

Tunnel stability in a clay layer with overlying coarse sand was investigated using geotechnical centrifuge at City University London (Grant and Taylor, 2000). The test was conducted with the plane-strain box with the tunnel being represented by a latex lined cylindrical cavity (Figure 2-15). Air pressure was used to maintain the shape of cavity and as the centrifuge acceleration increased, the air pressure was adjusted to balance the increased load. Once the targeted acceleration level was reached, the ground movement was generated by reducing the air pressure supporting the cavity. The pressure reduction rate could be adjusted to create drained or undrained behaviour in the clay. With the LVDTs mounted at the surface of the model, the surface deformation could be measured. Three miniature pore pressure transducers were employed to monitor pore pressure changes during ground movement. Also a standpipe would provide a constant water level in the model. There are also other similar test setups using expandable tubes to create uplift (Wichman, 2005).

Discussion:

If this setup is to be used, a certain thickness of sand should be placed at the bottom of plane-strain box to accommodate the expandable tube, which will influence the thickness of caprock that could be simulated as the plane-strain box has limited space. Also, it is of difficulty to control the air/fluid pressure in the tube to make the caprock deform in a controlled manner. More importantly, the caprock deformation induced by tube expansion is not necessarily comparable to that in the SAGD process.

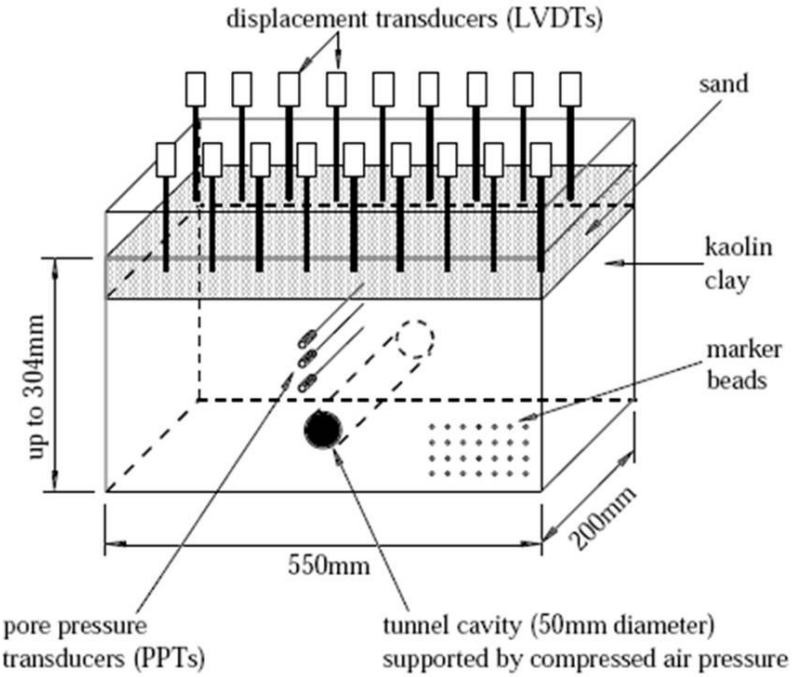

Figure 2-15 Schematic of centrifuge model on tunnels (Grant and Taylor, 2000).

2.3.2.2 Compaction Grouting

Compaction grouting is typically used in cohesionless soils to reduce ground settlement during underground construction. High viscosity, stiff or low slump paste is injected into the ground to form an approximately columnar or spherical "bulb" (Lee et al., 2001). Because of high injection pressure and volume, soils around the injection point will be compacted. In the centrifuge tests conducted by Lee et al. (2001), injectors were made of copper tubes being squashed flat. Drainage holes were drilled at both ends and also on the

top and bottom surfaces of the squashed tubes for fluid injection. A tight fitting 1mm-thick rubber sleeve was put onto the squashed tube and clamped at both ends (Figure 2-16). These injectors were connected to a hydraulic actuator which could precisely control injection rate and record injected fluid volume into the dry sand. A pressure transducer was connected to the outlet of the fluid chamber to measure the injection pressure (Figure 2-17).

Discussion:

Such setups are similar to those for studying tunnel stability; however, they have the advantages of direct measurements of injection pressure and injected fluid volume. Also, the injectors were made of copper tubes which could endure much higher injection pressure compared to the latex. But they have the same problem of not being able to mimic the displacement at the base of caprock in SAGD process.

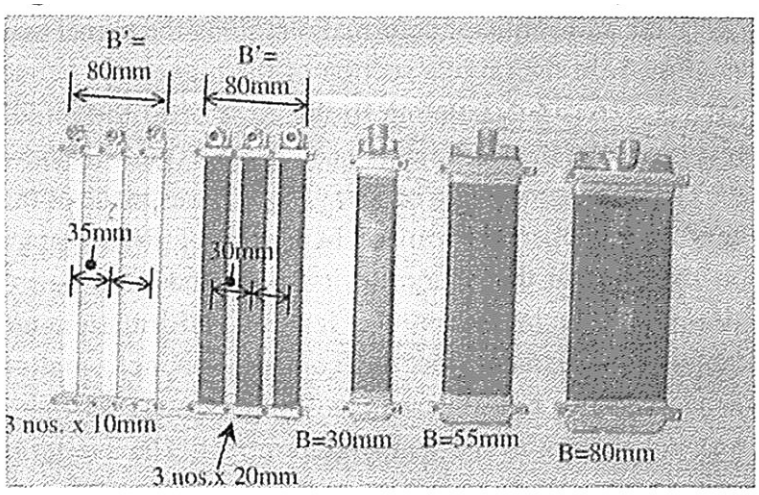

Figure 2-16 Multi-point and strip injectors used in centrifuge testing (Lee et al., 2001).

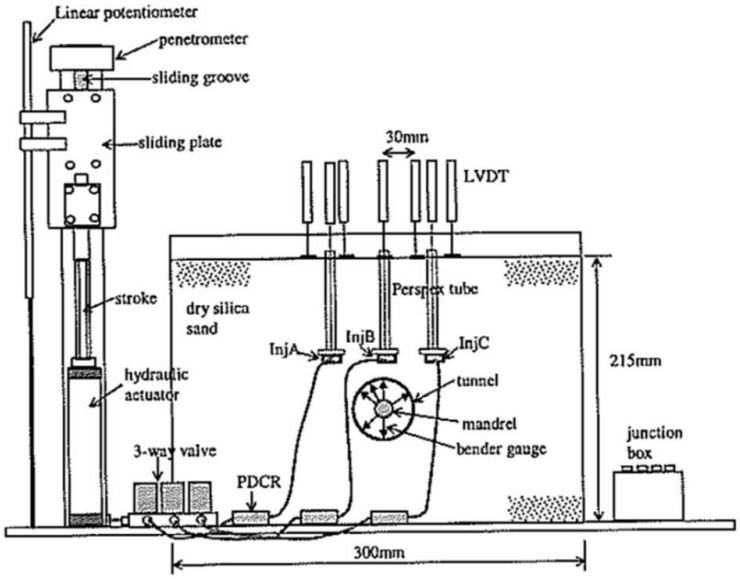

Figure 2-17 Schematic view of a multi-point injection centrifuge model set-up (not to scale) (Lee et al., 2001).

2.3.2.3 Upheaval Resistance of Buried Offshore Pipelines

The upheaval resistance of buried offshore pipeline has been a popular research topic in the area of offshore geotechnical engineering. Figure 2-18 shows the testing apparatus for conducting such experiments at University of Dundee (Bransby, 2002). The pipe was pulled out of the formation using a rigid hanger arrangement to ensure that the pipe moved vertically with uniform displacement. Both 1g and centrifuge tests were conducted using INSTRON machine and special centrifuge actuator respectively.

Discussion:

Rigid hanger arrangement shall penetrate through the test materials which will naturally destroy the material integrity. This should be avoided for caprock integrity tests. However, such devices can precisely control the displacement and displacement rate which provided valuable ideas for the development of a displacement controlled caprock failure mechanism.

Figure 2-18 Laboratory test apparatus (left) and centrifuge model package (right) (Bransby, 2002).

2.3.2.4 Faulting

Faulting caused by earthquakes was studied at HKUST using a displacement controlled device (Cai, 2011). A specially designed mechanical device was buried at the bottom of plane-strain box and then the test materials were placed on top of it. The displacements of test material were measured using particle image velocimetry (PIV). The pore pressure changes inside the materials were observed using Druck PDCR81 miniature transducers. Rigid and flexible boundary conditions were both explored in this research. For flexible boundary condition, a separate device was employed as shown in Figure 2-19b.

Discussion:

This test setup can be used as a reference case for the design of the device for studying SAGD caprock integrity. The influence of the oilsands reservoir expansion at the base of caprock can be simulated using a similar device as shown in Figure 2-19. The deformation of caprock can be captured using the PIV system as well. Internal pore

pressure changes inside the caprock could also be monitored using similar miniature pore pressure transducers like the Druck PDCR81.

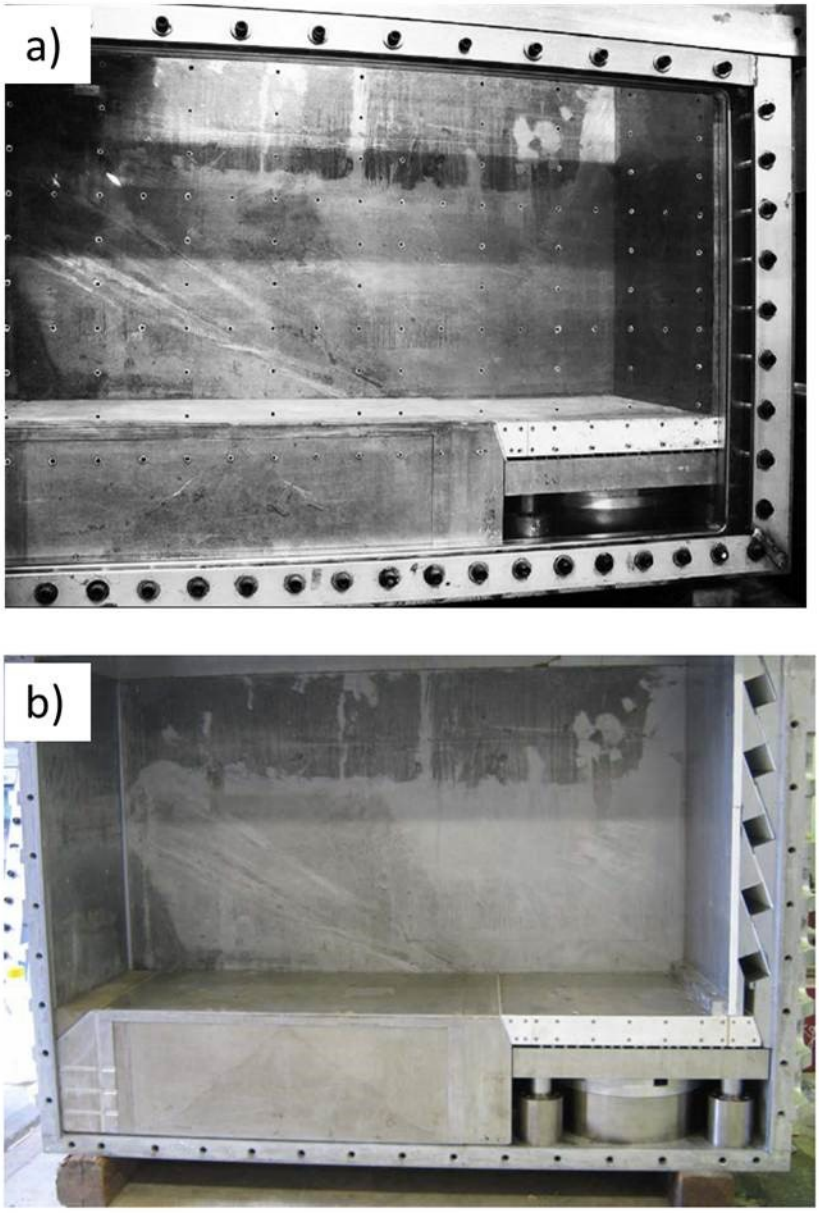

Figure 2-19 Model container and the bedrock fault system with a) rigid boundary conditions and b) flexible boundary conditions utilized in centrifuge test at HKUST (modified after Cai, 2011).

Chapter 3 : Geotechnical Centrifuge Experimental Research Facility and Centrifuge Testing Program

In this chapter, a brief introduction is presented about the newly established **Geo**technical **C**entrifuge **E**xperimental **R**esearch **F**acility (GeoCERF). The preparation procedure of overconsolidated Speswhite kaolin block, measurement of the mechanical properties of the overconsolidated Speswhite kaolin, installation procedure of the Kulite miniature pore pressure transducer and the image-based deformation measurement system at GeoCERF will be discussed in detail.

3.1 Geotechnical Centrifuge Experimental Research Facility

The **Geo**technical **C**entrifuge **E**xperimental **R**esearch **F**acility (GeoCERF) is located at the lowermost level of the Natural Resources Engineering Facility (NREF) at University of Alberta. The beam centrifuge at GeoCERF has a nominal capacity of 50g-ton that means a maximum payload of 500kg can be spun at 100g or 335kg at 150g. It has a 2m rotation radius from the rotation axis to the swing basket platform.

Figure 3-1 shows the scheme of the centrifuge control system, which is based on an industrial programmable logic controller (PLC). The PLC-based control system comprises a Control/Drive Panel, a Local Control Panel, and Machine Instrumentation (TBS, 2012). Speed, automatic balancing, drive overload protection, access interlocks, start and stop sequences as well as other safety related machine functions can be controlled by the PLC system (TBS, 2012). There are two in-flight computers (PCs) accommodated in the center cabinet (Figure 3-1). The data acquisition system (DAS) is

connected to in-flight PC1, and the high resolution camera is connected to in-flight PC2. Both in-flight PCs are remote accessed and controlled at the control room. Additional details of this centrifuge can be found at Zambrano et al. (2014).

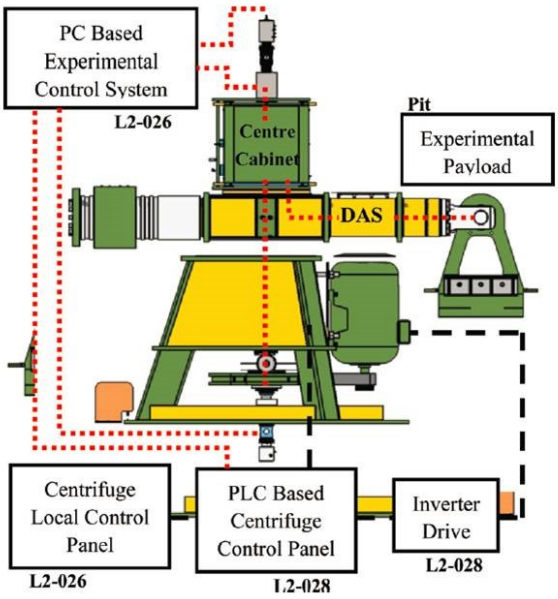

Figure 3-1 GeoCERF centrifuge control system (Zambrano et al., 2014).

3.2 Preparation and Properties of Overconsolidated Speswhite Kaolin Block

The Clearwater shale is a heavily overconsolidated material and demonstrates a significantly dilative behavior under shearing as discussed in Chapter 2. At this stage, no in-situ caprock material will be used in the centrifuge models due to the variability of its properties. Alternatively, the commonly used Speswhite kaolin in centrifuge community is utilized to explore the possibility of making overconsolidated kaolin samples which could demonstrate similar behaviors as those of the Clearwater shale under shearing.

The behavior of the overconsolidated kaolin under shearing highly depends on the overconsolidation ratio (OCR). Following is a statement on the OCR influences on clay

behaviors from the report of "Geotechnical centrifuge use at University of Cambridge Geotechnical Center, August – September 1991" (Gilbert, 1992):

> *Overconsolidation ratio (OCR) for prototype soil is about 1.5; its behaviour would therefore be the contractive behaviour associated with the "wet" side of the critical state line (CSL). However, in order to achieve the same strength profile in Speswhite as in the "aged" prototype clay, it would be necessary to consolidate Speswhite to an OCR of about 3.5 that would produce strongly dilative behaviour (which is associated with the "dry" side of the CSL). Behaviour on the dry side of the CSL is so different from that of the wet side that it was decided, instead, to scale down stress and strength in the model in order to match the wet side CSL behaviour between model and prototype.*

Thus, the methodology of preparing overconsolidated Speswhite kaolin is to consolidate the sample to the maximum capacity of the consolidation setup to create a highest pre-consolidation pressure, through which, the kaolin block can get a high OCR. At the time of conducting this research, the maximum consolidation pressure which could be exerted on top of the kaolin block is 1.45MPa.

3.2.1 Preparation of Overconsolidated Kaolin Block

3.2.1.1 Speswhite Kaolin

Speswhite kaolin has been widely used in centrifuge community and its properties are well documented. Figure 3-2 gives a summary of the most important parameters of the Speswhite kaolin (Cao, 2003). Also, Valls-Marquez et al. (2006) conducted experiments on the void ratio change of Speswhite kaolin under different stresses (Figure 3-3).

Property	Value
Material	Speswhite kaolin
Specific gravity (*Gs*)	2.61
Coefficient of earth pressure at rest for normally consolidated clay (k_0)	0.64
Liquid limit (*LL*)	69%
Plastic limit (*PL*)	38%
Plastic index (*PI*)	31%
Vertical permeability (k_v)	2 to 3 x 10^{-6} mm/second
Horizontal permeability (k_h)	3 to 5 x 10^{-6} mm/second
Coefficient of virgin consolidation (c_v)	~0.1 mm^2/second
Coefficient of virgin compressibility, $\lambda\,(e-\ln p')$	0.26
Coefficient of rebound compressibility, $\kappa\,(e-\ln p')$	0.01~0.05
Vane shear stress, s_u/σ'	0.19 $OCR^{0.59}$
Sensitivity at 58% water content	1.3
Initial specific volume V (@ p'=1 kPa)	3.58

Figure 3-2 Speswhite kaolin parameters determined by C-CORE and others (Cao, 2003).

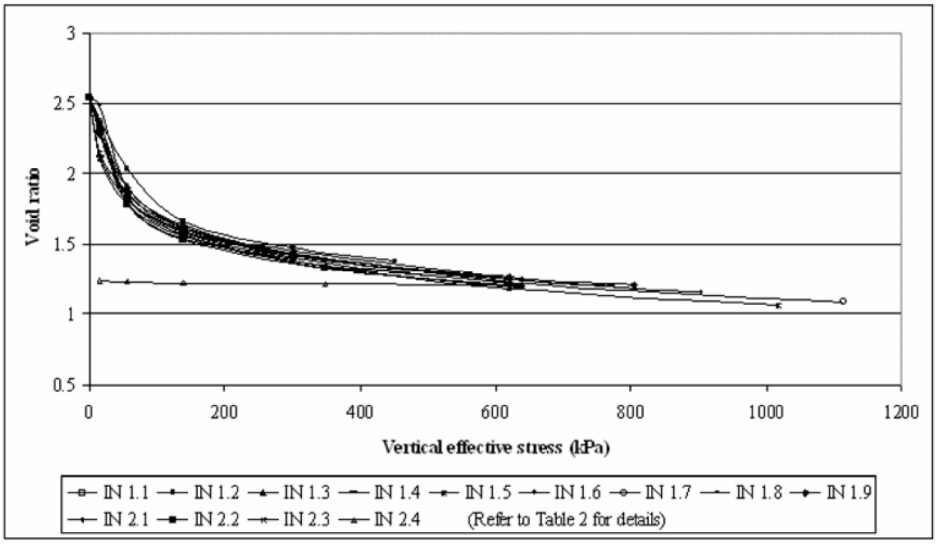

Figure 3-3 Void ratio changes with σ'_v during the Ko consolidation of Speswhite kaolin slurry under variable conditions (Valls-Marquez et al., 2006).

Based on the consolidation test results on Speswhite kaolin conducted at GeoCERF, the void ratio of Speswhite kaolin versus consolidation pressures is plotted as shown in Figure 3-4. This plot can help get a good estimation of the Speswhite kaolin powder required to make a certain thickness of kaolin block at different stress levels.

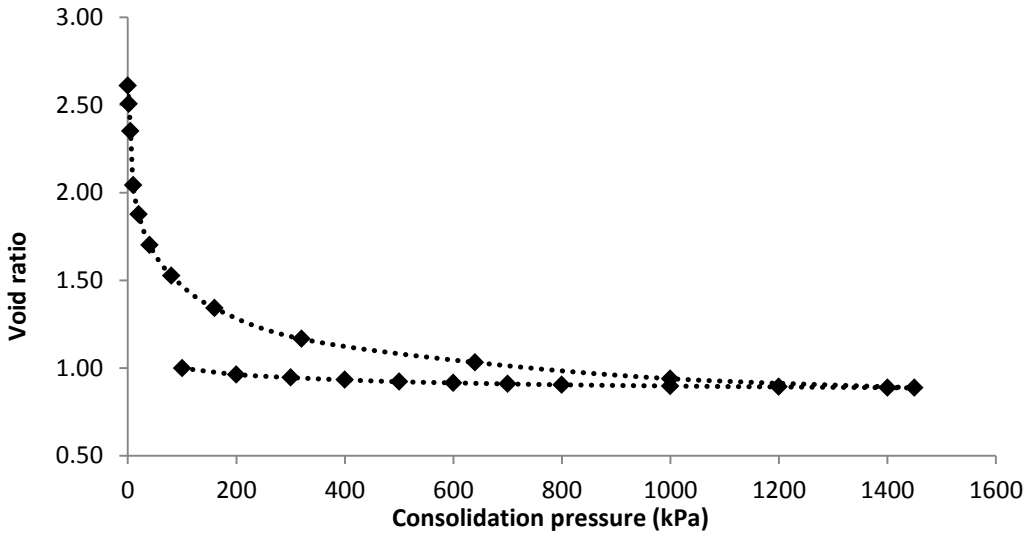

Figure 3-4 Loading and unloading curve of the Speswhite kaolin.

3.2.1.2 Preparation Procedures of Overconsolidated Kaolin Block

The overconsolidated kaolin block is contained within the plane-strain box at GeoCERF (Figure 3-5).

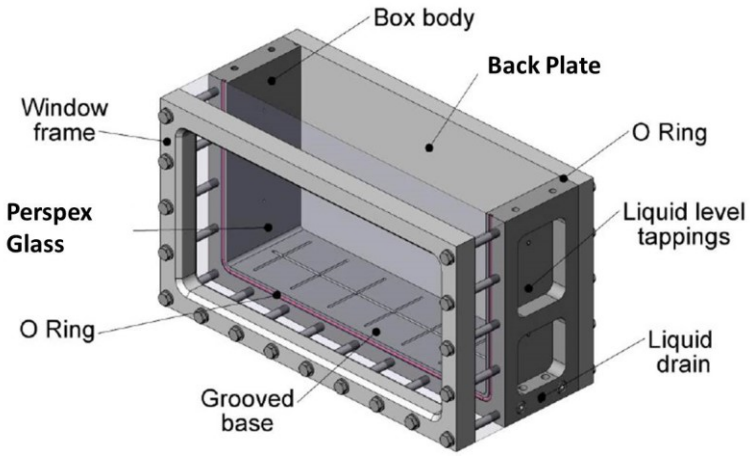

Figure 3-5 Arrangement of the plane-strain box (modified after TBS, 2012).

Speswhite kaolin powder is mixed with de-ionized water for minimizing chemical effects and bacterial growth within the sample as it will stay in the plane-strain box for 3~4 weeks. The kaolin slurry is mixed at 100% water content under vacuum for two hours to create smooth slurry. The mixer at the GeoCERF (Figure 3-6) can provide a vacuum of ~ -60kPa.

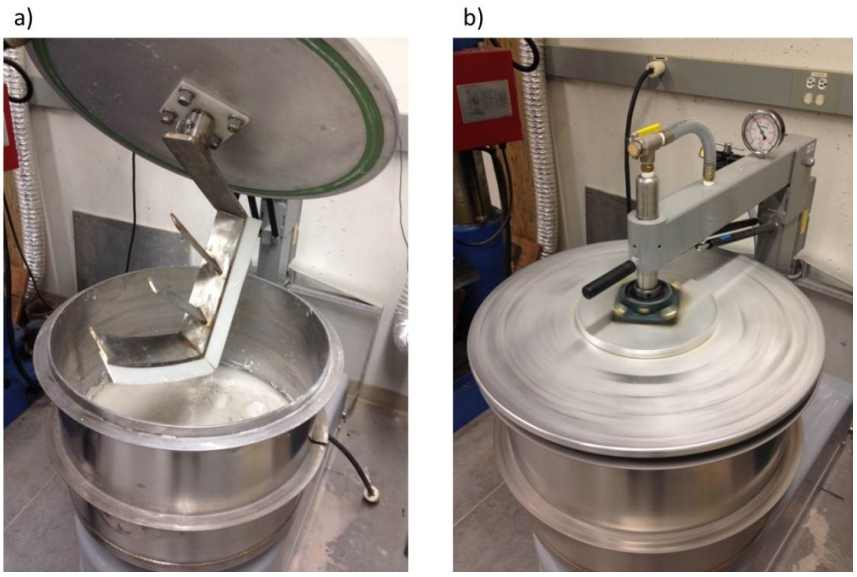

Figure 3-6 Vacuum mixer at GeoCERF.

It is not easy to adjust the kaolin block thickness after consolidation; thus it is essential to get a good estimation of how much Speswhite kaolin powder is required before mixing. According to Figure 3-4, the void ratio of Speswhite kaolin at different consolidation pressures is known. Thus, the Speswhite kaolin powder required to make a certain thickness of kaolin block can be calculated with the knowledge that Speswhite kaolin has a specific gravity of 2.61. As the water content is 100%, the water needed is also known. According to the results of several trial tests, 37.8kg of Speswhite kaolin powder is required to be mixed at 100% water content to make a 20cm kaolin block for the final shearing test at 100g.

The plane strain box is cleaned and a thin layer of transparency is attached to the aluminum plate, which will be replaced by the Perspex glass after consolidation is finished. The back plate and the aluminum plate are subsequently coated with silicon grease. As the Speswhite kaolin will stay in the plane-strain box for three to four weeks, it is necessary to have such a layer of grease for two purposes: 1) reduce the wall-clay friction 2) protect the aluminum plate. A porous stone covered by filter paper is placed at the bottom of the plane-strain box to facilitate bottom drainage (Figure 3-7).

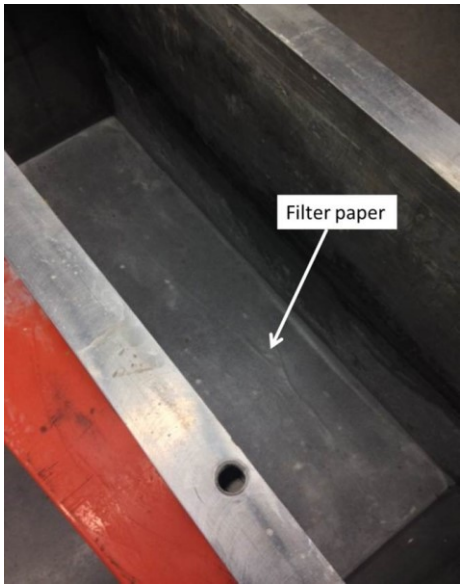

Figure 3-7 The plane-strain box with porous stone and filter paper at the bottom.

When the slurry is ready, it is carefully scooped to the plane-strain box, taking care to avoid intrusion of air bubbles (Figure 3-8).

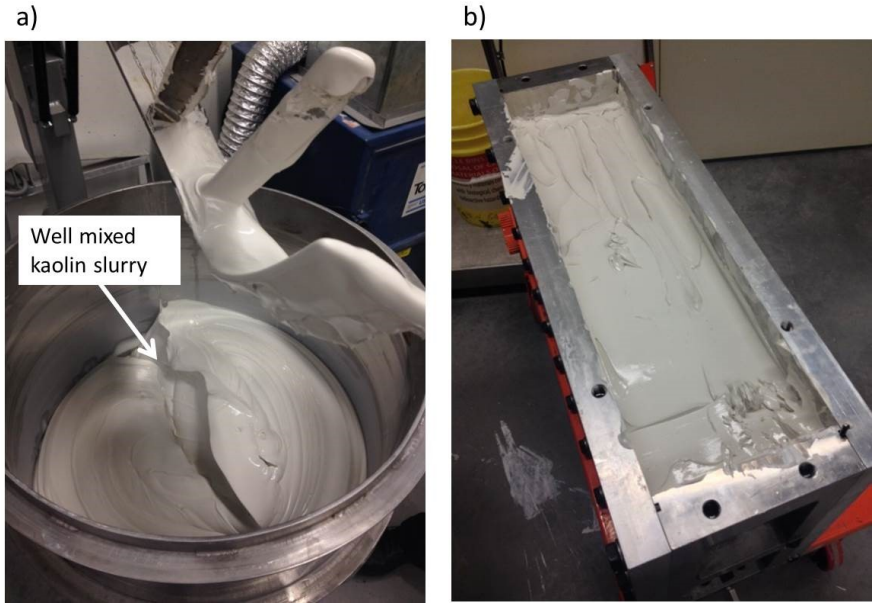

Figure 3-8 Moving kaolin slurry into the plane-strain box.

After moving kaolin slurry to the plane-strain box, another filter paper and porous stone are placed on top of it. To prevent extrusion of kaolin slurry during consolidation, the porous stone is made just the size of the plane-strain box. Distance from the porous stone

to the top of the plane-strain box is measured at different locations to ensure that the porous stone is positioned horizontally (Figure 3-9b).

To shorten the consolidation time, double drainage is maintained during the consolidation. At the top of the kaolin block, dissipated water is kept. At the bottom of the kaolin block, drainage channels are connected to standpipe**.** By this way, the kaolin block is kept saturated during consolidation.

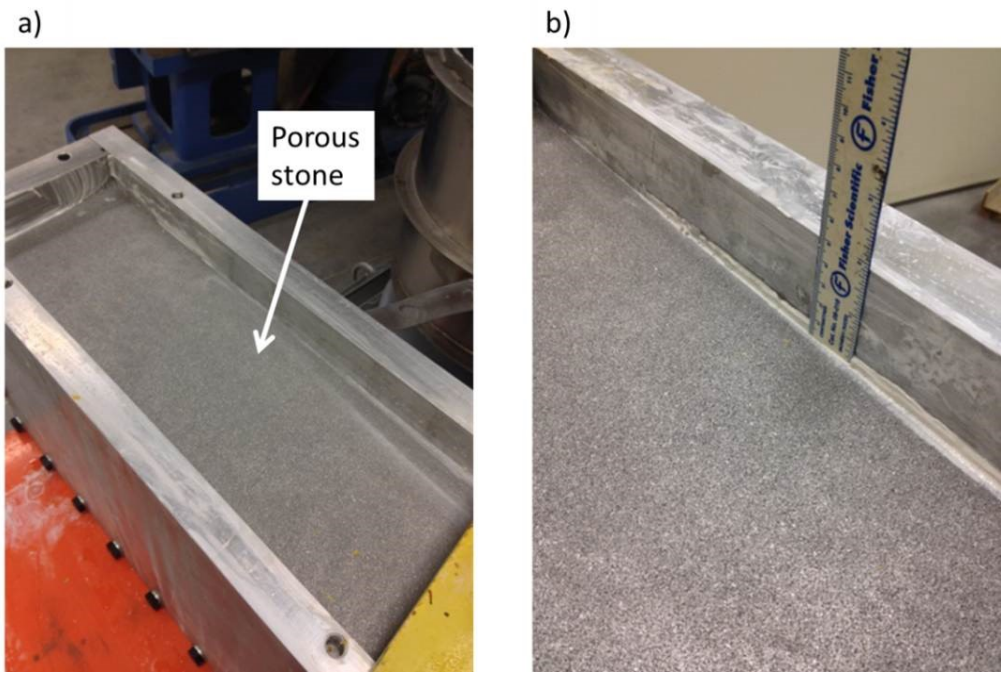

Figure 3-9 Porous stone on top of the kaolin slurry.

Then the loading plate is gently positioned on top of the porous stone, which will exert an equivalent consolidation pressure of 1.9kPa. The loading plate is left on the kaolin block overnight for stabilization (Figure 3-10).

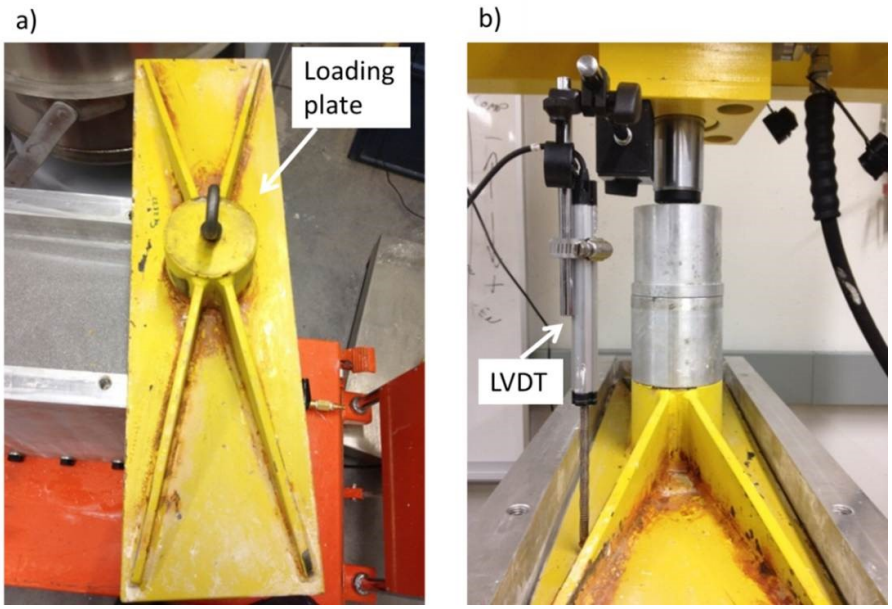

Figure 3-10 The loading plate for consolidation.

Then the consolidation pressure is increased to 5kPa. After the first increment, the consolidation pressure could be increased after about 80% of consolidation is achieved which could be roughly judged by observing the derivation of the consolidation curve from its linear portion (log scale) as shown in the Figure 3-11.

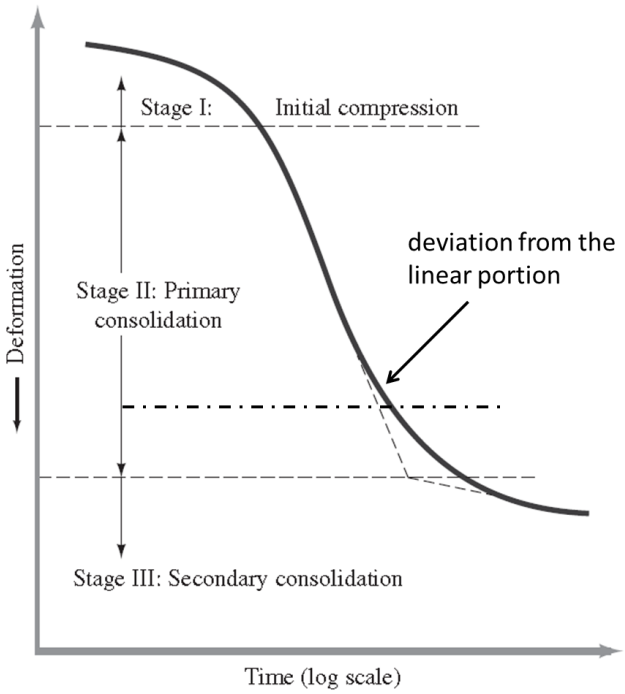

Figure 3-11 The consolidation curve (modified after Das, 2007).

The consolidation pressure is successively doubled until the required maximum consolidation pressure is achieved (2kPa, 5kPa, 10kPa, 20kPa, 40kPa, 80kPa, 160kPa, 320kPa, 640kPa, 1000kPa, 1450kPa). It typically takes 2 to 3 days for one consolidation stage to finish.

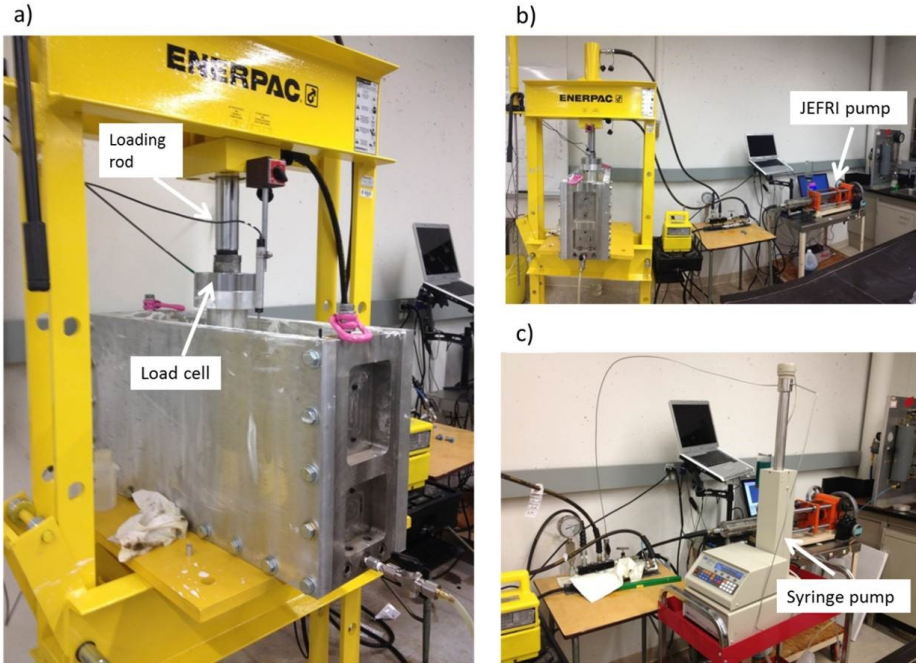

Figure 3-12 The consolidation setup at GeoCERF.

Before applying the maximum consolidation pressure, the Kulite miniature pore pressure transducers (PPTs) should be installed. The bottom drainage is closed to prevent suction at the bottom of the kaolin block. Then the consolidation pressure is released step by step. The height of the kaolin block should be measured immediately before and after unloading. The PPTs are installed at certain depths inside the kaolin block through the tappings at the side wall of the plane-strain box. Detailed PPT installation procedures will be described in section 3.3.

After the installation of Kulite PPTs, the bottom drainage is restored and then the consolidation pressure on the kaolin block is resumed to its former level. When the primary consolidation is finished, the final consolidation pressure of 1450kPa is loaded.

After the 1450kPa consolidation, the kaolin block should be unloaded for the following centrifuge tests. It is important to unload the kaolin block step by step (in an increment of 100kPa) to eliminate the possibility of air bubble nucleation within the kaolin block (Take, 2003). After each stage of unloading, the pore pressures within the kaolin block are in suction which will dissipate in a controlled manner in the presence of excess pore fluid (Taylor, 1995). Before the final unloading from 100kPa to 0kPa is performed, the kaolin block is isolated from potential sources of water that could permit elastic swelling: the bottom drainage is closed and any free water on the top surface of the kaolin block is removed (Take, 2003). After unloading, the top of the kaolin block should be covered with a plastic film to prevent evaporation.

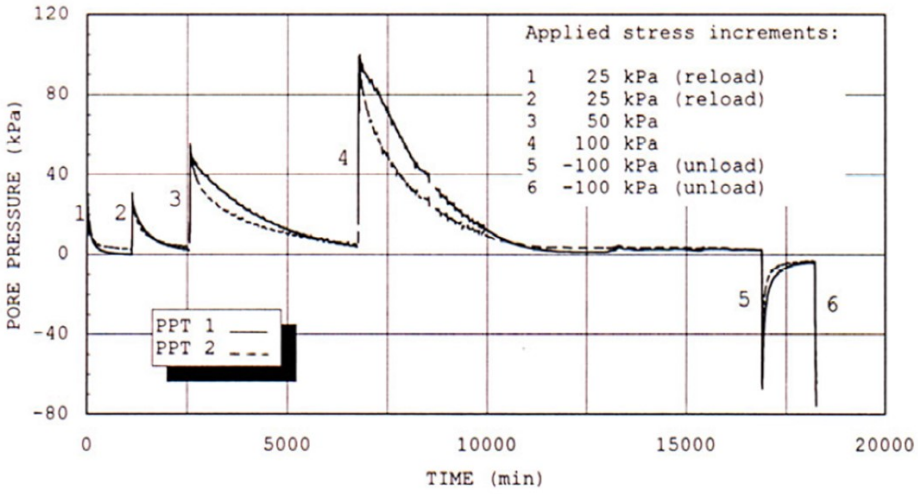

Figure 3-13 Pore pressures in a clay sample under 1 g consolidation (Konig et al., 1994).

3.2.2 Properties of Overconsolidated Speswhite Kaolin

3.2.2.1 Triaxial Test

Triaxial tests are commonly conducted to measure the mechanical properties of geotechnical materials. Typically, three types of triaxial tests could be carried out: unconsolidated-undrained (UU), consolidated-undrained (CU) and consolidated-drained (CD). Figure 3-14 shows the diagram of typical triaxial test equipment, and the drainage conditions (drained or undrained) during shearing could be controlled by the drainage valve.

Consolidated-drained triaxial compression tests are conducted using the GDS system at Geomechanical Reservoir Experimental Facility (GeoREF). For GDS system, there are two GDS pumps: one for the cell pressure and one for the top back pressure (back pressure exerted at the top of sample). Another ISCO pump is connected at the bottom of sample for bottom back pressure. This ISCO pump will exert higher pressure at the bottom of sample than the GDS back pump to conduct permeability tests. One important feature of the system is that the volume change in the sample during consolidation and shearing could be directly observed.

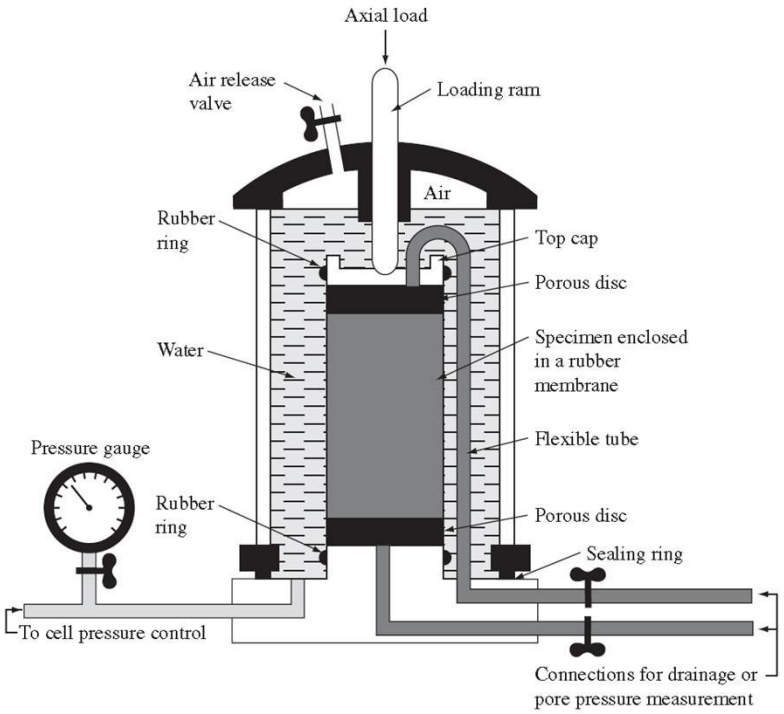

Figure 3-14 Diagram of triaxial test equipment (Das, 2007).

3.2.2.2 Sample Coring for Triaxial Test

Triaxial samples are cored right after the Speswhite kaolin block is unloaded instead of after inflight consolidation because in-flight consolidation would cause various stress histories across the sample length which should be avoided. During sample coring, it is important to avoid the Kulite Pore Pressure Transducer. Five samples are cored out of the kaolin block with five Shelby tubes of 2.5 inch inner diameter. The Shelby tubes are carefully pressed all the way down to the kaolin block bottom by the same hydraulic ram for consolidation (Figure 3-15a). It is difficult to pull the Shelby tube out of the kaolin block. Therefore, the aluminum plate of the plane-strain box is removed, and the Shelby tubes are cut out using a wire saw (Figure 3-16).

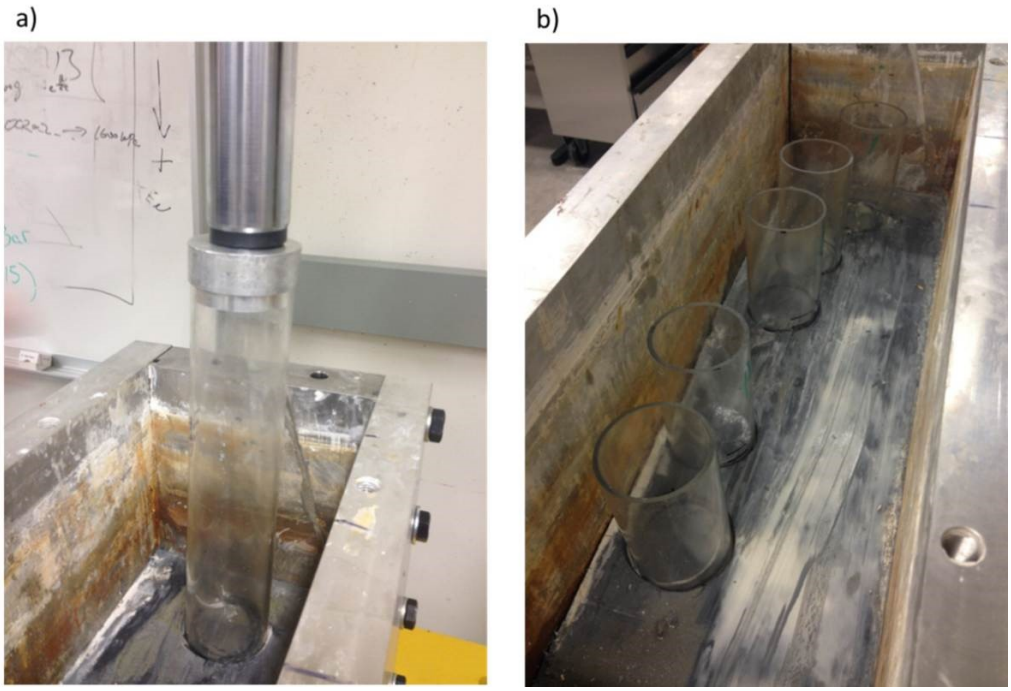

Figure 3-15 a) Shelby tube being pushed down into the kaolin block by hydraulic ram and b) five Shelby tubes pushed all the way down to the bottom of kaolin block.

Figure 3-16 Cutting the Shelby tube out of the kaolin block.

3.3.2.3 Properties of Overconsolidated Kaolin from Consolidated-drained Triaxial Test

Three consolidated-drained triaxial tests are conducted on overconsolidated Speswhite kaolin samples at different effective confining stresses of 300kPa, 700kPa, and 1000kPa respectively (Table 3-1). Constant pressure head permeability tests are carried out before and after shearing for each sample to measure the permeability of the overconsolidated Speswhite kaolin samples, which can be found in Appendix B.2. The mechanical properties of overconsolidated Speswhite kaolin samples are determined as shown in Table 3-3. Detailed descriptions of the triaxial test results on these kaolin samples can be found in Appendix B.

Table 3-1 Triaxial test program for overconsolidated Speswhite kaolin samples.

	Back pressure (kPa)	Cell pressure (kPa)	Effective confining pressure (kPa)	Permeability test pressure head (kPa)
Test #1/Sample #1	500	800	300	30
Test #2/Sample #4	500	1200	700	70
Test #3/Sample #5	500	1500	1000	100

Table 3-2 Overconsolidated Speswhite kaolin triaxial test sample properties.

	Height (mm)	Diameter (mm)	Weight (g)	Bulk Density (kg/m^3)	Dry Density (kg/m^3)	Initial Void Ratio	Initial Water content
Test #1/Sample #1	138.35	63.2	781.15	1799.8	1264.7	1.06	42.31
Test #2/Sample #4	140.35	63.5	792.48	1783.5	1256.3	1.08	41.97
Test #3/Sample #5	138.00	63.4	776.67	1782.9	1264.1	1.06	41.04

Table 3-3 Mechanical properties of overconsolidated Speswhite kaolin samples.

Bulk Modulus (MPa)	Shear Modulus (MPa)	Friction Angle (°)	Cohesion (kPa)	Dilation Angle (°)	Tension (kPa)
11.11	3.70	15	30	0	0

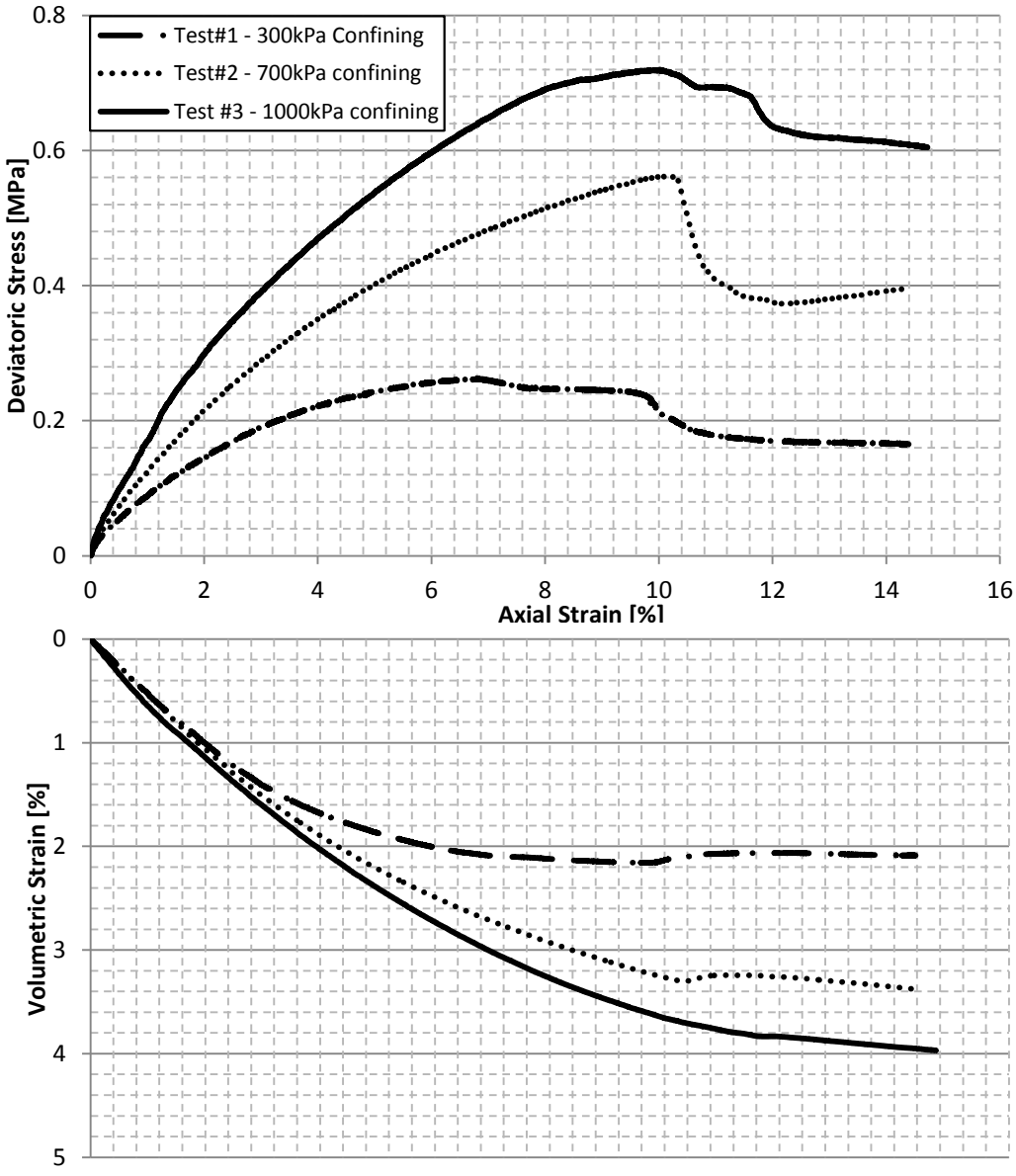

Figure 3-17 Deviatoric stress – axial strain - volumetric strain test results for overconsolidated Speswhite kaolin samples.

3.3 Instrumentation for Centrifuge Application

3.3.1 Pore Pressure Measurement

3.3.1.1 Kulite Miniature Pore Pressure Transducer

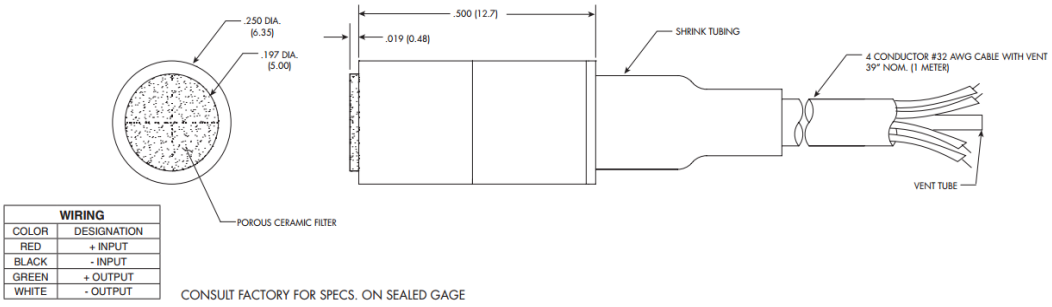

Figure 3-18 Configuration of the Kulite XCL-11-250 pore pressure transducer.

The Kulite XCL-11-250 Series is typically used for high-demanding pore pressure monitoring, such as in corrosive environments and during earthquake; meanwhile, these pore pressure transducers have small dimensions (Figure 3-18), which make it a good choice for geotechnical centrifuge application. Table 3-4 shows the working conditions of the specific Kulite XCL-11-250 used within GeoCERF.

Table 3-4 Specifications of the Kulite XCL-11-250 miniature pore pressure transducer.

Operational Mode	Sealed Gage
Rated Pressure	1700kPa
Maximum Pressure	3400kPa
Rated Electrical Excitation	10 VDC/AC
Maximum Electrical Excitation	15 VDC/AC

3.3.1.2 Installation of Kulite Miniature Pore Pressure Transducer

The Kulite XCL-11-250 Miniature Pore Pressure Transducer (PPT) is to be installed in the middle of the kaolin block for internal pore pressure monitoring and recording.

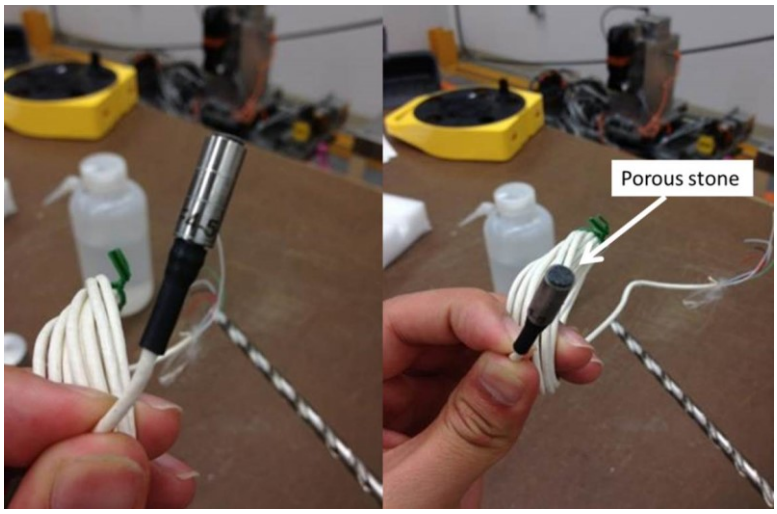

Figure 3-19 Kulite XCL-11-250 Miniature Pore Pressure Transducer (1/4 inch diameter cylinder probe).

The Kulite PPT should be installed after most of the consolidation has finished as large vertical deformation will damage the transducer lead. That is the reason why it is installed before the last consolidation increment.

The installation will proceed with the consolidation pressure removed. During installation, the sample undergoes swelling and suction is developing within the sample. Thus it is necessary to plan ahead and have all required equipment ready before installation to make the process go quick and smooth. The quicker the process, the less the time required for the subsequent consolidation "recovery" after resuming consolidation.

The Kulite PPT is installed through the tappings at the sides of the plane-strain box. There are three tappings at each side of the plane-strain box which are equidistantly located. The tappings are internally threaded and during consolidation they are closed with plugs.

The Kulite PPT should be connected to the data logger during installation for observation and recording of PPT readings. A hollow brass pusher rod with the same diameter as the transducer is put on the transducer lead. The pusher rod will be used to push the

transducer into position. Before inserting the Kulite PPT into the kaolin block, it is kept in water for saturation (Figure 3-20). The readings recorded when the Kulite PPT is in water is considered as the reference reading for future readings.

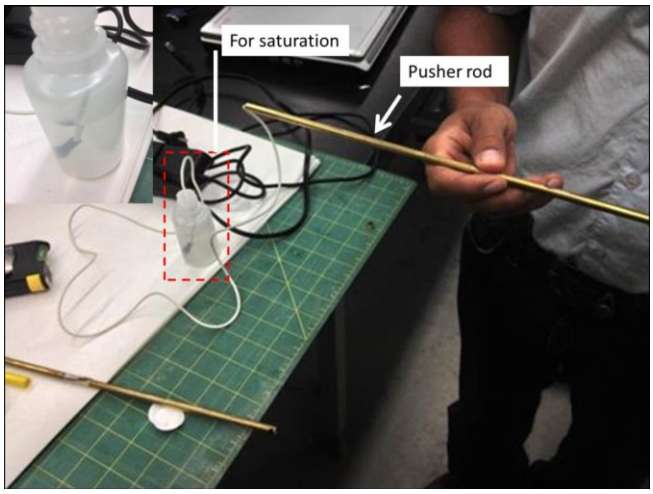

Figure 3-20 Saturation of Kulite pore pressure transducer before installation.

Remove the plug of the tapping where the Kulite PPT will be inserted from. A handheld drill is used to auger through the kaolin block until 5mm short of the desired installation position (Figure 3-21). An adjustable cart is used to make the dill seated horizontally at the same height of the tapping. For convenience and accuracy, required drilling depth is marked on the drilling rod.

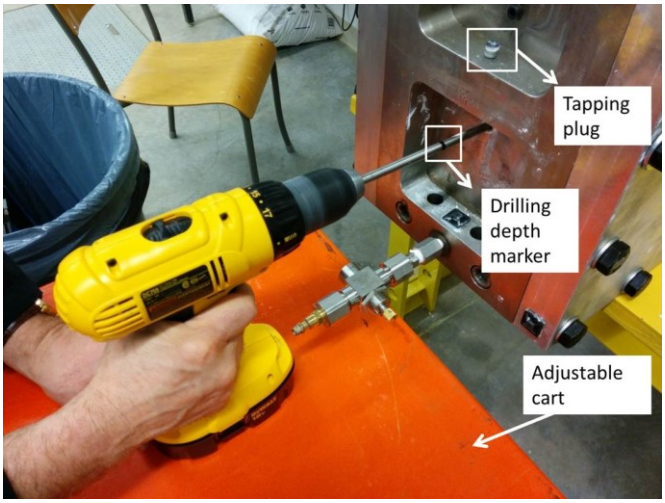

Figure 3-21 Drilling a "tunnel" for Kulite pore pressure transducer installation.

When the drilling is finished, the drill rod is gently pulled out and a tunnel is created. The Kulite PPT is set in its receptacle on the end of the pusher rod (Figure 3-22) and a filter paper is put on the porous stone of the transducer to avoid clogging. Some water is sprinkled onto the filter paper for saturation. Before insertion, it is necessary to mark the installation depth on the pusher rod and the transducer lead to track where the transducer is in case that some inner parts of the tunnel collapsed. Then the transducer is quickly inserted into the tunnel. When it is sensed that the transducer has hit the end of the tunnel (precisely judged by the marker on the pusher rod), the transducer is pushed another 5mm to firmly seat the transducer (Figure 3-22).

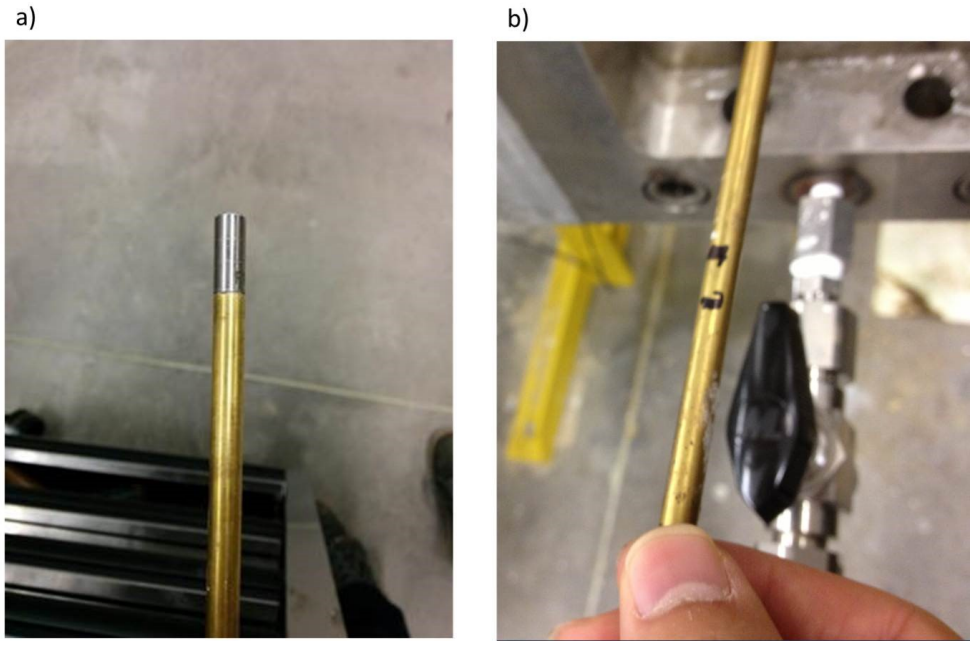

Figure 3-22 Insert the transducer into the sample using a hollow brass rod.

At this time, the pusher rod is pulled back slightly (leaving the transducer in place), and then the tunnel should be refilled by kaolin slurry which is to be injected by a syringe with air pressure supply. The syringe consists of an O-ring sealed piston chamber (which has been filled with kaolin slurry) with a long one-eighth-inch tube attached to its end (Figure 3-23). The one-eighth-inch tube is inserted to the end of tunnel and then the air pressure is supplied to continuously inject kaolin slurry into the tunnel until the kaolin

slurry goes out of the tunnel. After the kaolin slurry goes out, the injection still continues for a while to ensure that no air bubble is trapped inside.

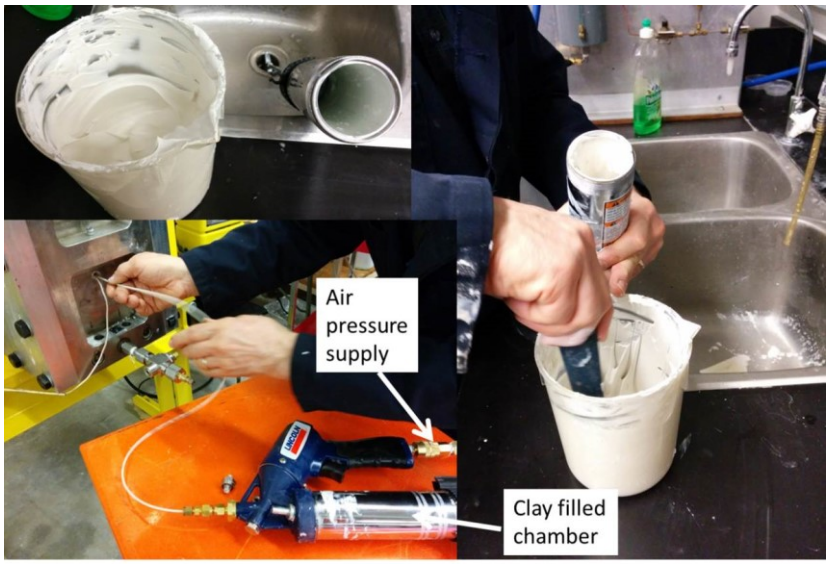

Figure 3-23 Fill the syringe with kaolin slurry.

When the tunnel is filled with kaolin slurry, a nut with O-ring inside (Figure 3-24) is used to close the tapping while giving the transducer lead some flexibility as in the subsequent experiments the transducer will be stretched due to kaolin block deformation. When installation is finished, the consolidation pressure is restored to the former level.

Figure 3-24 Closure of the tapping after installation of Kulite pore pressure transducer.

3.3.2 Image-based Deformation Measurement

Particle Image Velocimetry (PIV) is a texture-driven displacement measurement technique (Figure 3-25) based on image processing and has been successfully employed in experimental fluid mechanics long before White (2002) and Take (2003) introduced this technique to the geotechnical centrifuge application.

By using digital imaging, multi-threshold centroiding, particle image velocimetry and close-range photogrammetry, White (2002) and Take (2003) developed a texture-driven displacement measurement system especially for geotechnical centrifuge application. Detailed theory background of this technique will not be covered here and could be found at Take (2003). A MATLAB application package named GeoPIV (White, 2002; White et al., 2003) is available for non-commercial usage and can be used to analyze the displacement in image space. With the aid of control markers, the displacement could be transformed to the object space.

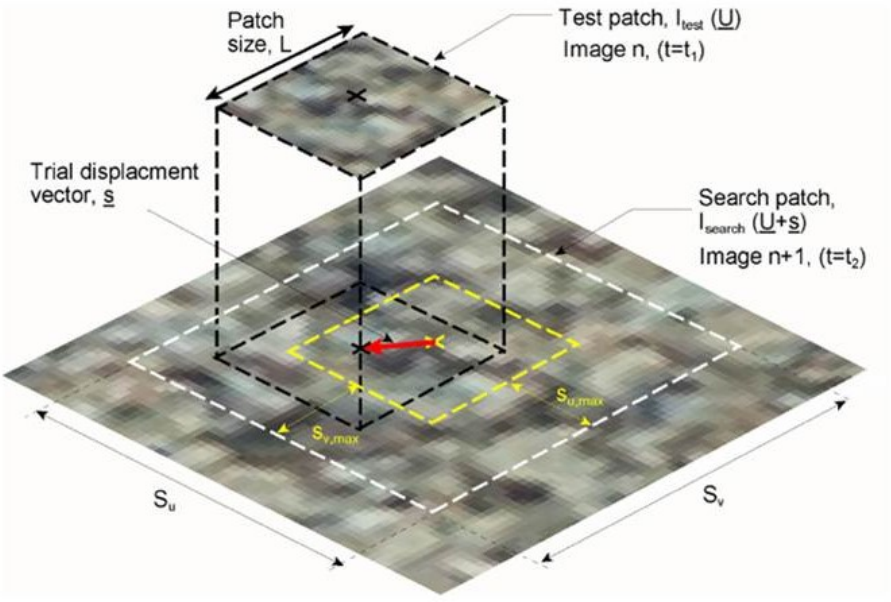

Figure 3-25 Visual description of PIV matching algorithm (Take, 2003).

3.3.2.1 PIV System at GeoCERF

To survive high centrifugal forces while taking high-quality images, the camera and lens should have solid quality. The IDS UI-6280RE camera and Cinegon 1.8/4.8mm compact c-mount lens are used (Figure 3-26). The IDS camera has a 2/3" Sony 5 megapixel monochrome and color CCD sensor which can deliver a resolution of 2448 x 2050 pixels. A global shutter system allows it to capture sharp images of moving objectives. The Cinegon lens has high-standard optical performance and through its fine internal thread precise focusing could be achieved. Also the lockable focus and iris setting mechanism can maintain the optical settings during continuous use.

Figure 3-26 a) IDS UI-6280RE-C-HQ camera (en.ids-imaging.com) b) Schneider KMP-IR Cinegon 4.8/1.8 lens (www.schneideroptics.com).

Camera mounting kit is used to hold the camera in place at high g-force environment and the height and position of the camera can be adjusted by using different pre-set holes as shown in Figure 3-27.

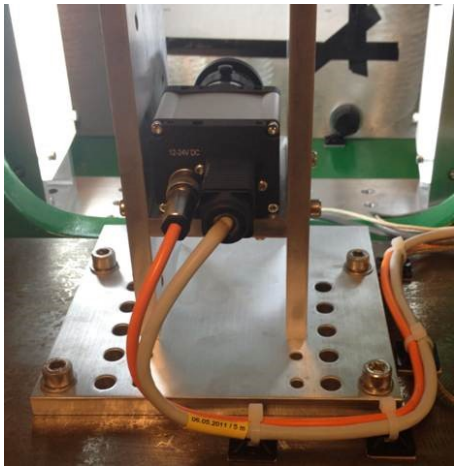

Figure 3-27 Mounting kit for IDS camera.

Two LED illumination towers are available on the centrifuge swing platform to facilitate better lighting conditions with the help of illumination diffuser filter and polarising filter sheet (Figure 3-28). The angle and position of the LED towers can be adjusted.

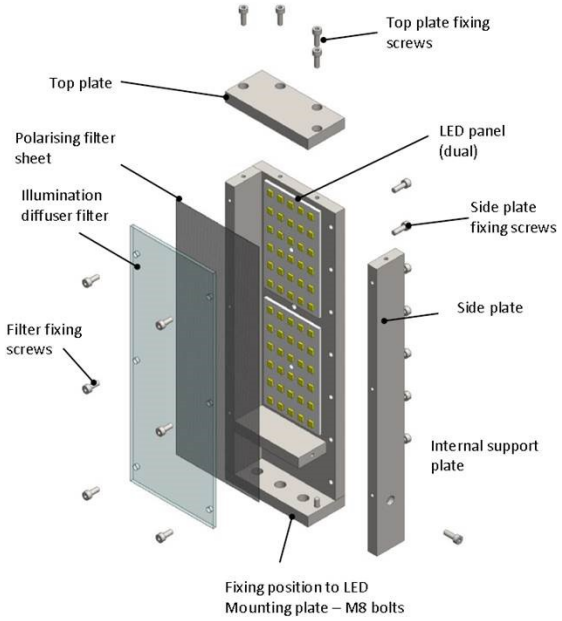

Figure 3-28 LED illumination tower construction (TBS, 2013).

3.3.2.2 Texture of Clay

One of the key points for conducting successful PIV analysis relies on the material textures. The Speswhite kaolin has a uniform white color that is not suitable for PIV analysis. To create sufficient texture for the Speswhite kaolin, a thin layer of uniform fine red sand is softly blown onto the Perspex glass before assembling the plane-strain box. To hold the sand in place during assembly, a thin layer of silicon grease is coated onto the Perspex glass.

3.3.2.3 Control Markers

The control markers are the most important component for transforming the image-space displacement vectors to object-space displacement vectors. Basically, control markers are made of round black dots with white background. At GeoCERF, control markers are

made permanent on the Perspex glass using drill bits. Firstly, 6.5mm diameter and 0.25mm deep holes are drilled. Then 4.5mm diameter and 0.75mm deep holes are dilled (Figure 3-29). The smaller diameter holes are then filled with black pigment (Figure 3-30). After the black pigment dries out, white pigment is painted above and fills the bigger diameter hole. Finally, a coating is put on top to protect the control markers from scratching.

For each test, the Perspex glass should be covered with a thin layer of transparency to prevent scratching of the glass as well as the control markers. Attention should be paid to avoid trapping air, which may cause some areas of higher brightness in captured images.

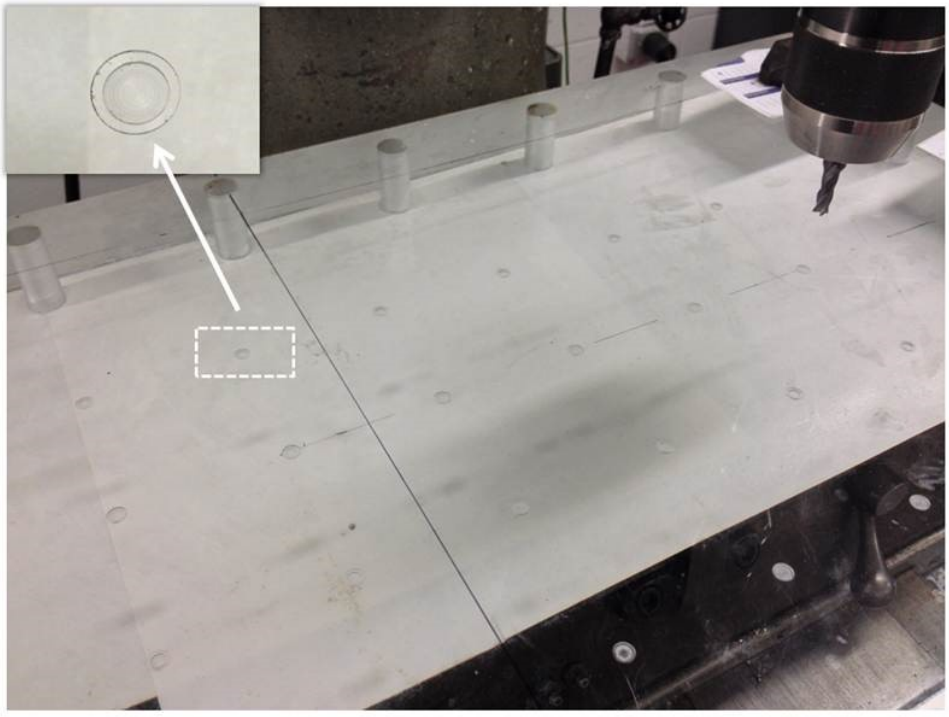

Figure 3-29 Making of permanent control markers on the Perspex glass.

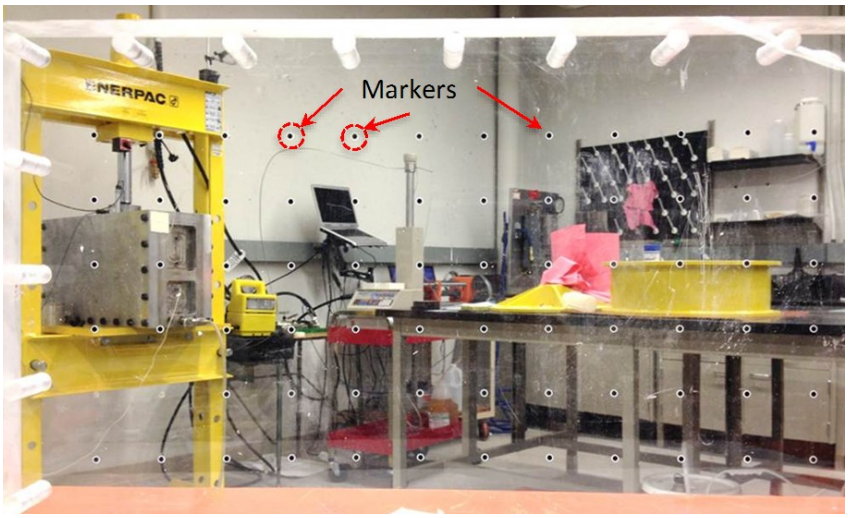

Figure 3-30 Control markers after being filled with black pigment.

3.3.2.4 Good Practice for PIV Measurements

These sections are courtesy of Dr. Jonathan Black at the University of Sheffield.

Considering the distortion caused by wide angle lens

Wide angle lenses have the advantages of covering much wider areas of the testing package, even the full extent of the plane-strain box. The mounting positions of the camera can be adjusted depending on the areas of interest for different tests. However, images captured through wide angle lenses have large distortion especially at the edges. It would be favourable if the area of interest is placed at the center of the image.

If conducted appropriately, the distortions can be corrected using control markers. As the control markers are coplanar with the front face of the kaolin block, the refraction influence of the thick Perspex glass could be automatically corrected.

Regarding the LED illumination, and glare reduction

The lighting conditions have significant influences on the quality of images for PIV analysis. With the equipment available at GeoCERF, a few things could be considered to facilitate good lighting conditions.

1) The LED towers are supplied with light diffuser panels and polarizing light filters, which should be installed. The light exiting the LED towers is vertically polarized. As a consequence, the illumination from the incident and reflected ray from the Perspex glass will be reduced.
2) The positioning of LED towers is important as the lighting angle is critical to optimal imaging. If the positioning is not appropriate, there would be the reflection of the LED towers on the Perspex glass which could destroy the material textures on captured images. Usually, the LED towers should be placed at a shallow angle to the Perspex glass so that light is illuminated across the glass instead of pointing directly at the window. Another trick of positioning the LED towers is to avoid the area of interest; by this way, the glare on the Perspex glass would not influence much of the PIV analysis.
3) The illumination intensity of the LED towers could be adjusted. The exposure time of the camera should be adjusted accordingly to capture images of good quality.
4) There still might be some reflection of the LED towers on the Perspex even though great efforts have been devoted to find the right positioning of the LED towers. A polarizer for the camera lens could be used to help reduce glare.
5) The lighting on the ceiling of the centrifuge chamber is not continuous, thus there would be non-uniform lighting conditions during spinning. The images captured during spinning might have different brightness on certain areas which will influence the PIV analysis results to some extent. It is recommended to turn off the chamber lights during spinning if the image quality can be guaranteed.

Chapter 4： Numerical Study of SAGD Caprock Integrity

This chapter is devoted to the numerical study of SAGD caprock integrity as well as the feasibility study of centrifuge physical modeling of caprock integrity.

Without sufficient field data, reservoir geomechanical simulations of SAGD caprock integrity play an important role in bridging the prototype and the centrifuge model. A synthetic one well-pair SAGD project which will act as the prototype is created based on the geology of the Joslyn SAGD project. The shearing zone development in caprock is thoroughly analyzed along with the displacement profile evolution at the base of the caprock. As the overconsolidated Speswhite kaolin used in the centrifuge model has a different behaviour under shearing compared to that of caprock shale, a parametric analysis is carried out to study the influences of different parameters on caprock behaviour during SAGD process. The feasibility study of conducting caprock integrity test using geotechnical centrifuge is also presented.

4.1 Prototype - Synthetic One Well-pair SAGD

4.1.1 The Prototype Configuration

4.1.1.1 Joslyn Steam Release Incident

The 2006 Joslyn incident is the only major failure of SAGD caprock (Total E&P, 2007). Also, at the time, the Joslyn SAGD project was the shallowest commercial SAGD project. Thus it is of importance to study the geology of the project and review the failure mechanism.

The report of "Summary of Investigations into the Joslyn May 18th 2006 Steam Release" (Total E&P, 2007) provides a detailed post-incident analysis, of which geological and geomechanical analysis are of great importance to this study.

Geology:

The geology of the failure areas can be simplified as followings:

- ***Layer A:*** *A ~28 m thick bitumen bearing Middle McMurray reservoir at the base of which a horizontal SAGD injector and a horizontal SAGD producer are drilled above one another, the producer being close to the reservoir base and the injector about 5 m above the producer.*
- ***Layer B:*** *A ~25 m thick Middle / Upper McMurray and Wabiskaw interval with alternating shale and bitumen and gas bearing reservoir intervals. This interval is not regarded as a SAGD development target. It presents some potential for long term seal confinement and temporary pressure buffering.*
- ***Layer C:*** *A 2 m water bearing interval (Wabiskaw 3).*
- ***Layer D:*** *A massive mostly shaley interval up to surface (~35 m thick, Clearwater and Quaternary).*

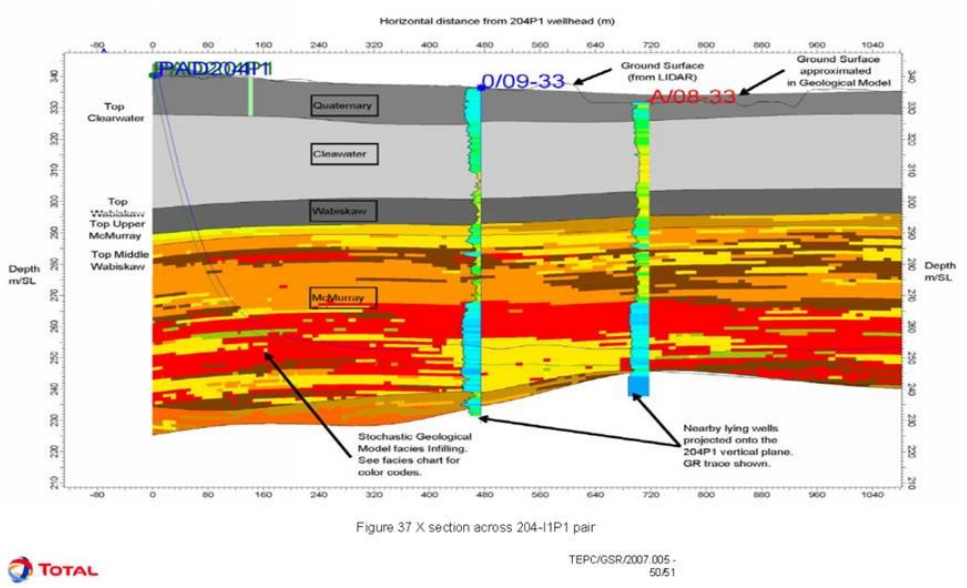

Figure 4-1 Section across 204-I1P1 well pair where steam release happened (Total E&P, 2007).

Failure mechanism:

According to the post-incident analysis (Total E&P, 2007), most likely the final failure of caprock is caused by the pore pressure build-up at the bottom of caprock. When the pore pressure exceeds the vertical stress, shoulder failure initiates from the base of caprock and propagates through the caprock as shown in Figure 4-2b.

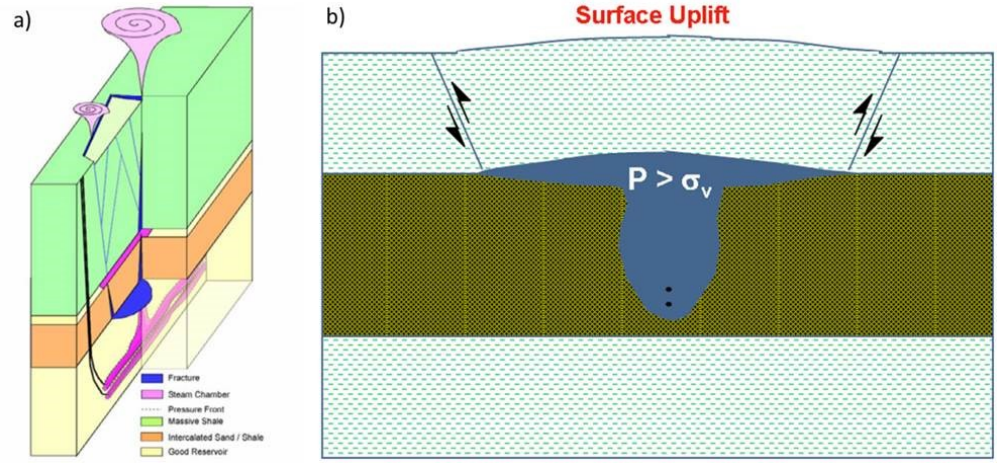

Figure 4-2 a) Steam release – May 18th 2006, b) failure of a shale barrier by shear on the shoulders of a zone with a pressure greater than the vertical stress (Total E&P, 2007).

4.1.1.2 Configuration of the Synthetic One Well-Pair SAGD

For SAGD projects, the horizontal wells are typically 1000m long, while the vertical depths are only a few hundred meters. The ratio of vertical dimension to horizontal dimension is low especially for shallow reservoirs (less than 100m deep). Thus it is reasonable to study SAGD caprock integrity two-dimensionally (i.e. a plane-strain problem) and the plane-strain box at GeoCERF will be used to contain the centrifuge model.

Only caprock and overburden will be simulated in the centrifuge models, which will be spun at 100g. The dimensions (Figure 4-3), and mechanical strength of the plane-strain box will constrain the depth and thickness of caprock which could be simulated. To maximize testing space in the plane-strain box, the overburden in centrifuge models are simulated using closely packed lead bars.

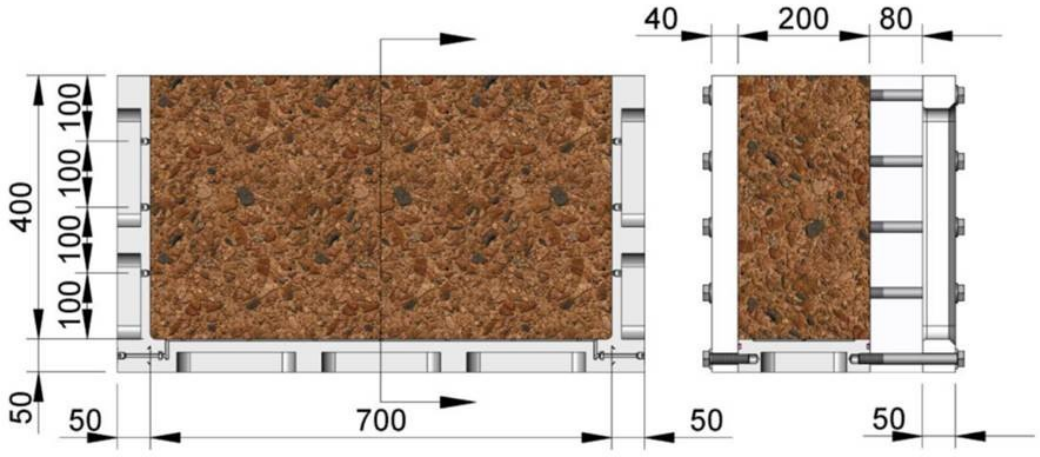

Figure 4-3 The dimensions (units in mm) of the plane-strain box at GeoCERF (TBS, 2012).

Based on the geology of the Joslyn SAGD project and the capacity of the plane-strain box at GeoCERF, the synthetic one well-pair SAGD project has such dimensions as shown in Figure 4-4.

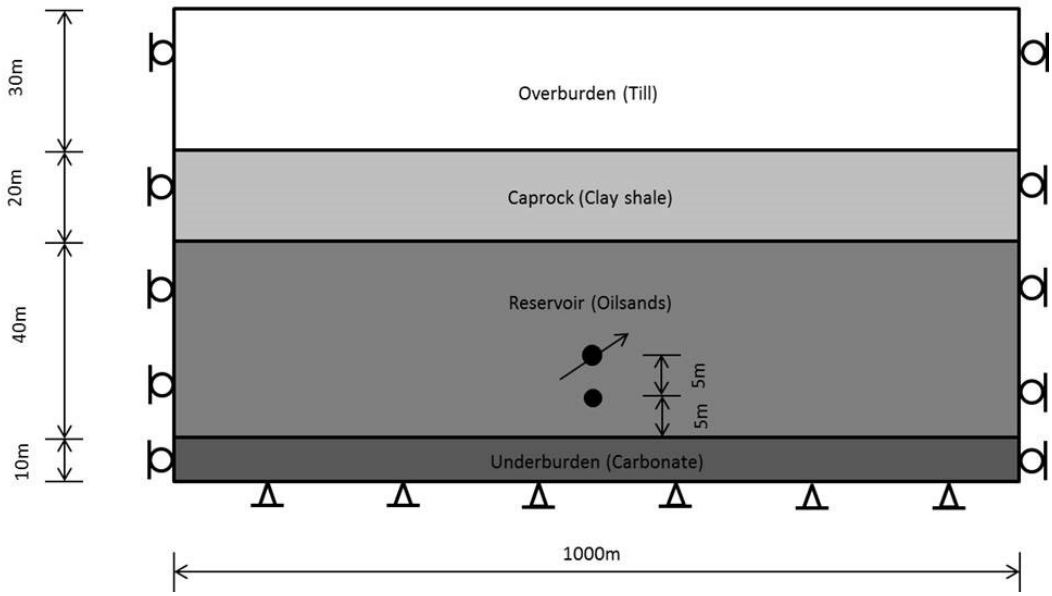

Figure 4-4 Schematic view of the synthetic one well-pair SAGD model (lateral and vertical dimensions are not at scale) and the boundary condition for geomechanical simulation.

Typically, the producer well is located around 5 meters above the top of underburden and the injector well is 5m above the producer well. To avoid possible tensile failures at the base of caprock, the bottom hole pressure (BHP) in the injector well is determined based on the minimum in situ stress, which is typically the vertical stress for shallow SAGD projects. Current regulations state that the BHP should not exceed 80% of the minimum in situ stress at the base of caprock. To create a pressure difference between injector and producer wells, the BHP in the producer well is set 200kPa lower than the injector well pressure. This pressure difference helps with steam chamber conformance and aids in the movement of bitumen-water mixture into the producer.

However, the purpose of this simulation is to explore the failure mechanisms of caprock under high injection pressure. Thus, the injection pressure gradient is picked as 16kPa/m, which creates an injection pressure of 1280kPa at the heel of the injector well.

4.1.2 Reservoir Geomechanical Simulations

The reservoir-geomechanical coupling could be achieved by three methods: fully coupled, sequential coupled and one-way coupled (decoupled) (Figure 4-5). Theoretically, the fully coupled method is the most accurate as fluid flow and deformation equations are solved simultaneously; however, this method is not practical due to its complexity. As an alternative, sequential coupling is most commonly used with acceptable accuracy and much less time consumption. Fully coupled and sequential coupled methods are more intended for studying the geomechanical effects on reservoir oil productions; they are not necessary for this study as the research focus is the stress and strain field alteration in the caprock (Deisman et al., 2012). Thus, the decoupled reservoir geomechanical simulation routines developed within Reservoir Geomechanics Research Group (RG^2) using ITASCA FLAC (geomechanical simulator) and CMG STARS (reservoir simulator) is employed for this study. Reservoir simulation is conducted first and then the updated pore pressure and temperature at each time step are fed to the geomechanical simulator to calculate the stress and strain field in caprock. For reservoir simulations, only reservoir and underburden are included. Thus, the grid system for CMG STARS is 1000m × 50m and each element is 1m by 1m rectangle. In geomechanical simulations, the grid system includes overburden, caprock, reservoir and underburden; thus the geomechanical model has a dimension of 1000m × 100m with each element being 1m by 1m rectangle. The horizontal displacement at the sides and bottom of the model is fixed, and no vertical displacement is allowed at the bottom of the model (Figure 4-4).

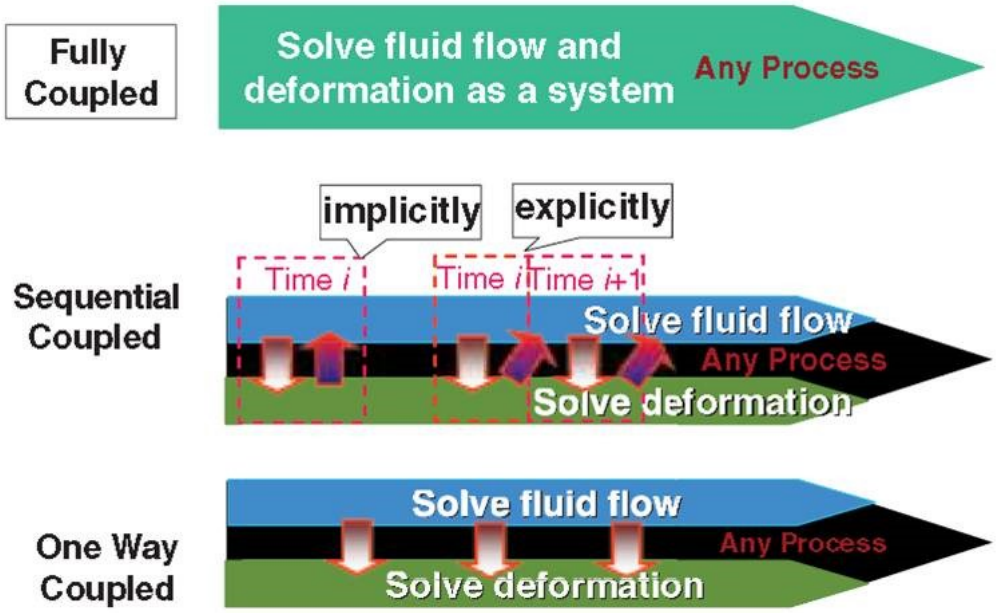

Figure 4-5 Methods of coupled reservoir and geomechanical simulation (Gu et al., 2011).

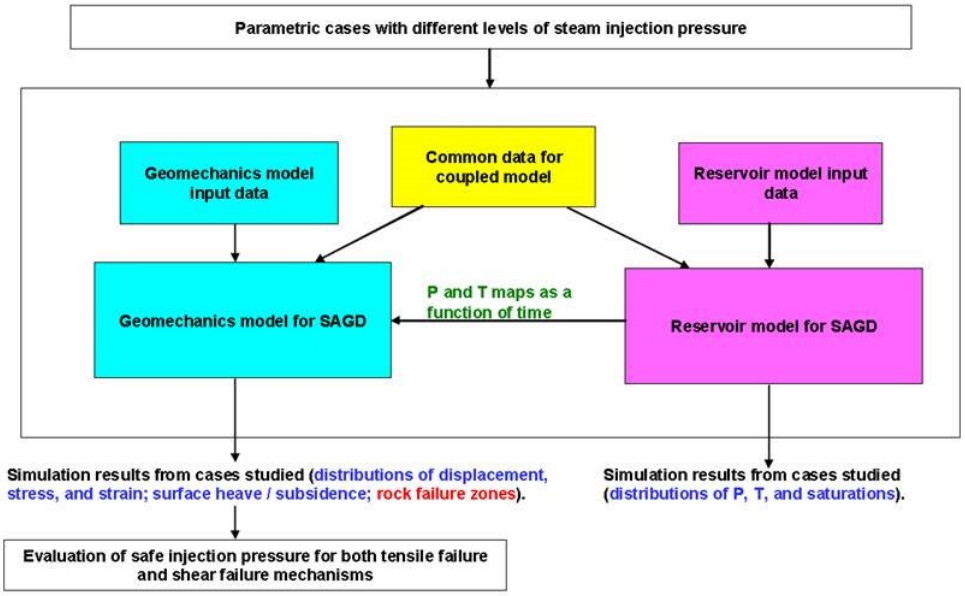

Figure 4-6 One-way coupling workflow between geomechanics and reservoir models (Chin et al., 2012).

For reservoir simulations, the input parameters for reservoir and underburden are chosen as the typical values in literature (Table 4-1).

Table 4-1 Reservoir and underburden properties for reservoir simulation in Reference Case.

	Porosity	Permeability: $K_I=K_J$ (Darcy)	Permeability: K_K (Darcy)	Thermal Conductivity of Rock (J/m-day-C)	Thermal Conductivity of Oil phase (J/m-day-C)
Reservoir	0.35	2	1	1.33E+5	1.33E+5
Underburden	0.01	0.001	1E-6	1.73E+5	1.33E+5

Caprock behaviour in geomechanical simulations is described using an elasto-perfectly plastic constitutive model with Mohr-Coulomb failure criterion. In the centrifuge models, caprock will be mimicked using the overconsolidated Speswhite kaolin block. Thus the mechanical properties of the over-consolidated Speswhite kaolin are assigned to the caprock layer in the geomechanical simulations.

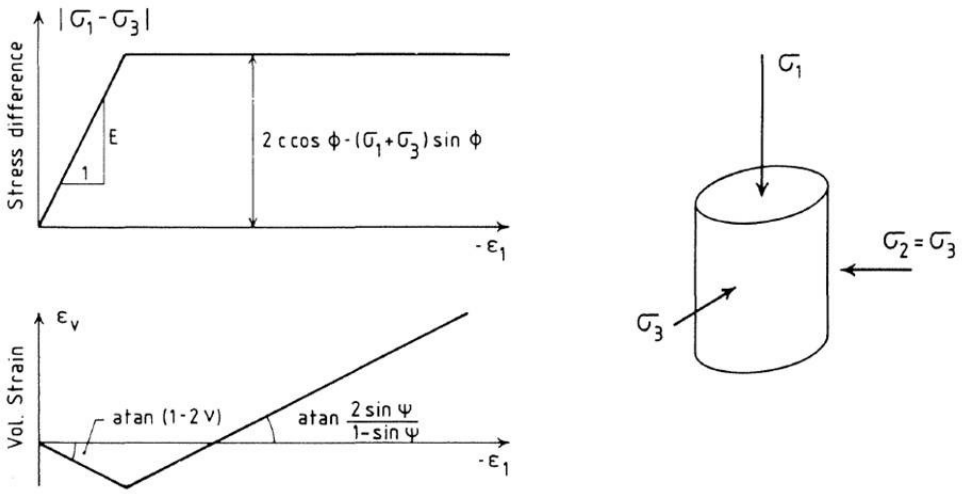

Figure 4-7 Bilinear idealization of triaxial test results (Vermeer, 1984).

Table 4-2 Mechanical properties of each layer for FLAC simulation in Reference Case.

	Thickness (m)	Density (kg/m^3)	Parameters for Elasto-plastic Model with M-C criterion					
			Bulk Modulus (MPa)	Shear Modulus (MPa)	Friction Angle (°)	Cohesion (kPa)	Dilation Angle (°)	Tension (kPa)
Overburden	30	2200	1.56	0.52	Elastic			
Caprock	20	1800	15.6[1]	5.2[1]	17[1]	0[1]	0	0
Reservoir	40	2250	333	200	45	0	35	0
Underburden	10	2250	353	136	Elastic			

4.2 Caprock Behavior in Reference Case

Caprock in this research is deemed as homogeneous material without any pre-existing faults or weak planes inside. Consequently, no failures along the faults or weak planes are considered. Shearing failure and tensile failure are the major failure modes of caprock to be explored in this research using reservoir geomechanical simulation approach.

To simplify the problem and comply with the boundary conditions in the centrifuge model, no pore pressure and temperature changes in caprock are considered for this research. Pore pressure and temperature fronts growths, vertical and horizontal displacement profile evolution at the base of caprock and the shearing zone development in caprock at different times are thoroughly analyzed to figure out how the caprock behave in the SAGD process. The one well-pair SAGD model is symmetrical to the well pair; thus only displacement and stress plots at the left half of the model would be presented. For horizontal displacement plots, the negative value means the horizontal displacement is towards the left boundary of the model.

[1] It should be noticed that the parameters listed in Table 4-2 are different from those reported in Table 3-3. This is because after this numerical analysis is conducted, two more triaxial tests on overconsolidated Speswhite kaolin samples are repeated and the measured mechanical properties are updated. The purpose of this numerical analysis is mainly for providing an approach to explore the possible failure modes of caprock to simulate in centrifuge models. It is not intended for a specific simulation case. Also a parametric analysis is conducted after this simulation to study the influence of different parameters on the caprock behavior during SAGD process. Thus numerical analysis is not re-run with the updated parameters.

The simulation case with the geomechanical properties listed in Table 4-2 is named as the Reference Case. According to geomechanical simulation results, the shearing zones in caprock start at 1260 days since the start of SAGD operation (Figure 4-8). Then the shearing zones propagate upward until going through the whole caprock formation at 1530 days (Figure 4-11). In FLAC geomechanical models, the caprock layer is from 50m to 70m and the reservoir is from 10m to 50m in elevation. If the zones are black, it means these zones have remained elastic. The red zones represent the shearing failure and yellow zones show that these zones were once in plastic state, but presently are elastic. The white zones stand for tension failure. The FLAC simulation model has a width of 1000m. To clearly demonstrate the shearing failure zones, only the center areas of the simulation are plotted (the center line of the simulation is at 500m in the longitudinal direction, i.e. the location of the single well pair of SAGD).

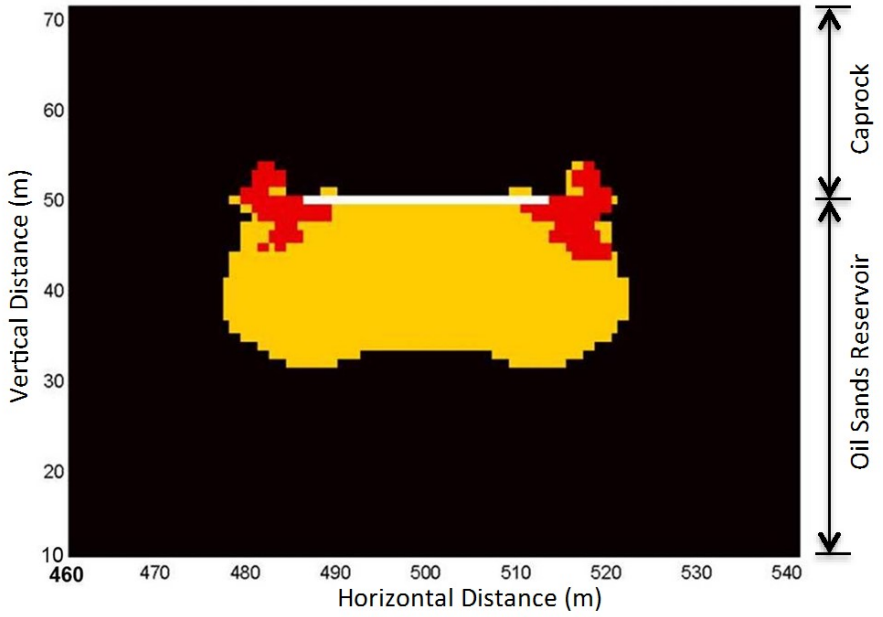

Figure 4-8 Shearing zones at 1260 days. Black zones = elastic, red zones = shear failure, yellow zones = previously failed but now elastic, white zones = tensile failure.

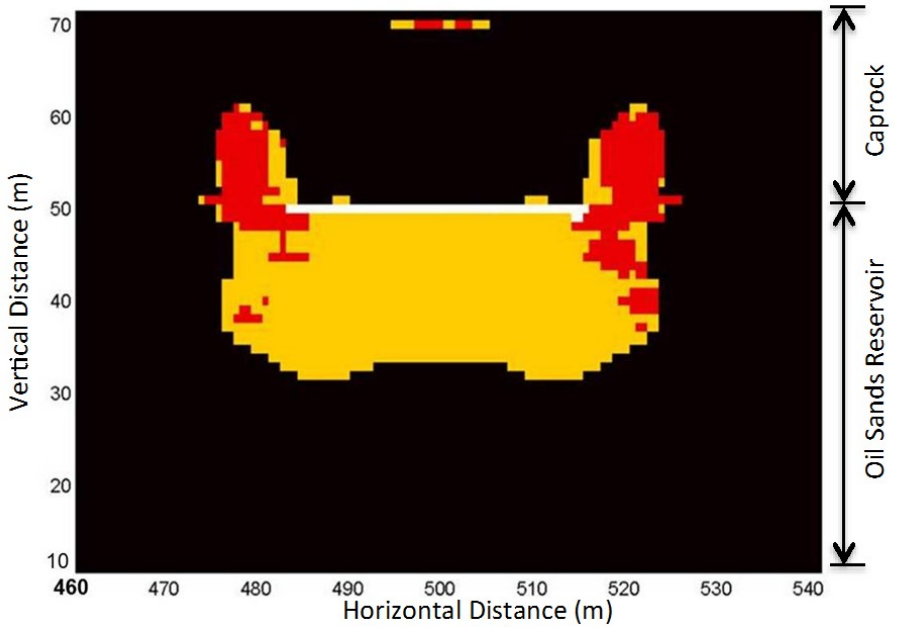

Figure 4-9 Shearing zones at 1350days. Black zones = elastic, red zones = shear failure, yellow zones = previously failed but now elastic, white zones = tensile failure.

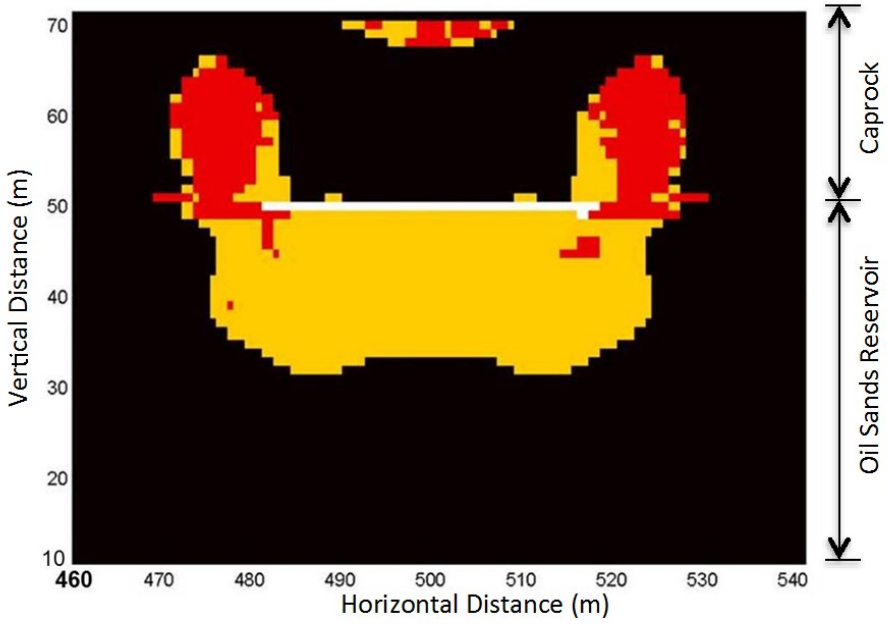

Figure 4-10 Shearing zones at 1440days. Black zones = elastic, red zones = shear failure, yellow zones = previously failed but now elastic, white zones = tensile failure.

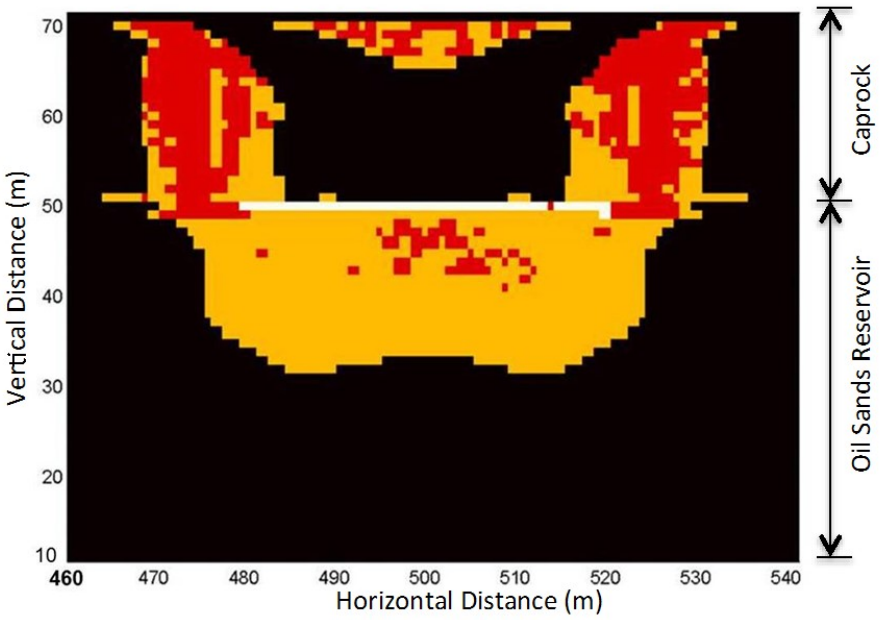

Figure 4-11 Shearing zones at 1530days. Black zones = elastic, red zones = shear failure, yellow zones = previously failed but now elastic, white zones = tensile failure.

4.2.1 Period before the Pressure Front Reaches the Caprock (0 ~ 900 days)

Initially, the steam chamber grows vertically (Figure 4-12 to Figure 4-15). As discussed in Chapter 2, the propagation of the temperature front falls behind the pressure front. According to reservoir simulations, the pressure front first reaches the base of caprock at 900 days (Figure 4-14), while the temperature front arrives at the base of caprock at 1080 days (Figure 4-15).

During this period (0 ~ 900 days), the vertical displacement at the base of caprock is relatively small. As shown in Figure 4-16, the influenced areas are from 400m to 500m in the horizontal direction (left half). The horizontal displacement is comparable to the vertical displacement in terms of magnitude. The maximum vertical displacement at the base of caprock happens right above the well-pair, while the maximum horizontal displacement shifts from the center of the model.

During this period, no shearing zones in caprock are observed.

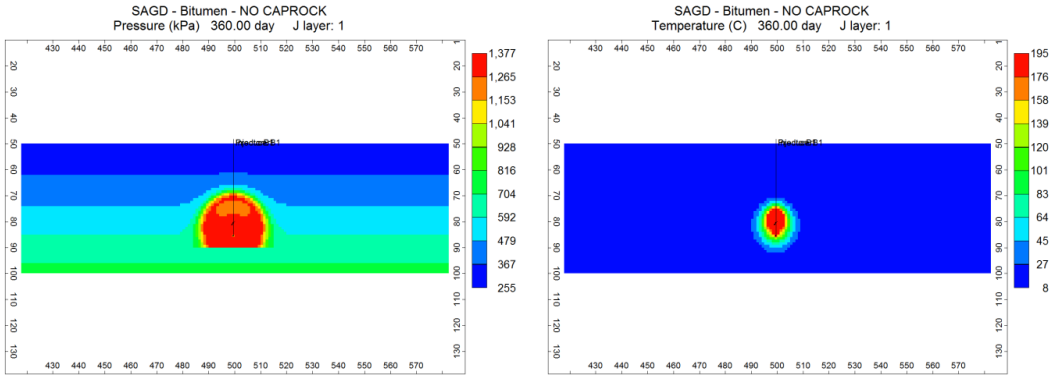

Figure 4-12 Pore pressure and temperature distributions in CMG STARS at 360 days.

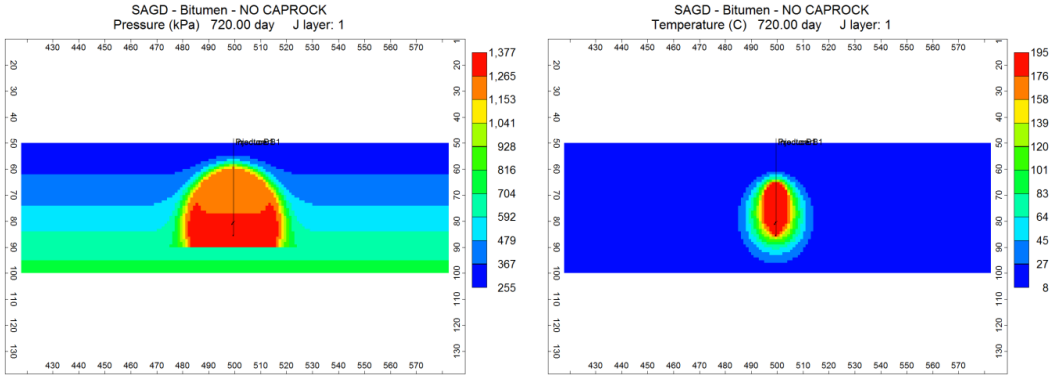

Figure 4-13 Pore pressure and temperature distributions in CMG STARS at 720 days.

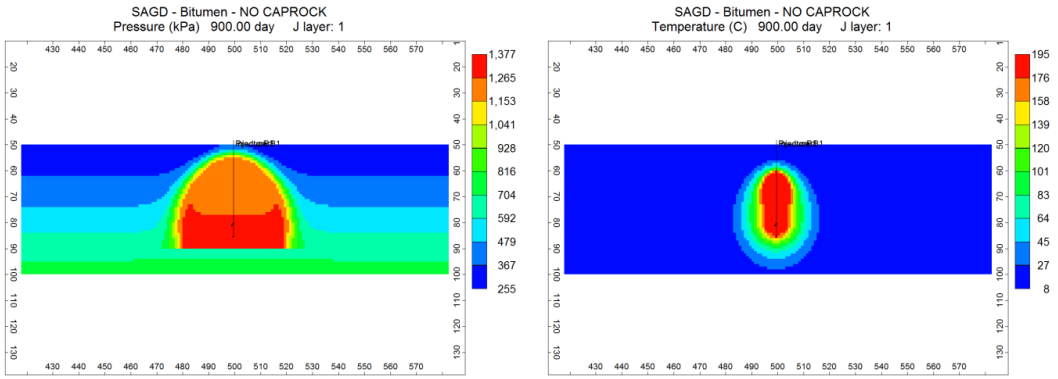

Figure 4-14 Pore pressure and temperature distributions in CMG STARS at 900 days.

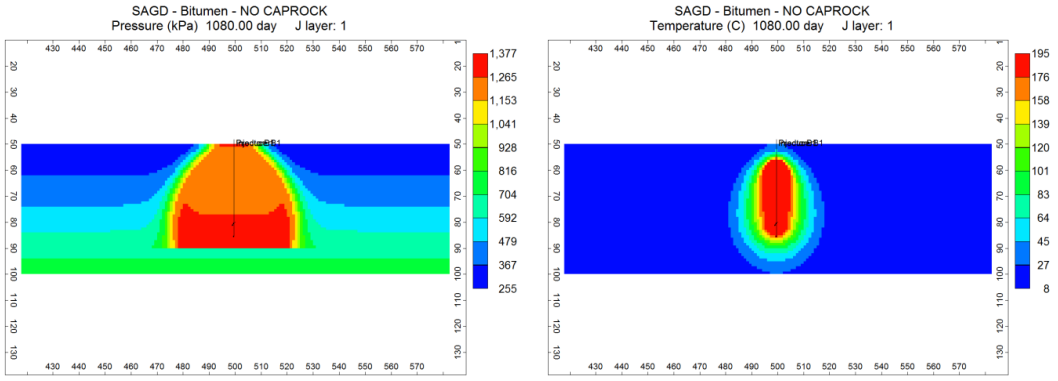

Figure 4-15 Pore pressure and temperature distributions in CMG STARS at 1080 days.

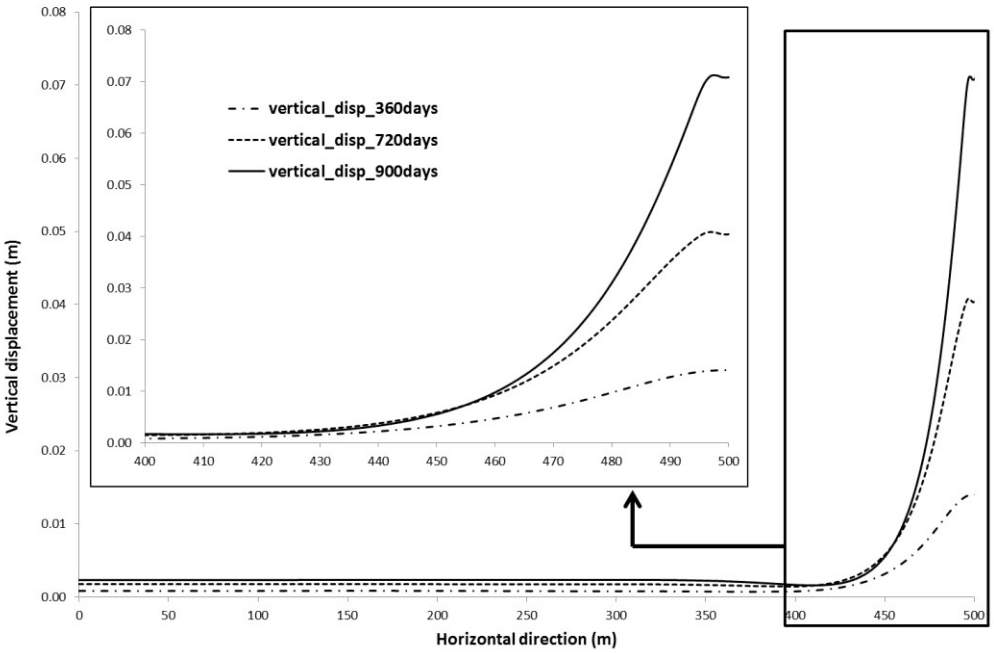

Figure 4-16 Vertical displacement at the base of caprock at 360 days, 720 days and 900 days.

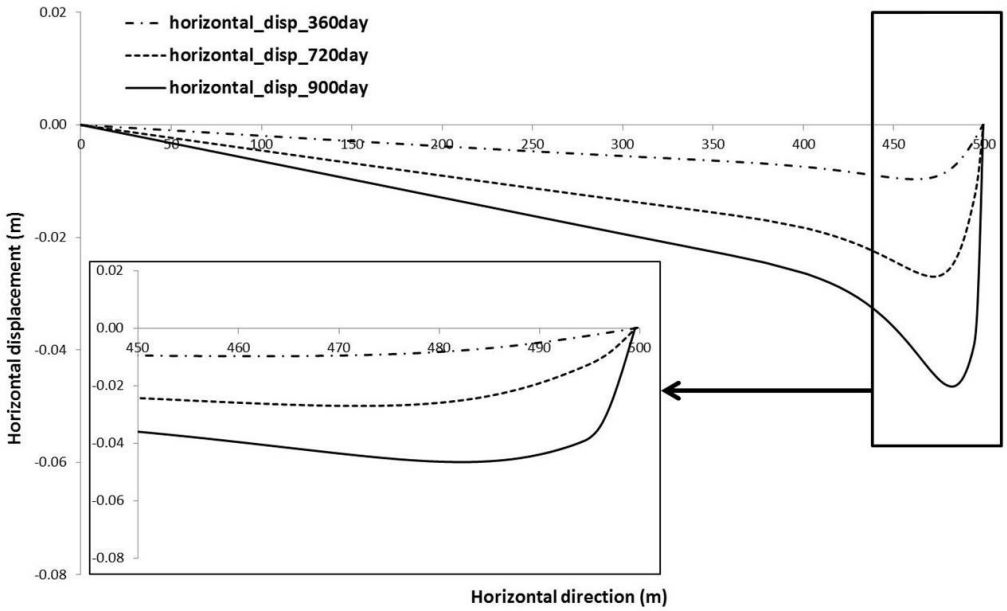

Figure 4-17 Horizontal displacement at the base of caprock at 300 days, 720 days and 900 days.

4.2.2 Transition Period after Pressure Front Reaches Caprock Base and before Temperature Front Reaches Caprock Base (900 ~ 1080 days)

The period from 900 days to 1080 days is a transition period as the pressure and temperature front do not reach the base of caprock concurrently. During this period, changes in the characteristics of vertical and horizontal displacement profiles at the base of caprock are observed. For vertical displacements, it is found that there is a large increase at 488m in the horizontal direction at 1080 days because the pressure front propagates to 488m at 1080 days (Figure 4-18). Horizontal displacements towards the well-pair are observed at areas close to the well-pair (Figure 4-19).

At 1080 days, the maximum vertical displacement is around 0.4m (Figure 4-18); while the maximum horizontal displacement is around 0.07m (Figure 4-19), which indicates that from 1080 days on, the vertical displacement will become the dominant factor to influence the caprock behaviour in terms of stress and strain alteration.

No shearing zones are observed during this period.

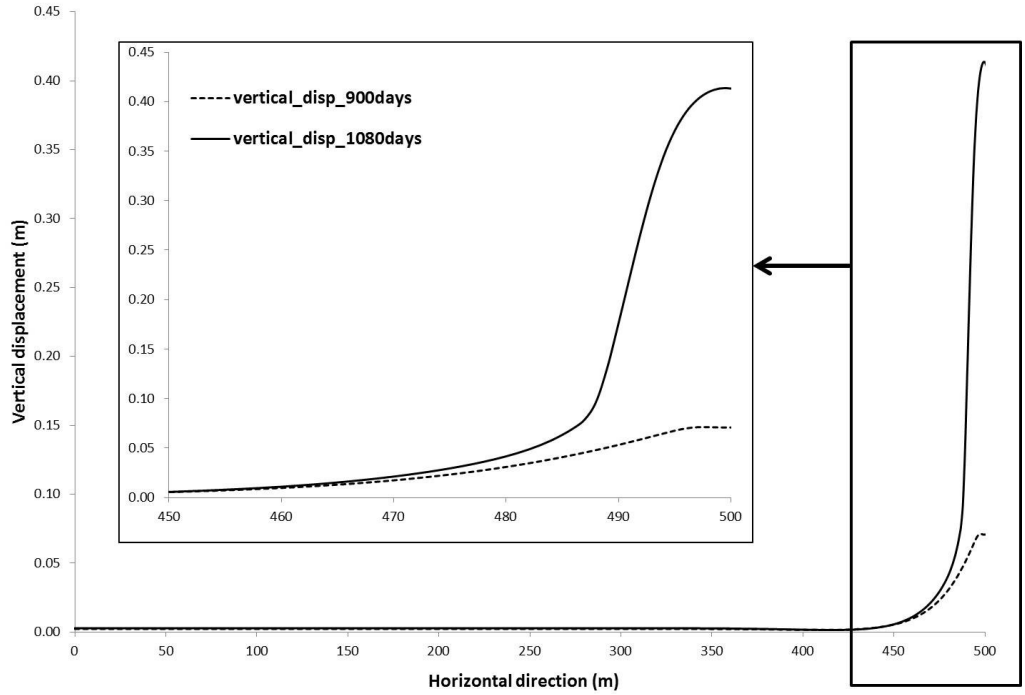

Figure 4-18 Vertical displacement at the base of caprock at 900 days and 1080 days.

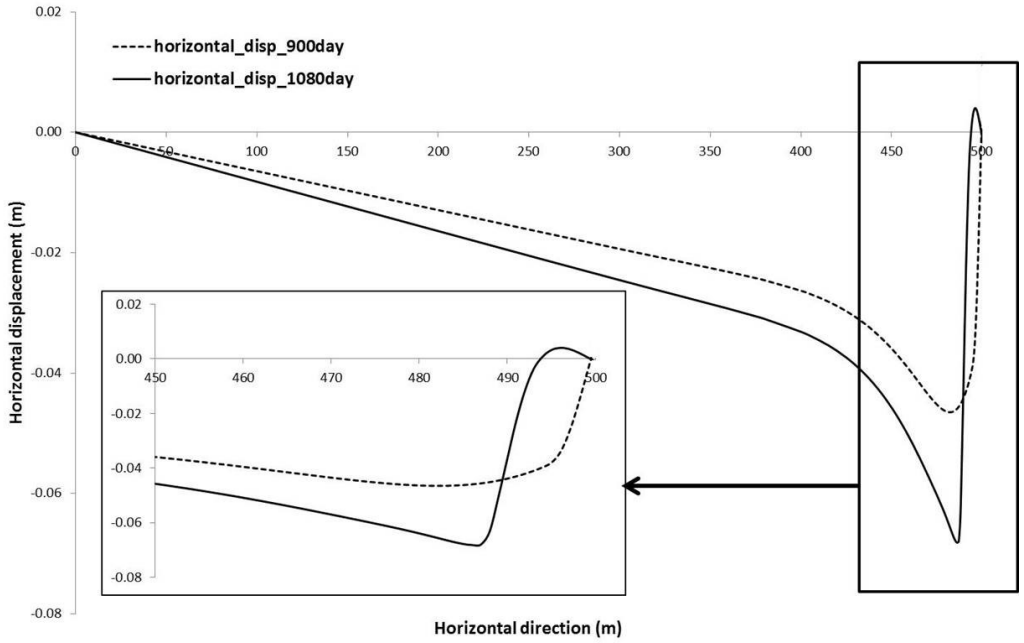

Figure 4-19 Horizontal displacement at the base of caprock at 900 days and 1080 days.

4.2.3 Lateral Spreading of Steam Chamber at the Base of Caprock until Caprock Shearing Failure (1080 ~ 1530 days)

From 1080 days on, both temperature and pressure fronts will be spreading at the base of caprock (Figure 4-20 to Figure 4-23). As shown in Figure 4-24, the vertical displacement before 900 days is negligible. After the pressure front reaches the base of caprock at 900 days, the growth rate of vertical displacement bursts up. It is important to notice that tensile failure of oilsands happens at the base of caprock as the steam injection pressure exceeds the minimum principal stress at the base of caprock. As the steam chamber spreads at the base of caprock, the oilsands tensile failure zones expand concurrently. Pore pressures building up at the base of caprock as well as oilsands reservoir expansion is the source of the large vertical displacement at the caprock base which causes the development of shearing zones in caprock starting from the edges of the oilsands tensile failure zones (Figure 4-8 to Figure 4-11). Caprock shearing failure happens when the shearing zones go through the whole caprock formation at 1530 days (Figure 4-11).

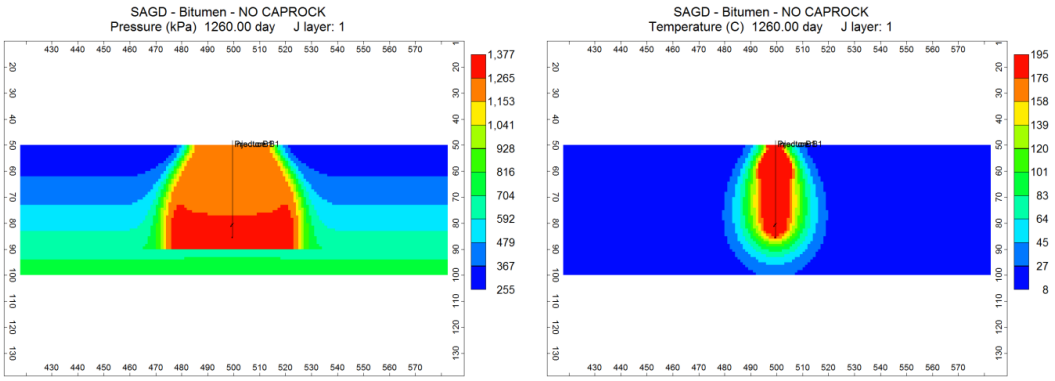

Figure 4-20 Pore pressure and temperature distributions in CMG STARS at 1260 days.

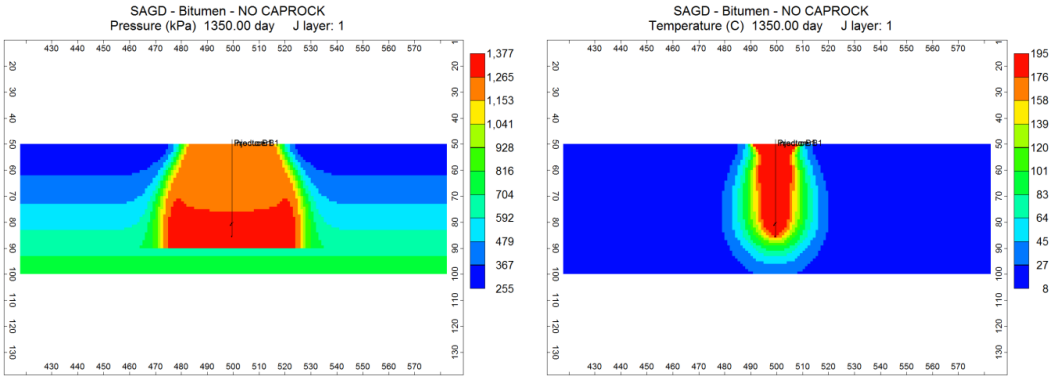

Figure 4-21 Pore pressure and temperature distributions in CMG STARS at 1350 days.

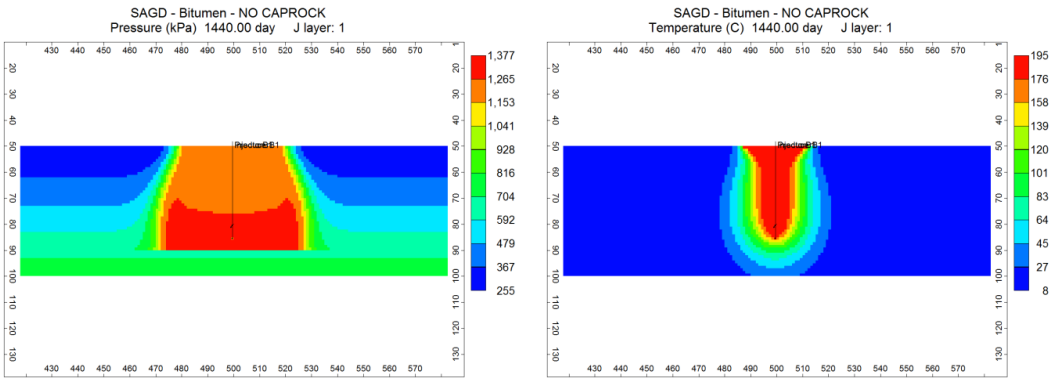

Figure 4-22 Pore pressure and temperature distributions in CMG STARS at 1440 days.

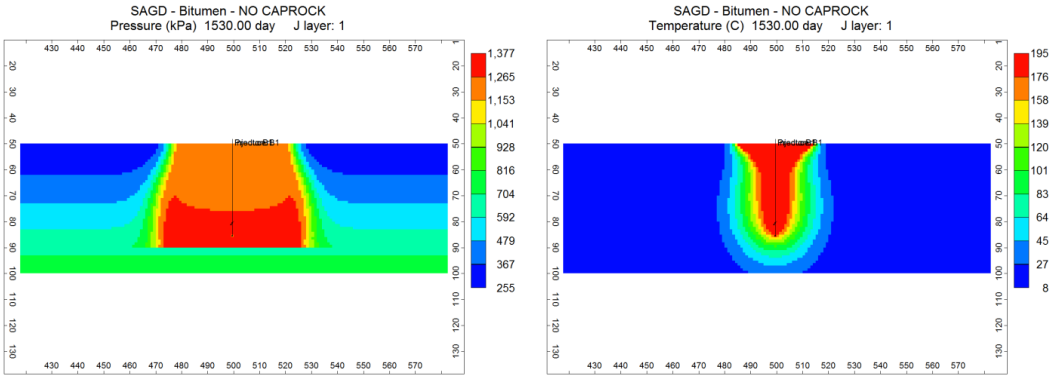

Figure 4-23 Pore pressure and temperature distributions in CMG STARS at 1530 days.

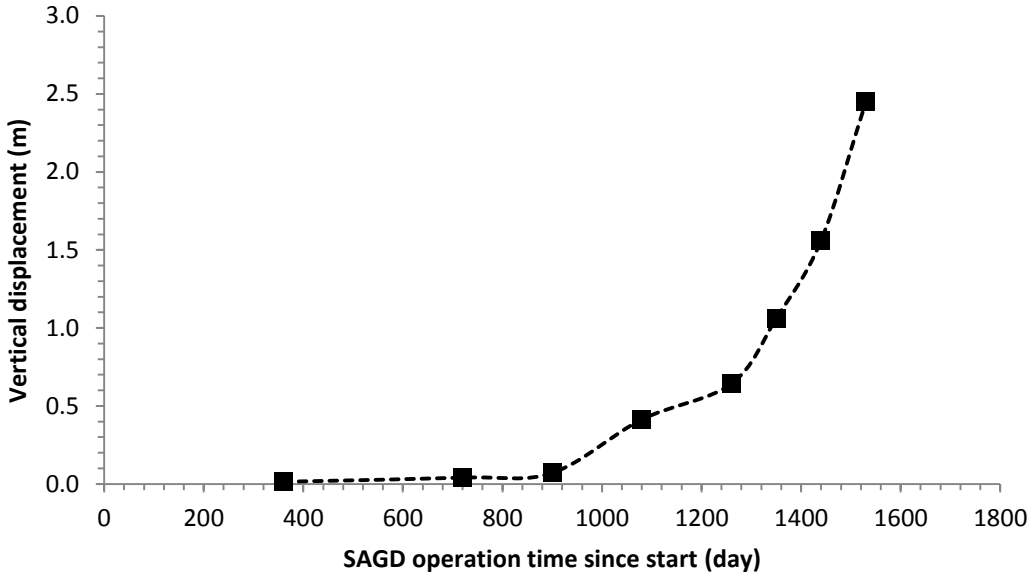

Figure 4-24 Maximum vertical displacement at the base of caprock during SAGD process.

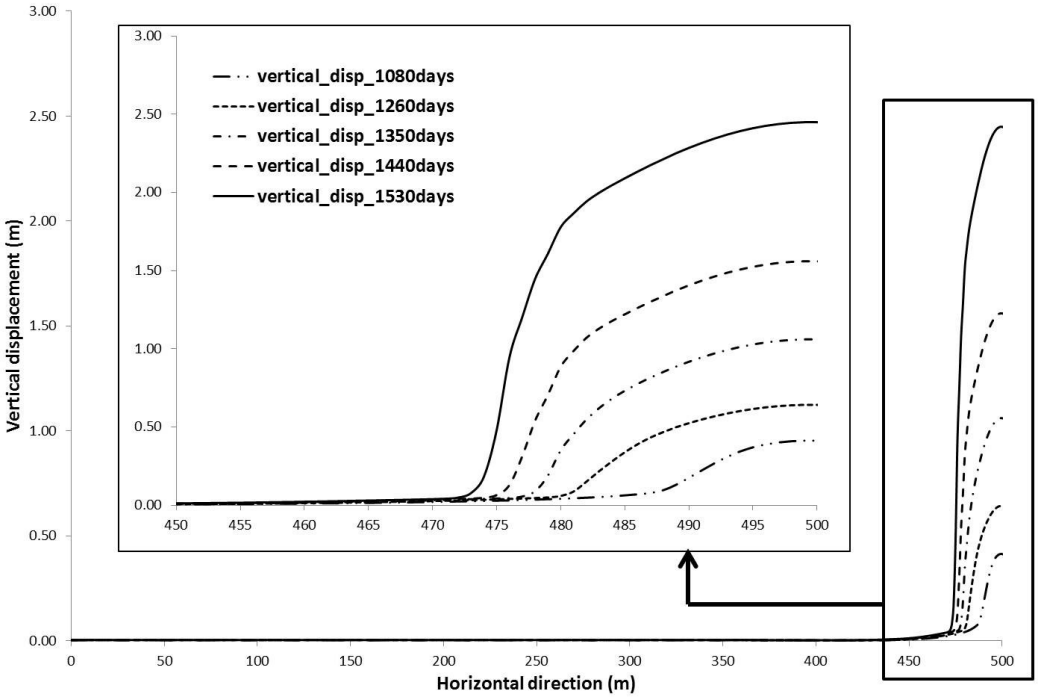

Figure 4-25 Vertical displacement at the base of caprock at 1080 days, 1260days, 1350 days, 1440 days, and 1530 days.

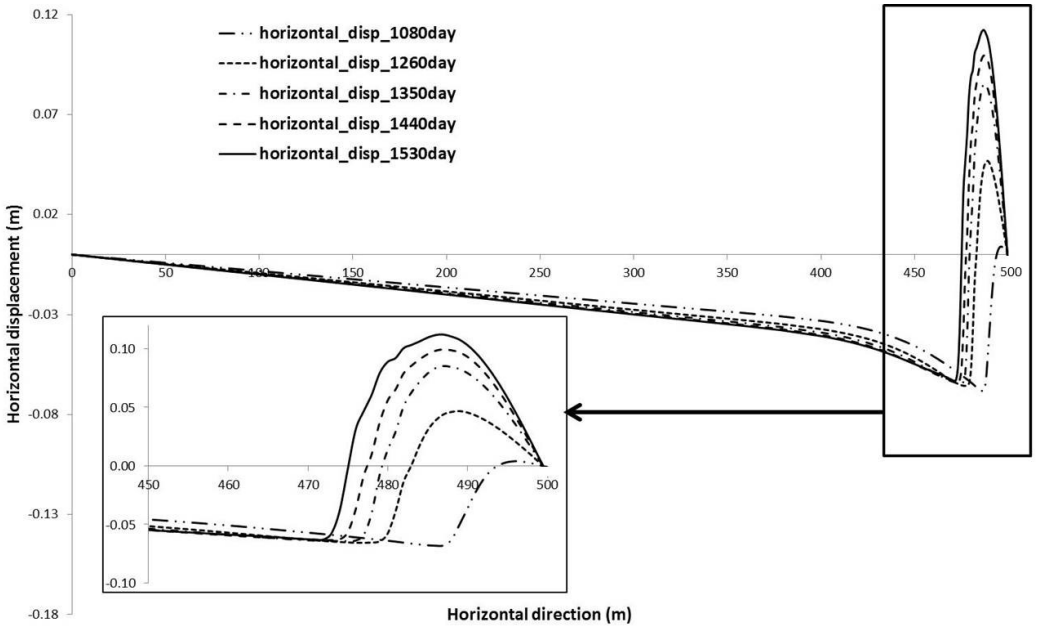

Figure 4-26 Horizontal displacement at the base of caprock at 1080 days, 1260days, 1350 days, 1440 days, and 1530 days.

4.3 Parametric Analysis

There are significant differences in geomechanical properties between caprock shale and overconsolidated Speswhite kaolin used in the centrifuge models in terms of material stiffness, strength and dilation behaviour after shearing. The caprock shale has much larger strength and stiffness compared to those of the overconsolidated Speswhite kaolin. Also, the caprock shale has a strong dilative behaviour after failure, while the overconsolidated Speswhite kaolin demonstrates a contractive behaviour after failure. A parametric analysis is necessary to study the influences of stiffness, strength and dilation on caprock behaviour during SAGD process. For each case, only one parameter is changed with other parameters remaining the same as shown in Table 4-3.

Table 4-3 Geomechanical parameters for caprock in each case of the parametric analysis.

	Bulk Modulus (MPa)	Shear Modulus (MPa)	Friction Angle (°)	Cohesion (kPa)	Dilation Angle (°)	Tension (kPa)
Reference Case	15.6	5.2	17	0	0	0
Case 1-1	***78***	***26***	17	0	0	0
Case 1-2	***156***	***52***	17	0	0	0
Case 2-1	15.6	5.2	17	0	***10***	0
Case 2-2	15.6	5.2	17	0	***20***	0
Case 3-1	15.6	5.2	***25***	0	0	0
Case 3-2	15.6	5.2	***35***	0	0	0

4.3.1 Influences of Stiffness

Case 1-1 and Case 1-2 have bulk modulus and shear modulus of 5 times and 10 times of those in the Reference Case respectively. Stiffness is an important element of material properties as it reflects the relations between stress change and strain change. The stiffer the material, the higher the stress is required to generate the same strain change in material and vice versa.

For SAGD operations, there are limited vertical constraints on caprock deformation and the horizontal deformation is greatly constrained by the continuity of the caprock formation. Since the material stiffness increases while material strength remains the same, less deformation is required to generate the stress conditions leading to the caprock shearing failure. For Case 1-1 and Case 1-2, caprock shearing failure both happens at 1440 days while for the Reference Case, it happens at 1530 days.

Same as in the Reference Case, vertical displacement at the base of caprock is the dominant force causing caprock shearing failure in Case 1-1 and Case 1-2. As the stiffness increases, the maximum vertical displacement at caprock shearing failure decreases (Figure 4-28). However, the shape and characteristics of the vertical displacement profile are the same for Case 1-1, Case 1-2 and the Reference Case. The patterns of the caprock shearing failure are almost the same as shown in Figure 4-27.

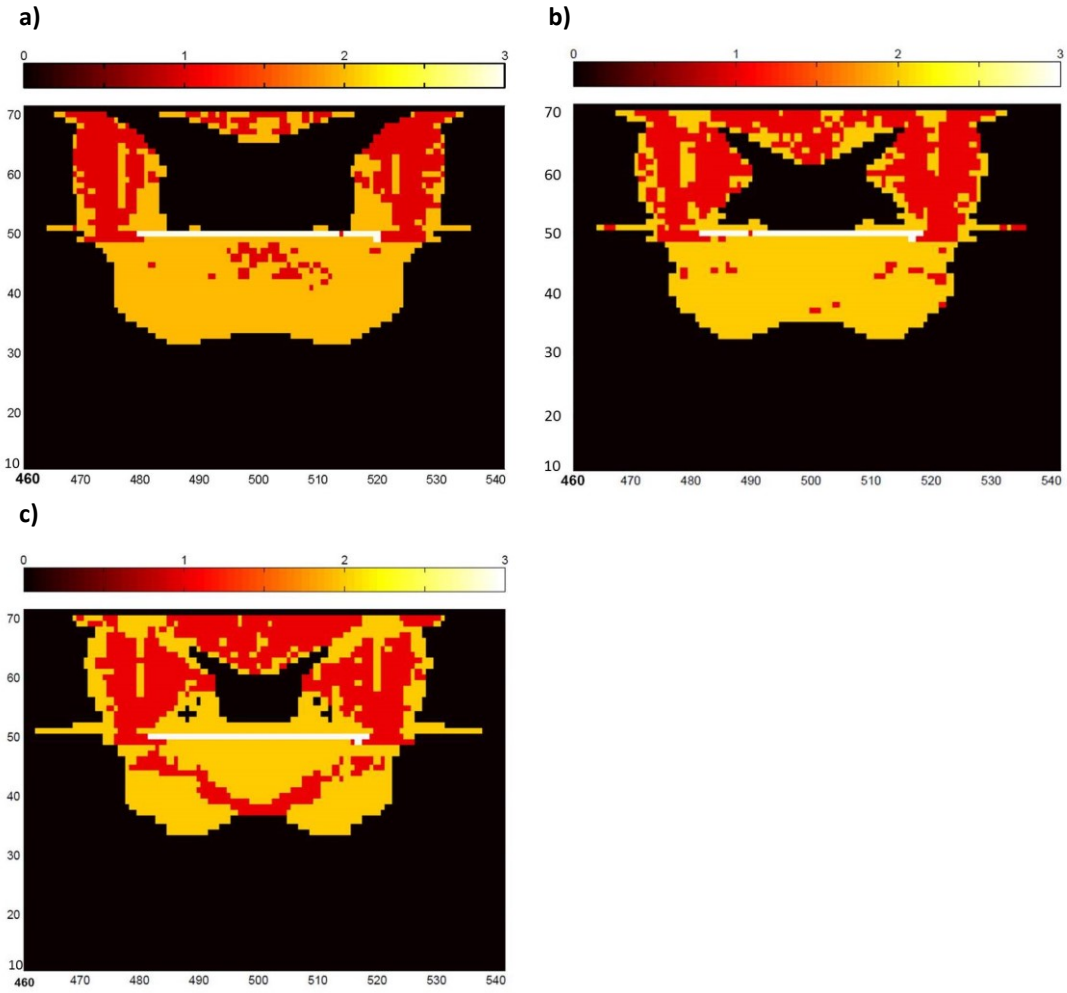

Figure 4-27 Patterns of caprock shearing failure for a) Reference Case b) Case 1-1 c) Case 1-2 (unit in m).

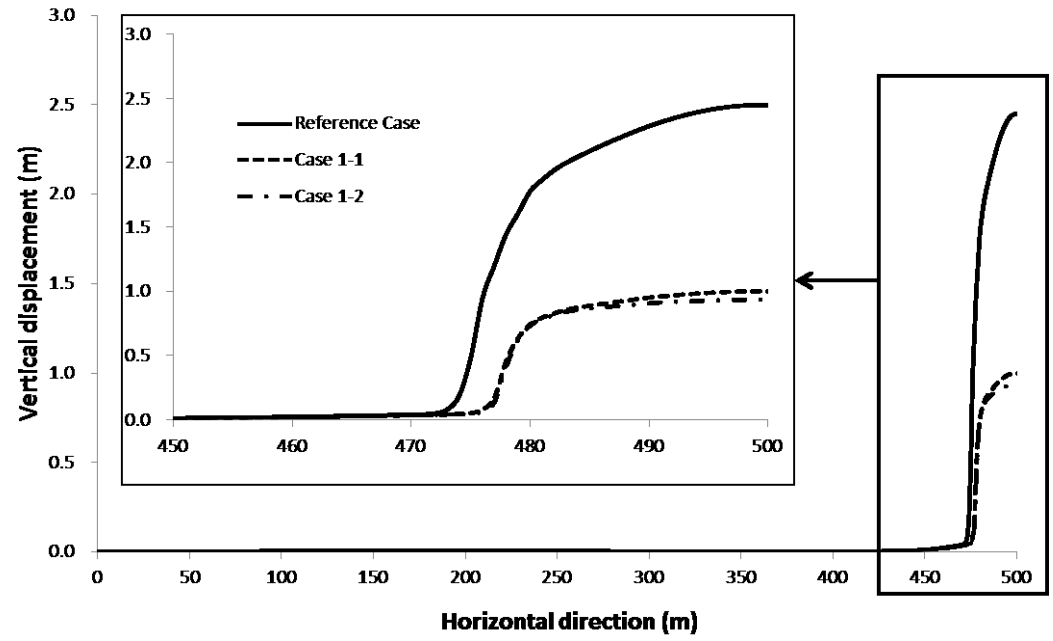

Figure 4-28 Vertical displacement at the base of caprock for Case 1-1 and Case 1-2 and the Reference Case.

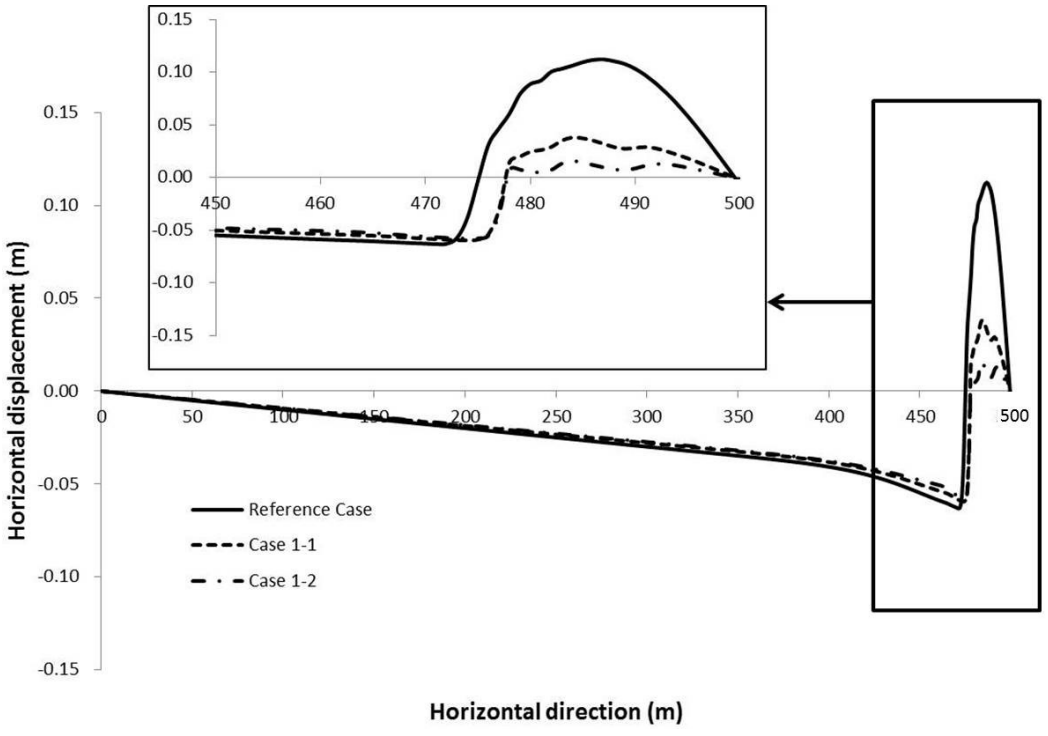

Figure 4-29 Horizontal displacement at the base of caprock for Case 1-1 and Case 1-2 and the Reference Case.

4.3.2 Influences of Dilation

For Case 2-1 and Case 2-2, dilation angles of 10 and 20 degrees are assigned to the caprock respectively. The dilation angle reflects the volume increase of material after shearing failure. Thus, the caprock in Case 2-1 and Case 2-2 has the same behaviours as those in the reference case before the shearing zones start developing.

Caprock shearing failure happens at the same time of 1530 days for the Reference Case, Case 2-1 and Case 2-2. According to Figure 4-30, the dilation angle has minor influences on the patterns of the caprock shearing failure. It could observed from Figure 4-30 that as the dilation angle increases, the shearing zones tend to grow more outward in the horizontal direction. This phenomenon might be caused by the horizontal constraints of the formation. There is limited vertical displacement constraints, thus the caprock dilation after failure will not generate much increase in vertical stress. However, the caprock dilation after failure in the horizontal direction will encounter large resistance; therefore, there would be large increase in the horizontal stress which in turn help further development of the shearing zones horizontally.

The vertical displacement at the base of caprock is the dominant factor which causes the caprock shearing failure in Case 2-1 and Case 2-2. As the dilation angle increases, the vertical displacement decreases (Figure 4-31). This is because that the volume increase of caprock material after shearing will help the development of the shearing zones in caprock and thus at caprock shearing failure, less vertical displacement is required.

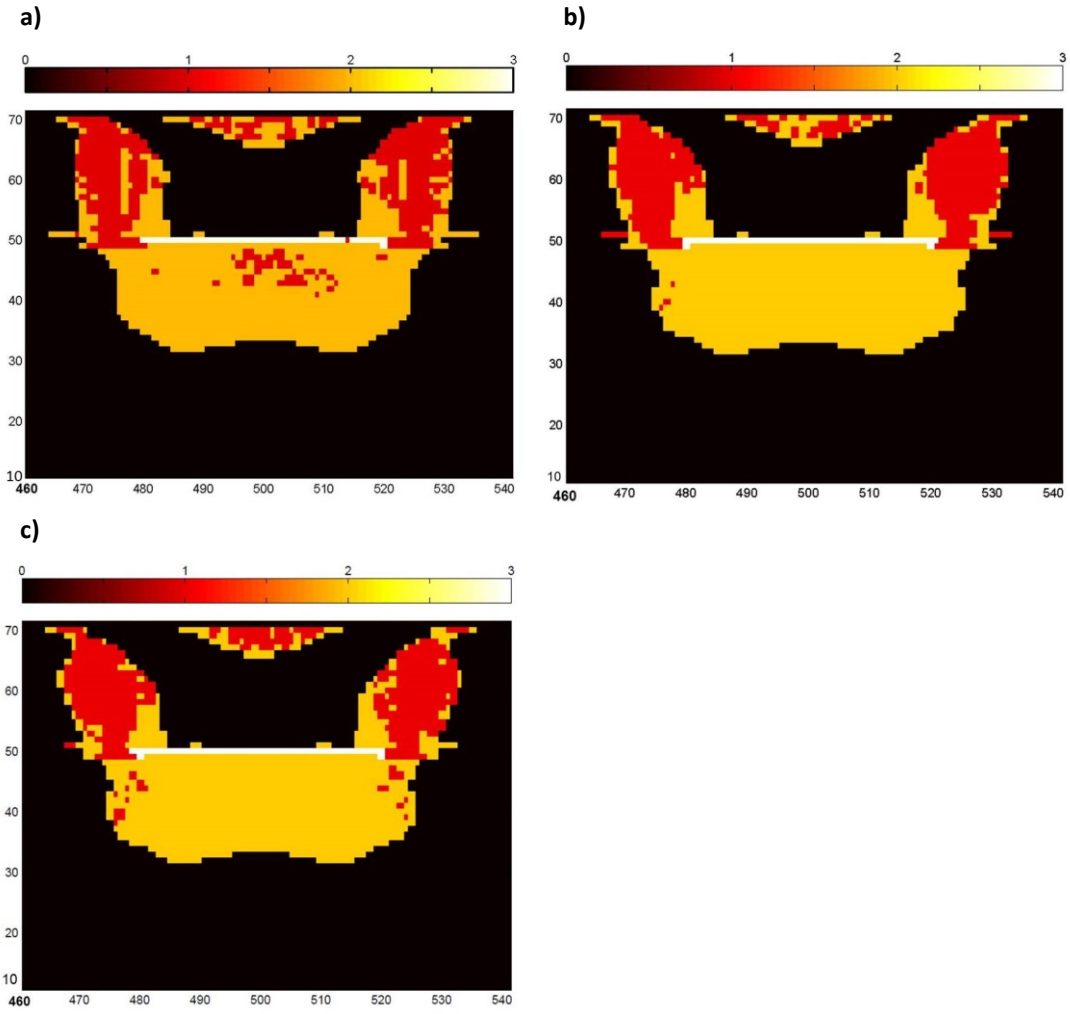

Figure 4-30 Patterns of caprock shearing failure for a) Reference Case b) Case 2-1 c) Case 2-2 (unit in m).

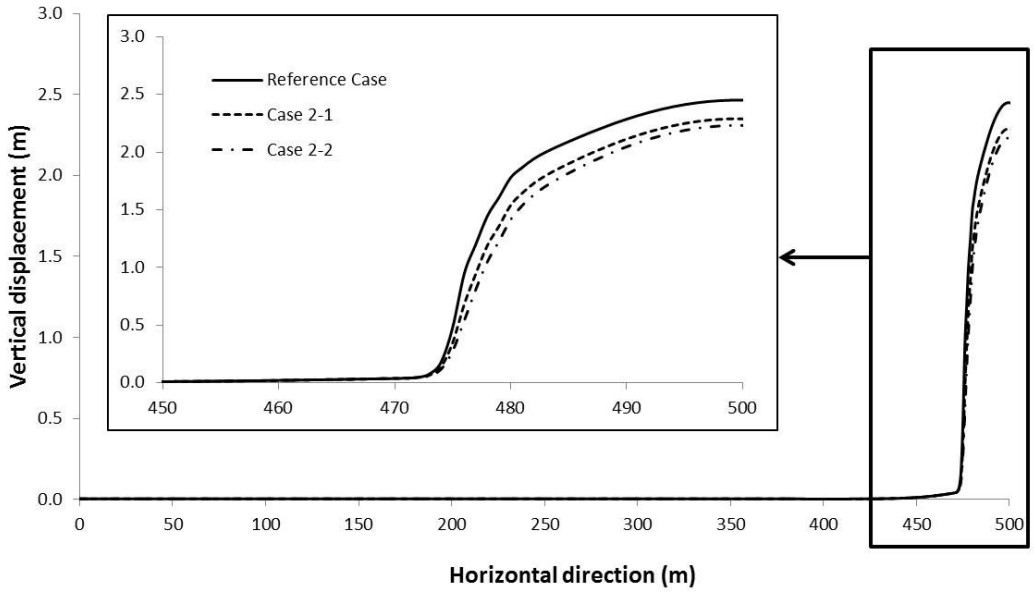

Figure 4-31 Vertical displacement at the base of caprock at caprock shearing failure.

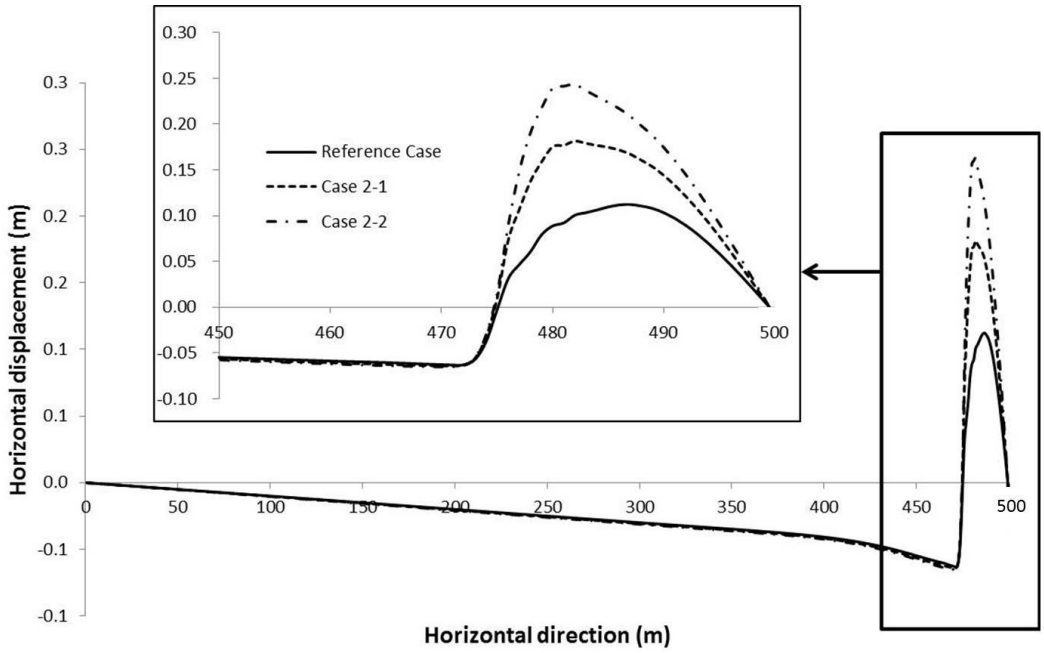

Figure 4-32 Horizontal displacement at the base of caprock at caprock shearing failure.

4.3.3 Influences of Friction Angle

Comparing the Reference Case, Case 3-1, and Case 3-2, caprock shearing failure happens at 1530 days, 1980 days, and 2340 days respectively. As expected, the higher the friction

angle, the longer it takes to fail the caprock. Therefore, when caprock shearing failure happens, the shearing zones will have a larger bottom span (Figure 4-33 and Figure 4-34). Also, it takes more vertical displacement to reach the caprock shearing failure as the material stiffness is same but the friction angle is higher (Figure 4-35).

Comparing the patterns of caprock shearing failure for all three cases, they are almost the same besides the bottom span as the longer it takes to fail the caprock, the wider the steam chamber will be spreading at the base of caprock.

Similarly, vertical displacement at the base of caprock is the driving force which leads to caprock shearing failure. Comparing the vertical displacement profiles at the base of caprock for all three cases, they all have the same characteristics. The major differences are the maximum vertical displacements as well as the span of the displacement profiles.

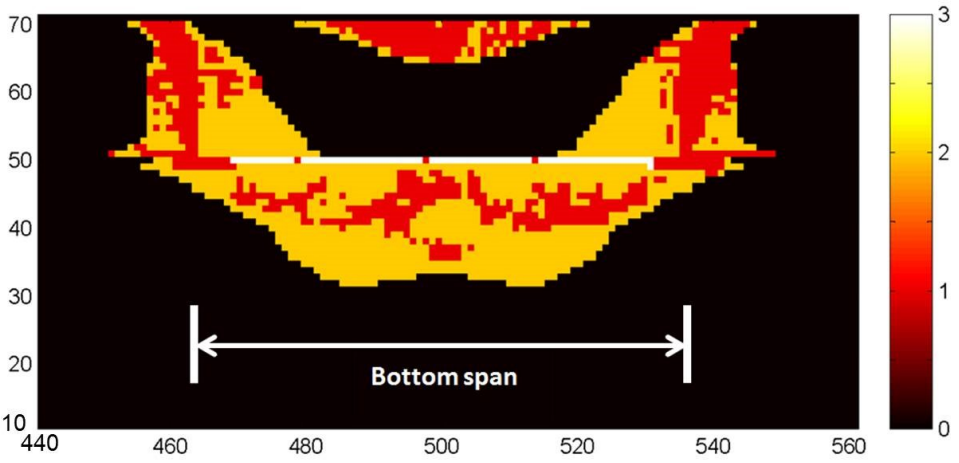

Figure 4-33 Patterns of caprock shearing failure for Case 3-1 (unit in m).

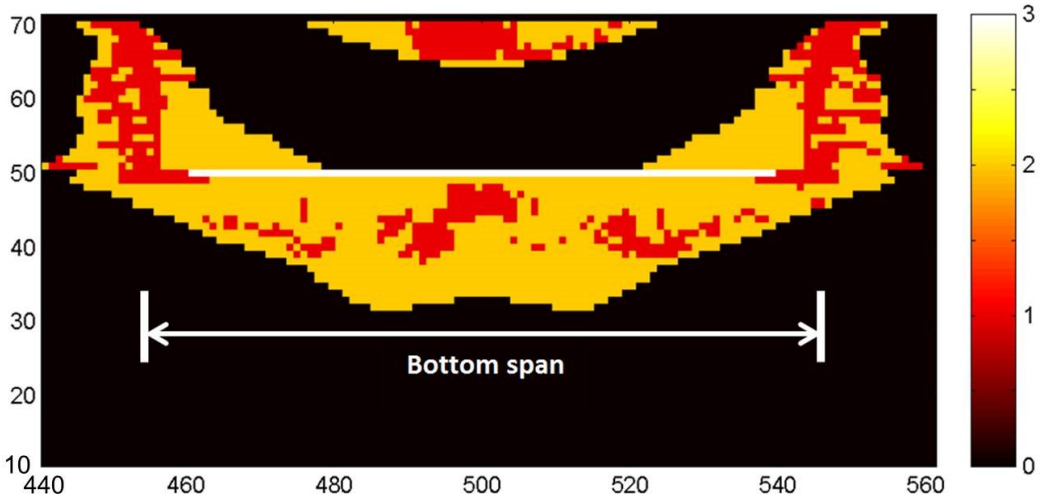

Figure 4-34 Patterns of caprock shearing failure for Case 3-2 (unit in m).

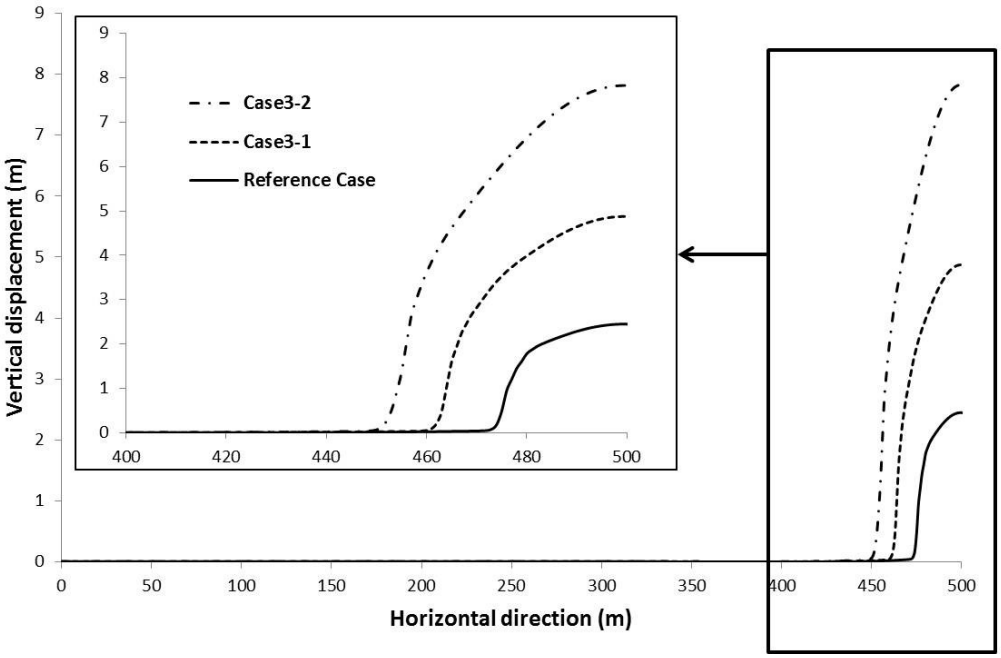

Figure 4-35 Vertical displacements at the base of caprock at caprock shearing failure for Case 3-1, Case 3-2 and Reference Case.

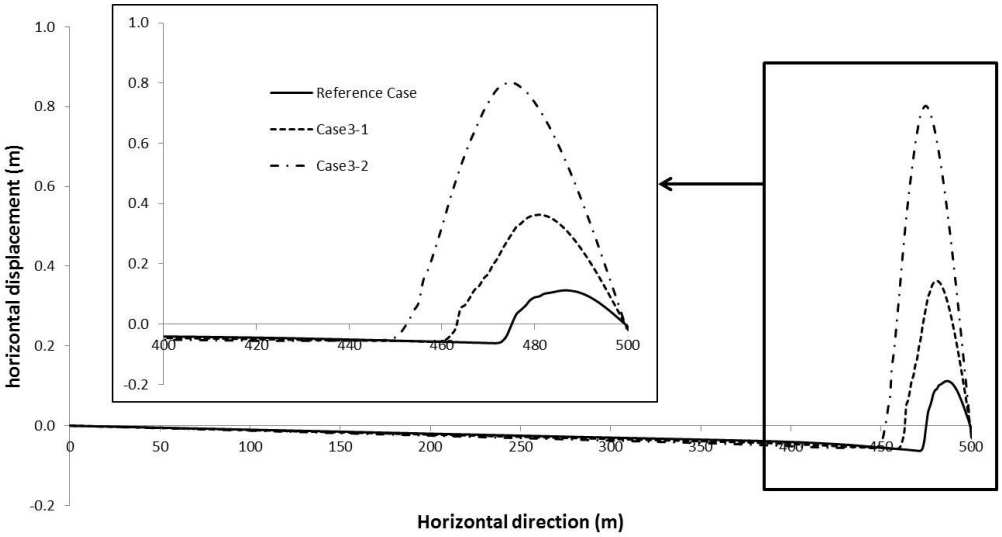

Figure 4-36 Horizontal displacements at the base of caprock at caprock shearing failure for Case 3-1, Case 3-2 and Reference Case.

4.4 Feasibility Study of Centrifuge Modeling of Caprock Integrity

There is no simple way of fully applying the displacement profile from the reservoir geomechanical simulations at the base of caprock in centrifuge models. Alternatively, a simplified displacement profile should be figured out to fulfill the following requirements: **1)** containable in the plane-strain box **2)** executable at 100g centrifuge spinning **3)** can generate similar stress and strain fields in the caprock comparing to those in the prototype.

4.4.1 Polyline Simplified Displacement

In geomechanical simulations, oilsands reservoir is the source of deformation at the base of caprock. Theoretically, if the displacements at the base of caprock are fully simulated, the caprock should have the same behaviors as those in reservoir geomechanical simulations.

As shown in Figure 4-37, the horizontal to vertical displacement ratio is close to zero in the main displacement areas. So it is also necessary to verify the dominant role of vertical

displacement in failing the caprock. Thus two geomechanical simulation cases are run: one with both polyline simplified vertical displacement (PSVD) and polyline simplified horizontal displacement (PSHD); the other one with only the polyline simplified vertical displacement (PSVD). The results of displacement vectors, stress contours and patterns of caprock shearing failure in the caprock formation from these two cases are compared to those from reservoir geomechanical simulations.

In physical models, polyline simplified displacements are easier to exert than the smooth displacements generated by oilsands reservoir expansion. As shown in Figure 4-38 and Figure 4-39, dashed polyline simplified vertical and horizontal displacements as close as possible to the actual displacements are plotted. In a separate geomechanical simulation using FLAC, only the caprock and overburden are included with the polyline simplified displacements applied at the base of caprock. The caprock formation in this FLAC analysis is from 0 to 20m in elevation.

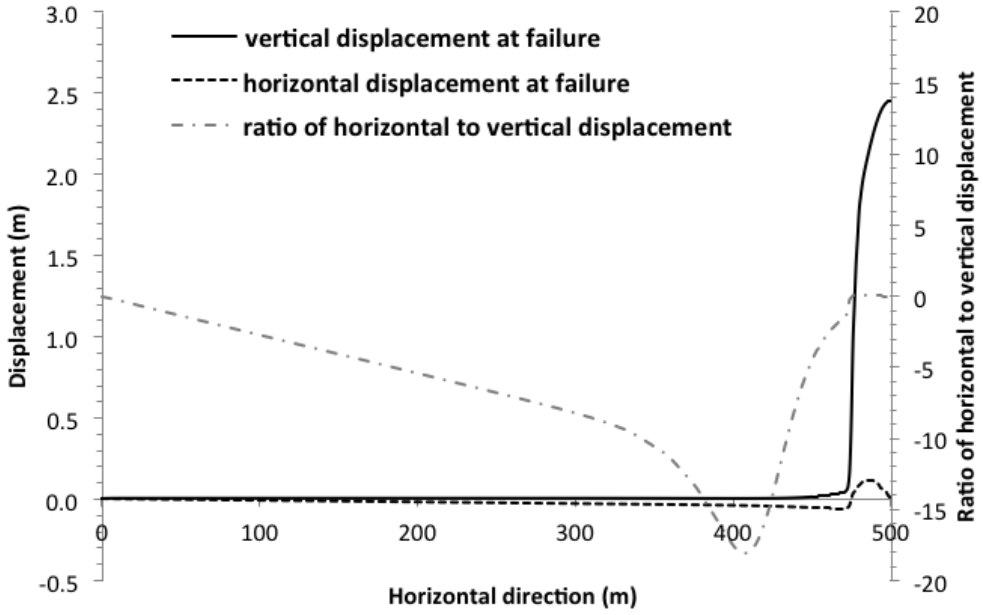

Figure 4-37 Vertical and horizontal displacements at the base of caprock at caprock shearing failure in the Reference Case.

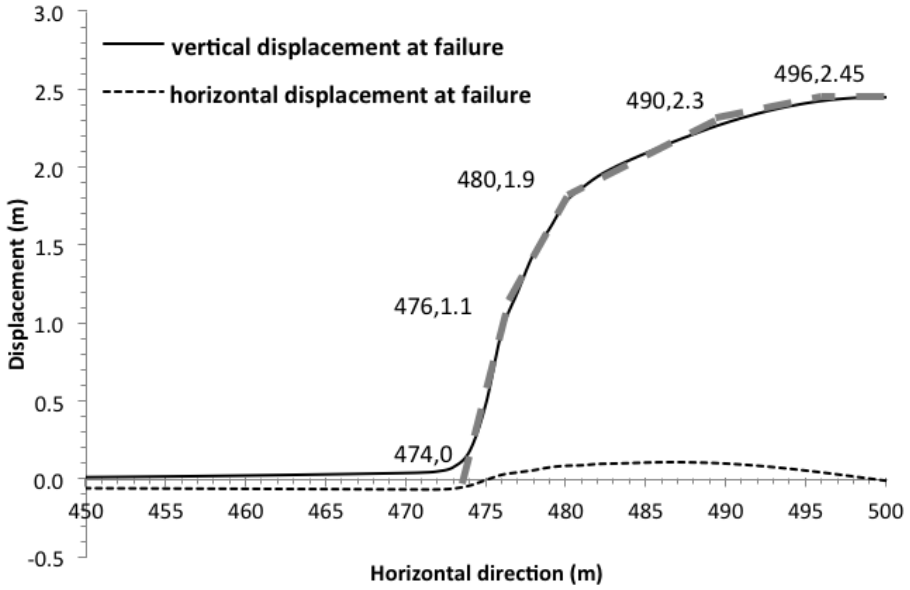

Figure 4-38 Polyline simplified vertical displacement.

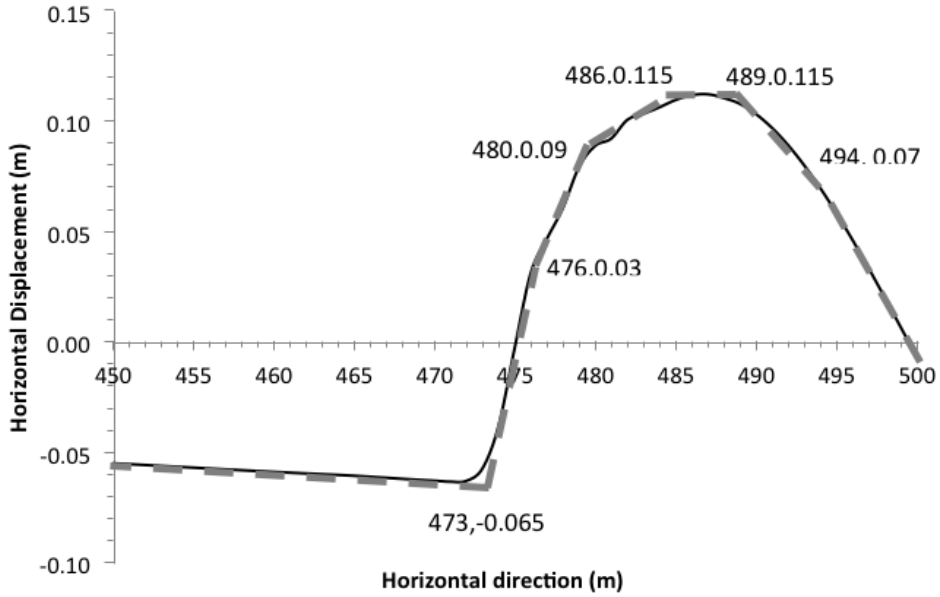

Figure 4-39 Polyline simplified horizontal displacement (from 0 m to 473m, the horizontal displacement changes linearly from 0m to -0.065m, which is not demonstrated in this figure for the purpose of clearly illustrating the horizontal displacement from 473m to 500m).

1) Displacement vectors

Comparing Figure 4-40a, and Figure 4-40b, the displacement vectors are almost the same. However, for FLAC simulation with only PSVD, at areas of 450m to 470m and 530m to 550m in the horizontal direction, there are some displacement vectors towards the center

of the simulation (Figure 4-40c). This happens because that material close to the major uplifting areas is stretched.

a) Displacement vectors in reservoir-geomechanical analysis

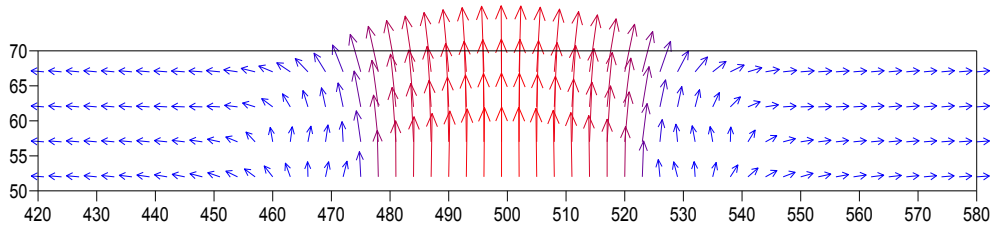

b) Displacement vectors in FLAC analysis with both PSVD and PSHD

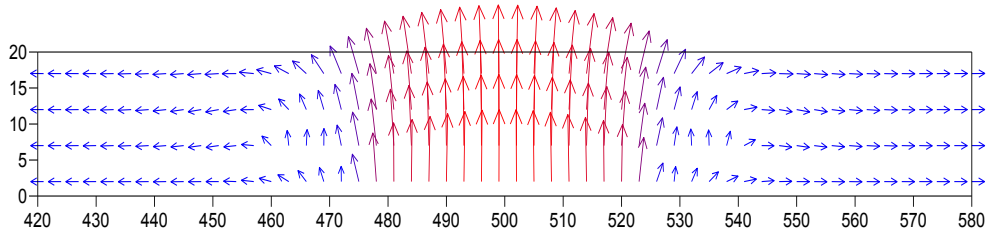

c) Displacement vectors in FLAC analysis with ONLY PSVD

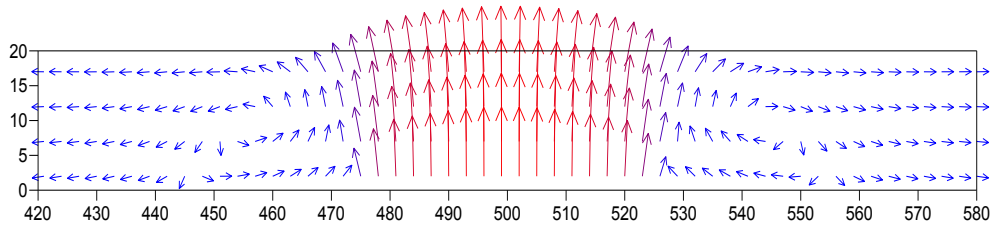

Figure 4-40 Displacement vectors in a) reservoir-geomechanical analysis, b) FLAC analysis with both PSVD & PSHD, and c) FLAC analysis with only PSHD (unit in m).

2) Stress contours

All horizontal stress, vertical stress and shear stress contours are plotted. The stress contours from the FLAC analysis are fairly comparable to the stress contours from reservoir geomechanical simulations in terms of both magnitudes and trends. From 480m to 520m in the horizontal direction at the base of caprock, there is stress concentration observed. These stress concentration points correspond to the turning points of the polyline simplified displacement profile.

a) Horizontal stress contours in reservoir-geomechanical analysis (kPa)

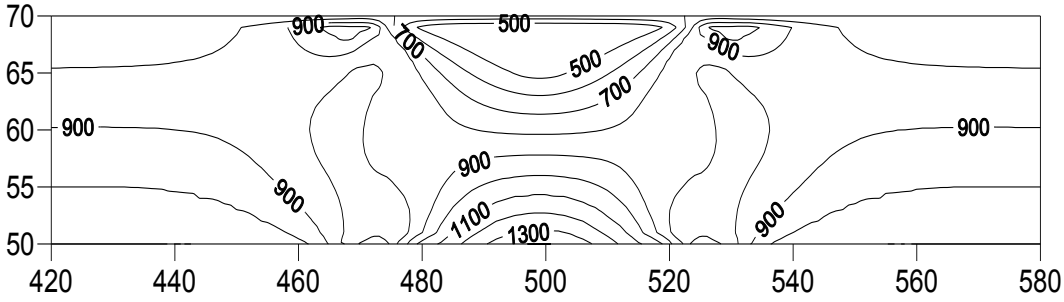

b) Horizontal stress contours in FLAC analysis with both PSVD and PSHD (kPa)

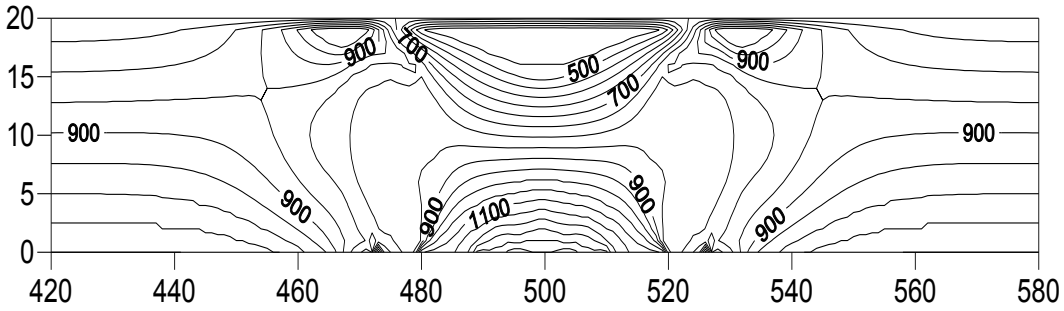

c) Horizontal stress contours in FLAC analysis with ONLY PSVD (kPa)

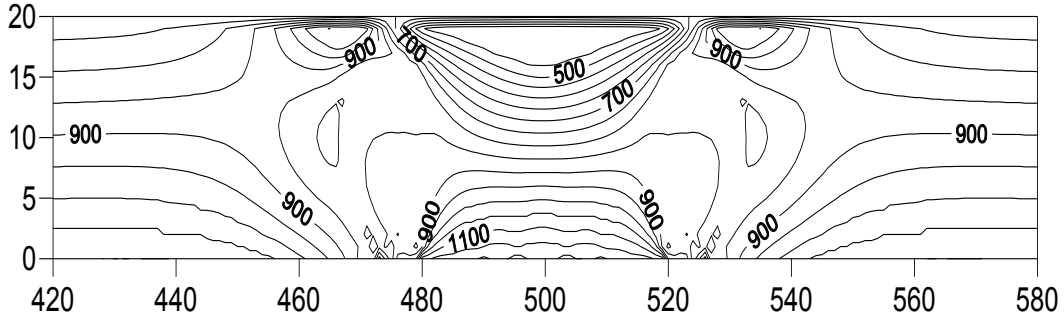

Figure 4-41 Horizontal stress contours in a) reservoir-geomechanical analysis, b) FLAC analysis with both PSVD & PSHD, and c) FLAC analysis with only PSHD (unit in m).

a) Vertical stress contours in reservoir-geomechanical analysis (kPa)

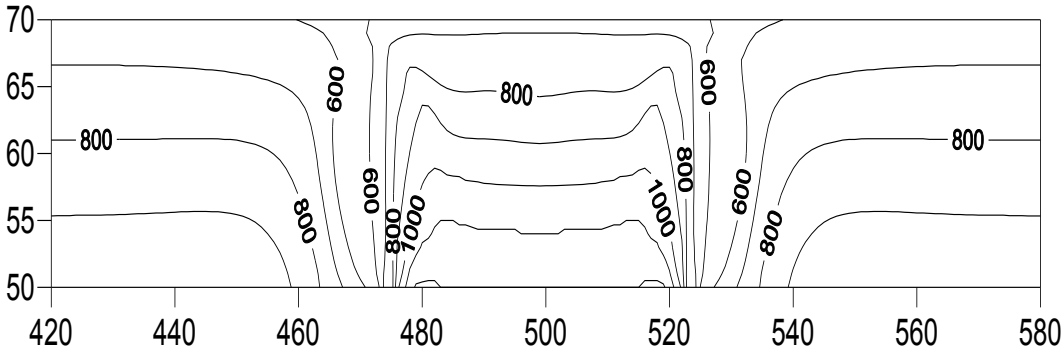

b) Vertical stress contours in FLAC analysis with both PSVD and PSHD (kPa)

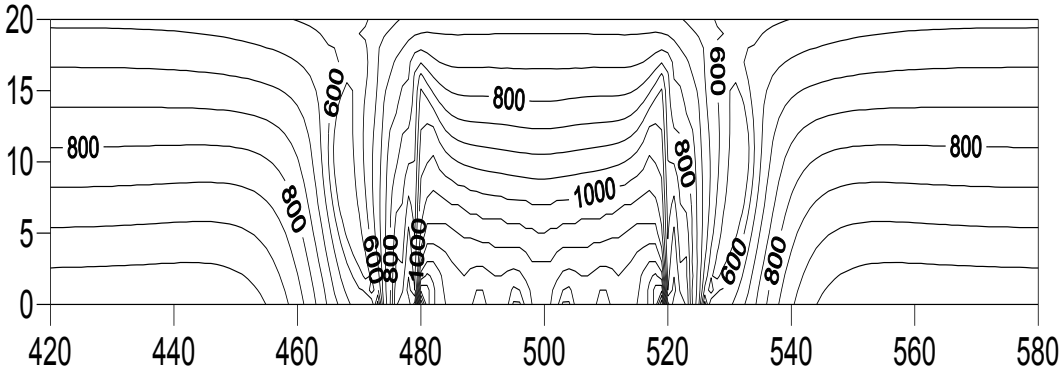

c) Vertical stress contours in FLAC analysis with ONLY PSVD (kPa)

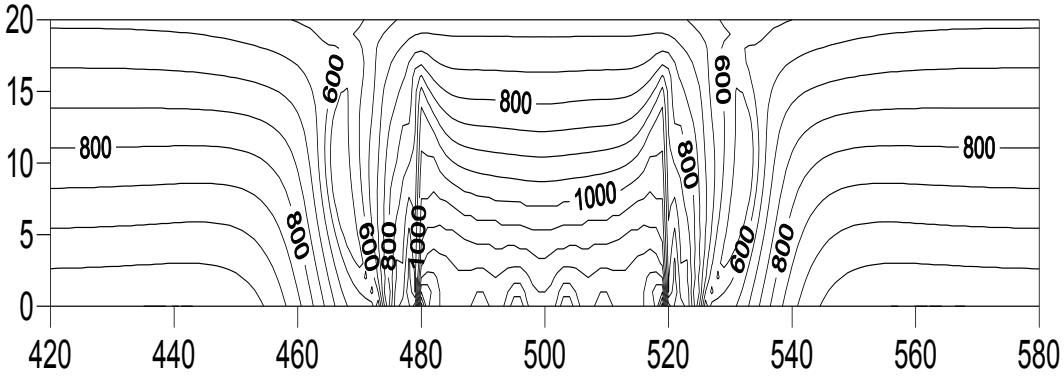

Figure 4-42 Vertical stress contours in a) reservoir-geomechanical analysis, b) FLAC analysis with both PSVD & PSHD, and c) FLAC analysis with only PSHD (unit in m).

a) Shear stress contours in reservoir-geomechanical analysis (kPa)

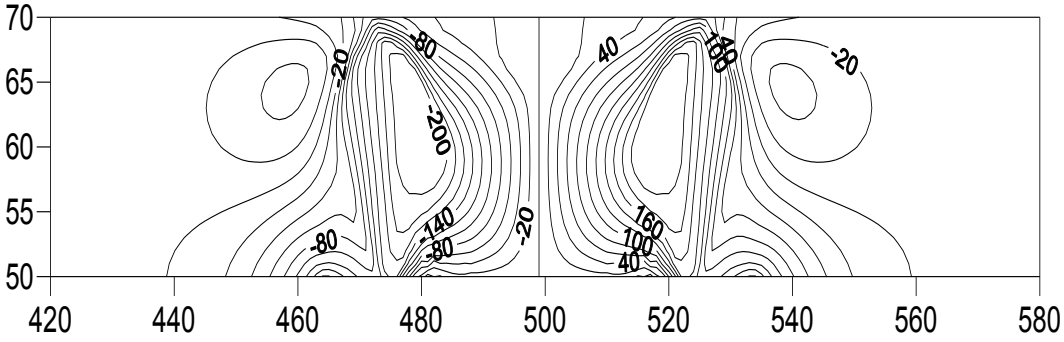

b) Shear stress contours in FLAC analysis with both PSVD and PSHD (kPa)

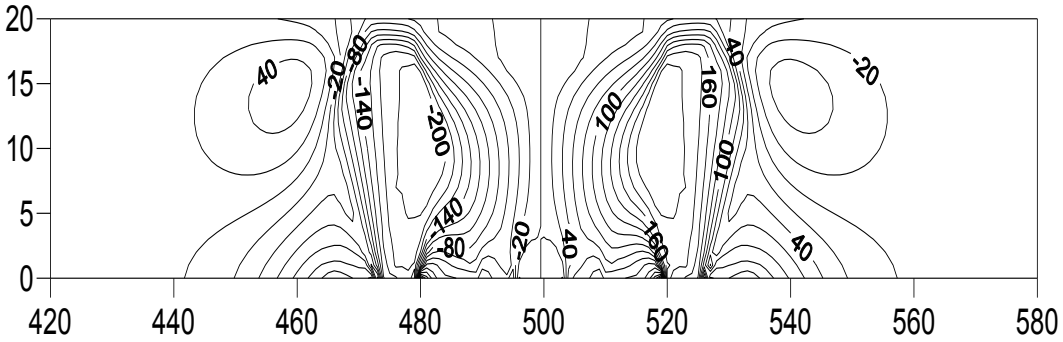

c) Shear stress contours in FLAC analysis with ONLY PSVD (kPa)

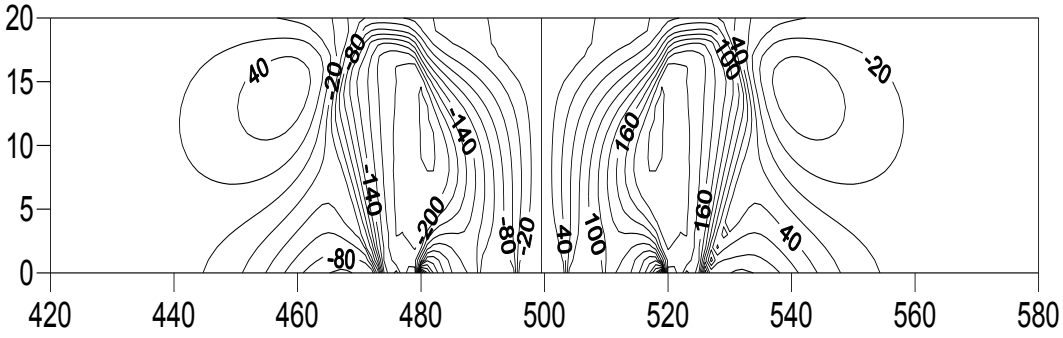

Figure 4-43 Shear stress contours in a) reservoir-geomechanical analysis, b) FLAC analysis with both PSVD & PSHD, and c) FLAC analysis with only PSHD (unit in m).

3) Patterns of caprock shearing failure

According to Figure 4-44, both the FLAC simulations with PSVD & PSHD and only PSVD have similar patterns of caprock shearing failure comparing to those in the reservoir- geomechanical simulation.

a) Patterns of caprock shearing failure in reservoir-geomechanical analysis

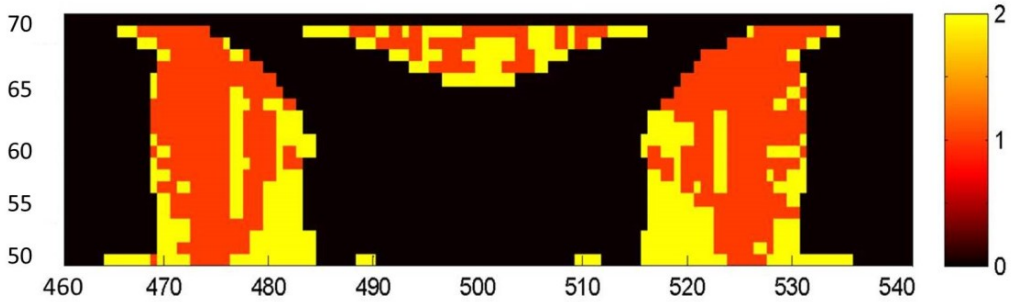

b) Patterns of caprock shearing failure in FLAC analysis with both PSVD & PSHD

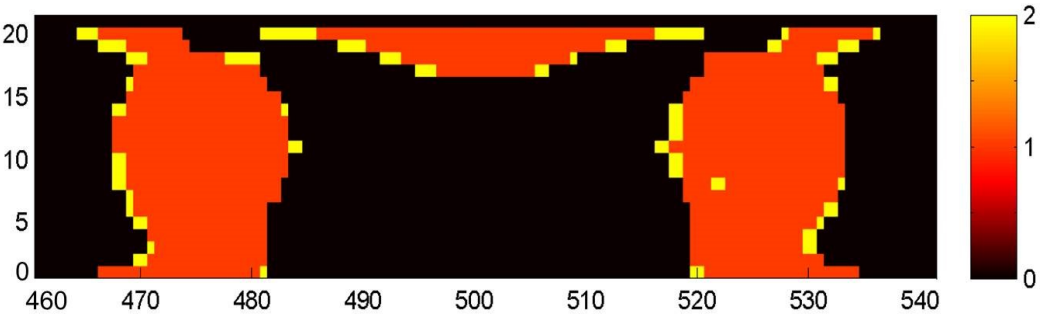

c) Patterns of caprock shearing failure in FLAC analysis with only PSHD

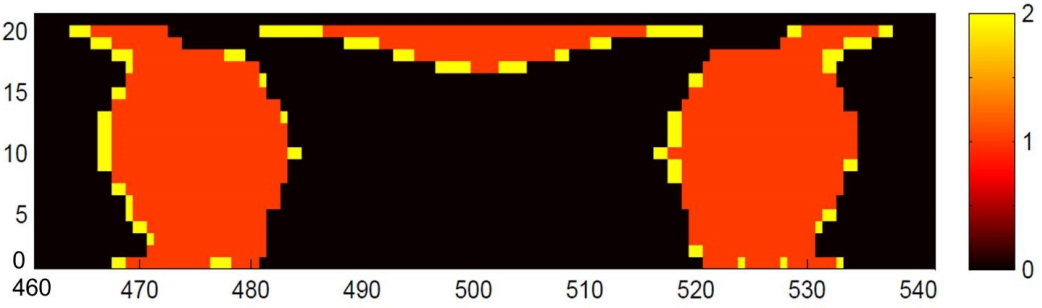

Figure 4-44 Patterns of caprock shearing failures in a) reservoir-geomechanical analysis, b) FLAC analysis with both PSVD & PSHD, and c) FLAC analysis with only PSHD (unit in m).

4) Summary

By comparing the displacement vectors, stress contours and the patterns of caprock shearing failure, the polyline simplified displacements at the base of caprock are proven to be capable of replacing oilsands reservoir for studying the caprock behavior in SAGD process. Both horizontal and vertical displacements are generated at the base of caprock. Ideally, both of them should be applied in centrifuge models to fully simulate the caprock behavior. However, it is of difficulty to implement both of them.

At the time of caprock shearing failure, the vertical displacement dominates and the influence of the horizontal displacement is negligible. The FLAC simulation with only polyline simplified vertical displacement (PSVD) applied at the base of caprock shows that the displacements, stresses and patterns of caprock shearing failure are highly comparable to those in reservoir-geomechanical simulations, which indicates that it is reasonable to simulate the caprock behavior in physical modeling by applying only polyline simplified vertical displacement (PSVD) at the base of caprock.

4.4.2 Centrifuge Simplified Vertical Displacement

Even though the polyline simplified vertical displacement (PSVD) is good enough to simulate caprock behavior in physical models, it is found that such a displacement profile is still difficult to implement in experimental environments. Consequently, further simplification is required and bilinear displacement profile is explored.

The polyline simplified vertical displacement has a span of 52m, while the plane strain box at GeoCERF has a length of 70cm and the centrifuge test is to be conducted at 100g. Thus the prototype which could fit into the plane-strain box should be no more than 70m long. To reduce the boundary effects of the plane-strain box, a ratio of no larger than 1/3 is recommended for model actuation area versus plane-strain box length.

As shown in Figure 4-45, two vertical displacement profiles will be exerted at the base of caprock in FLAC analysis with only caprock and overburden: one is the simplified vertical displacement (SVD) and another is the centrifuge simplified vertical displacement (cSVD). Basically, the cSVD would have the same shape as in Figure 4-45a; however, to fit into the plane-strain box, the plateau area would only be 10m long for cSVD. Similar as in section 4.4.1, the displacement vectors, stress contours and patterns of caprock shearing failure zones in the caprock formation would be compared to those in the reservoir geomechanical simulation to verify the feasibility of using cSVD to study caprock behavior in centrifuge models.

a)

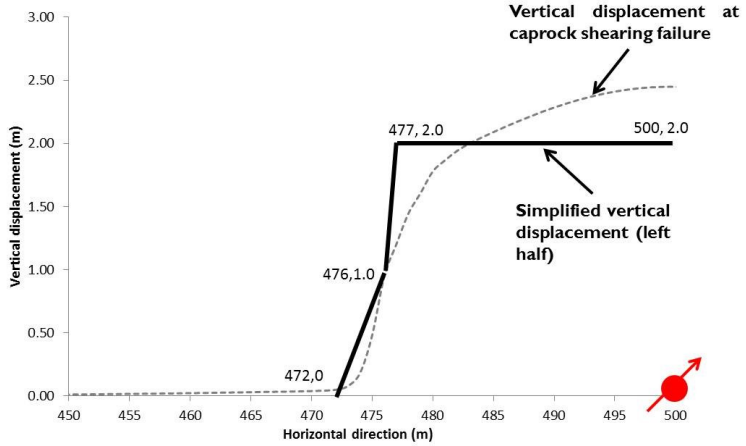

b)

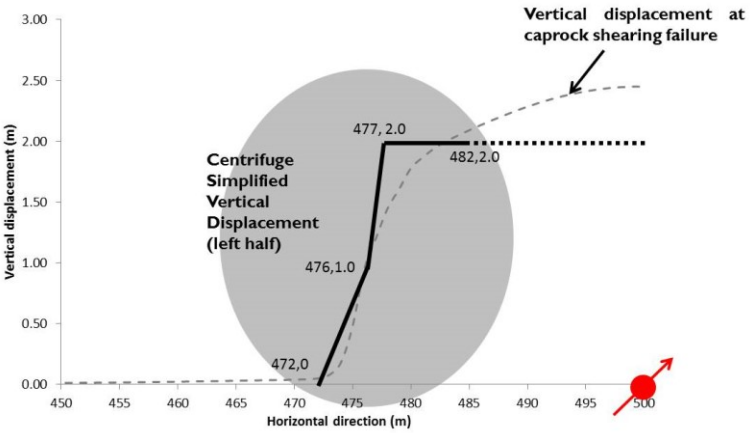

Figure 4-45 a) Simplified vertical displacement (SVD) and b) centrifuge simplified vertical displacement (cSVD).

1) Displacement vectors

a) Displacement vectors in reservoir-geomechanical analysis

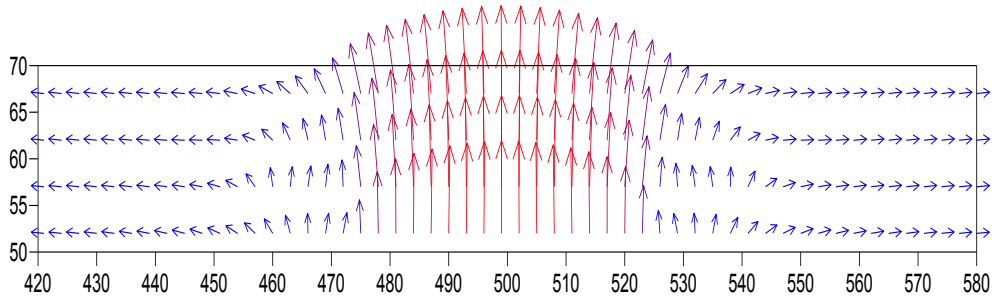

b) Displacement vectors in FLAC analysis with SVD

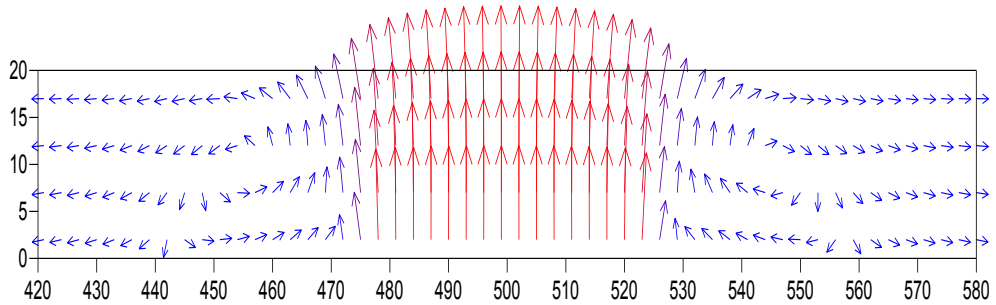

c) Displacement vectors in FLAC analysis with cSVD

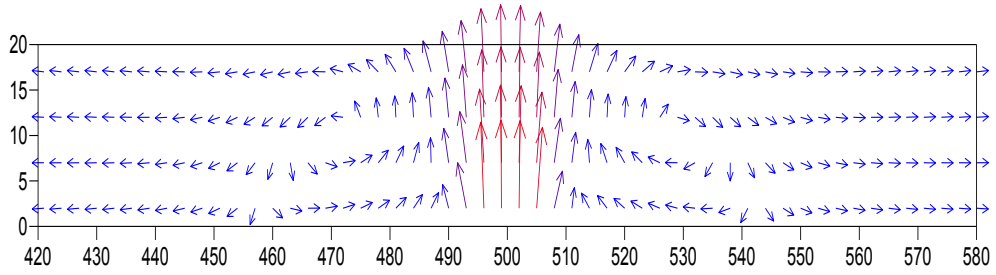

Figure 4-46 Displacement vectors in a) reservoir-geomechanical analysis, b) FLAC analysis with SVD and c) FLAC analysis with cSVD (unit in m).

2) Stress contours

a) Horizontal stress contours in reservoir-geomechanical analysis (kPa)

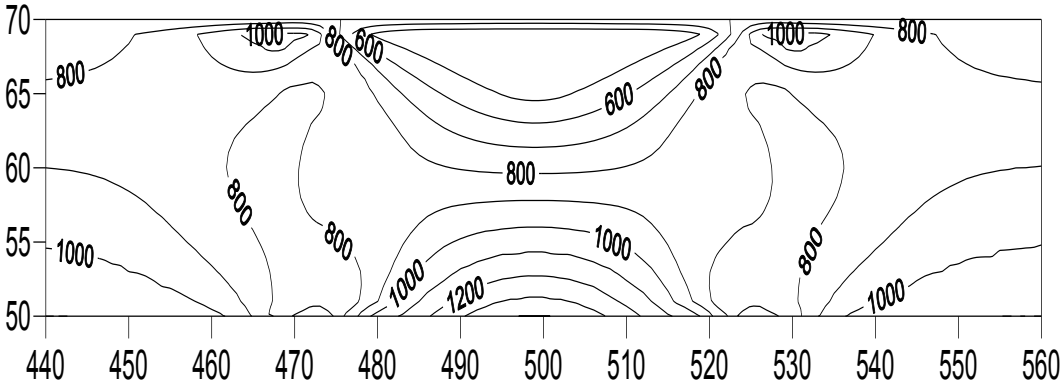

b) Horizontal stress contours in FLAC analysis with SVD (kPa)

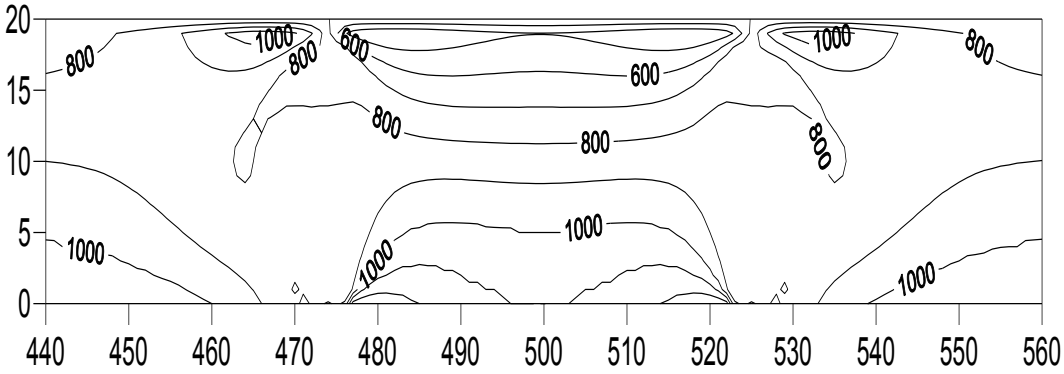

c) Horizontal stress contours in FLAC analysis with cSVD (kPa)

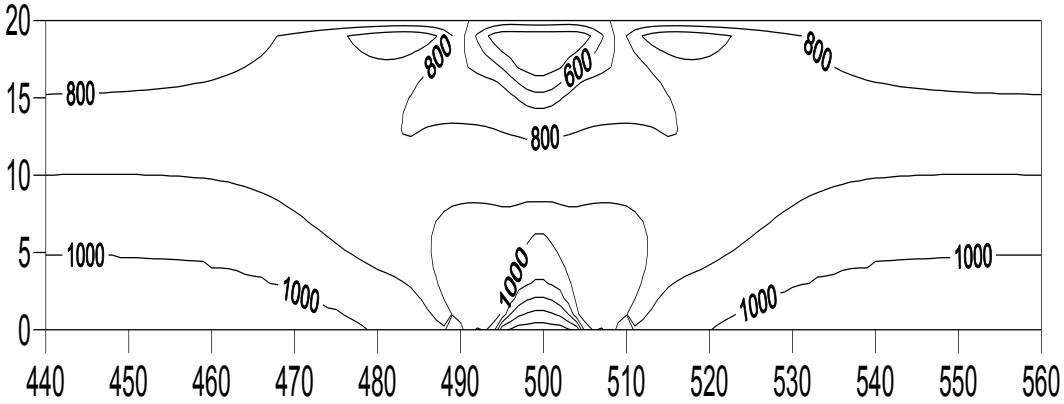

Figure 4-47 Horizontal stress contours in a) reservoir-geomechanical analysis, b) FLAC analysis with SVD and c) FLAC analysis with cSVD (unit in m).

a) Vertical stress contours in reservoir-geomechanical analysis (kPa)

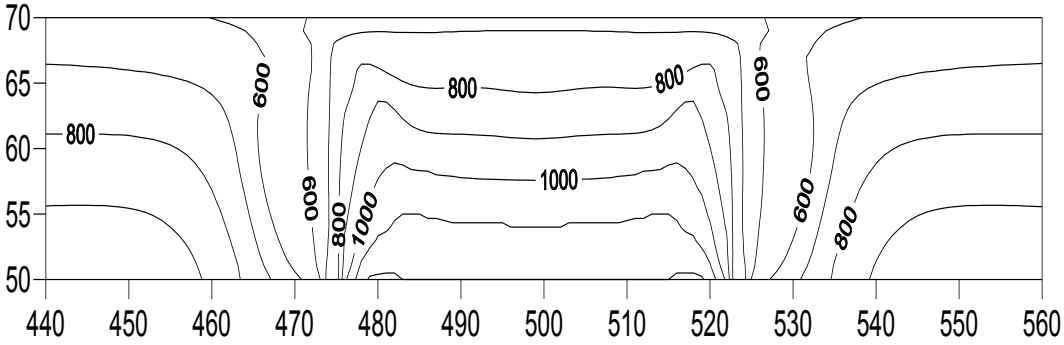

b) Vertical stress contours in FLAC analysis with SVD (kPa)

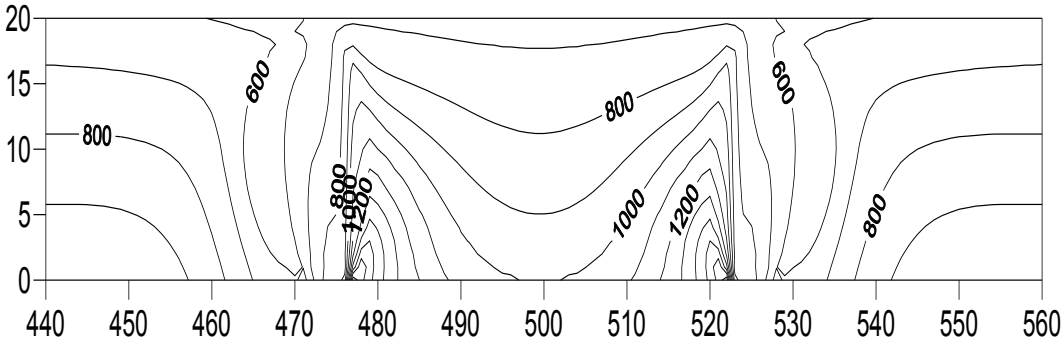

c) Vertical stress contours in FLAC analysis with cSVD (kPa)

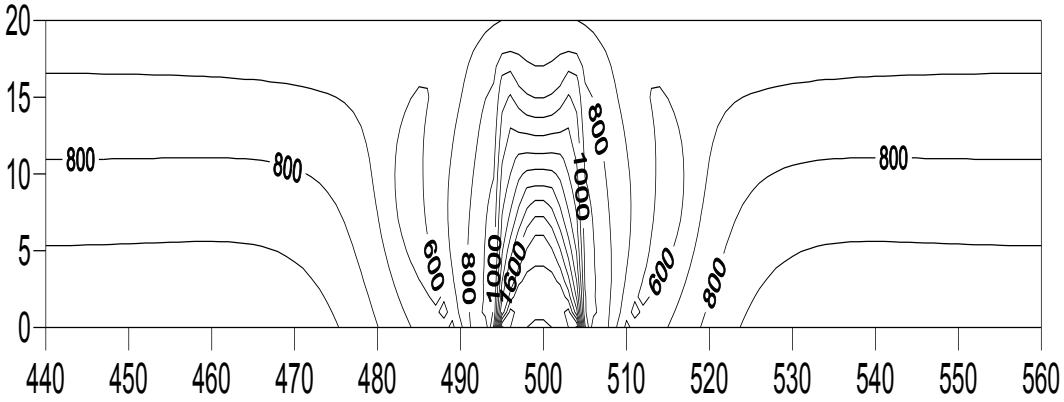

Figure 4-48 Vertical stress contours in a) reservoir-geomechanical analysis, b) FLAC analysis with SVD and c) FLAC analysis with cSVD (unit in m).

a) Shear stress contours in reservoir-geomechanical analysis (kPa)

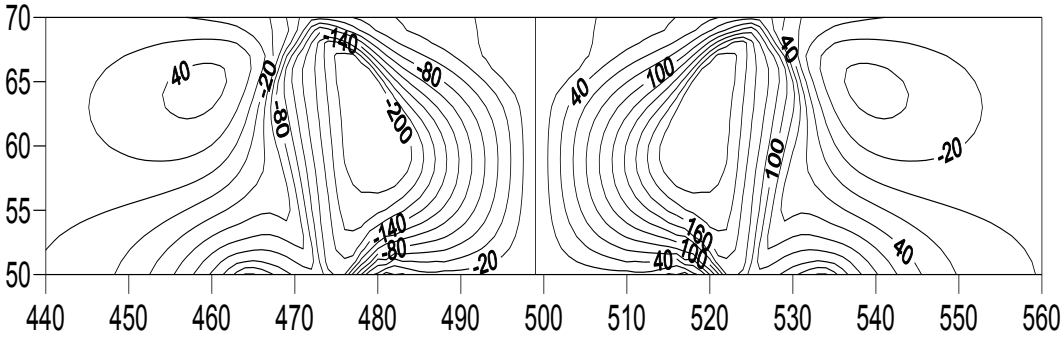

b) Shear stress contours in FLAC analysis with SVD (kPa)

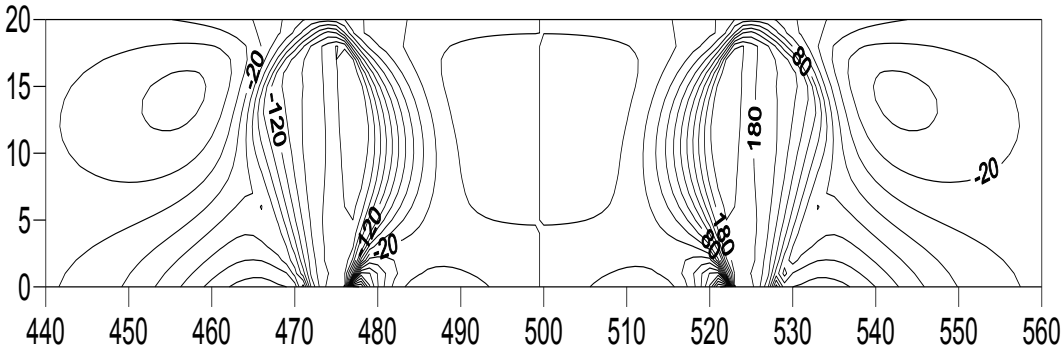

c) Shear stress contours in FLAC analysis with cSVD (kPa)

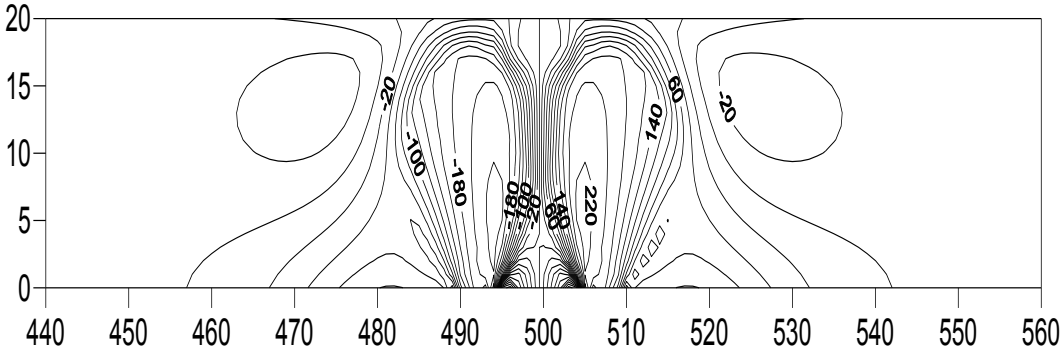

Figure 4-49 Shear stress contours in a) reservoir-geomechanical analysis, b) FLAC analysis with SVD and c) FLAC analysis with cSVD (unit in m).

3) Patterns of caprock shearing failure

a) Patterns of caprock shearing failure in reservoir-geomechanical analysis

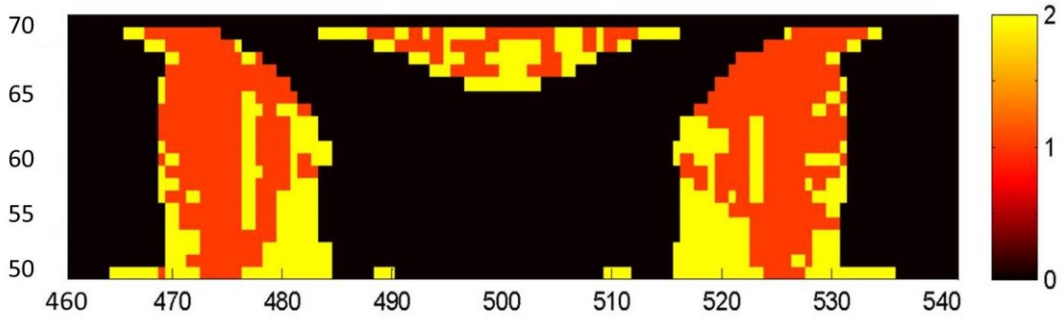

b) Patterns of caprock shearing failure in FLAC analysis with SVD

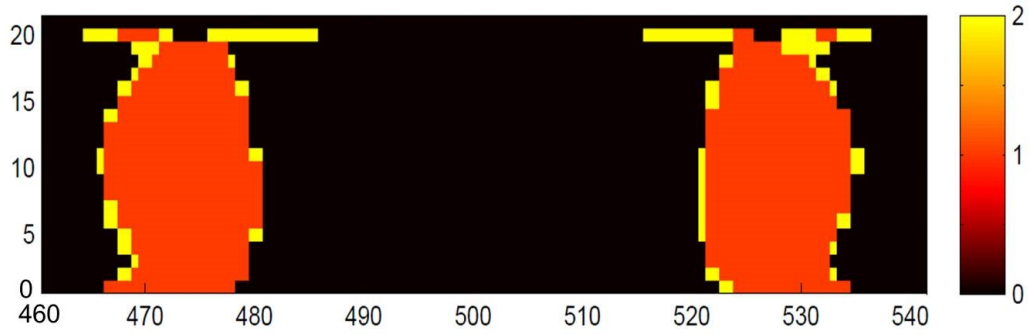

c) Patterns of caprock shearing failure in FLAC analysis with cSVD

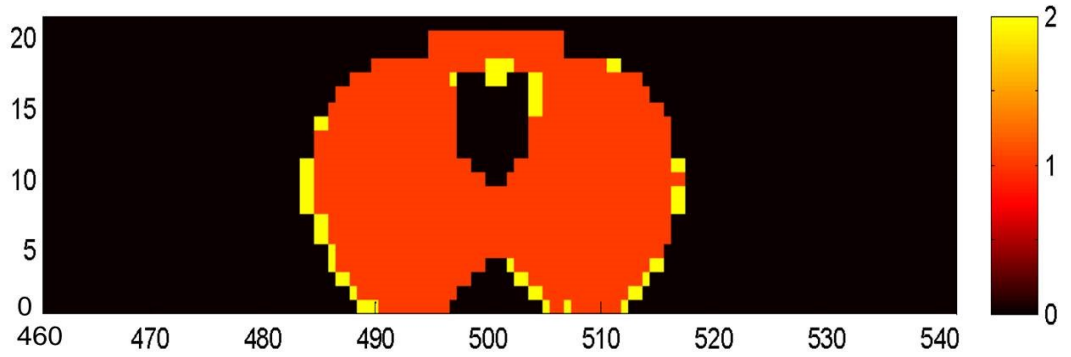

Figure 4-50 Patterns of caprock shearing failure in a) reservoir-geomechanical analysis, b) FLAC analysis with SVD and c) FLAC analysis with cSVD (unit in m).

4) Summary

It is found that the simplified vertical displacement (SVD) at the base of caprock can generate fairly comparable stress and strain fields and patterns of shearing failure zones in the caprock compared to those in reservoir-geomechanical simulations.

Because of the shrinkage of the plateau area of the centrifuge simplified vertical displacement (cSVD), it is apparent that the stress and strain fields as well as the patterns of caprock shearing failure are squashed to the center of the model (Figure 4-46 to Figure 4-50). The cSVD can capture the characteristics of the caprock behavior during SAGD process to some extent. This research focuses on the feasibility study of centrifuge modeling of caprock integrity, and the cSVD will be exerted at the base of caprock in centrifuge modeling.

4.5 Summary and Discussion

Numerical study of SAGD caprock integrity in this chapter proposes an approach to explore the caprock failure modes to simulate in centrifuge physical modeling. A thorough analysis of the caprock behavior during SAGD process in the Reference Case is conducted. The pressure and temperature front growths, displacement profile evolution at the base of caprock and the shearing zone development in caprock are analyzed simultaneously. Tensile failure of oilsands at the base of caprock is observed, as the steam injection pressure is higher than the minimum principal stress. As the steam chamber expands horizontally, the oilsands tensile failure zones propagate concurrently. The pore pressure building up as well as the reservoir expansion at the base of caprock is the source of the large vertical displacement at caprock base which causes the development of shearing zones in caprock from the edges of the oilsands tensile failure zones. Caprock shearing failure happens when the shearing zones go through the whole caprock formation.

Caprock in centrifuge models is mimicked using overconsolidated Speswhite kaolin and triaxial test results reveal that there are significant geomechanical property differences between caprock shale and overconsolidated Speswhite kaolin. Thus, a parametric analysis is conducted to study the influence of property difference on caprock behavior during SAGD process. According to the parametric analysis results, the caprock shearing failure driven by the vertical displacement at the base of caprock is commonly observed for caprock with different geomechanical properties. The property differences will influence the span and magnitude of the vertical displacement profiles at the base of caprock when caprock shearing failure is reached but generally, the shape and characteristics of the vertical displacement profiles are the same.

Ideally, the displacement profile from reservoir geomechanical simulations should be fully simulated in centrifuge models. However, constrained by the dimensions of the plane-strain box and the complexity of fully implementing the vertical displacement profile, an alternative solution is the centrifuge simplified vertical displacement (cSVD). A separate FLAC model with only caprock and overburden is built with cSVD applied at the base of caprock. The calculated stress and strain fields along with patterns of the caprock shearing failure are compared to those from reservoir geomechanical simulations and the cSVD can capture the characteristics of caprock behavior during SAGD process to a certain extent. The boundary effects of the plane-strain box are also explored (see Appendix D). For this feasibility study of centrifuge modeling of caprock integrity, the cSVD will be exerted in the centrifuge model; however, further improvements are required in the future study.

Chapter 5 : Design and Commissioning of the Geomechanical Caprock Deflection Mechanism

A custom-designed electromechanical device named Geomechanical Caprock Deflection Mechanism (GeoCDM) (Figure 5-1) is designed and commissioned within Geotechnical Centrifuge Experimental Research Facility (GeoCERF) to apply the centrifuge simplified vertical displacement (cSVD). Commissioning of GeoCDM is thoroughly conducted to validate the mechanical performance and ensure the successive running of 100g centrifuge test of caprock integrity. 1g load test and 100g centrifuge tests are both carried out. Necessary modification of GeoCDM is conducted concurrently.

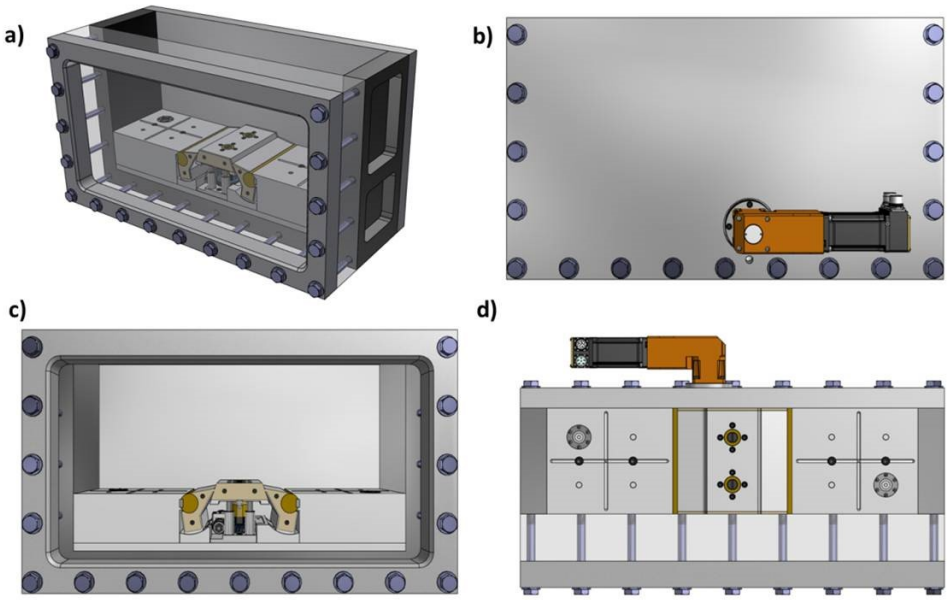

Figure 5-1 Schematic view of GeoCDM a) isometric view b) back view c) front view d) top view.

5.1 Mechanical Design of GeoCDM

The GeoCDM is comprised of two parts: the driving system and the transmission system (Figure 5-2). The driving system provides the power to drive the transmission system and includes a Parker BE233D servo motor which is controlled by a Parker AR-08CE controller, and a Parker RX23-100-S2 gearhead with a reduction ratio of 100:1. The

Parker Motor has a rated torque of 1.33Nm at the rated speed of 3741rpm. The transmission system is made up of the rotation shaft, two sets of worm gears, the center-lifting table, left and right flanks and two fixed side blocks.

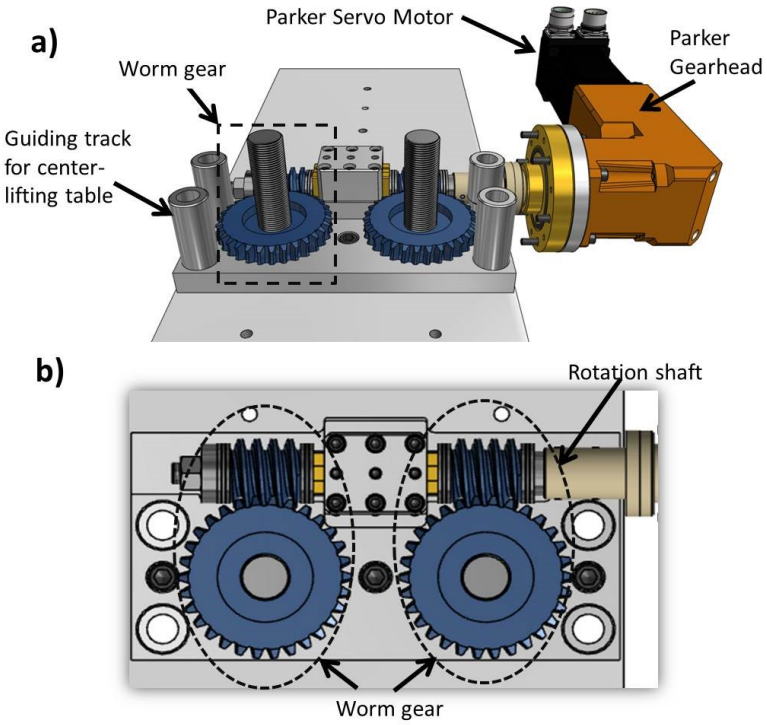

Figure 5-2 a) Driving system and transmission system of GeoCDM b) top view of the worm gears and the rotation shaft.

The driving system and transmission system are interconnected by locking the key (in the Parker gearhead) into the key-way (in the rotation shaft). The worm ratio for the transmission system is 30:1, which means 30 rotations of the horizontal shaft (or the gearhead shaft) will make one rotation of the vertical shaft of the worm gear. And one rotation of the vertical shaft will move the center-lifting table up by 1.5mm. Since the gearhead has a reduction ratio of 100:1, thus 3000 rotations of the Parker servo motor is required to uplift the center-lifting table by 1.5mm.

The center-lifting table has a width of 10cm and each flank has a width of 5cm. Figure 5-3 and Figure 5-4 shows the GeoCDM shapes at initial position and after 20mm uplift.

The GeoCDM is designed to uplift under a uniform load of 2MPa along the uplifting area of the center-lifting table and left and right flanks.

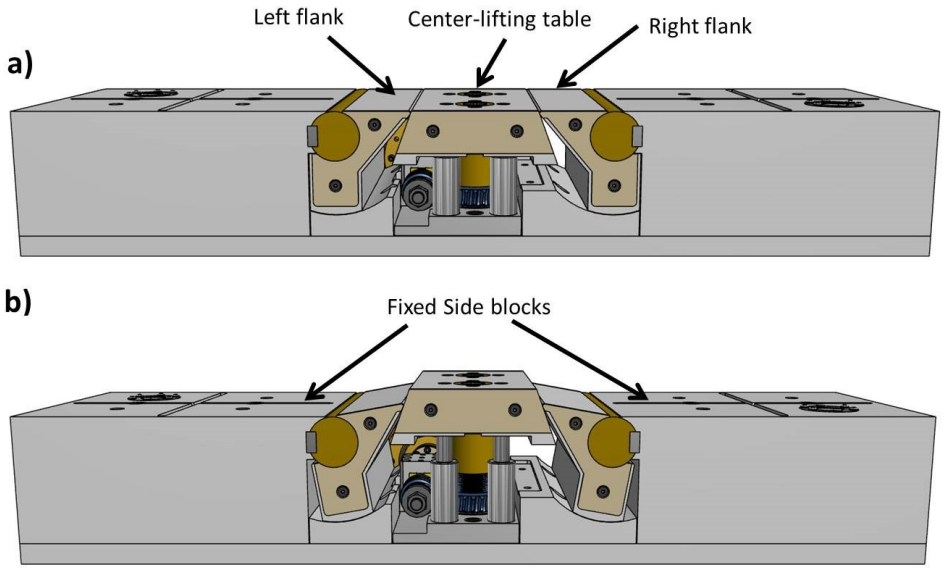

Figure 5-3 a) Front view of GeoCDM at 0mm poisition b) front view of GeoCDM at 20mm poisition.

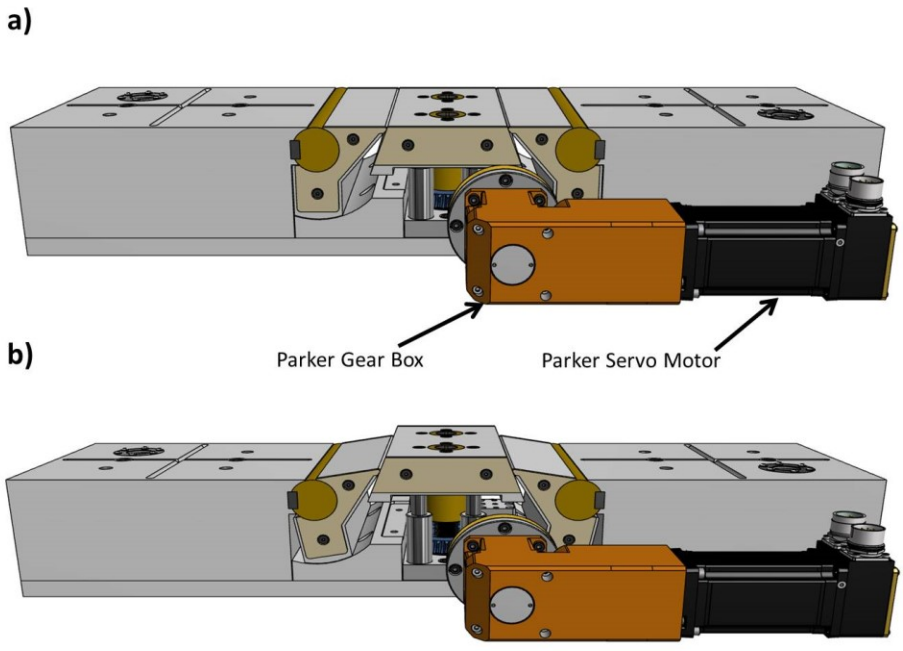

Figure 5-4 a) Back view of GeoCDM at 0mm poisition b) back view of GeoCDM at 20mm poisition.

5.2 Commissioning of GeoCDM

To validate the mechanical performance of GeoCDM under the design load and during centrifuge spinning, commissioning work is conducted including both 1g load test and 100g centrifuge tests. For 1g load tests, there is no simple way of applying constant pressure on top of the left and right flanks. Alternatively, all forces on the uplifting area are converted to a load on top of the center-lifting table. 2MPa uniform pressure on top of the uplifting area is equal to a force of 62kN. Following 1g load test, 100g dry test (without water) and 100g wet tests (with water) are conducted to ensure that GeoCDM and corresponding instrumentations are working appropriately during 100g centrifuge spinning.

5.2.1 1g Load Test

1g load tests are conducted to confirm whether the Parker servo motor has the capacity to uplift the center-lifting table under the design load, during which the center-lifting table displacement and displacement rate are calibrated.

5.2.1.1 Torque Wrench Test

To protect the mechanical parts and the driving motor of the GeoCDM from unexpected overloading, a torque wrench test is conducted to determine the torque required to uplift the center-lifting table under a certain amount of load (Table 5-1). The torque wrench test results are valuable inputs for the right choice of the driving motor.

Table 5-1 Torque wrench test results.

Load (kN)	Torque Required (N·m)
30	> 130 inch· pound (14.68 N·m) *
40	150 inch· pound/16.94N·m
50	165 inch· pound/ 18.64N·m
60	200 inch· pound/ 22.60N·m
70	220 inch· pound/ 24.86N·m

**** 130 inch· pound is the capacity of the original stepper motor.***

5.2.1.2 Assembly of GeoCDM for 1g Load Tests

All components of GeoCDM are installed on a base plate (Figure 5-5). For 1g load tests, only the center-lifting table of GeoCDM would be installed. First, the rotation shaft and worm gears are installed on the base plate (Figure 5-6). Then, the base plate is carefully placed at the base of the plane-strain box. The axis of the rotation shaft should be aligned with the axis of the pre-drilled hole at the back plate of the plane-strain box (Figure 5-7).

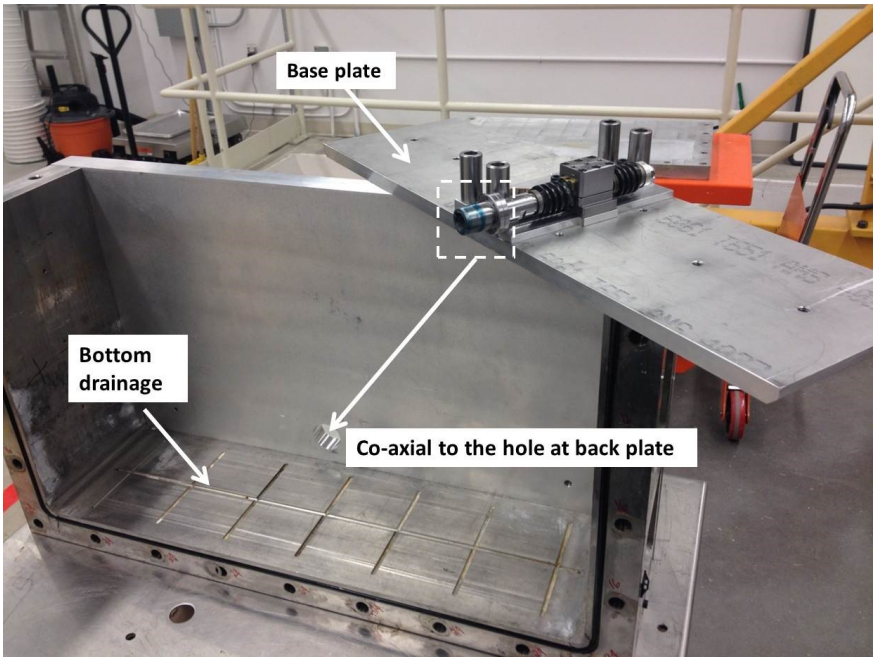

Figure 5-5 The base plate for installation of GeoCDM.

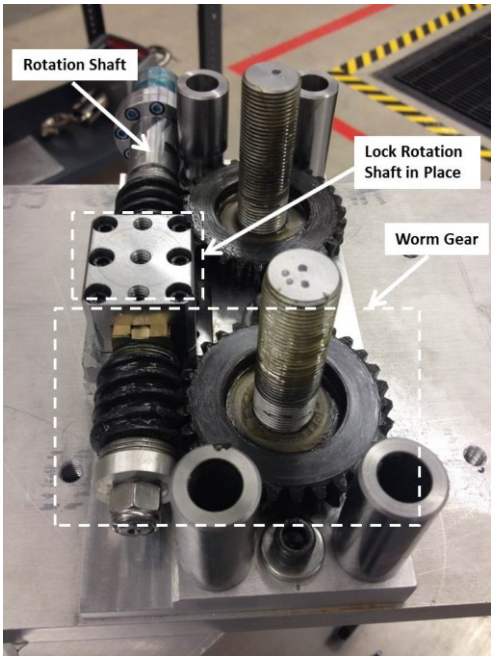

Figure 5-6 Installation of rotation shaft and the worm gears at the base plate.

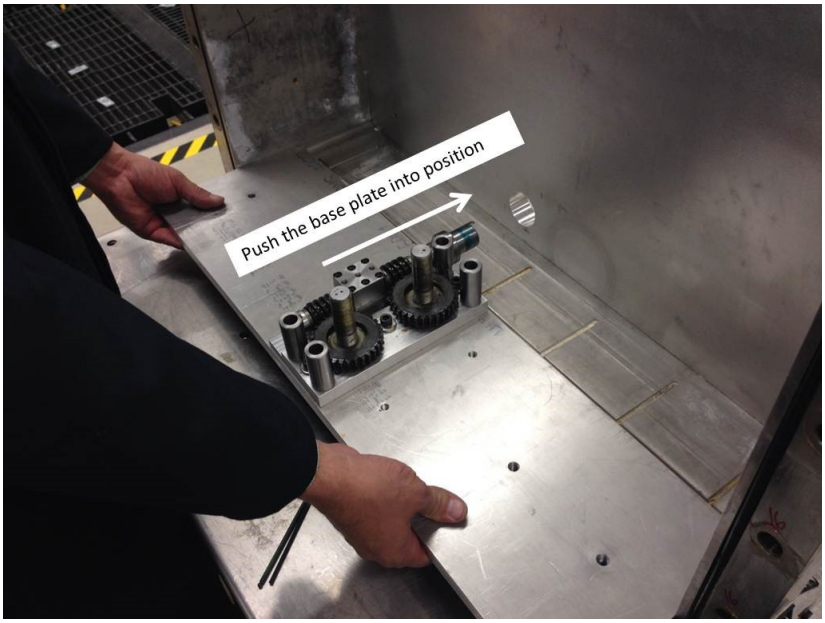

Figure 5-7 Place the base plate at the base of the plane-strain box.

At the back plate, a brass flange with an oil seal is installed to seal the GeoCDM chamber and provide the centralizing bushing for the rotation shaft (Figure 5-8a). Then another aluminum flange is installed onto the brass one for the purpose of holding the Parker Servo Motor in position (Figure 5-8b). The key in the Parker gearhead and the key-way

in the rotation shaft should be aligned so that the Parker servo motor could drive the rotation shaft (Figure 5-9).

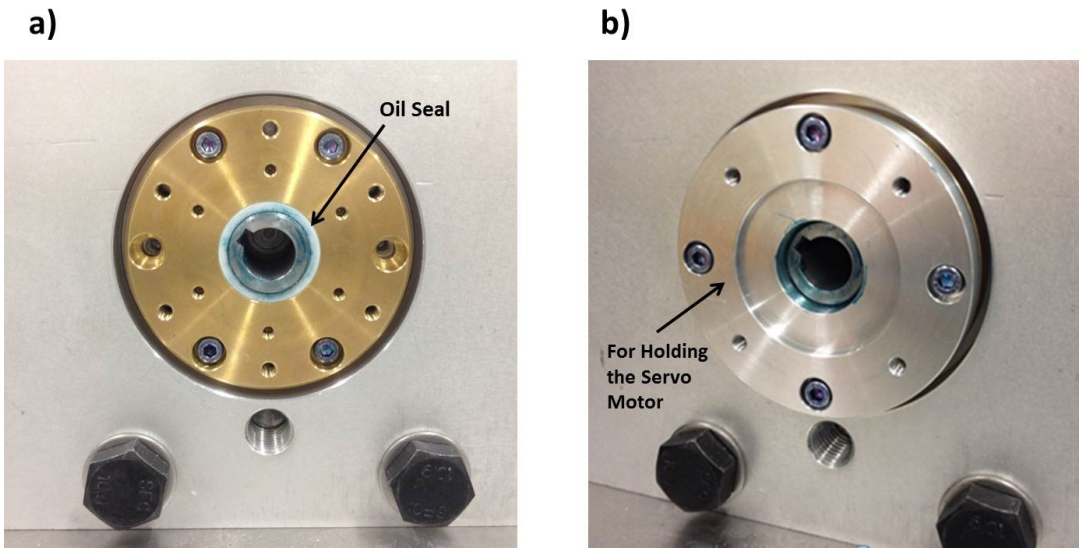

Figure 5-8 a) Installation of the brass flange at the back plate b) installation of the aluminum flange onto the brass flange.

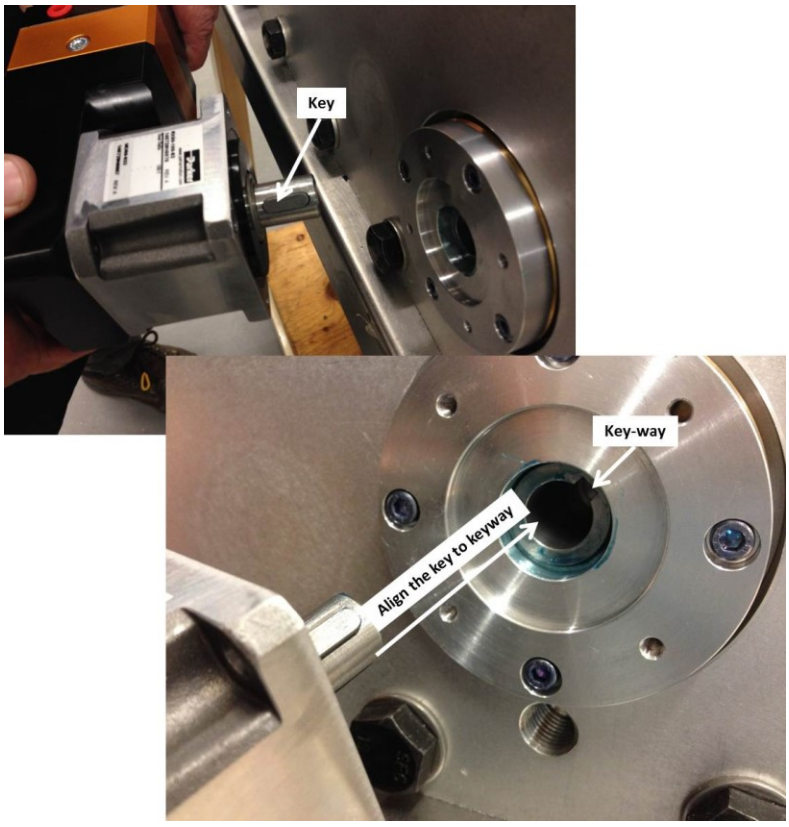

Figure 5-9 Installation of the Parker servo motor.

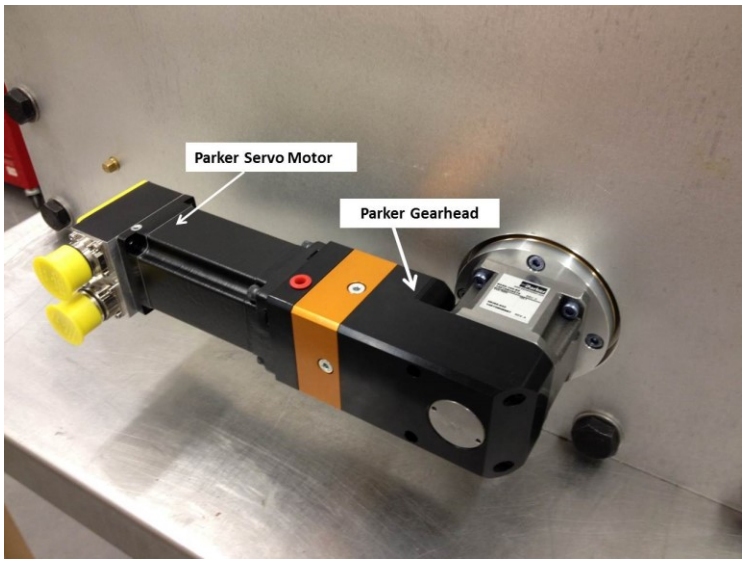

Figure 5-10 Parker servo motor with the Parker gearhead after installation.

An aluminum plate as shown in Figure 5-11 is used to lock the worm gears in place (Figure 5-11). Then the center-lifting table is installed. It is important to make sure that the two brass threaded inserts are at the same level; otherwise the center-lifting table would be tilted (Figure 5-11).

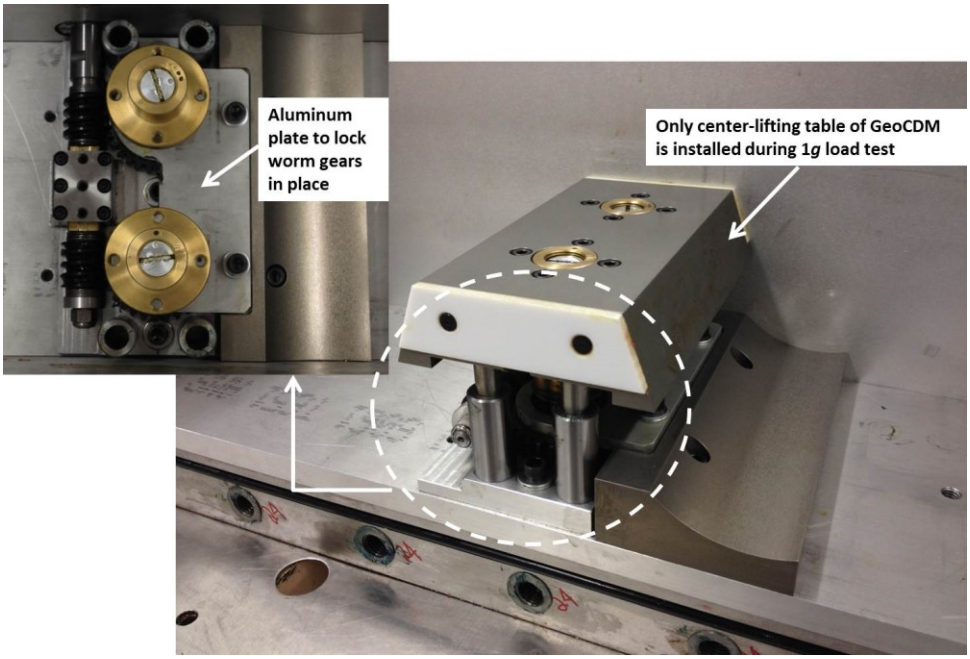

Figure 5-11 The center-lifting table after installation.

5.2.1.3 62kN Load Test on GeoCDM

The same setup of 1g consolidation is used for the 1g load tests. An ISCO pump is employed to apply pressure on top of the GeoCDM. The ISCO pump pressure (kPa) to load (kN) exerted on top of the GeoCDM has a ratio of 254:1, based on which, the required ISCO pump pressures for applying a certain value of load could be calculated. In real application, the load cell reading should be relied on to get the exact ISCO pressures.

Because of the high load on top of the GeoCDM, it is of great significance to make sure that all the spacers between the top of the GeoCDM and the loading ram should be centered (Figure 5-12b). Otherwise, it might damage the GeoCDM or bring out inaccurate data. Instead of directly doing 62kN test, load on top of the GeoCDM is gradually increased at a sequence of 20kN, 40kN and 62kN. A dial gauge is used to observe the movement of GeoCDM (Figure 5-12).

There is slack in the transmission system; thus before commencing the 1g load test, it is necessary to let the system run for a while until the movement of the center-lifting table is observed through the dial gauge, which will ensure that the transmission system is fully engaged.

20mm/4hr test and 20mm/24hr tests were conducted under the load of 62kN (Figure 5-13, Figure 5-14 and Figure 5-15). The displacement was off by 0.33% and 0.34% respectively. For 20mm/4hr test, only manual readings from dial gauge were taken. For 20mm/24hr test, both manual and laser readings were taken. The displacement measured by laser was 20.778mm that is 3.89% higher than the target value. This large discrepancy happened because of the laser head not being appropriately installed (i.e. not perpendicular to the center-lifting table). The measured velocity for the 20mm/24hr test according to manual readings was 0.828 mm/hr and had a discrepancy of only 0.6%

compared to the target velocity of 0.833mm/hr. These results indicate that the electromechanical system is capable of lifting the GeoCDM under the design load of 62kN.

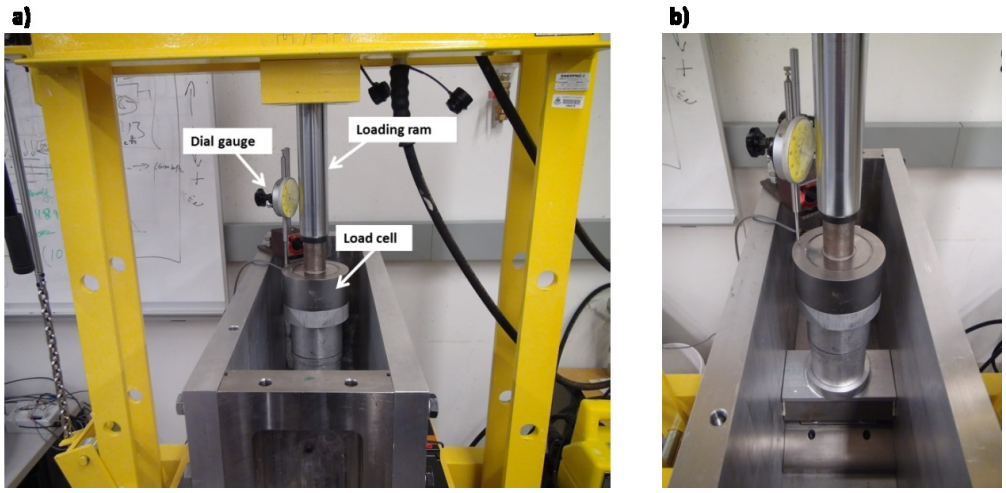

Figure 5-12 The setup for 1g load tests.

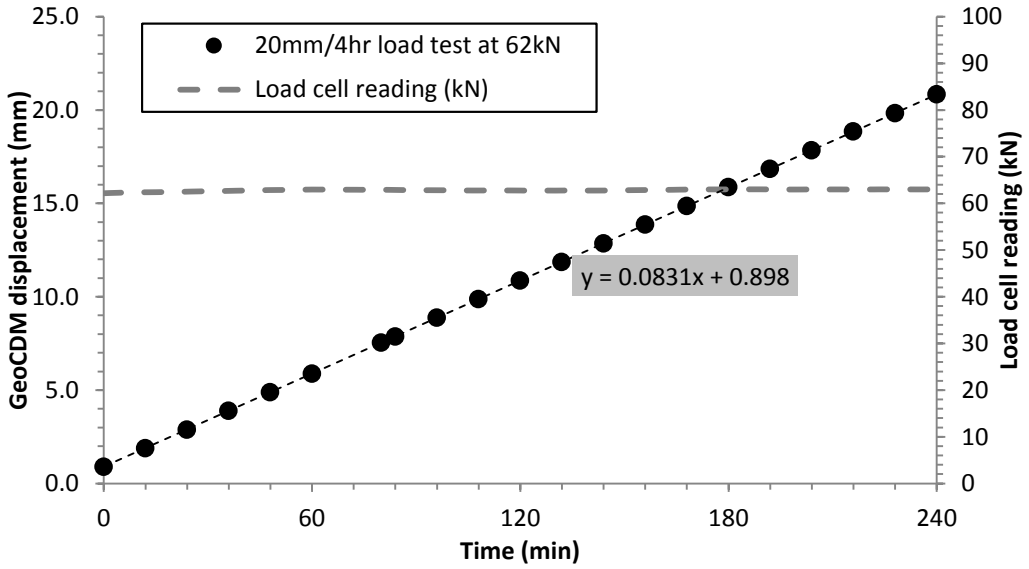

Figure 5-13 The GeoCDM displacement for the 20mm/4hr load test at 62kN.

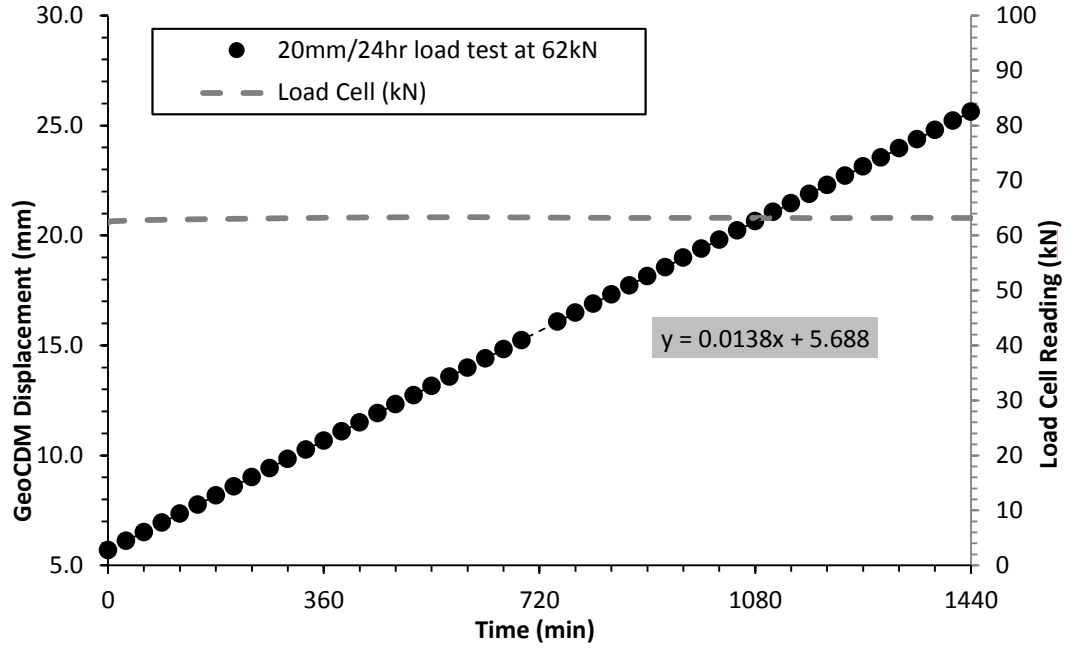

Figure 5-14 The GeoCDM displacement for the 20mm/24hr load test at 62kN (manual readings).

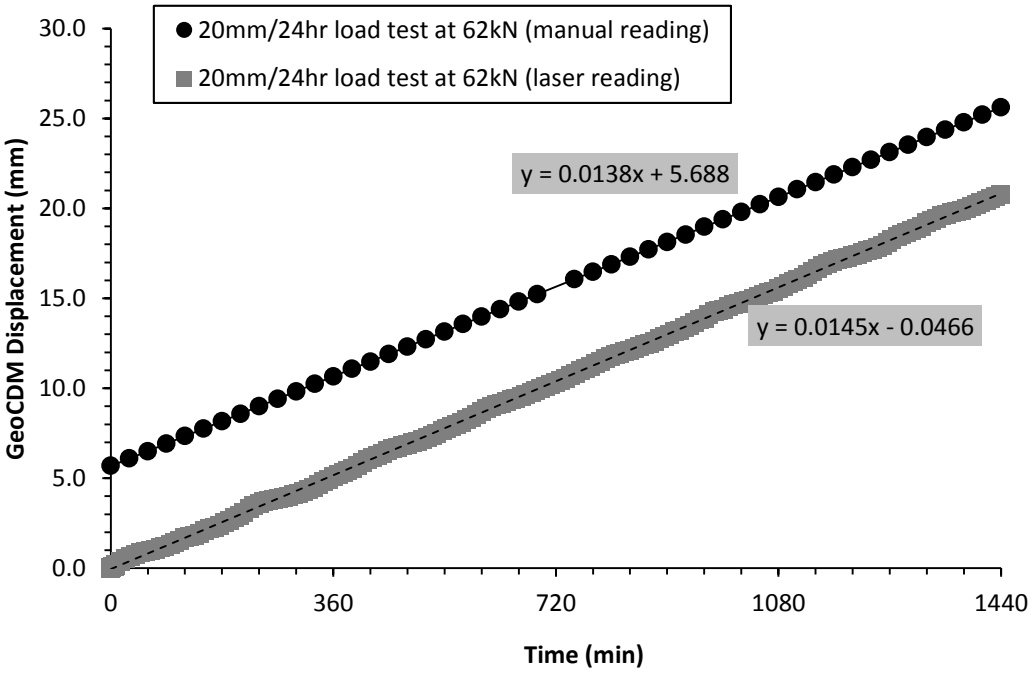

Figure 5-15 The GeoCDM displacement for the 20mm/24hr load test at 62kN (both manual and laser readings).

5.2.2 100g Centrifuge Test

Following the 1g load test, the GeoCDM were tested at 100g at different conditions: dry condition (without water on top of GeoCDM), and wet condition (with water on top of GeoCDM).

5.2.2.1 100g Dry Test

In the 100g dry test, a LVDT was mounted on top of the center-lifting table to measure the displacement of GeoCDM (Figure 5-16). A 20mm/1hr test was conducted. For the 100g dry test, no pre-running of the GeoCDM was carried out. Slacking was observed as shown in Figure 5-18 and there was no movement of the center-lifting table during the initial 30 seconds. According to the LVDT measurements, the velocity of the GeoCDM during 100g spinning was 19.83mm/hr, which has a discrepancy of 0.8% compared to the target velocity of 20mm/hr.

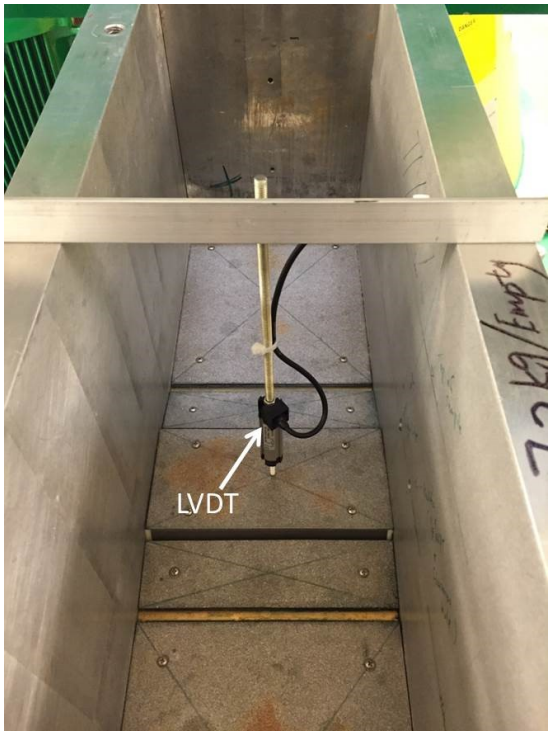

Figure 5-16 LVDT for measuring the GeoCDM displacement during 100g test.

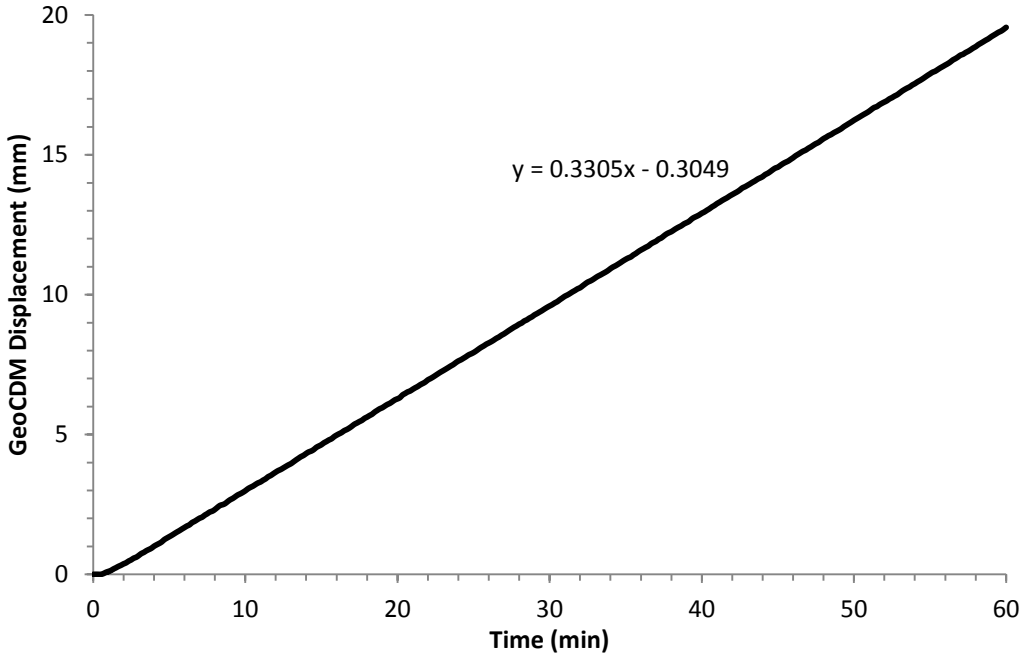

Figure 5-17 GeoCDM displacement during 100g dry test.

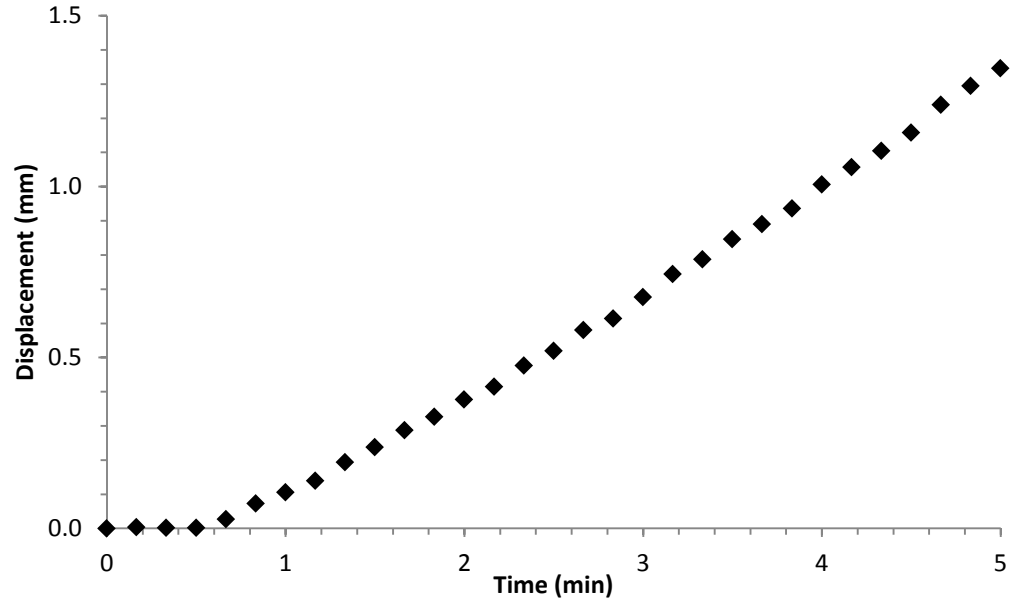

Figure 5-18 GeoCDM displacement in the initial 5 minutes of the 100g dry test.

5.2.2.2 100g Wet Test (without mineral oil on top of water)

100g wet test was conducted to test whether there is any leakage problem in the test setup and to check the influence of evaporation as the water surface was subject to the wind

caused by centrifuge spinning. A certain thickness of water was placed on top of the GeoCDM and an external pore pressure transducer was connected to the top of the GeoCDM. The plane-strain box was being spun at 100g with water surface open to atmosphere. Pre-running of the GeoCDM was conducted. And according to Figure 5-19, the center-lifting table of the GeoCDM started to move right at the start of the driving system.

As shown in Figure 5-20, pore pressure at the top of the GeoCDM kept decreasing which means the evaporation was severe during centrifuge spinning. Thus measures should be taken to prevent the evaporation during centrifuge spinning.

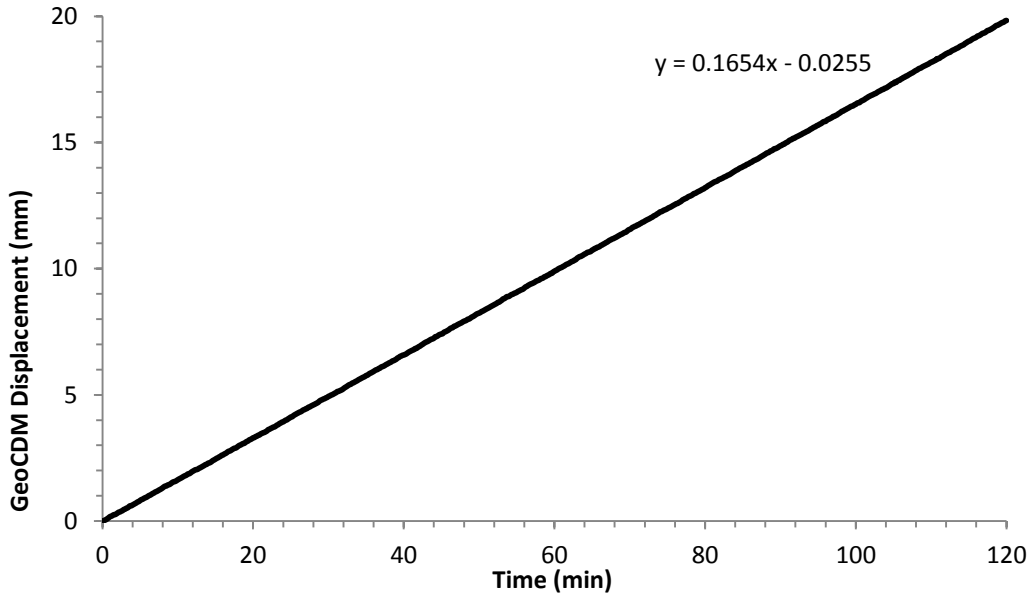

Figure 5-19 GeoCDM displacement during the 100g wet test.

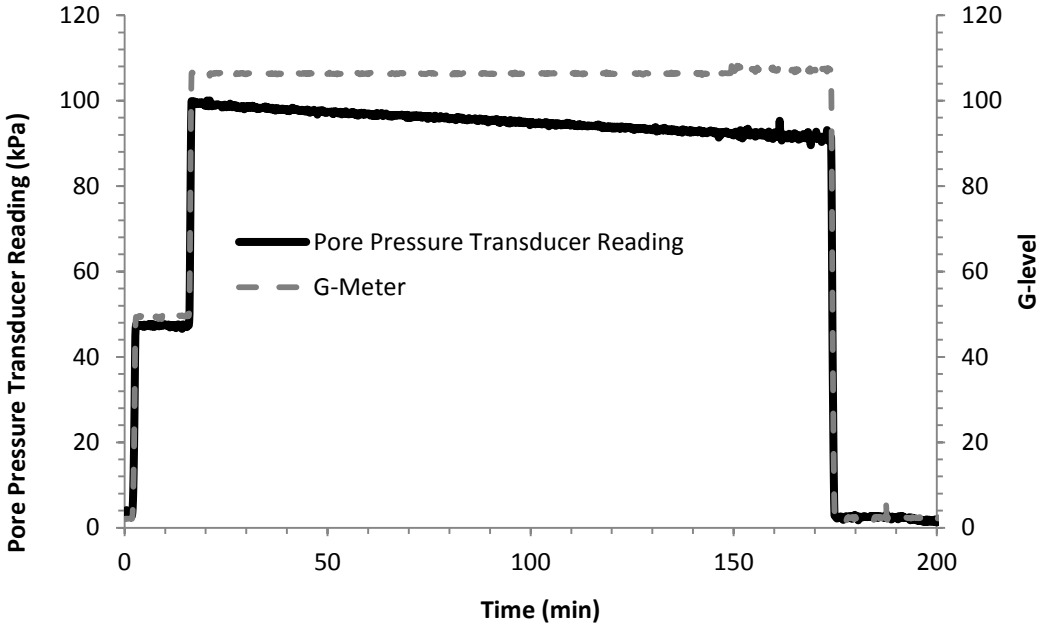

Figure 5-20 Pore pressures at the top of the GeoCDM (100g wet test without mineral oil on top of water).

5.2.2.3 100g Wet Test (with mineral oil on top of water)

The 100g wet test without mineral oil on top of water has shown that the evaporation of water due to the large open area of the plane-strain box has great influence on the water level. A solution is found by placing mineral oil on top of water. Also, on top of the plane-strain box, a thin aluminum plate is placed to reduce the wind generated during high-speed spinning of centrifuge. As shown in Figure 5-21, this method is effective in preventing evaporation during centrifuge spinning.

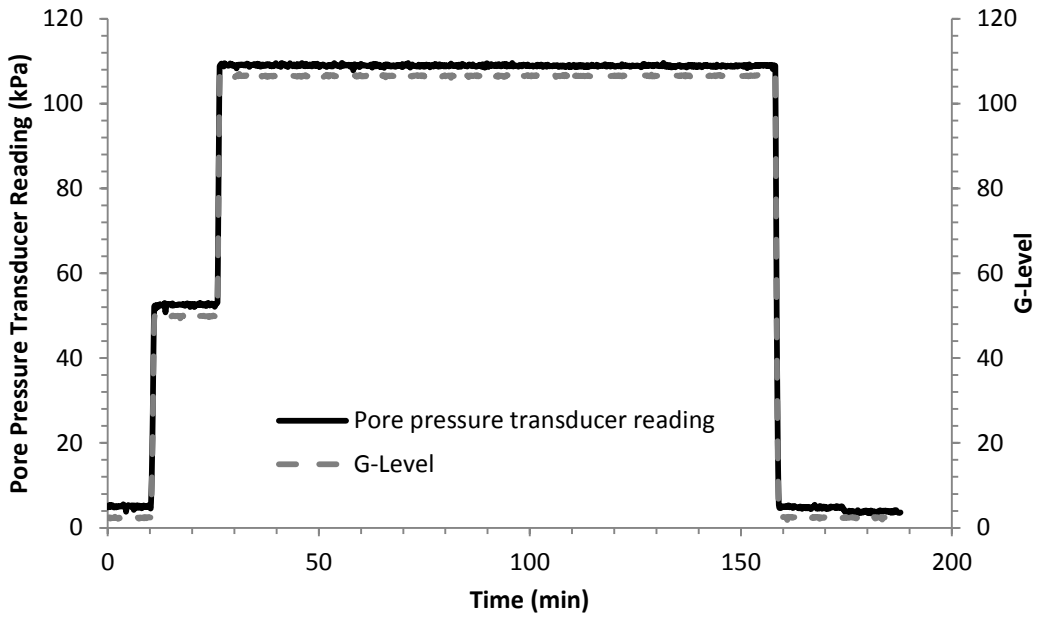

Figure 5-21 Pore pressures at the top of the GeoCDM (100g wet test with mineral oil on top of water).

5.3 Summary and Discussion

The mechanical design of the Geomechanical Caprock Deflection Mechanism (GeoCDM) as well as the installation procedure of GeoCDM is described in details. Commissioning work of GeoCDM was conducted at both 1g and 100g. According to 1g load tests, the GeoCDM is proven to be working effectively under the design load of 62kN. Both dry and wet tests were carried out at 100g. The instrumentation and cabling of the GeoCDM work approriately at 100g environment. A thin layer of light mineral oil on top of water can effectively prevenet evapation caused by the wind during centrifuge spinning. Slacking was observed in the transmission system when initating the GeoCDM. At this stage, without direct measurement of the GeoCDM movement, a pre-running of GeoCDM could be used to reduce the influences of the slacking in the transmission system.

Chapter 6 : GeoCDM Centrifuge Testing Program and Preliminary Testing Results

In this chapter, the GeoCDM centrifuge testing setup as well as the detailed testing procedure is presented. Two preliminary tests are conducted: one with the commercial clay block and another with the over-consolidated Speswhite kaolin.

6.1 GeoCDM Centrifuge Testing Setup

Figure 6-1 illustrates the elements of the GeoCDM setup used in this centrifuge testing program. The main components of the setup are the plane-strain box with its extension, pore pressure transducers (PPTs), PIV system and Mariotte Bottle.

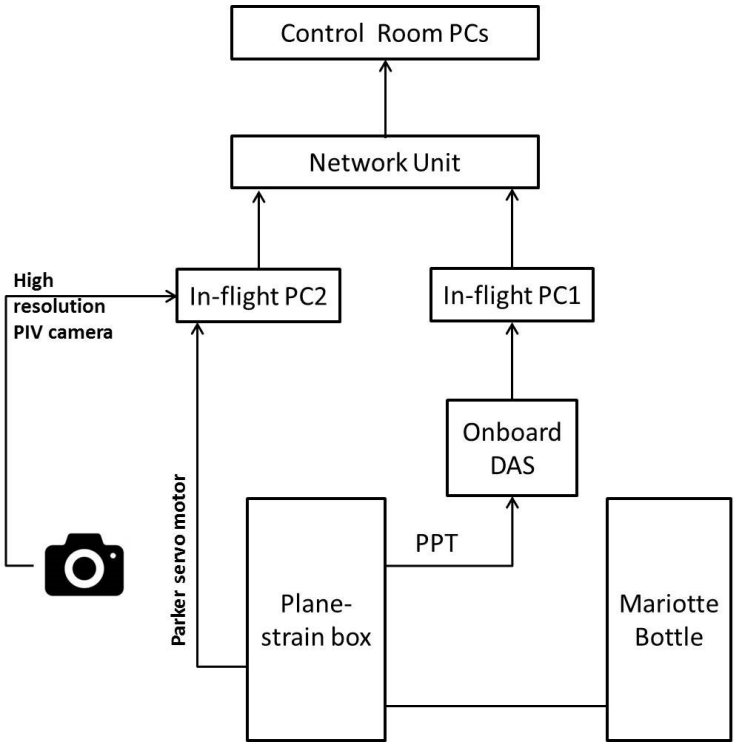

Figure 6-1 Elements of the GeoCDM centrifuge setup.

6.1.1 Plane-strain Box with Extension

An extension is necessary when the centrifuge model height is larger than the internal height (40cm) of the plane-strain box. To prevent leakage in the connection area, a layer of gasket is placed in between the plane-strain box and the extension. Ideally, the extension should be firmly tied down to the plane-strain box using screws on top of the back plate and the Perspex glass. However, it is not acceptable to drill holes in the Perspex glass to accommodate the screws. Thus, a frame as shown in Figure 6-4 is installed to tie down the extension to prevent leakage at the Perspex glass side. A thin aluminum plate is placed on top of the extension to reduce the influences of the wind caused by centrifuge spinning.

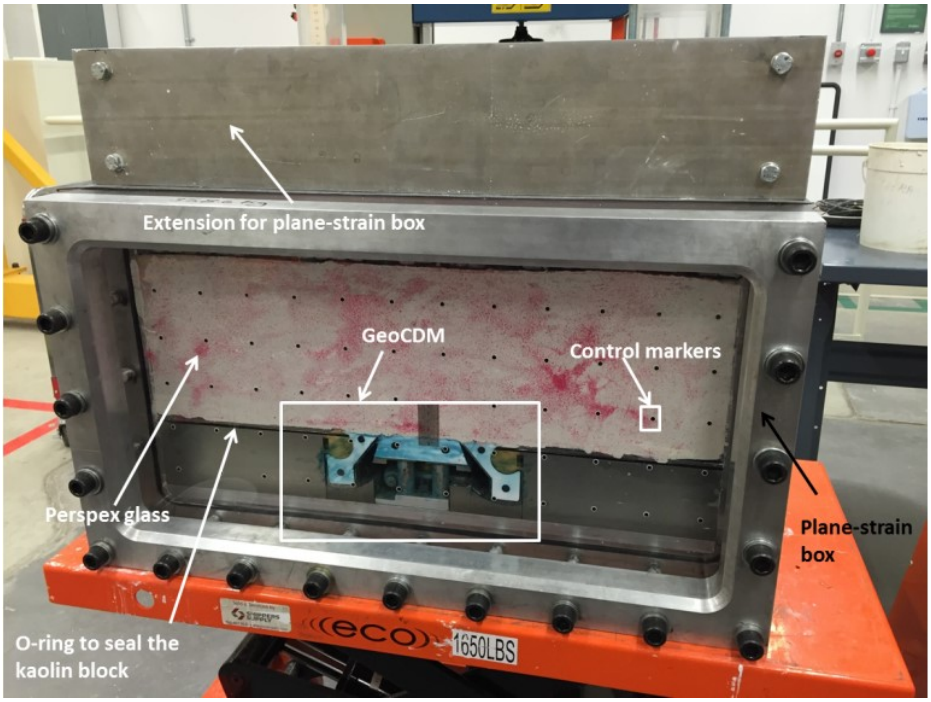

Figure 6-2 The plane-strain box with extension.

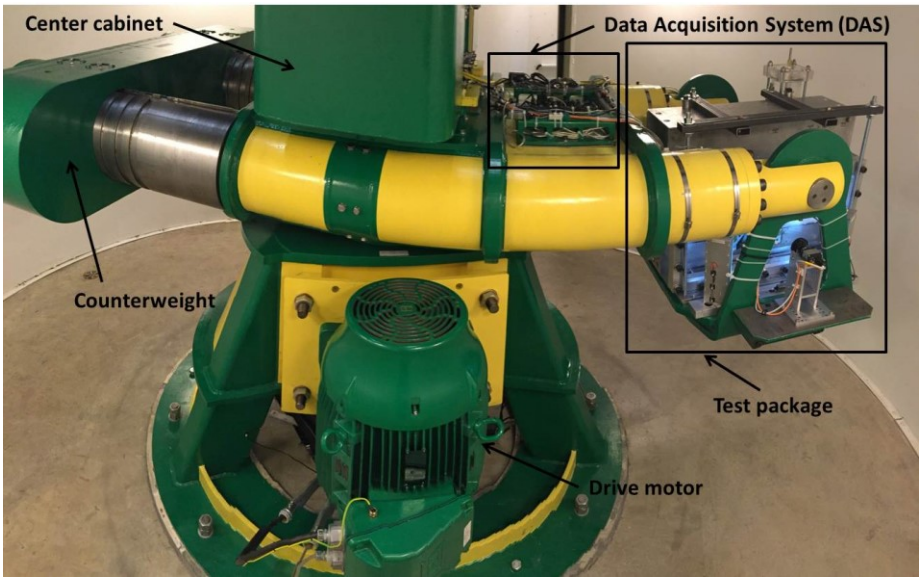

Figure 6-3 Overview of the centrifuge testing setup.

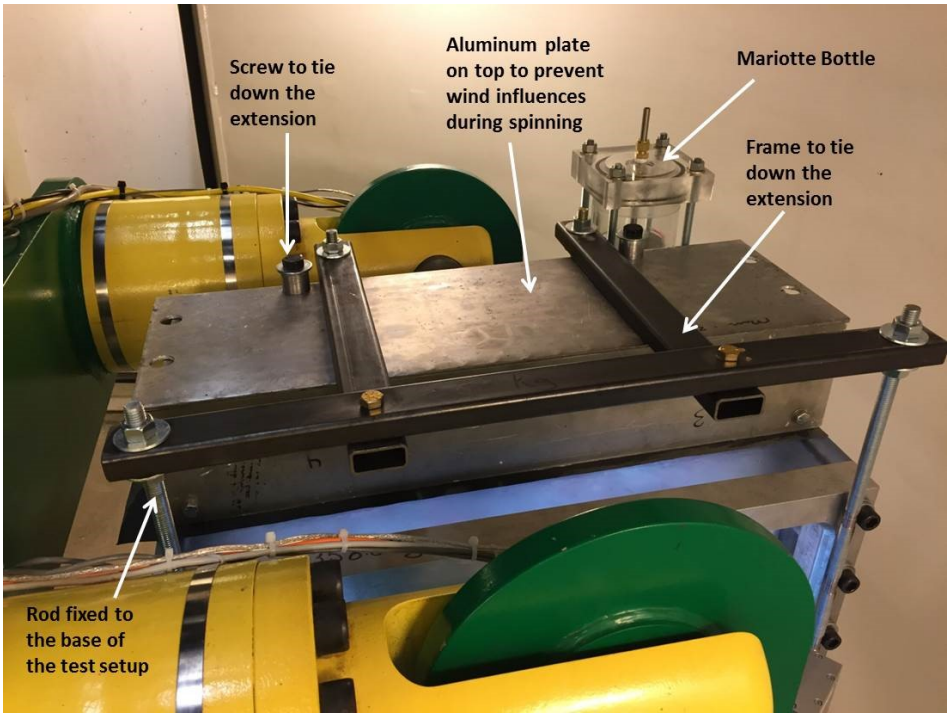

Figure 6-4 The GeoCDM centrifuge test setup.

6.1.2 Instrumentation

Instrumentation include the Kulite miniature pore pressure transducer (PPT) for internal pore pressure measurement and an external pore pressure transducer for pore pressure monitoring at the base of the overconsolidated Speswhite kaolin block (Figure 6-5). Two Kulite PPTs are installed in case that one of them may fail during testing. One Kulite PPT

is installed right in the center of the kaolin block, 5cm left of which is installed another one in the length direction. The external PPT is connected to an external fitting right at the top of the GeoCDM (Figure 6-5 and Figure 6-6).

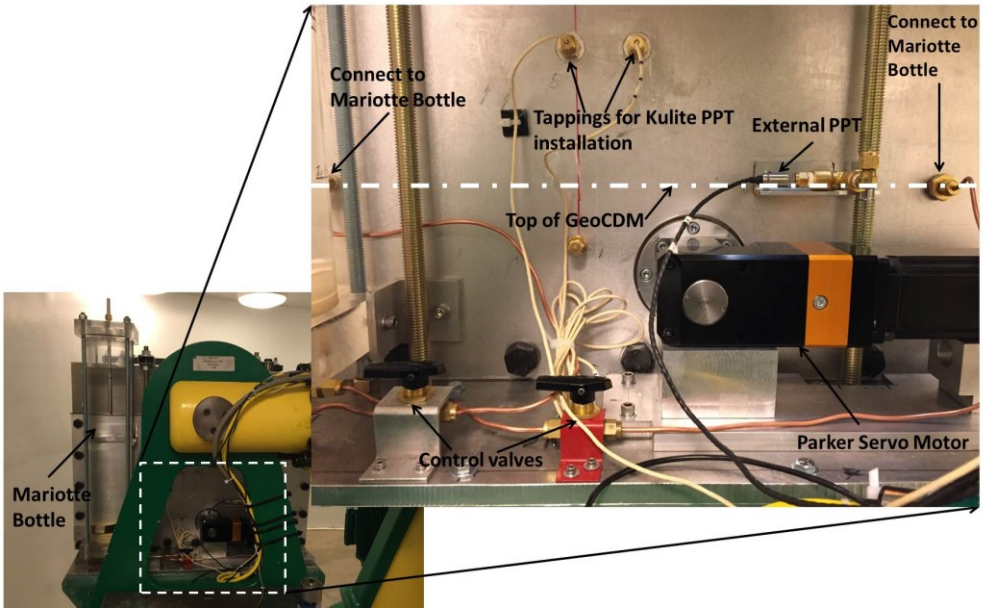

Figure 6-5 Instrumentations and Mariotte Bottle for GeoCDM centrifuge testing setup.

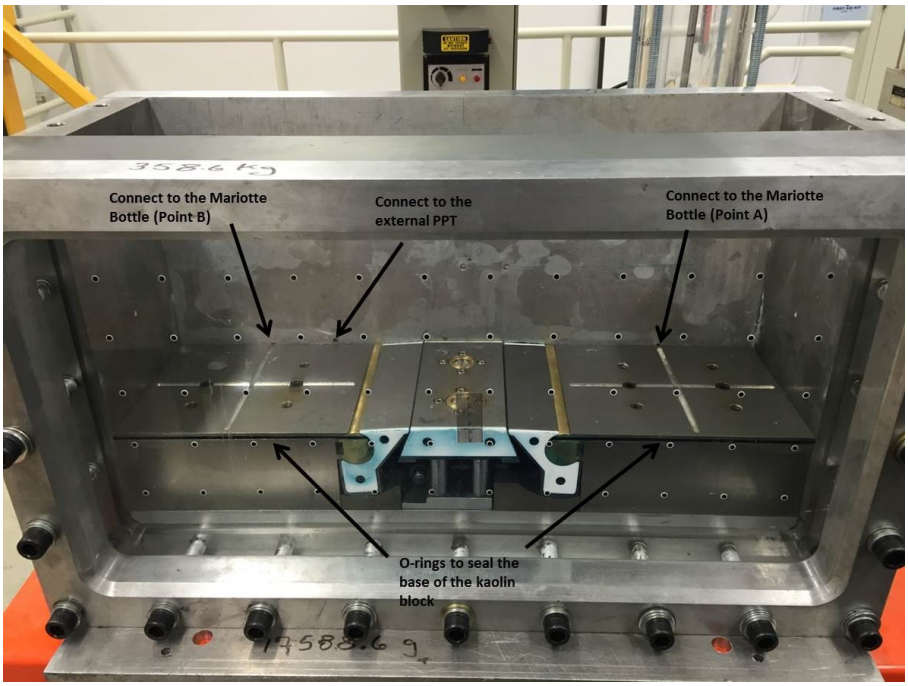

Figure 6-6 Front view of the plane strain box with Perspex glass.

6.1.3 PIV Setup

At GeoCERF, an IDS UI-6280RE-C-HQ camera body with a Schneider KMP-IR Cinegon 4.8/1.8 wide-angle lens is employed to take pictures of the centrifuge model at 100g spinning (Figure 6-7). A Matlab application package named GeoPIV (White, 2002; White et al., 2003) is used to analyze sample displacement in image-space. With the aid of control markers on the Perspex glass (Figure 6-6), the image-space displacement can be transformed into the object-space displacement.

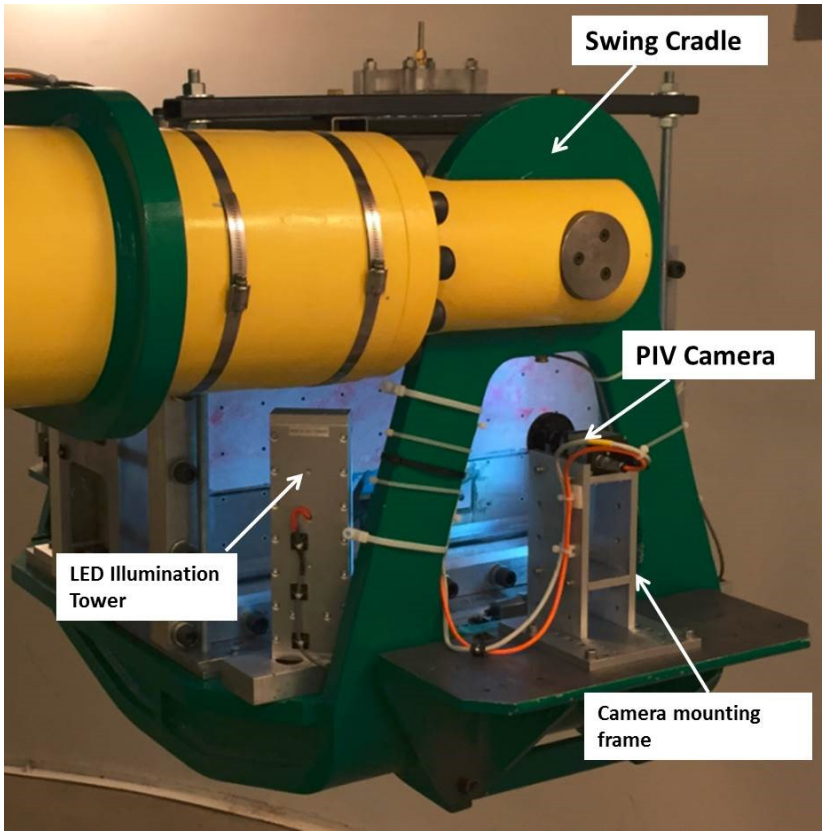

Figure 6-7 The PIV Setup.

6.1.4 Mariotte Bottle

Mariotte Bottle (Thorel et al. 2002) has been successively used in centrifuge applications to maintain the water table inside the centrifuge model. As shown in Figure 6-8a, the Mariotte Bottle is capped at the top with a tube connecting to atmosphere. The lowermost point of the tube (point A) determines the water table to be maintained during testing

(Figure 6-8b). As shown in Figure 6-5, the Mariotte Bottle is connected to the top of the GeoCDM at two locations using copper tubes. Communication between the Mariotte Bottle and the top of the GeoCDM can be controlled using the control valves (Figure 6-5). The position of the steel tube inside the Mariotte Bottle can be adjusted according to the water table to be maintained inside the plane-strain box.

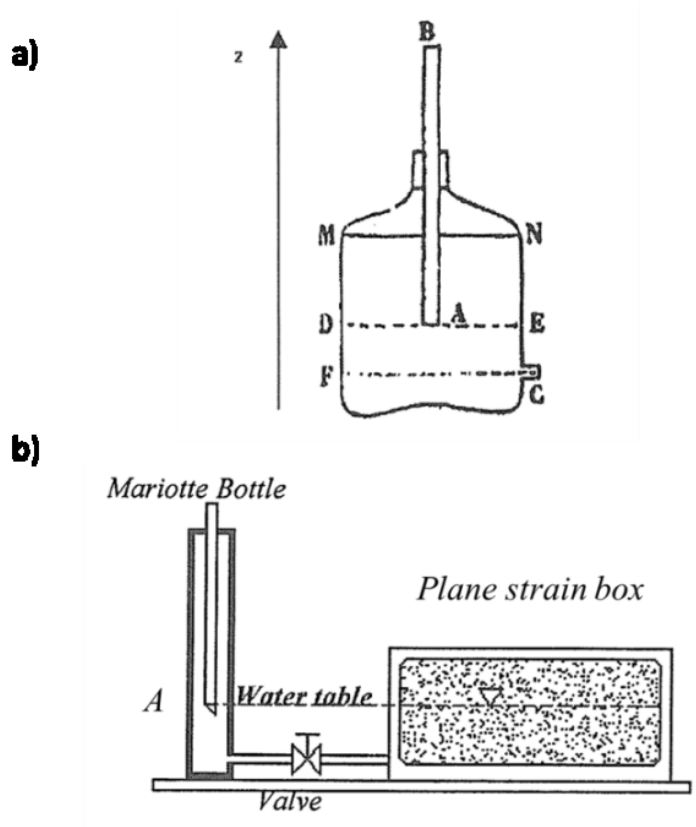

Figure 6-8 a) Schematic Mariotte Bottle b) Mariotte Bottle connected to plane-strain box (after Thorel et al., 2002)

6.2 GeoCDM Centrifuge Testing Procedure

6.2.1 Installation of GeoCDM at the Base of Plane-strain box

Before preparation of overconsolidated Speswhite kaolin, the GeoCDM has to be installed appropriately at the base of the plane-strain box. Most importantly, all the moving parts should be lubricated appropriately using lubricant grease (Figure 6-9). The mechanical parts of GeoCDM will be submerged in water for about one month, which

will cause rusting of the metal parts without any protection. During 1g consolidation and 100g GeoCDM uplifting, there might be some debris or kaolin materials falling in between the worm gears. The lubricant grease will protect the metal from rusting during the consolidation stage, which takes 3 to 4 weeks. And during GeoCDM uplift at 100g, it also helps the gears move smoothly at high gravitational fields.

The center-lifting table should be installed horizontally; otherwise, it will be locked between the back plate and the Perspex glass during GeoCDM uplift. The top of the GeoCDM is covered with porous stone, which is fixed using screws. A piece of geotextile and a piece of filter paper are placed on top of the porous stone successively.

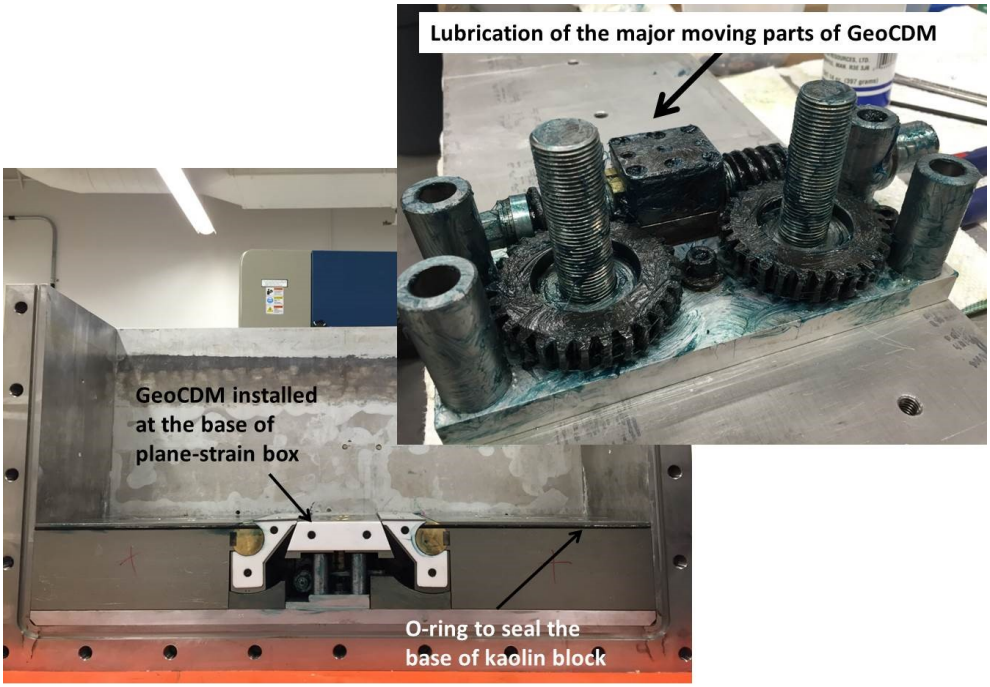

Figure 6-9 Installation of GeoCDM at the base of plane-strain box and lubrication of GeoCDM.

As shown in Figure 6-10b, the side blocks have hollow parts and O-ring is used to prevent fluid from leaking into these hollow parts. Two screws are employed to fix each side block to the base plate. A hole in the center of each side block is drilled to facilitate the bottom drainage during 1g consolidation (Figure 6-10a).

The height of the center-lifting table of the GeoCDM is measured before and after test for the purpose of checking the movement of the GeoCDM during shearing/deflection of the kaolin block.

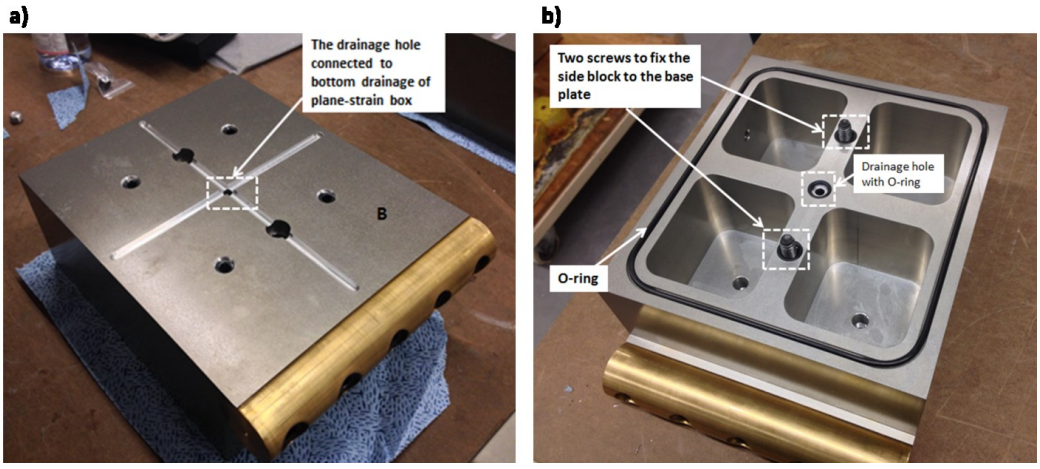

Figure 6-10 The side blocks of GeoCDM.

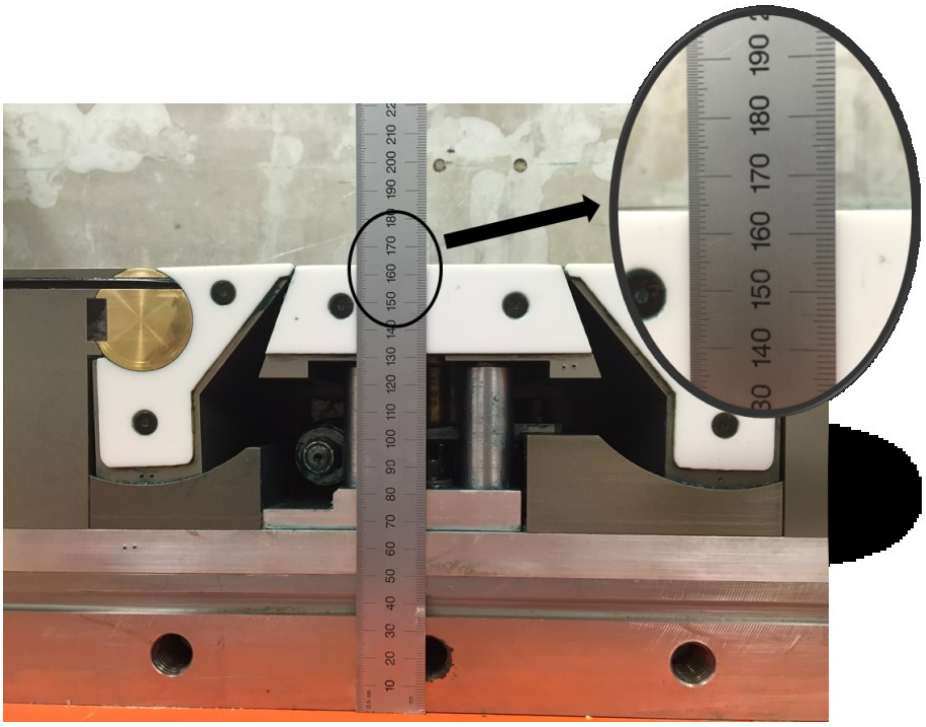

Figure 6-11 Measure the height of the center-lifting table.

6.2.2 Preparation of Over-Consolidated Speswhite Kaolin

Based on previous test results, Speswhite kaolin powder of 37.8kg mixed with water at 100% water content should be used to make smooth kaolin slurry to make 20cm thick Speswhite kaolin block.

During consolidation stage, an aluminum plate instead of the Perspex glass will be used to protect the glass from scratching. The surface of the aluminum plate is cleaned and then attached with a thin layer of transparency, which is used to prevent the reaction between water and the aluminum plate. Silicone grease is coated to both the aluminum plate and the back plate to reduce friction during consolidation.

After installation of the aluminum plate and the extension, the GeoCDM should be saturated with deionized water. Then, kaolin slurry is carefully scooped into the plane-strain box to avoid intrusion of air bubbles. The surface of the kaolin slurry should be made as flat as possible, and then a piece of filter paper and a piece of geotextile is placed above the slurry successively. A whole piece of porous stone is placed above the geotextile and then the loading frame as shown Figure 6-12 is carefully placed above the porous stone. The kaolin slurry is left overnight for stabilization and then it is consolidated step by step. For each step, the consolidation pressure should not exceed two times the consolidation pressure for the previous step. For this test, a consolidation sequence of 5kPa, 10kPa, 20kPa, 40kPa, 80kPa, 160kPa, 320kPa, 640kPa, 1000kPa, and 1450kPa is used. To ensure the saturation of the base of the kaolin block, two bottom drainage ports are connected to standpipes with deionized water (Figure 6-12).

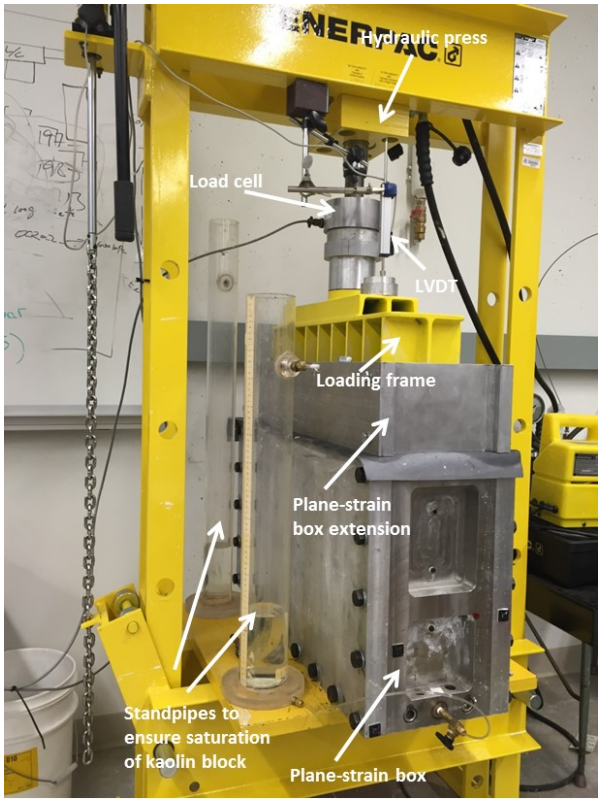

Figure 6-12 The 1g consolidation setup.

6.2.3 Installation of Kulite Pore Pressure Transducer

The installation procedure of the Kulite PPT is described in details in section 3.2. The Kulite PPT should be installed right before the last stage of consolidation (1450kPa). After completion of 1000kPa consolidation, pressure on top of the kaolin block should be released to prepare for the installation of Kulite PPT. During installation, the sample undergoes swelling and suction is developed within the sample. It is necessary to plan ahead and have all necessary equipment prepared to make the installation proceed smoothly and quickly. The Kulite PPT should be connected to the data logger during installation for observation and recording of PPT readings. The readings recorded when the Kulite PPT is kept saturated in water is considered as the reference for future readings. The Kulite PPT is installed through the tappings made at the back plate of the plane-strain box.

6.2.4 Replacement of the Aluminum Plate with Perspex Glass

After the 1450kPa consolidation is done, the kaolin block should be unloaded for the following centrifuge tests. It is important to unload the sample step by step to eliminate the possibility of nucleation within the kaolin block (Take, 2003).

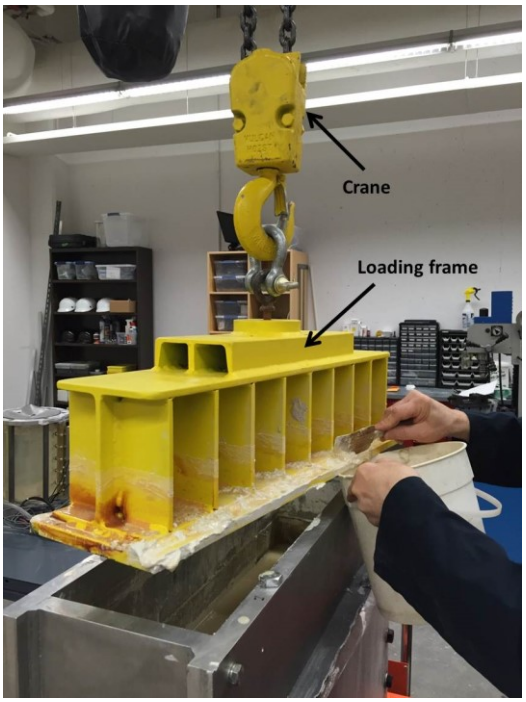

Figure 6-13 Remove the loading frame.

After releasing the pressure on top of the kaolin block, the plane-strain box is moved to the preparation room (L2-028) and the crane is used to remove the loading frame as suction is developed in between the loading frame and the top of the kaolin block (Figure 6-13). Water/kaolin mixture on top of the kaolin block is removed using a vacuum cleaner after removal of the loading frame.

Then the aluminum plate should be removed. A new method is adopted instead of directly pulling the plate off the plane-strain box. If the plate is directly pulled off, kaolin will be pulled off at the same time, creating a significantly disturbed surface. The new method is to make the aluminum plate seated on the edge of a cart with fixed height and then increase the height of the adjustable cart, during which, the aluminum plate will be

separated from the plane-strain box with the aid of self-weight (Figure 6-14). Using this method, a smooth kaolin surface can be created.

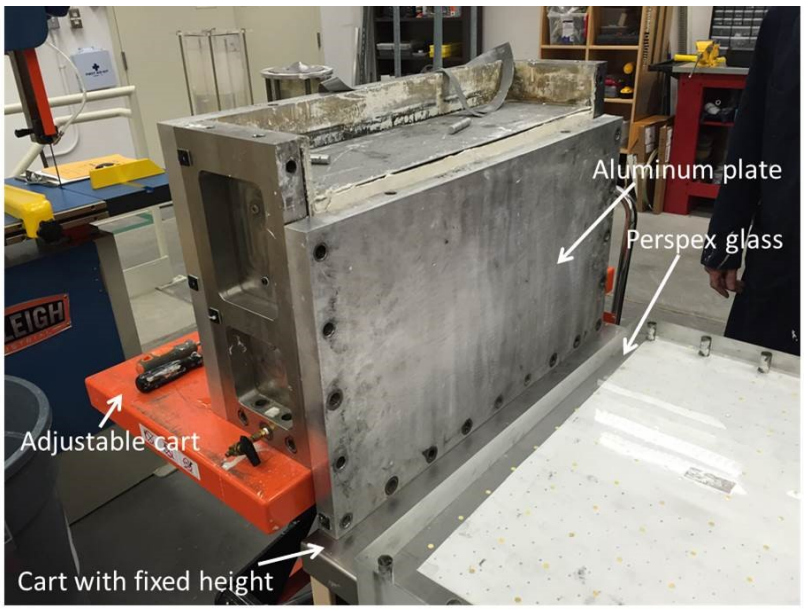

Figure 6-14 Remove the aluminum plate.

The surface of the Perspex glass is attached with a thin layer of transparency to protect the control markers as well as the Perspex glass itself. A thin and uniform layer of silicone grease is coated onto the transparency and then red dyed sand is blown softly onto the Perspex glass, which will help increase the texture of the kaolin block. Then the Perspex glass is installed onto the plane-strain box.

6.2.5 Preparation of the GeoCDM Test Package

To maximize the testing space in the plane-strain box, the overburden is simulated using closely packed lead bars. After installation of the Perspex glass, a layer of geotextile is placed on top of the kaolin block and then lead bars are carefully placed on top of it.

Mariotte Bottle is installed on the back plate and the position of the steel tube inside the bottle is adjusted based on the water table to be maintained in the centrifuge model. Deionized water is filled into the Mariotte Bottle and the copper tubes are connected to

the top of the GeoCDM. Then the plane-strain box is craned into the swing cradle of the centrifuge (Figure 6-15), where all the instrumentation connection, PIV camera setup and cabling work are finished.

Above the kaolin block, there is a certain thickness of deionized water, which should be poured into the plane-strain box a few hours before the centrifuge spinning. If soaked in water for a long period, the top of the kaolin block will be softened. There is 5mm thick light mineral oil on top of the water to prevent water evaporation during long hour centrifuge spinning.

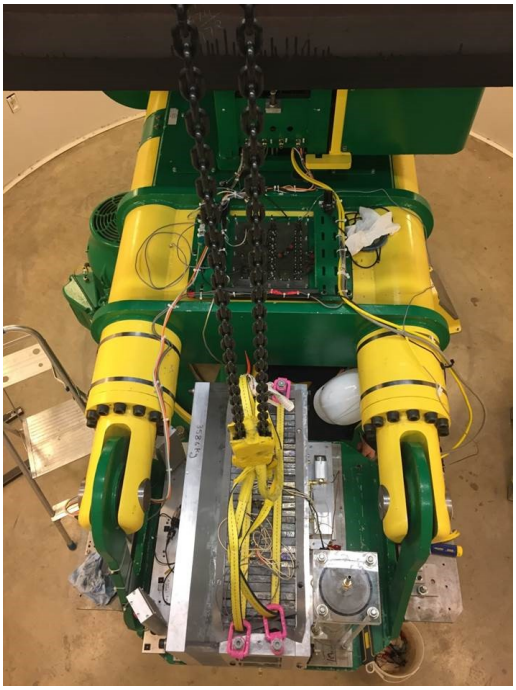

Figure 6-15 Crane the plane-strain box to the swing cradle.

The camera position, lens focus and aperture, LED light tower angles, and LED light brightness of the PIV system should be fine adjusted to take clear images of the centrifuge model without obvious glares on the Perspex glass. The data acquisition system (DAS) should also be readied by entering the calibrations for each instrument and checking whether the initial readings of each instrument make sense. The communication between the control software and the Parker servo motor should be tested to ensure the

appropriate working condition of the motor as well as the communication network. All these work should be conducted one day before the centrifuge testing.

6.2.6 100g Consolidation

During centrifuge testing, the g-level is increased step by step until reaching 100g. At 100g, the kaolin block undergoes consolidation due to the increase of overburden pressure. It takes time to dissipate excessive pore pressures inside the kaolin block. There are direct measurements of pore pressures in the middle and at the base of the kaolin block; thus the degree of consolidation can be judged based these readings.

6.2.7 100g GeoCDM Uplifting

Once 100g consolidation is finished, the GeoCDM is readied to uplift/shear the kaolin block at a certain velocity. The major controlling parameters of the Parker servo motor are Proportional Gain and Derivative Gain (Figure 6-16), which should be tuned before starting the servo motor. Currently, the target movement of GeoCDM is controlled by the "Incremental Distance" on the motor control interface (Figure 6-17). An incremental distance of 1200 means 1mm travel of the GeoCDM center-lifting table based on current settings. And the movement of GeoCDM could be observed from the indicator of "Actual Position -Scaled" (Figure 6-17). To minimize the influences of slack in the transmission system, the GeoCDM is pre-run for an incremental distance of 200 before uplifting/shearing the kaolin block.

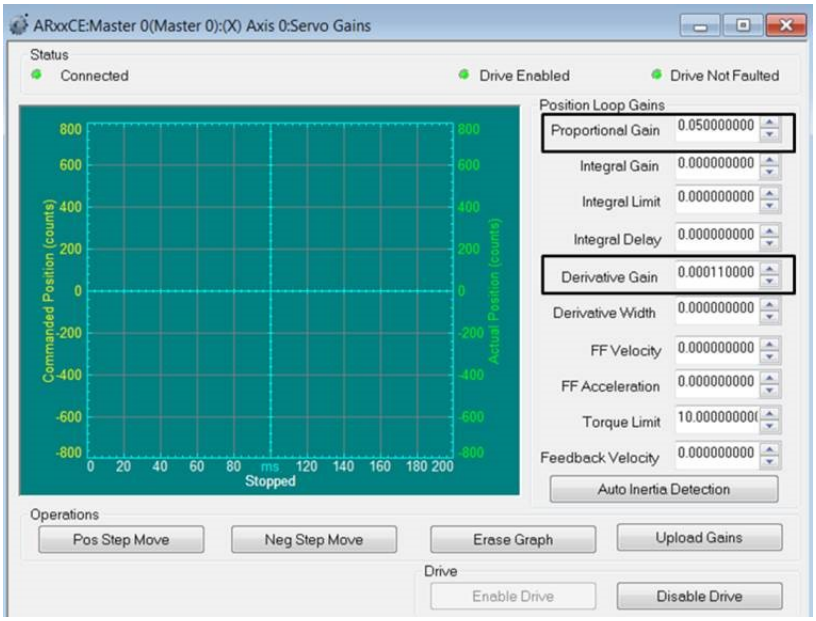

Figure 6-16 The Parker servo motor tuning interface.

Figure 6-17 The Parker servo motor control interface.

6.3 Preliminary GeoCDM Centrifuge Tests

6.3.1 100g GeoCDM Centrifuge Test with Commercial Clay Block (Test #1)

Preparing an overconsolidated Speswhite kaolin block takes about four weeks. Thus, a quick 100g centrifuge test was conducted with precast commercial clay blocks placed in the plane-strain box to test the GeoCDM setup, including the PIV system. The external PPT was installed to monitor the pore pressure changes at the base of the clay block. No Kulite PPTs were installed for this test.

The test setup is presented in Figure 6-18 and the GeoCDM was set to deflect the clay block by 20mm in 6 hours. The clay block had a thickness of 16cm at Earth's gravity and 74kg of lead bars were placed on top of it. At 100g, these lead bars will apply a vertical pressure of 520kPa. Above the top of the clay block, there was 8cm thick water. A thin layer of mineral oil was put on top of water to prevent evaporation and the position of steel tube inside the Mariotte Bottle was adjusted according to the water level inside the model.

The centrifuge model was spun at 50g first for 15 minutes to let the system stabilize. Then the g-level was increased to 100g. The uplifting of the GeoCDM was initiated 45min after the g-level was increased to 100g.

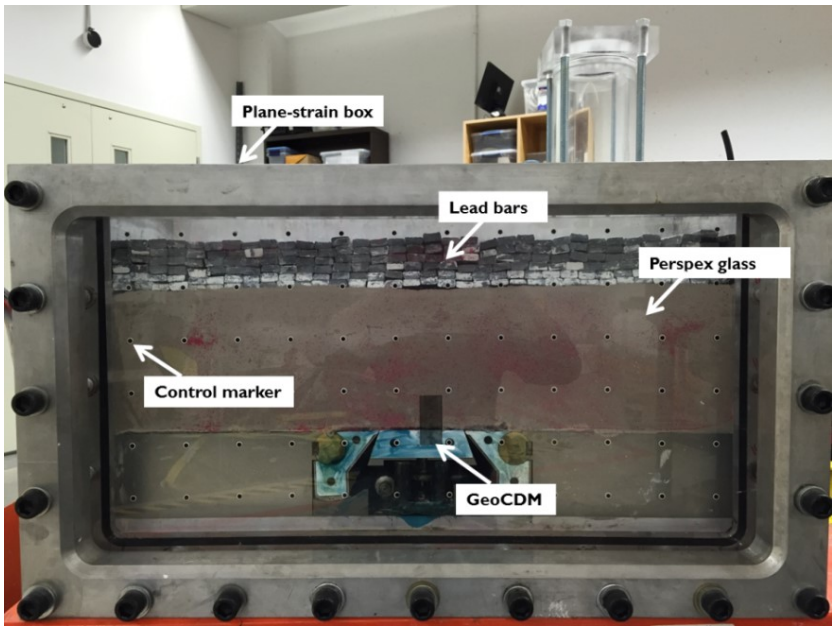

Figure 6-18 Plane-strain box with commercial clay block and lead bars.

6.3.1.1 Pore Pressure Readings

The pore pressure readings at the base of the kaolin block were supposed to be maintained at around 240kPa during GeoCDM uplifting. However, as shown in Figure 6-19, the pore pressure kept decreasing, which happened mainly because of the unsaturation of the clay block.

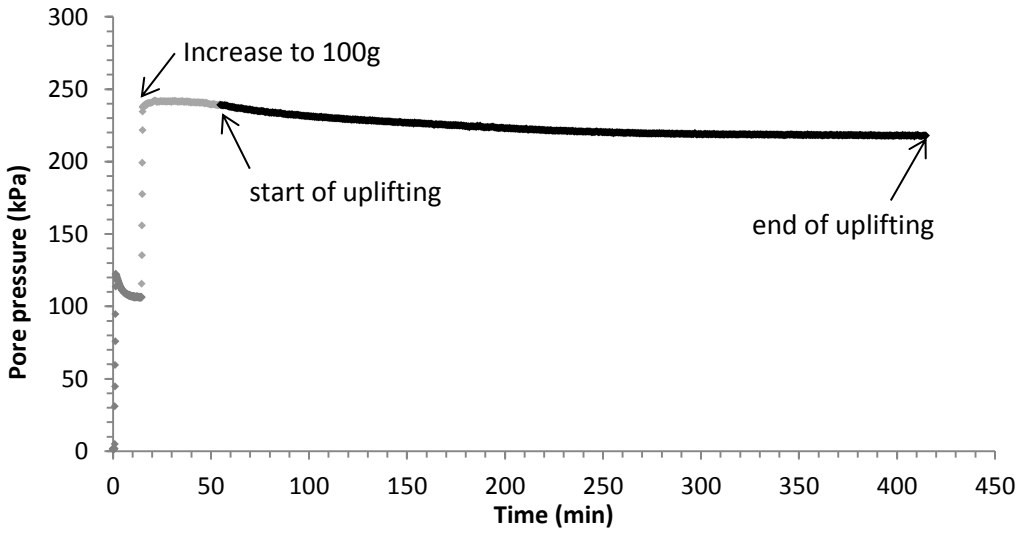

Figure 6-19 Pore pressure readings at the base of the GeoCDM.

6.3.1.2 PIV Results

The positions of the center-lifting table before and after test were measured and the maximum GeoCDM uplift was measured at 19.9mm. The measured movement agrees with the GeoPIV analysis results, which verifies the capacity of PIV tracking soil displacement within the GeoCDM setup. Figure 6-20 shows a linear GeoCDM movement during the 20mm/6hr test, which indicates a good mechanical performance of GeoCDM at 100g as well as the accuracy of PIV analysis results.

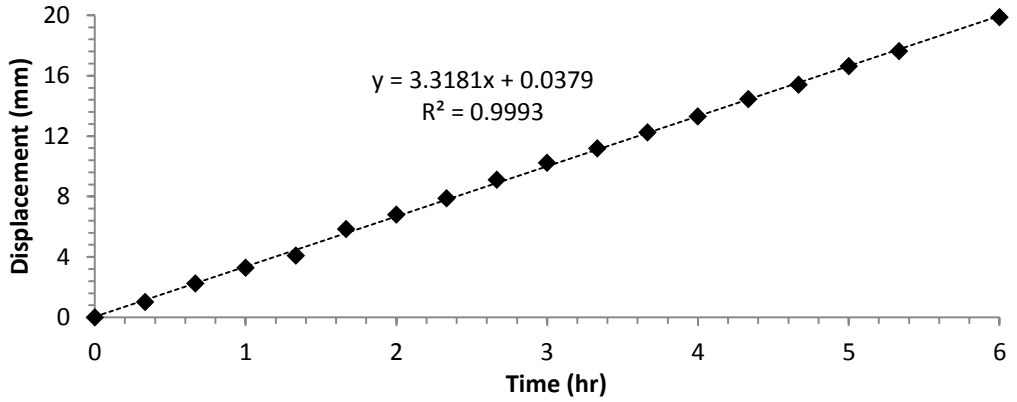

Figure 6-20 GeoPIV analyzed GeoCDM movement.

Figure 6-22 shows the image-space displacement vectors across the whole area of caprock and overburden when the GeoCDM moves up by 5.5mm. Figure 6-23 is the zoomed view of the displacement vectors around GeoCDM areas. And Figure 6-24 is the transformed object-space displacement vectors. The direction and magnitude of the displacement vectors at the center-lifting table area prove that the PIV system works within the GeoCDM setup. However, there are some displacement vectors missing in areas A, B, C, D and E (Figure 6-24). For area A, the PIV analysis is impeded because of the ruler attached to the Perspex glass, which does not move during GeoCDM uplift. For areas B, C, D and E, there are no reasonable results because of the imperfect sealing at the base of caprock. As the testing went on, more materials were forced down to the base

of the plane-strain box at high gravitational field, which significantly destroyed the material textures (Figure 6-21). Most of the materials were leaking along the areas indicated by the bold black lines as shown in Figure 6-21; meanwhile, some materials were leaking through the uplifting area of the GeoCDM.

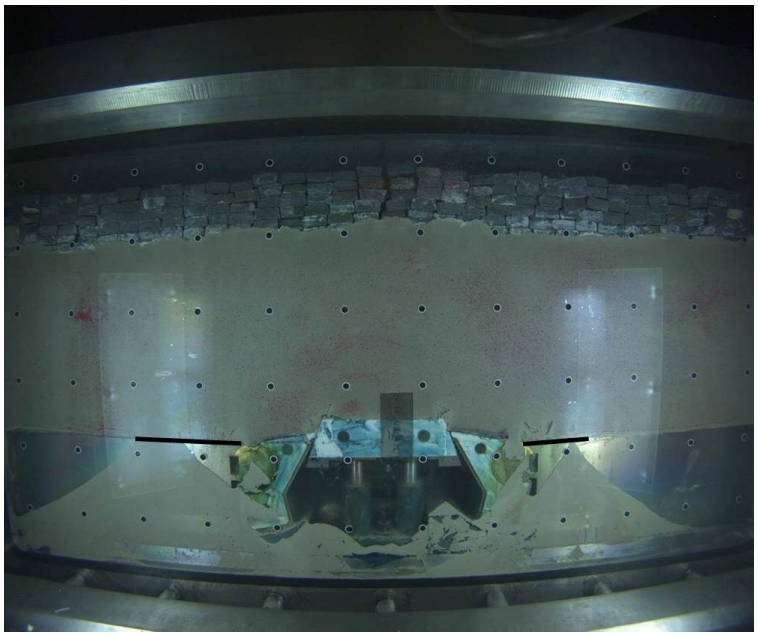

Figure 6-21 The centrifuge model at the end of the test #1.

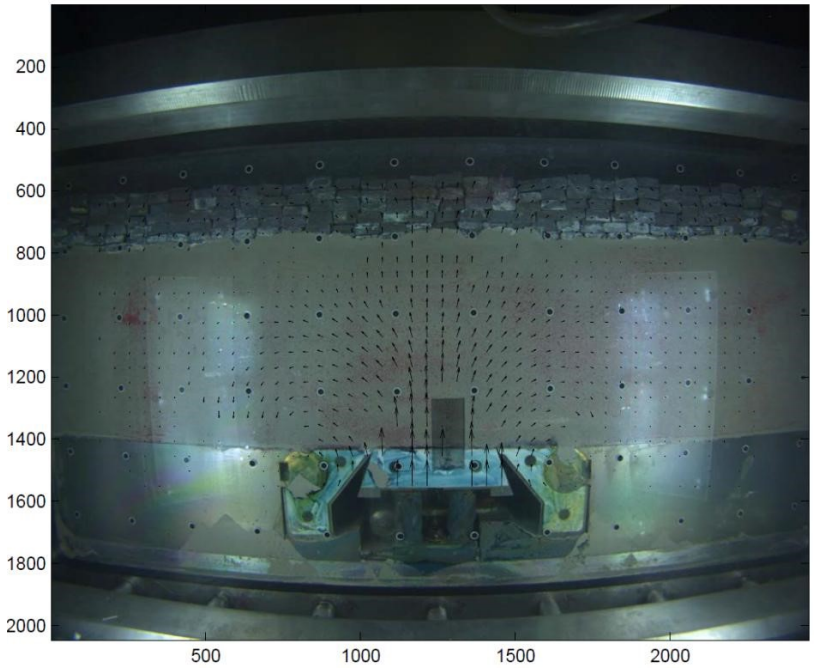

Figure 6-22 Image-space displacement vectors when the GeoCDM moves up by 5.5mm (unit in pixel).

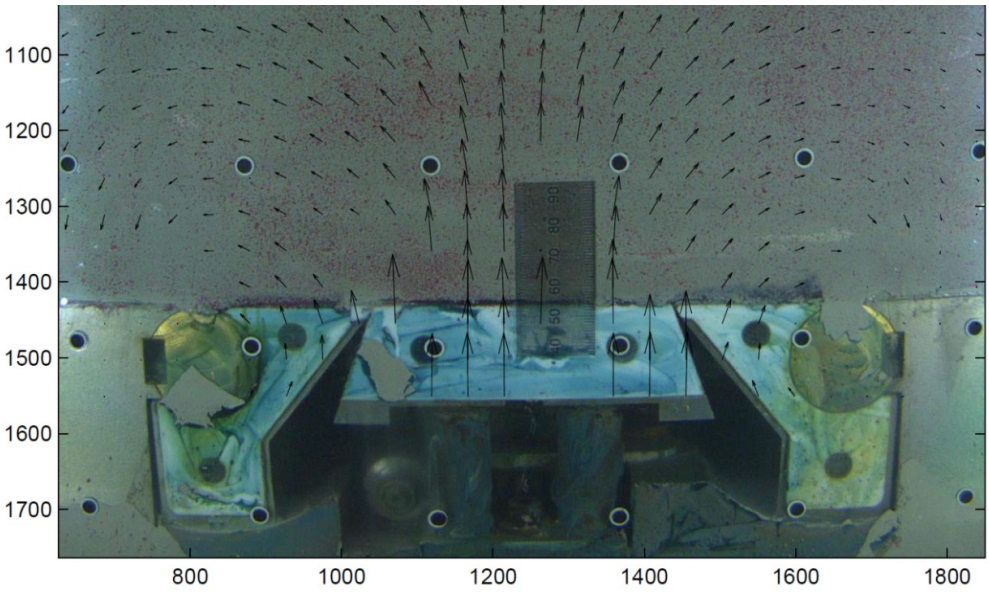

Figure 6-23 Zoomed view of the displacement vectors at the GeoCDM area when the GeoCDM moves up by 5.5mm (unit in pixel).

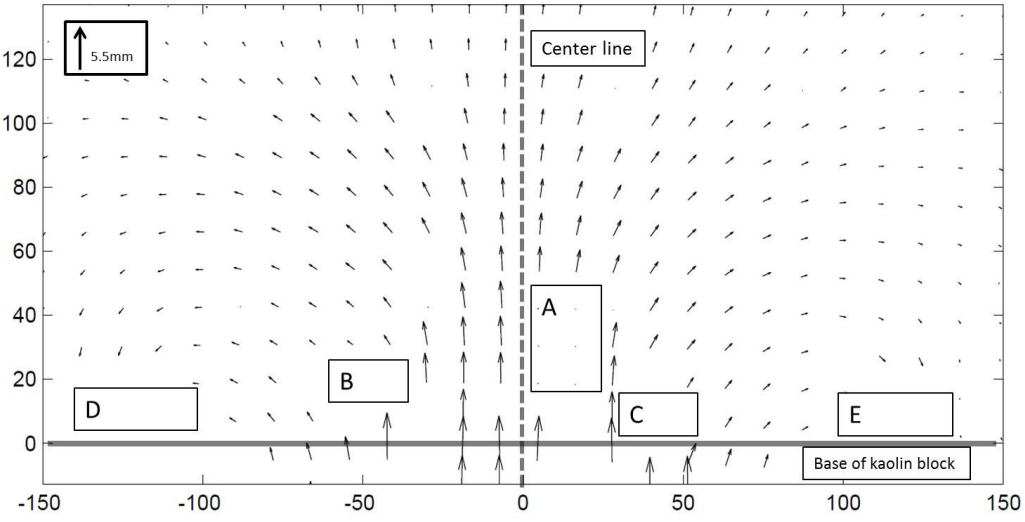

Figure 6-24 Object-space displacement vectors when the GeoCDM moves up by 5.5mm (unit in mm).

6.3.2 Preliminary 100g Test results with Overconsolidated Speswhite Kaolin (Test #2)

A 100g GeoCDM centrifuge test with over-consolidated Speswhite kaolin was conducted following the testing procedures described in section 6.2. The kaolin block had a thickness of 20cm with 86.2kg of lead bars overlying it. At 100g, these lead bars will

exert a vertical pressure of 600kPa. Water table was 10cm above the top of the kaolin block and the position of the tube inside the Mariotte Bottle was adjusted accordingly. PIV camera position was adjusted to take images which can cover the full area of the Perspex glass as shown in Figure 6-25. The aperture and focus of the camera lens were fine adjusted to take clear images of the centrifuge model, which is vital for the post-test soil displacement analysis. Two O-rings were installed within the grooves fabricated at the top of the side blocks to prevent kaolin materials from leaking to the base of the plane-strain box according to results of Test #1.

The centrifuge was run at 50g first for about 30 minutes to let the system stabilize. Then the g-level was increased to 100g. When the 100g consolidation was finished, the GeoCDM was set to uplift by 20mm in 36 hours.

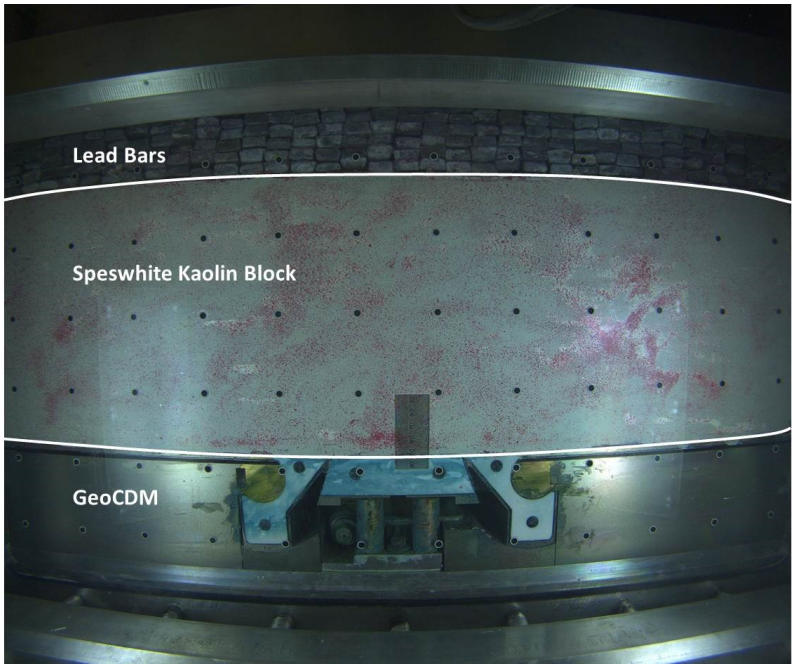

Figure 6-25 An image of the GeoCDM setup taken by PIV camera before centrifuge spinning.

6.3.2.1 Pore Pressure Readings

As discussed in Section 6.2, two Kulite PPTs and one external PPT were used during testing. The Kulite PPT installed in the center of the kaolin block did not work

appropriately. Figure 6-26 shows the pore pressure readings in the middle (Kulite PPT) and at the base (external PPT) of the kaolin block.

Figure 6-27 shows the pore pressure changes in the middle of the kaolin block from the start of 100g consolidation to the start of GeoCDM uplift, according to which, it can be judged that the primary consolidation was finished when the GeoCDM started to uplift.

Ideally, pore pressure at the base of the kaolin block should be maintained during 100g consolidation and GeoCDM uplift if the Mariotte Bottle worked appropriately. However, as shown in Figure 6-26, pore pressure at the base of the kaolin block kept decreasing, which was caused by the leaking through the connection area of the plane-strain box and its extension at the Perspex glass side. As the water table inside the plane-strain box decreases, Mariotte Bottle tries to compensate the water head loss. Consequently, the water level inside the Mariotte Bottle will decrease. Once the water level gets lower than the lowermost point of the tube, the Mariotte Bottle fails. According to post-test observations, water level inside the Mariotte Bottle was 3.6cm below the steel tube.

During GeoCDM uplift, the pore pressure difference in the middle and at the base of the kaolin block was maintained at around 100kPa, which is reasonable as half of the kaolin block thickness is around 10cm. At 100g, 10cm water head equals to 100kPa water pressure.

After the centrifuge was stopped, pore pressure at the base of the kaolin block was reduced to around 2kPa, while pore pressure in the middle became negative, as the pressure on top of the kaolin block was reduced and thus suction was developed. Then the magnitude of the negative pressure would decrease gradually as shown in Figure 6-26.

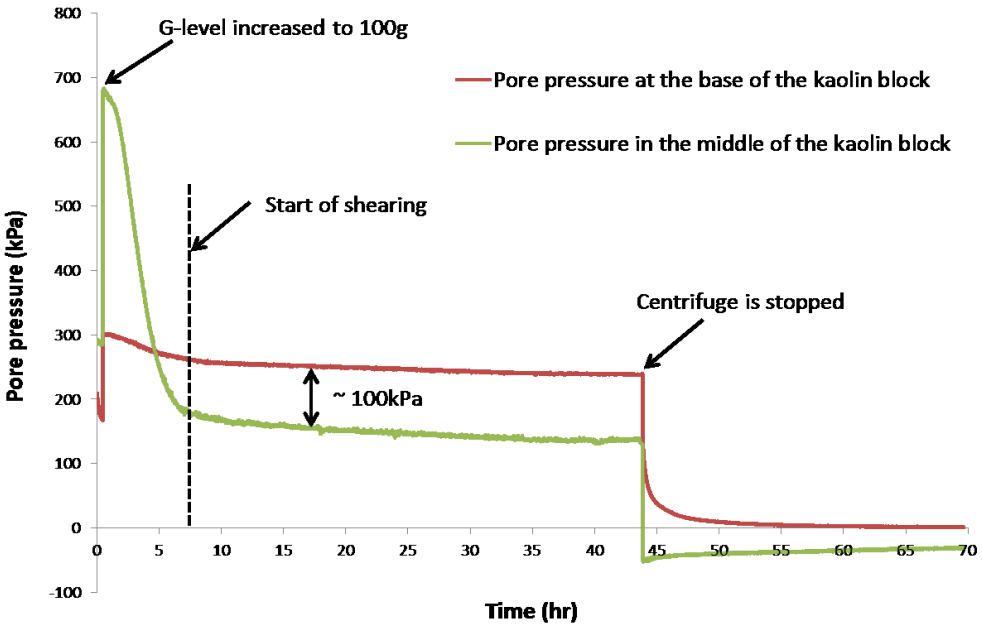

Figure 6-26 The pore pressure readings in the middle and at the base of the kaolin block during and after centrifuge spinning.

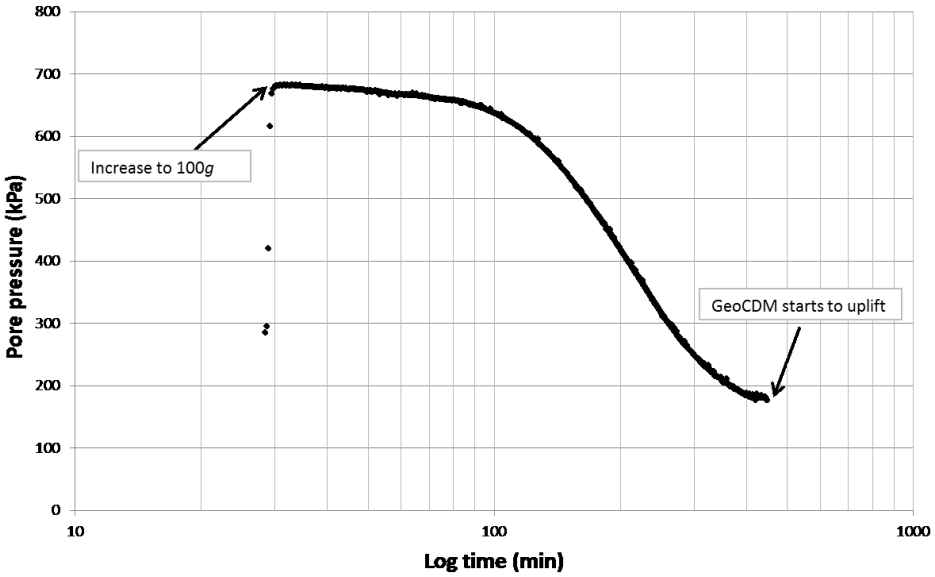

Figure 6-27 The pore pressure in the middle of the kaolin block during 100g consolidation.

6.3.2.2 PIV Results

As discussed in section 6.3.1.2, the sealing at the base of the caprock is a problem. O-rings are used in the side block areas. When the g-level is increased to 100g, the lateral stress exerted on the Perspex glass becomes much larger, causing tiny gaps between the

GeoCDM and the glass. However, the base of the kaolin block is sealed using O-rings only at the areas of the fixed side blocks (Figure 6-25). kaolin material attached to the Perspex glass along with the red dyed sand is forced down to the base of the plane-strain box through the gaps in the uplifting area of the GeoCDM (Figure 6-28), which will destroy the material textures and result in poor PIV analysis outcomes. As the testing goes on, situation becomes worse as more materials are forced down and wider areas are influenced. Figure 6-29 shows the PIV analyzed image-space displacement vectors for in-flight consolidation. Most materials forced down are from Area A; thus the material textures in that area are significantly destroyed and no reasonable displacement vectors could be generated by PIV analysis. During GeoCDM uplift, the displacement vectors in Area A are of the greatest significance; however, without sufficient material textures, no reasonable results could be produced from PIV analysis either.

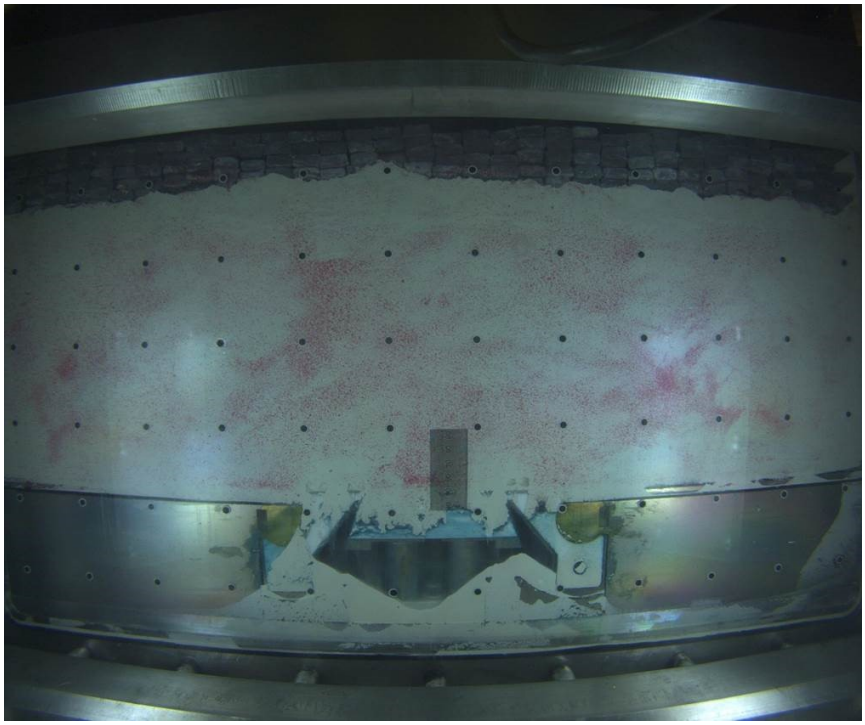

Figure 6-28 The PIV image taken at the end of 100g consolidation.

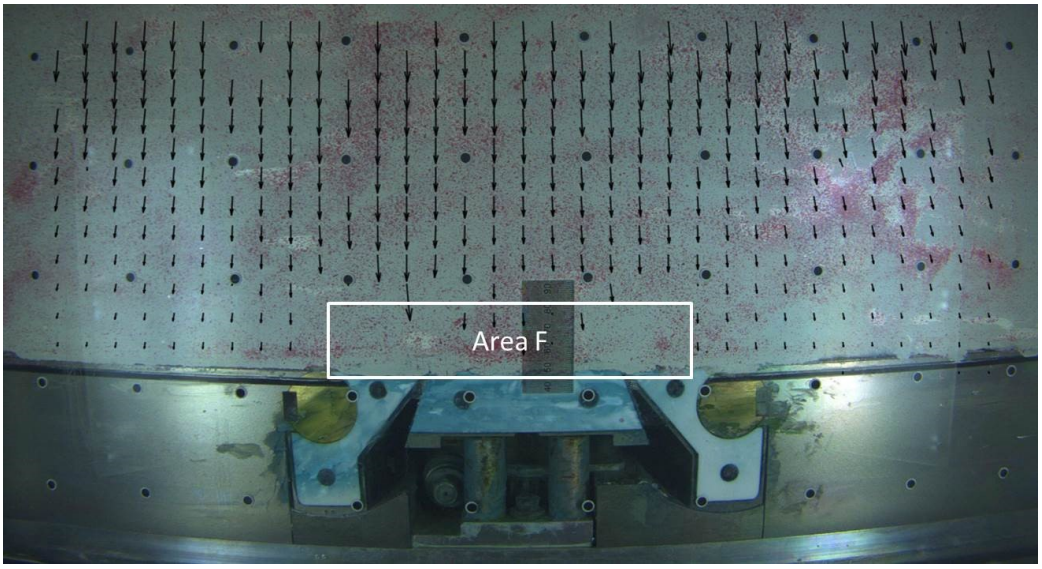

Figure 6-29 Image-space displacement vectors for in-flight consolidation

6.4 Summary and Discussion

In this chapter, a detailed description of the GeoCDM centrifuge testing setup is presented and the full procedure of conducting GeoCDM centrifuge testing is discussed. Two preliminary GeoCDM centrifuge tests were conducted. The first one (Test #1) was conducted using precast commercial clay block to test the GeoCDM as well as the PIV system and the second test (Test #2) followed the full procedure of GeoCDM centrifuge testing described in section 6.2.

- GeoCDM

In Test #2, the transmission system of the GeoCDM was submerged in water for more than one month. The lubricant grease worked effectively in preventing rusting of the metal parts. Even though the lubricant grease is lighter than water, it remained on the surface of the mechanical parts of the GeoCDM instead of migrating up to the base of the kaolin block during 100g centrifuge spinning. Also the lubricant grease helped facilitating the smooth movement of the transmission system of the GeoCDM. The PIV analyzed displacement of the GeoCDM in Test #1 indicates a smooth mechanical performance of GeoCDM at 100g.

- Pore Pressure Transducers

Internal pore pressure changes of the kaolin block are monitored using the Kulite miniature pore pressure transducers (PPTs) installed in middle of the kaolin block, based on which the degree of in-flight consolidation can be judged. Also, the kaolin block is set to be uplifted/sheared in a drained condition, which can be identified according to the Kulite PPT readings. If the kaolin block is uplifted/sheared in a drained condition, the Kulite PPT readings should remain unchanged. The pore pressure at the base of the kaolin block is maintained using the Mariotte Bottle and monitored using an external PPT. According to Test #2 results, the Kulite PPT works well in monitoring the pore pressure changes inside the kaolin block. Both Test #1 and Test #2 results indicate that the external PPT functions well within the GeoCDM setup.

- PIV system

The deformation of the kaolin block during centrifuge spinning is measured by the PIV system. Caprock integrity in this research is studied as a plane-strain problem, thus the measured deformation of the plane attached to the Perspex glass can represent the deformation of the whole kaolin block. PIV analysis of the kaolin block deformation is significantly dependent on the material textures, which are created by adding red dyed sand to the surface of the kaolin block attached to the Perspex glass.

The GeoCDM movements as well as kaolin block deformation during uplifting were successfully tracked by the PIV system in Test #1, which was a 7-hour test. However, there were test materials leaking to the base of the plane-strain box from the top of the side blocks, which compromised the PIV analysis results. When g-level was increased to 100g, the lateral stress exerted on the Perspex glass by the test material was significantly increased. Thus, tiny gaps were created between the GeoCDM and the Perspex glass

because of the Perspex glass deformation. For areas where significant leaking happened, no reasonable PIV results could be generated due to lack of sufficient material textures.

To prevent the leaking at the base of the kaolin block, two O-rings were installed at the top of the side blocks for Test #2, which was a 48-hour test. For Test #2, material leaking from the top of the side blocks was successfully prevented, which indicates that the O-rings are appropriate for preventing material leaking within the GeoCDM setup. However, the lateral stress exerted on the Perspex glass was higher than that in Test #1 and the testing hour was much longer than Test #1. Consequently, material leaking was concentrated in the uplifting area of the GeoCDM and more material texture destruction was experienced. Thus only the PIV analysis results for in-flight consolidation could be generated. No reasonable results of the GeoCDM uplifting could be made.

The test results reported in this thesis are the very early, initial tests conducted with the full system. Improvements in hardware configurations and testing protocols, based on these initial tests, have significantly improved the results of subsequent tests.

Chapter 7 : Conclusions and Recommendations

7.1 Conclusions

7.1.1 Numerical Work

Caprock in this research is deemed as homogeneous material without any pre-existing faults or weak planes inside. Consequently, no failures along the faults or weak planes are considered. Shearing failure and tensile failure are the two major failure modes of caprock to be explored in this research using decoupled reservoir geomechanical simulation approach.

A thorough analysis of caprock behaviour in the Reference Case is conducted by analyzing the shearing zone development in caprock along with the displacement profile evolution at the base of caprock. Tensile failures of oilsands at the base of caprock are observed as the steam injection pressure exceeds the minimum principal stress. As the steam chamber spreads horizontally, oilsands tensile failure zones propagate concurrently. Pore pressures building up at the base of caprock as well as the oilsands reservoir expansion are the source of the large vertical displacement at the base of caprock, which causes the development of shearing zones in caprock starting from the edges of the oilsands tensile failure zones. Caprock shearing failure happens when the shearing zones go through the whole caprock formation.

Overconsolidated Speswhite kaolin is employed to mimic the caprock in centrifuge models to eliminate the influences of the property variability of in-situ caprock materials. However, triaxial test results reveal that there is significant geomechanical difference between overconsolidated Speswhite kaolin and caprock shale in terms of material stiffness, strength and dilation after shearing failure. Consequently, parametric analysis is

a necessity to study the influences of different property on caprock behaviour in SAGD process. According to the parametric analysis results, caprock shearing failure driven by the vertical displacement at the base of caprock is commonly observed for caprock with different geomechanical properties. The geomechanical property differences will influence the span and magnitude of the vertical displacement profiles at the base of caprock when caprock shearing failure is reached. Other than that, the shape and characteristics of the vertical displacement profiles are the same. The patterns of the caprock shearing failure are also the same.

Ideally, the vertical displacement profile from reservoir geomechanical simulations should be fully applied at the base of caprock in centrifuge models. However, constrained by the dimensions of the plane-strain box and the complexity of fully implementing such vertical displacement profiles, an alternative solution of the centrifuge simplified vertical displacement (cSVD) is figured out based on three requirements as 1) containable in the plane-strain box 2) executable at 100g centrifuge spinning 3) can generate similar stress and strain fields in the caprock comparing to those in the prototype. A separate FLAC geomechanical model with only caprock and overburden is built with cSVD applied at the base of caprock. The calculated stress and strain fields along with patterns of the caprock shearing failure are compared to those from reservoir geomechanical simulations and the cSVD can capture the characteristics of caprock behavior during SAGD process to a certain extent. This research focuses on the feasibility study of centrifuge modeling of caprock integrity, and the cSVD will be exerted at the base of caprock in centrifuge modeling.

7.1.2 Experimental Work

Development of preparation procedure of overconsolidated Speswhite kaolin block and installation procedure of Kulite miniature pore pressure transducers for internal pore

pressure measurement as well as the establishment of the particle image velocimetry (PIV) system for soil deformation measurement during centrifuge spinning are achieved during this research. Coring cylindrical samples out of the kaolin block for triaxial tests is documented. Mechanical properties of the overconsolidated Speswhite kaolin as well as the permeability properties are obtained through consolidated drained triaxial tests.

Another main contribution of the experimental work is the successful development of the Geomechanical Caprock Deflection Mechanism (GeoCDM) for applying the centrifuge simplified vertical displacement (cSVD) at the base of caprock in centrifuge models. Commissioning work on GeoCDM has been conducted to test the performance of this device at both 1g and 100g. A Mariotte Bottle (Thorel et al., 2002) is manufactured for maintaining the hydrostatic pressures inside the centrifuge model. Combing all these components together, a thorough centrifuge testing program of SAGD caprock integrity is developed and two preliminary 100g tests were conducted.

Results of the preliminary 100g GeoCDM centrifuge tests are positive with improvements to be done for subsequent tests. The GeoCDM is proven to be working smoothly and effectively during 100g centrifuge spinning. Kulite miniature pore pressure transducers are appropriately installed in the middle of the kaolin block following the installation procedure described in Chapter 3 and work effectively in delivering the real-time monitoring of internal pore pressure changes of the kaolin block. The external pore pressure transducer also functions well within the GeoCDM setup. The PIV system is capable of tracking the GeoCDM movements as well as the soil deformation within the GeoCDM setup. However, the faulty hydro-mechanical sealing at the base of the caprock compromised the PIV analysis results because the material textures of the areas where material leaking happened were destroyed. Modifications on the sealing at the base of the kaolin block are undergoing for subsequent tests.

7.2 Recommendations

7.2.1 Numerical Work

A simple scenario of one well-pair SAGD project is studied in this research. Caprock is deemed homogeneous material and no weak planes and pre-existing faults are considered. There are a few things, which could be incorporated into the numerical models for future studies.

Only the tensile failure of oilsands is observed. No tensile failure of caprock is investigated as the pore pressures inside the caprock are assumed to be hydrostatic during the process of SAGD operations to comply with the boundary conditions of the centrifuge model. However, there are pore pressure increases at the areas close to the base of caprock. Thus tensile failure of caprock should also be investigated in the reservoir geomechanical simulations.

Simulations of one well-pair SAGD are conducted in this research. For practical SAGD projects, there are typically multiple well-pairs, which might introduce different caprock failure modes and different displacement profiles at caprock failure. Therefore simulations on SAGD projects with multiple well-pairs should be conducted. Also for caprock formations, there are typically weak planes or faults inside due to geologic process. Weak planes or faults should also be incorporated into the numerical model.

7.2.2 Experimental Work

According to the preliminary 100g GeoCDM centrifuge test results, appropriate sealing at the base of the kaolin block is vital for the success of the centrifuge testing of caprock integrity. Sealing at the side block areas with O-rings proved to be working effectively in preventing leaking. However, without sealing at the uplifting area, testing material leaking was severe. A similar sealing system using the O-rings is now under development

for the uplifting area. Sealing at the side block areas is straightforward as the side blocks are fixed. However, the uplifting area keeps deforming during testing; thus the developed sealing system should be adjustable to the continuous deformation of the uplifting area.

Triaxial test results have revealed that there are significant differences between the caprock shale and the overconsolidated Speswhite kaolin in terms of stiffness, strength, and dilation behaviour after shearing. For studying caprock failure mechanism, it is of essence to create synthetic materials with close properties to the caprock shale. Addition of cement to the Speswhite kaolin powder seems a promising approach to explore for next stage of this research. Cai (2012) mixed dry sieved clay powder with Portland cement to create artificially cemented clay specimens and used the moist temping method to prepare homogeneous clay specimens. According to the direct shear test results on both uncemented and cemented clay specimens, it is found that strength and stiffness of specimens were significantly increased after cementation and the volumetric response changed from contractive (for uncemented clay) to dilative (for cemented clay) (Cai, 2012).

SAGD caprock integrity is studied as a plane-strain problem; thus measurement of the deformation of the plane attached to the Perspex glass could represent the deformation of the kaolin block. However, it would be ideal to have measurements of the internal deformations of the kaolin block to compare to the PIV analyzed results and in some cases for backup purposes. The fibre optic sensors (FOS) with the advantages of small size and lightweight construction and access to different measurands such as strain and temperature present a promising solution to internal deformation measurements (Kister et al., 2007). Fibre Bragg Grating Sensors are the most prominent example of the multiplexed fibre optic sensors, allowing measurements at multiple points along a single

fibre line, which enables the mapping of the internal strain field of the kaolin block (Inaudi et al., 2007).

The centrifuge simplified vertical displacement (cSVD) is developed due to the constraints of the testing space of the plane-strain box. The prototype is symmetric to the well-pair; thus by making use of the symmetry, only half of the model needs to be simulated. Idinger et al. (2011) used this technique to study the face stability of the shallow tunnel. By this way the using of the testing space of the plane-strain box can be maximized. Alternatively, a larger sized plane-strain box could be made for future tests.

Currently, the reservoir geomechanical simulations of SAGD caprock integrity provide the linkage between the prototype and the centrifuge model. Access to the field data in SAGD project will help verify and improve both the numerical and centrifuge physical modeling.

References

Azad, A., and Chalaturnyk, R. J., 2011. Numerical Study of SAGD: Geomechanical-flow Coupling for Athabasca Oil Sands Reservoirs. In Proceedings of the 45th US Rock Mechanics/Geomechanics Symposium, June 26-29, San Francisco.

ASTM Standard D7181-11, 2011. Method for Consolidated Drained Triaxial Compression Test for Soils. Volume i, pp. 1–11. ASTM International.

Butler, R. M., 1980. Method for Continuously Producing Viscous Hydrocarbons by Gravity Drainage while Injecting Heated Fluids. UK Pat. Appl. GB 2,053,328 (1980), also US 4,344,485 (1982), and Canada 1,130,201 (1982).

Bransby, M. F., Newson, T. A., Davies, M. C. R., and Brunning, P., 2002. Physical Modelling of the Upheaval Resistance of Buried Offshore Pipelines. In Proceedings of the 4th International Conference on Physical Modelling in Geomechanics, St. Johns, pp. 899-904.

Collins, P. M., Walters, D. A., Perkins, T., Kuhach, J. D., and Veith, E., 2013. Effective Caprock Determination for SAGD Projects. Journal of Canadian Petroleum Technology, 52(2), pp. 112-119.

Collins, P. M., 2007. Geomechanical Effects on the SAGD Process. SPE Reservoir Evaluation and Engineering, 10(4), pp. 367-375.

Chalaturnyk, R. J., 1996. Geomechanics of the Steam-assisted Gravity Drainage Process in Heavy Oil Reservoirs. Ph.D. dissertation, University of Alberta, Canada.

Cai, Q., 2011. Centrifuge, Analytical and Numerical Modeling of Normal Fault Propagation in Uncemented and Cemented Soils. Ph.D. dissertation, Hong Kong University of Science and Technology, Hong Kong.

Cao, J., 2003. Centrifuge Modeling and Numerical Analysis of the Behavior of Suction Caissons in Clay. Ph.D. dissertation, Memorial University of Newfoundland, Canada.

Chin, L. Y., Tomberlin, T. A., Ramos, G. G., and Chalaturnyk, R. J., 2012. Evaluation of Caprock Stability by Coupled Modeling of Geomechanics and Reservoir Simulation under Steam Injection for Producing Oil Sands Reservoirs. In Proceedings of the 46th US Rock Mechanics/Geomechanics Symposium, June 24-27, Chicago.

Dusseault, M. B., Yin, S., Rothenburg, L., and Han, H., 2007. Seismic Monitoring and Geomechanics Simulation. The Leading Edge, 26 (5), pp. 610-620.

Das, B. M., 2007. Fundamentals of Geotechnical Engineering. Cengage Learning.

Deisman, N., and Chalaturnyk, R. J., 2012. Comparative Stress Distribution in Coupled and Uncoupled SAGD Reservoir Simulation. In Proceedings of the 21st Canadian Rock Mechanics Symposium, pp. 401-411.

Ebrahimi, M., 2012. Steam Assisted Gravity Drainage: a Recipe for Success. World Academy of Science, Engineering and Technology, 61.

Grant, R. J., and Taylor, R. N., 2000. Tunneling-induced Ground Movements in Clay. In Proceedings of the ICE-Geotechnical Engineering, 143(1), pp. 43-55.

Gilbert, P. A., 1992. Geotechnical Centrifuge Use at University of Cambridge Geotechnical Center August – September 1991. Geotechnical Laboratory, Department of the Army Waterways Experiment Station, Corps of Engineers.

Gu, F., Chan, M., and Fryk, R., 2011. Geomechanical-data Acquisition, Monitoring, and Applications in SAGD. Journal of Canadian Petroleum Technology, 50(6), pp. 9-21.

Glisic, B., Inaudi, D., and Nan, C., 2002. Pile Monitoring with Fiber Optic Sensors during Axial Compression, Pullout, and Flexure Tests. Transport Research Record, 1808, pp. 11–20.

Han, H., Khan, S., Ansari, S. A., and Khosravi, N., 2012. Prediction of Injection Induced Formation Shear. In SPE International Symposium and Exhibition on Formation Damage Control. Society of Petroleum Engineers.

Inaudi, D., and Glisic, B., 2007. Overview of Fiber Optic Sensing Technologies for Geotechnical Instrumentation and Monitoring. Geotechnical News 25(3), pp. 27-31.

Idinger, G., Aklik, P., Wu, W., and Borja, R. I., 2011. Centrifuge Model Test on the Face Stability of Shallow Tunnel. Acta Geotechnica, 6(2), pp.105-117.

Li, P., 2006. Numerical Simulation of the SAGD Process Coupled with Geomechanical Behavior. Ph.D. dissertation, University of Alberta, Canada.

Li, P., and Chalaturnyk, R. J., 2006. Permeability Variations Associated with Shearing and Isotropic Unloading during the SAGD Process. Journal of Canadian Petroleum Technology, 45(1), pp. 54-61.

Li, P., Chalaturnyk, R. J., and Polikar, M., 2004. Issues with Reservoir Geomechanical Simulations of the SAGD Process. Journal of Canadian Petroleum Technology, 43(5), pp. 30-40.

Laue, J., 2002. Centrifuge Technology. In Workshop on Constitutive and Centrifuge Modeling, Two Extremes, Monte Verita, Rotterdam, Balkema, pp. 75-105.

Lee, S. W., Bolton, M. D., Mair, R. J., Hagiwara, T., Soga, K., and Dasari, G. R., 2001. Centrifuge Modelling of Injection near Tunnel Lining. International Journal of Physical Modelling in Geotechnics, 1(1), pp. 9-24.

National Energy Board, 2006. Canada's Oil Sands, Opportunities and Challenges to 2015: An Update. https://www.neb-one.gc.ca/nrg/sttstc/crdlndptrlmprdct/rprt/archive/pprtntsndchllngs20152006/pprtntsndchllngs20152006-eng.pdf

Ko, H. Y., 1988. Summary of the State-of-the-art in Centrifuge Model Testing. Centrifuges in soil mechanics, pp. 11-18.

Konig, D., Jessberger, H. L., Bolton, M. D., Phillips, R., Bagge, G., and Rienzi, R., 1994. Pore Pressure Measurement during Centrifuge Model Tests: Experience of Five Laboratories. In Centrifuge 94: International Conference, pp. 101-108.

Kister, G., Winter, D., Gebremichael, Y. M., Leighton, J., Badcock, R. A., Tester, P. D., Krishnamurthy, S., Boyle, W. J. O., Grattan, K. T. V., and Fernando, G. F., 2007. Methodology and Integrity Monitoring of Foundation Concrete Piles Using Bragg Grating Optical Fibre Sensors. Engineering Structures, 29(9), pp. 2048-2055.

Samieh, A. M., and Wong, R. C., 1997. Deformation of Athabasca Oil Sand at Low Effective Stresses under Varying Boundary Conditions. Canadian Geotechnical Journal, 34(6), pp. 985-990.

Total E&P Canada Ltd., 2007. Summary of Investigations into the Joslyn May 18th 2006 Steam Release. http://www.aer.ca/documents/reports/Total_Canada_Report_JoslynSteamRelease_2010-02.pdf

Taylor, R. N., 1995. Geotechnical Centrifuge Technology. London: Blackie Academic.

TBS, 2012. Operating Manual for GT50/1.7 Geotechnical Beam Centrifuge. Thomas Broadbent & Sons Ltd.

TBS, 2013. Image Acquisition Manual for GT50/1.7 Geotechnical Beam Centrifuge. Thomas Broadbent & Sons Ltd.

Take, W. A., 2003. The Influence of Seasonal Moisture Cycles on Clay Slopes. Ph.D. dissertation, University of Cambridge, UK.

Thorel, L., Favraud, C., and Garnier, J., 2002. Mariotte Bottle in a Centrifuge: a Device for Constant Water Table Level. International Journal of Physical Modelling in Geotechnics, 2(1), pp. 23-26.

Yuan, Y., Xu, B., and Palmgren, C., 2013. Design of Caprock Integrity in Thermal Stimulation of Shallow Oil-sands Reservoirs. Journal of Canadian Petroleum Technology, 52(4), pp. 266-278.

Uwiera, M., Carlson, M. R., Walters, D. A., and Palmgren, C. T., 2011. Geomechanical Simulation of Caprock Performance for a Proposed, Low Pressure, Steam-Assisted Gravity Drainage Pilot Project. In Canadian Unconventional Resources Conference. Society of Petroleum Engineers.

Valls-Marquez, M., Chapman, D. N., and Ghataora, G. S., 2006. Preparation of Stiff Overconsolidated Clay Samples for the Study of Soil Deformations around Tunnel. IAEG2006, September 6-10, Nottingham, United Kingdom.

Vermeer, P. A., and De Borst, R., 1984. Non-associated Plasticity for Soils, Concrete and Rock. HERON, 29 (3).

White, D. J., 2002. An Investigation into the Behavior of Pressed-in Piles. Ph.D. dissertation, University of Cambridge, UK.

White, D. J., Take, W. A., and Bolton, M. D., 2003. Soil Deformation Measurement Using Particle Image Velocimetry (PIV) and Photogrammetry. Geotechnique, 53(7), pp. 619 -631.

Wichman, B. G. H. M., and Allersma, H. G. B., 2005. Centrifuge Modeling of Soil Upheave by Expanding Tubes. In Proceedings of the International Conference on Soil Mechanics and Geotechnical Engineering, 16(3).

Zambrano-Narvaez, G., and Chalaturnyk, R. J., 2014. The New GeoREF Geotechnical Beam Centrifuge at the University of Alberta, Canada. In Proceedings of the 8th International Conference on Physical Modelling in Geotechnics 2014 (ICPMG2014), Perth, Australia.

Appendix

Appendix A: Consolidated-Drained Triaxial Test Procedures Using GDS Systems

Preparation

1. Check if the right pump fluid is used. If not, both the ISCO pressure pump and GDS pressure pumps should be emptied and then refilled with the right fluid for a couple of times to make sure all the lines are both clean and saturated. Generally, brine and deionized water will be used in the testing system. The bottles for different fluid should be marked as it is hard to tell between brine and deionized water.

2. Saturate the base where the specimen will be seated. Inject deionized water from one side of the bottom back pressure channel and make sure the fluid comes out from another side. Then inject high-speed air into the channel for a while and finally refill the channel with the test fluid and close the valve. Repeat this procedure for cell pressure channel, and top back pressure channel.

3. Get two 2.5" porous stones ready by using ultrasonic cleaner and boiling in deionized water. Also cut two pieces of filter paper for the porous stones.

4. Check if the GDSLAB software is communicating well with the GDS system and getting reasonable readings from each instrument (LVDT, Load Cell, pore pressure transducer, GDS pumps and ISCO pump).

5. Connect the ISCO and GDS pumps to atmosphere to check if the pressure reading is zero. If not, the pressure reading has to be zeroed.

Setup

6. Put a porous stone and then a filter paper on top of the specimen pedestal, and saturate them with test fluid. Carefully place the specimen on top of the pedestal.
7. Use the membrane holder to place two layers of Latex rubber membranes over the specimen.
8. Put a filter paper and then a porous stone on top of the specimen. Flood the top of the specimen test fluid, and then carefully put on the loading cap. Place the port of the loading cap at the comfortable position for connecting to the top back pressure line.
9. Use the membrane holder to place three O-rings in the pedestal area to fix the bottom part of latex rubber membrane. Then flip over the membranes to cover the O-rings. In a similar way, put another three O-rings in the loading cap area to fix the top part of the membrane and flip the membranes over to cover the O-rings.
10. Attach the top back pressure line and saturate the line.
11. Connect the top back pressure line to the loading cap. Hand tight first and then use wrenches to turn 1/8 circle to make sure the connection is tight.
12. The end of the loading rod is screwed into the main shaft and may be loose. Before putting on the triaxial cell, make sure that the end of loading rod is firmly fixed to the main shaft. Otherwise during shearing, the loading rod will be wobbling.

13. Put on the triaxial cell and transfer it to the ELE load frame using a mobile crane.

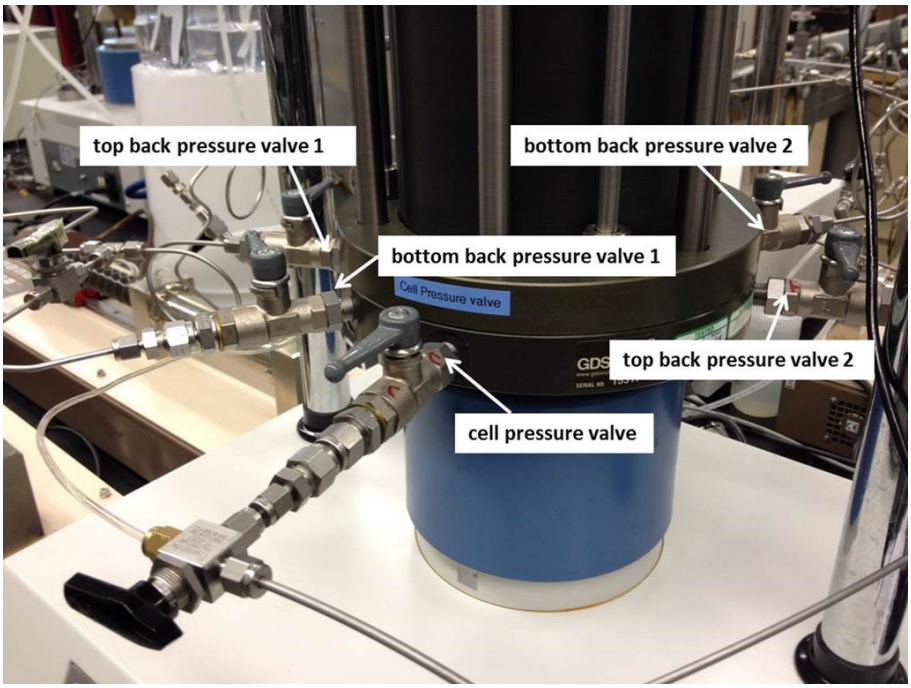

Figure A- 1 Connection ports at the base of the tri-axial cell.

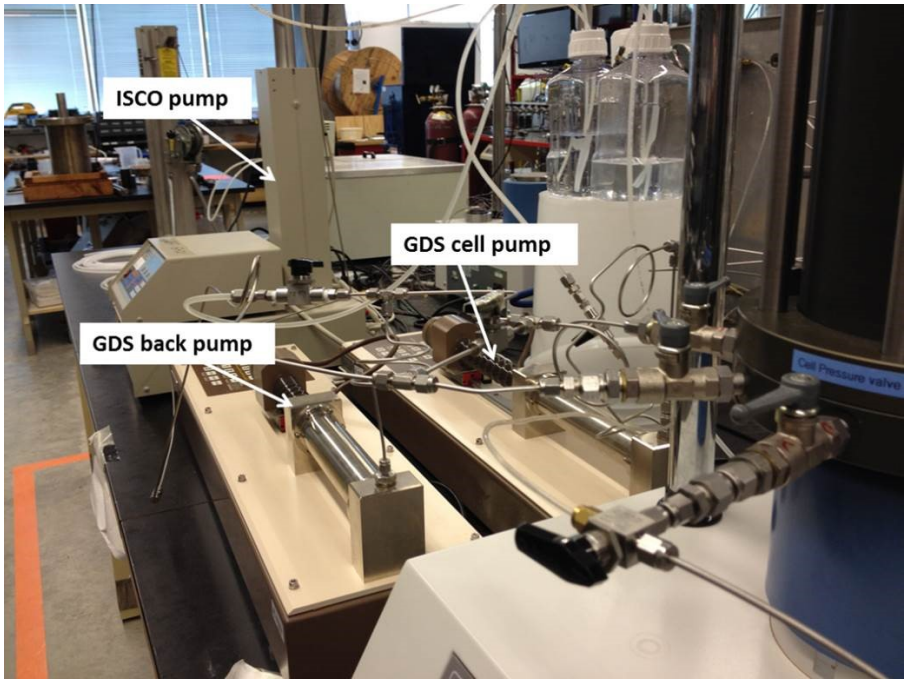

Figure A- 2 Pumps used in the GDS system.

14. Connect the cell pressure port at the base of the triaxial cell to tap water and fill it up. The outlet at the top of the triaxial cell should be connected to atmosphere using a tube. When water comes out from the tube, the tap water should be stopped and let some time for the air inside the triaxial cell to escape. Then close the outlet.
15. Close the cell pressure valve, detach the tap water line, saturate the port and then connect the GDS cell pressure pump line to the cell pressure port.
16. Turn the three-way valve to the air pressure system. Open the cell pressure valve and use the air pressure to pressurize the triaxial cell to 525kPa. Watch out the water level indicator in the water tank of the air pressure system and make sure no air is injected into the triaxial cell. Make sure at this time, the GDS cell pressure pump is stopped.
17. Turn the three-way valve to the GDS cell pressure pump, and the readings on the pump control panel should indicate a pressure close to 525kPa. Then start running GDS cell pressure pump at 525kPa.
18. Saturate the ports for top (GDS) and bottom (ISCO) back pressure pump lines. Then connect the ISCO pump to bottom back pressure port 1. Connect the GDS back pressure pump to top back pressure port 1 and connect the pore pressure transducer to bottom back pressure port 2. At this time, make sure all ports are closed.
19. Open the valve for the pore pressure transducer.
20. Keep the by-pass valve for ISCO and GDS back pressure pumps open. Open the valves for back pressure pumps. Run the GDS back pressure

pump and gradually increase the pressure to 500kPa. Make sure the pressure does not exceed the cell pressure.

21. Setup the GDS data logging system. At this time, the computer will take over the control of GDS system. Remember to reset the targeted pressure values each time the data logging is reset and also note that the volume reading for GDS back pressure pump will be automatically zeroed.

B-Test

22. Keep the back pressure at 500kPa and cell pressure at 525kPa overnight for back saturation.

23. Set the GDS back pressure pump in 'HOLD' mode using GDSLAB software. Increase the cell pressure by 50kPa each step and wait until the GDS back pressure pump readings stabilize. Repeat this step for at least 5 times.

24. If the B-value is more than 90% ~ 95% (depends on the material), then it means the specimen has been saturated.

Consolidation

25. Decrease the cell pressure gradually to 525 kPa and then run the GDS back pressure pump to restore the 500kPa back pressure. Let the system stabilize for a while.

26. For consolidation, effective consolidation pressure for each step should not exceed 2 times of that for the previous step. So consolidation pressure could be increased in such a way as 50kPa, 100kPa, 200kPa, 400kPa, 800kPa and etc. until the targeted effective stress level is reached.

27. To capture the full process of consolidation, for each consolidation step, the GDS back pressure pump should be set to 'HOLD' mode and then increase the cell pressure. When the GDS back pressure pump readings become stable, then restore the back pressure to 500kPa, which will start the consolidation.

28. During consolidation, the by-pass valve is kept open and ISCO back pressure pump is stopped.

Permeability test

29. Run the ISCO back pressure pump at 500kPa.

30. Close the by-pass valve for GDS and ISCO back pressure pumps.

31. The ISCO bottom back pressure pump will be used to exert higher pressure. And the pressure head for the permeability test should not exceed 10% of the effective consolidation pressure.

32. To make sure the overall back pressure within the specimen is maintained at 500kPa, the ISCO bottom back pressure pump should be running at (500+ permeability test pressure head/2) kPa and the GDS top back pressure pump should be running at (500- permeability test pressure head/2) kPa.

33. Monitor the ISCO and GDS back pressure pumps volume change for the initial one hour to ensure that the ISCO back pressure pump has enough volume remaining to pump out fluid and the GDS back pressure pump has enough capacity to receive fluid.

34. After the perm test, run both the GDS and ISCO back pressure pumps at 500kPa for a while. Then open the by-pass valve and stop the ISCO back pressure pump. Let the system stabilize.

35. Do the same for the permeability test after shearing.

36. For permeability test, it is essential to make sure that enough pump fluid is available for running overnight when no one is monitoring the process.

Shearing

37. Setup the LVDT and ensure that there would be enough travel of LVDT for the shearing.

38. Set the shearing rate based on the consolidation data and the equation recommended at ASTM D7181-11.

39. For some specimens, it would take long time for the loading rod to touch the specimen. Thus, in the beginning, a higher velocity could be used to shorten the waiting time for the rod to touch the specimen. However, during this period, someone has to be monitoring the load cell readings. Once significant increase of load cell reading (~50N) is observed, the movement of loading rod should be stopped. Then use the shearing rate to move the loading rod.

Disassemble the triaxial cell

40. Decrease cell pressure to 600kPa.

41. Decrease back pressure to 100 ~ 200kPa and then stop the GDS back pressure pump.

42. Disconnect both ISCO and GDS back pressure pump lines and open both the top and bottom back pressure valves to atmosphere for a while. Then close the valves.

43. Decrease the cell pressure to 200kPa, during which suction will be developing in the specimen. The suction will help maintain the shape of specimen.

44. Disconnect GDS cell pressure pump line and then connect the cell pressure port to a tube for chamber fluid drainage. Open the outlet on top of the triaxial cell and let the fluid drainage by gravity for a while.

45. Connect the outlet on the top of triaxial cell to air pressure which will fasten cell fluid drainage.

Appendix B: Triaxial Test Results on Overconsolidated Speswhite Kaolin Samples

Three consolidated-drained triaxial tests are conducted on overconsolidated Speswhite Kaolin samples using the GDS triaxial system within Geomechanical Reservoir Experimental Facility (GeoREF). Detailed testing procedures are described in Appendix A.

B.1 Summary of Sample Properties

Three samples are tested at different effective confining stresses: 300kPa, 700kPa and 1000kPa respectively (Table B-1). Constant pressure head permeability tests are conducted before and after shearing with a pressure head of no more than 10% of the effective confining stress.

Table B- 1 Testing program for overconsolidated Speswhite kaolin samples.

Test ID	Sample ID	Back pressure (kPa)	Cell pressure (kPa)	Effective confining pressure (kPa)	Permeability test pressure head (kPa)
Test #1	Sample #1	500	800	300	30
Test #2	Sample #4	500	1200	700	70
Test #3	Sample #5	500	1500	1000	100

Table B- 2 Triaxial test sample properties before testing.

Test ID	Sample ID	Initial Height (mm)	Initial Diameter (mm)	Initial Weight (mm)	Initial Water content (%)
Test #1	Sample #1	138.35	63.2	781.15	42.31
Test #2	Sample #4	140.35	63.5	792.48	41.97
Test #3	Sample #5	138.00	63.4	776.67	41.04

Table B- 3 Triaxial test sample properties before testing (continued).

Test ID	Sample ID	Initial Void Ratio	Initial Bulk Density (kg/ m^3)	Initial Dry Density (kg/ m^3)
Test #1	Sample #1	1.06	1799.8	1264.7
Test #2	Sample #4	1.08	1783.5	1256.3
Test #3	Sample #5	1.06	1782.9	1264.1

B.2 Summary of Permeability Test Results

For each sample, the constant pressure head permeability tests are conducted before and after shearing. The results are presented in Table B-4 and Figure B-1.

Table B- 4 Summary of permeability test results.

Test ID	Sample ID	Permeability before shearing (m/s)	Permeability after shearing (m/s)	Constant pressure head (kPa)	Effective Confining stress (kPa)
Test #1	Sample #1	7.692E-10	5.689E-10	30	300
Test #2	Sample #4	5.869E-10	4.181E-10	70	700
Test #3	Sample #5	5.382E-10	3.695E-10	100	1000

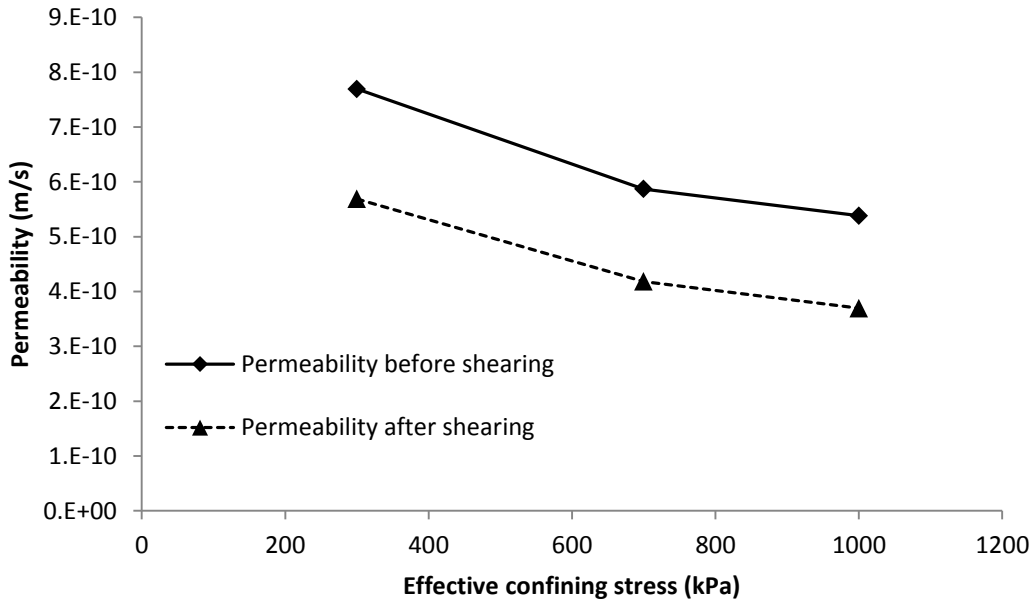

Figure B- 1 Permeability of overconsolidated Speswhite kaolin sample before and after shearing.

B.3 Summary of Sample Behavior under Shearing

Based on the consolidation data, the appropriate shearing rate is determined using the equation of $\varepsilon = 4\%/10t_{90}$ described in ASTM Standard D7181-11 (2011). The value of 4% is used based on the assumption that the failure will occur after 4% axial strain. The shearing rate of 4%/day is chosen for all three samples.

Test #1 - Sample #1:

Sample #1 demonstrates a strain-softening behaviour under shearing and the peak strength is reached at 6.8% axial strain (Figure B-4). During shearing, the sample shows a contractive behaviour. After failure, there is a slight dilation at around 10% axial strain. After that, the sample volume remains almost constant.

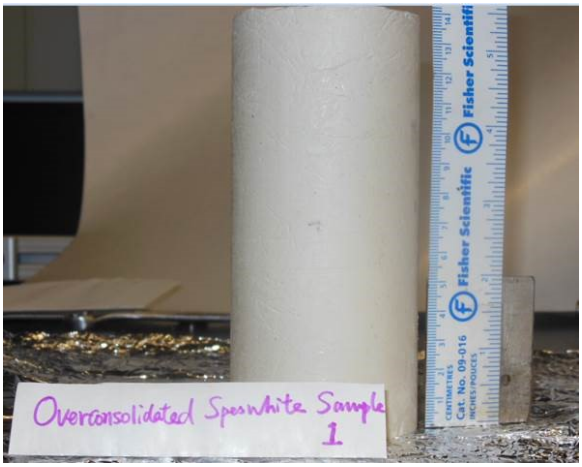

Figure B- 2 Sample#1 before shearing.

Figure B- 3 Sample #1 after shearing.

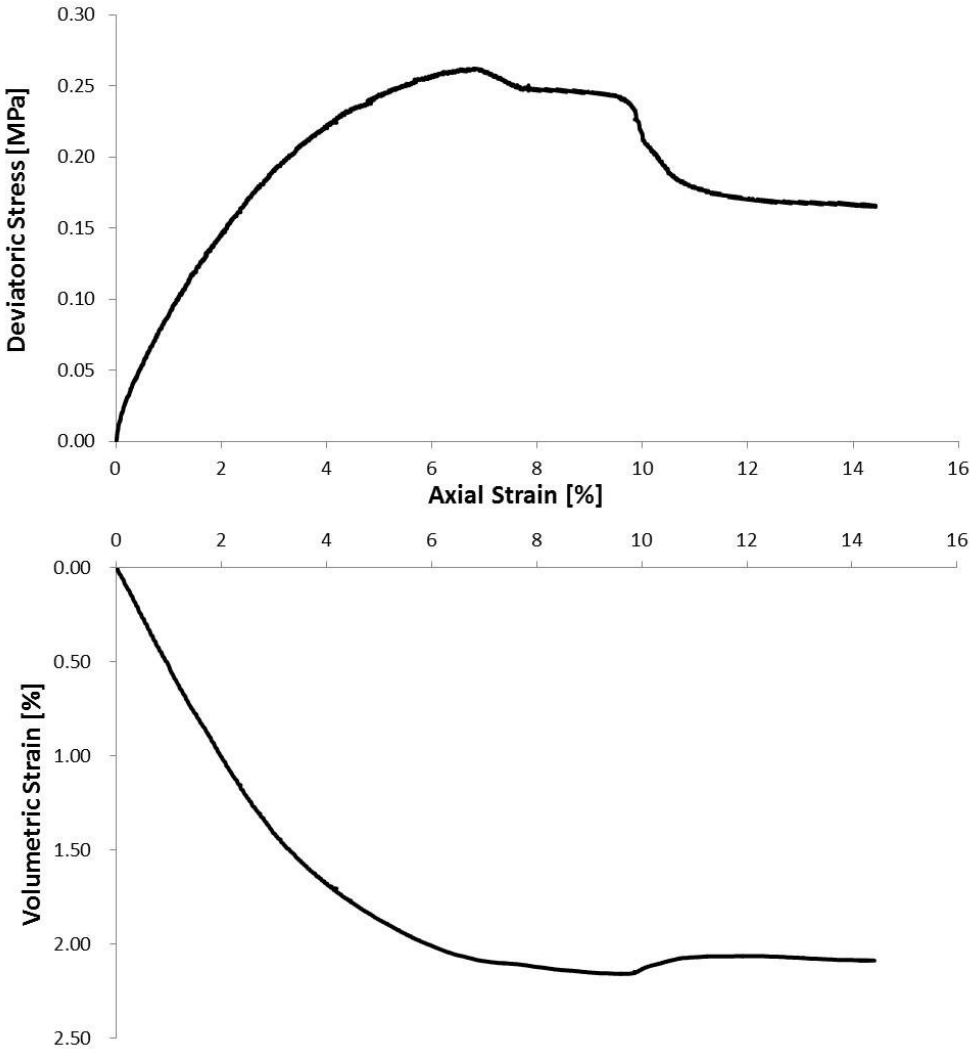

Figure B- 4 Deviatoric stress - axial strain – volumetric strain test results for sample #1.

Test #2 - Sample #4:

Sample #4 demonstrates a strain-softening behaviour and the peak strength is reached at 10% axial strain (Figure B-7). During shearing, the sample shows a contractive behaviour. After failure, there is a slight dilation at around 10% axial strain, after which the sample volume keeps decreasing (contraction).

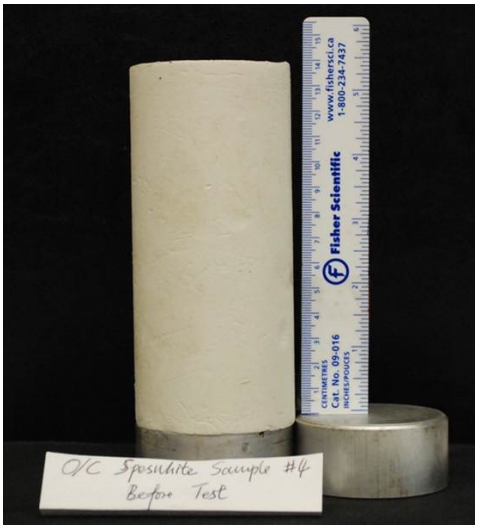

Figure B- 5 Sample #4 before shearing.

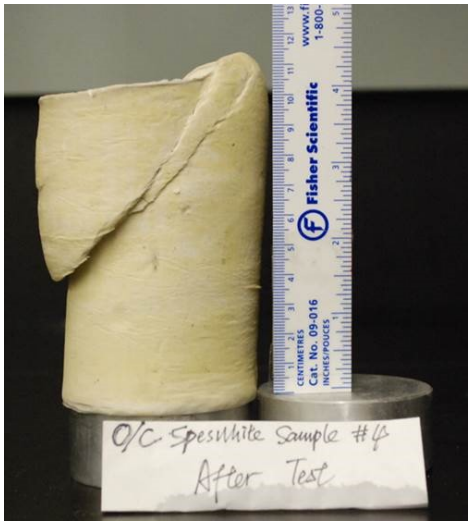

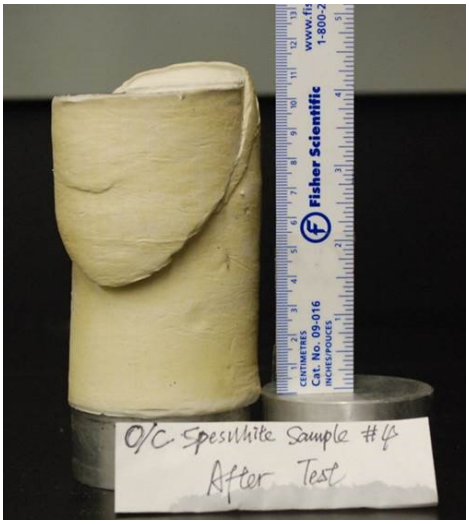

Figure B- 6 Sample #4 after shearing.

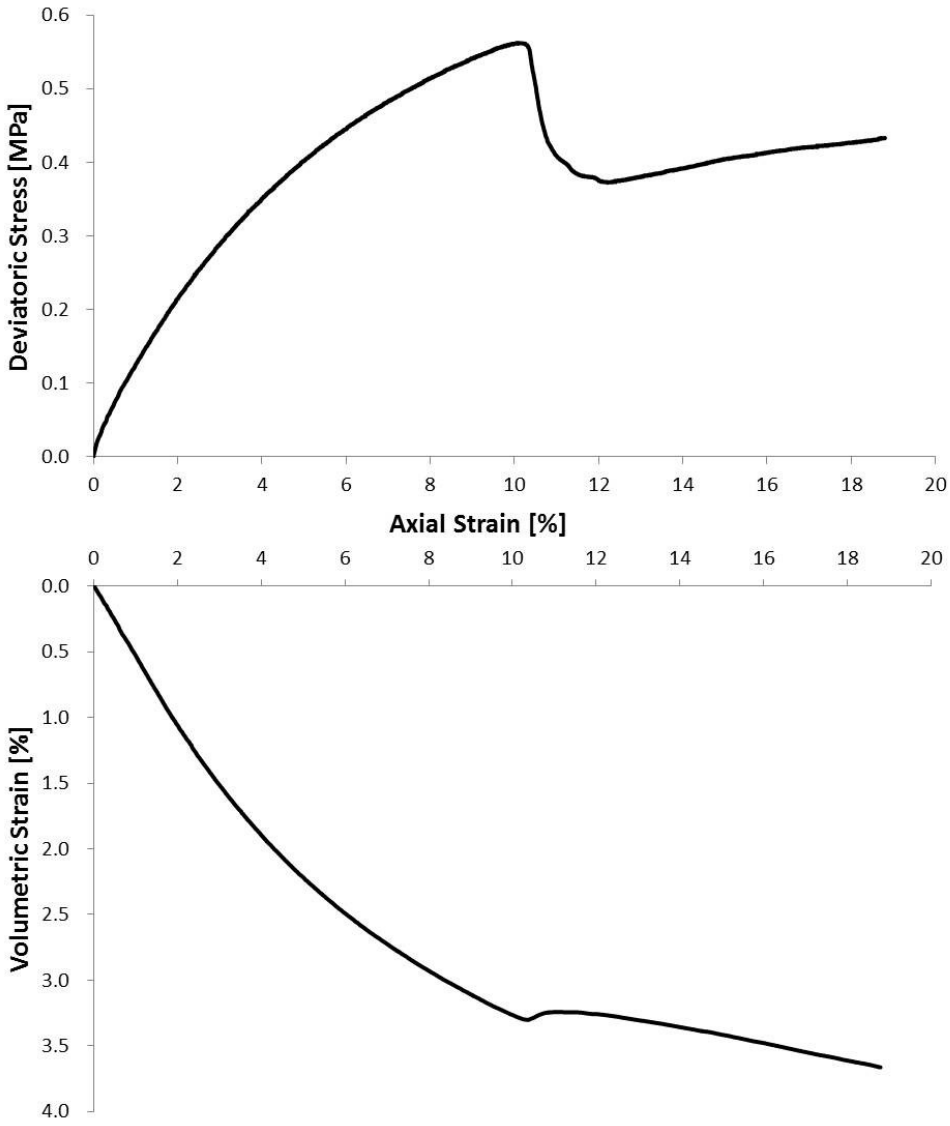

Figure B- 7 Deviatoric stress - axial strain – volumetric strain test results for sample #4.

Test #3 - Sample #5

Sample #5 demonstrates a strain-softening behaviour and the peak strength is reached at 10% axial strain (Figure B-10). During shearing, the sample shows a contractive behaviour and no dilation is observed for sample #5.

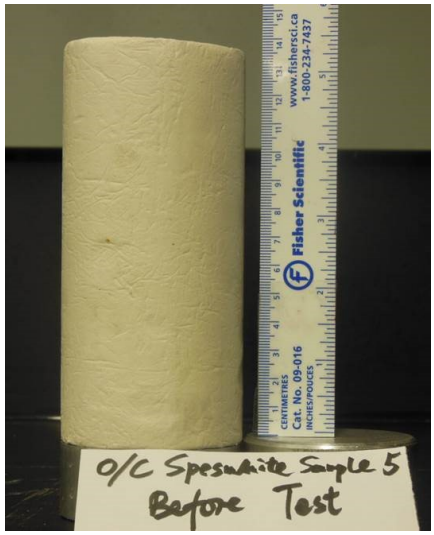

Figure B- 8 Sample #5 before shearing.

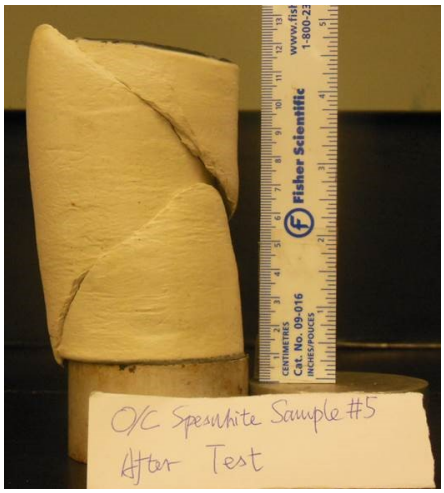

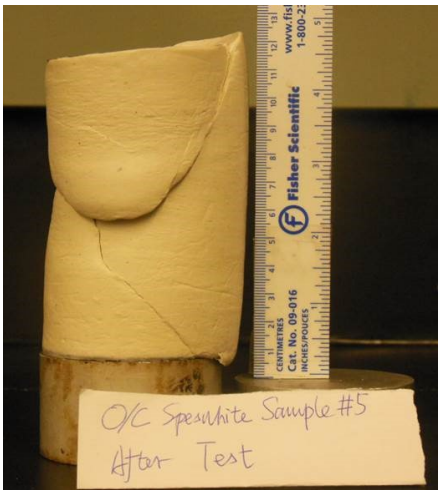

Figure B- 9 Sample #5 after shearing.

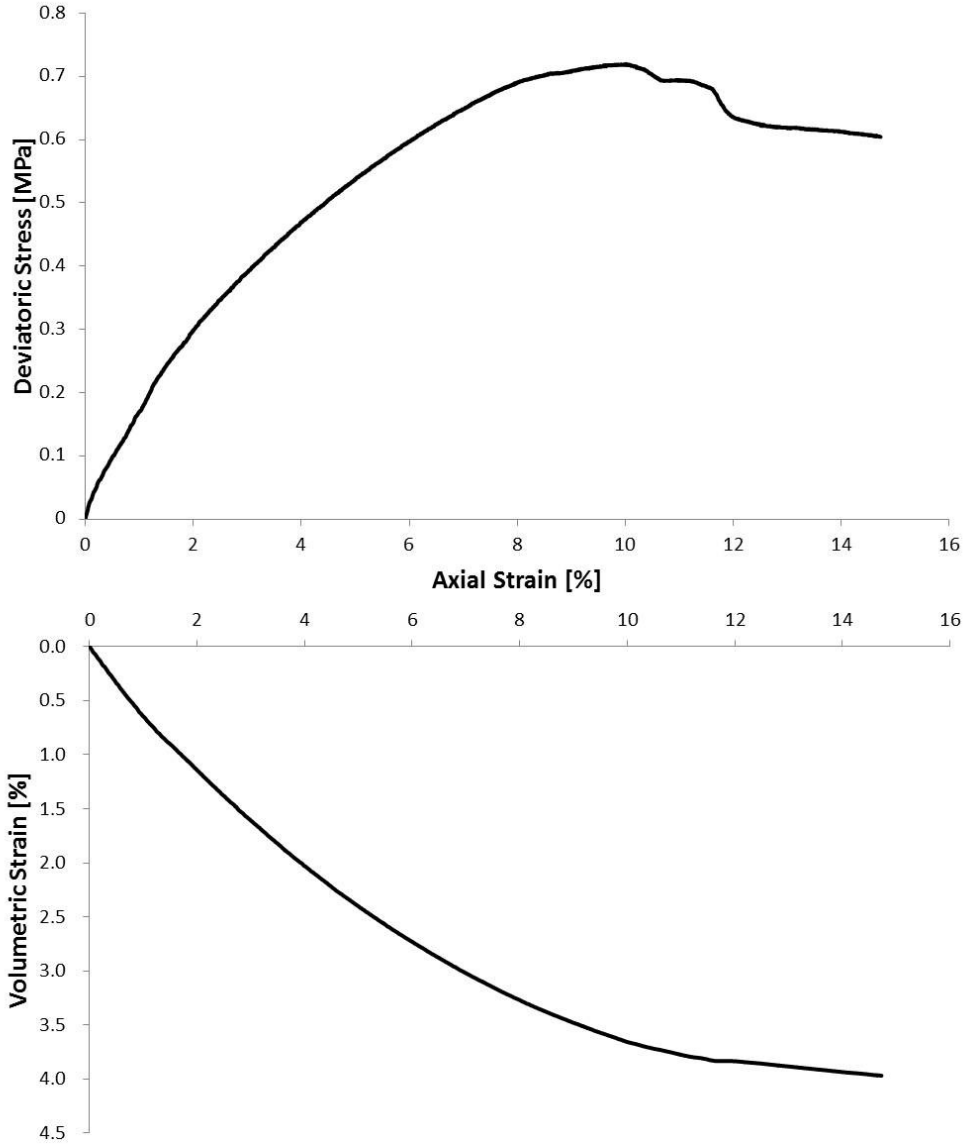

Figure B- 10 Deviatoric stress - axial strain – volumetric strain test results for sample #5.

B.4 Determination of Mechanical Properties of Overconsolidated Speswhite Kaolin

The main purposes of these triaxial tests are to determine the Young's modulus, Poisson's ratio, friction angle, cohesion, and dilation angle (if applicable) of the overconsolidated Speswhite kaolin sample for the input to the geomechanical simulator.

Young's Modulus:

E_{50} is used to describe the Young's Modulus of the overconsolidated Speswhite kaolin samples, and for each sample the E50 values are summarized in Table B-5.

Table B- 5 Young's modulus determined for each sample.

Test ID	Sample ID	Young's Modulus (E_{50})	Note
Test #1	Sample #1	7.6MPa	0.130MPa/1.7%
Test #2	Sample #4	9.7MPa	0.280MPa/2.9%
Test #3	Sample #5	13.3MPa	0.360MPa/2.7%

Poisson's ratio:

The Poisson's ratio is defined as the ratio of lateral strain versus axial strain. In the GDS system, there is no direct measurement of the lateral strain. Thus, the lateral strain is calculated based on the equation of $\varepsilon_v = \varepsilon_a + 2\varepsilon_l$. For saturated clay, the Poisson's ratio mostly falls in the range of 0.3 to 0.4.

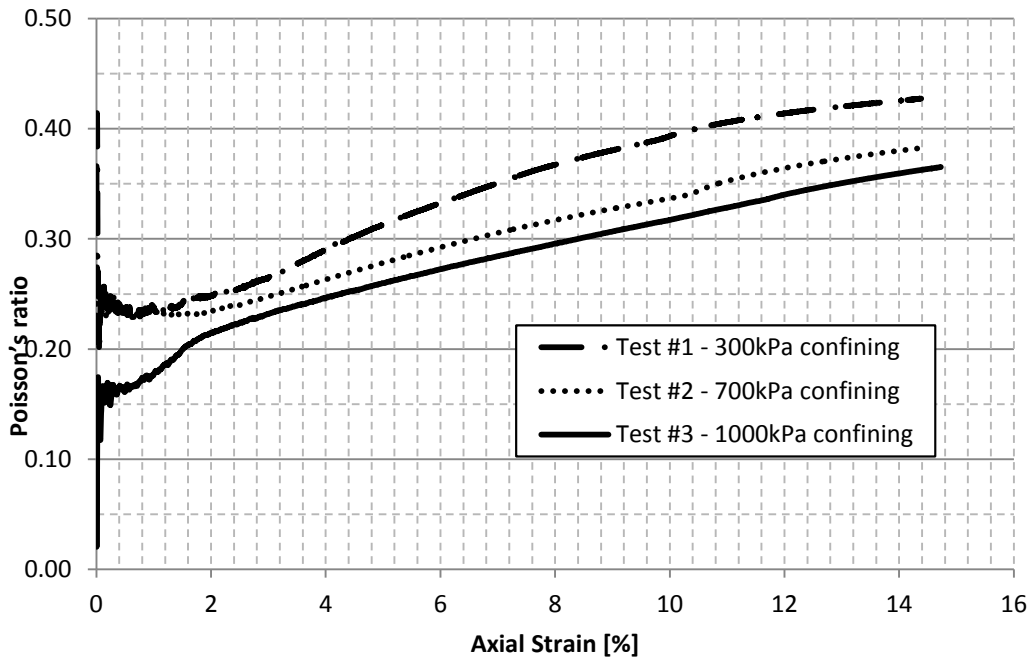

Figure B- 11 Calculated Poisson's ratio for each sample.

Friction angle and cohesion

Three different plots are used to determine the cohesion (c') and friction angle (φ') of the overconsolidated Speswhite kaolin: $\sigma_n - \tau$, $\sigma_3' - \sigma_1'$, and $p' - q'$ plots. For the $\sigma_n - \tau$ plots, these two parameters can be obtained directly. However, the parameters obtained from $\sigma_3' - \sigma_1'$, and $p' - q'$ plots should be transferred to the Mohr- Coulomb parameters using corresponding equations.

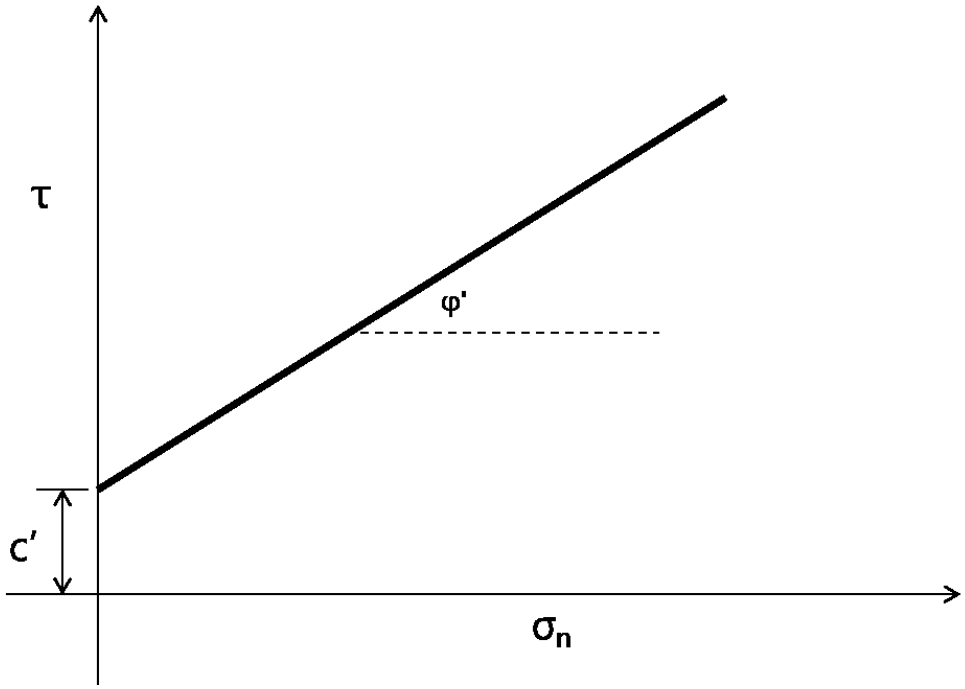

Figure B- 12 $\sigma_n - \tau$ failure envelope.

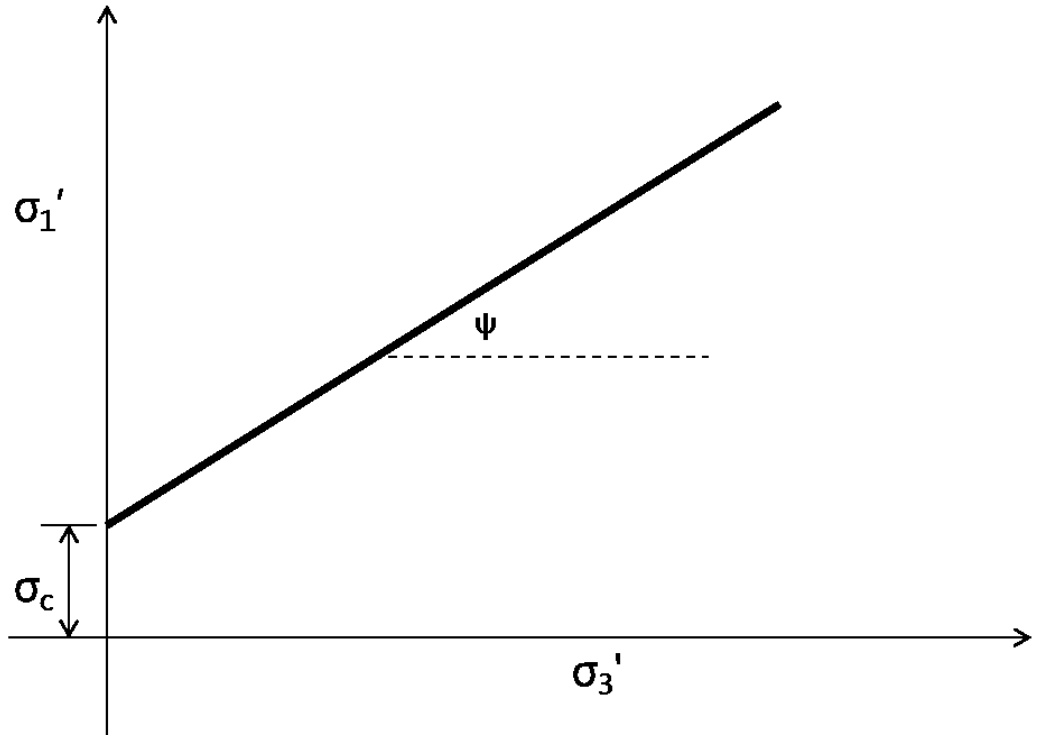

Figure B- 13 $\sigma_3' - \sigma_1'$ failure envelope.

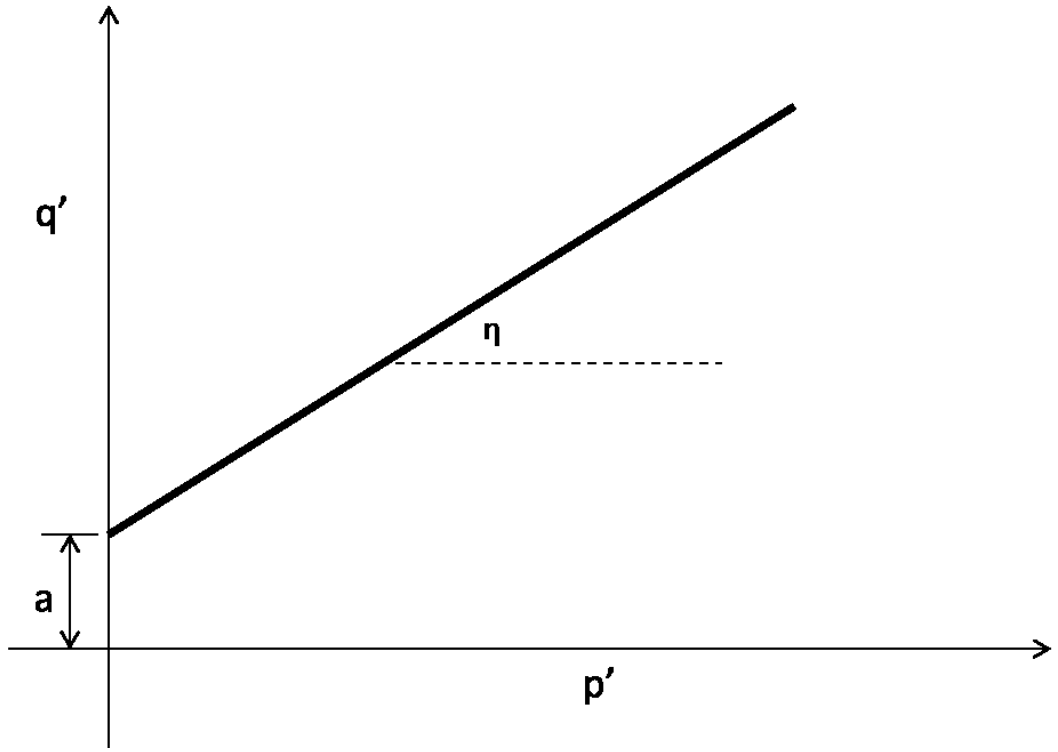

Figure B- 14 $p' - q'$ failure envelope.

For $\sigma_1 - \sigma_3$ plots:

$$\sigma_C = \frac{2c'\cos\varphi'}{1-sin\varphi'} \quad \text{..... (1)}$$

$$\tan\psi = \frac{1+sin\varphi'}{1-sin\varphi'} \quad \text{..... (2)}$$

For $p' - q'$ plots:

$$p' = \frac{\sigma_1' + 2\sigma_3'}{3} \quad \text{..... (3)}$$

$$q' = \sigma_1' - \sigma_3' \quad \text{..... (4)}$$

$$\tan\eta = \frac{6sin\varphi'}{3-sin\varphi'} \quad \text{..... (5)}$$

$$a = \frac{6c'\cos\varphi'}{3-sin\varphi'} \quad \text{..... (6)}$$

In which, σ_1' is the effective axial stress, σ_3' is the effective confining stress, φ' is the effective friction angle, c' is the cohesion, η is the failure envelope angle in $p' - q'$ plot and a is the q'-axis intercept of the failure envelop, ψ is the failure envelope angle in $\sigma_3' - \sigma_1'$ plot and σ_c is the σ_1'-axis intercept of the failure envelop.

Table B- 6 Summary of friction angle and cohesion determined by different methods.

Method	Cohesion (kPa)	Friction Angle (˚)
$\sigma_n - \tau$	30	15
$\sigma_3' - \sigma_1'$	31	14.5
$p' - q'$	28	14.7

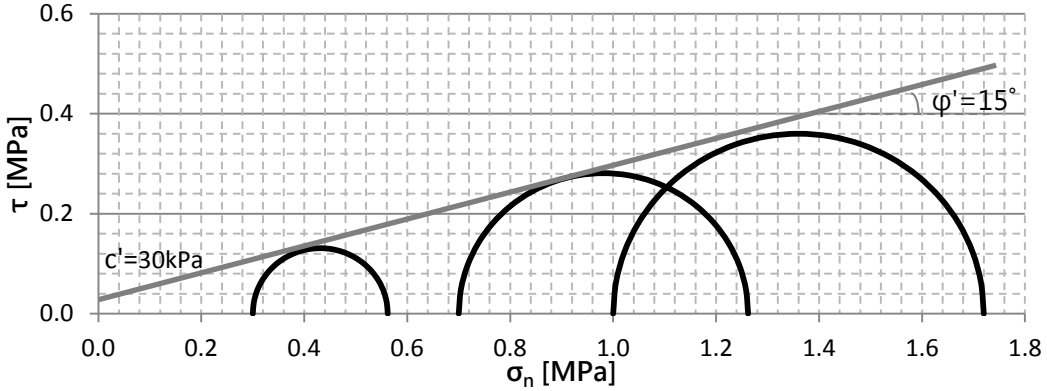

Figure B- 15 Mohr circle plots for determining friction angle and cohesion.

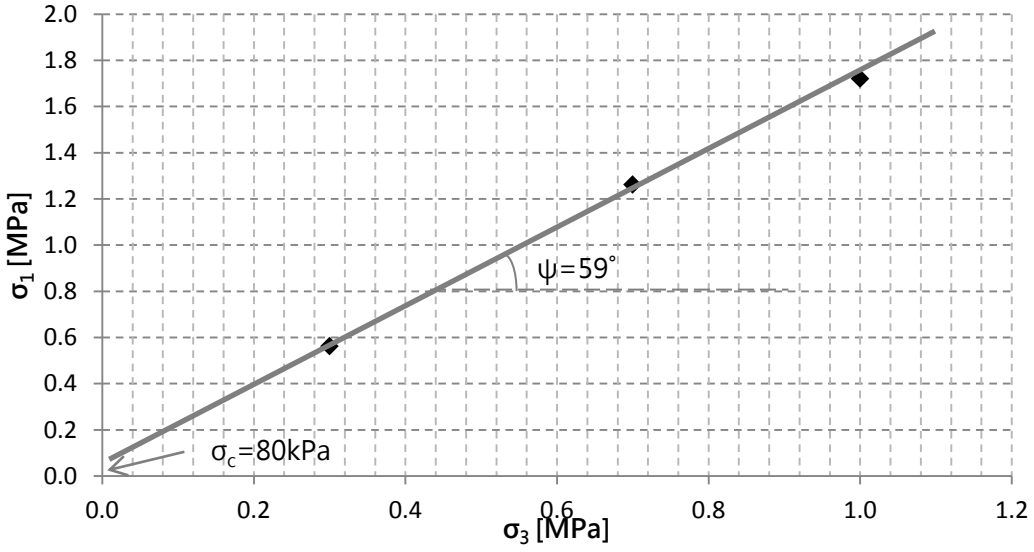

Figure B- 16 $\sigma_3' - \sigma_1'$ plots for determining friction angle and cohesion.

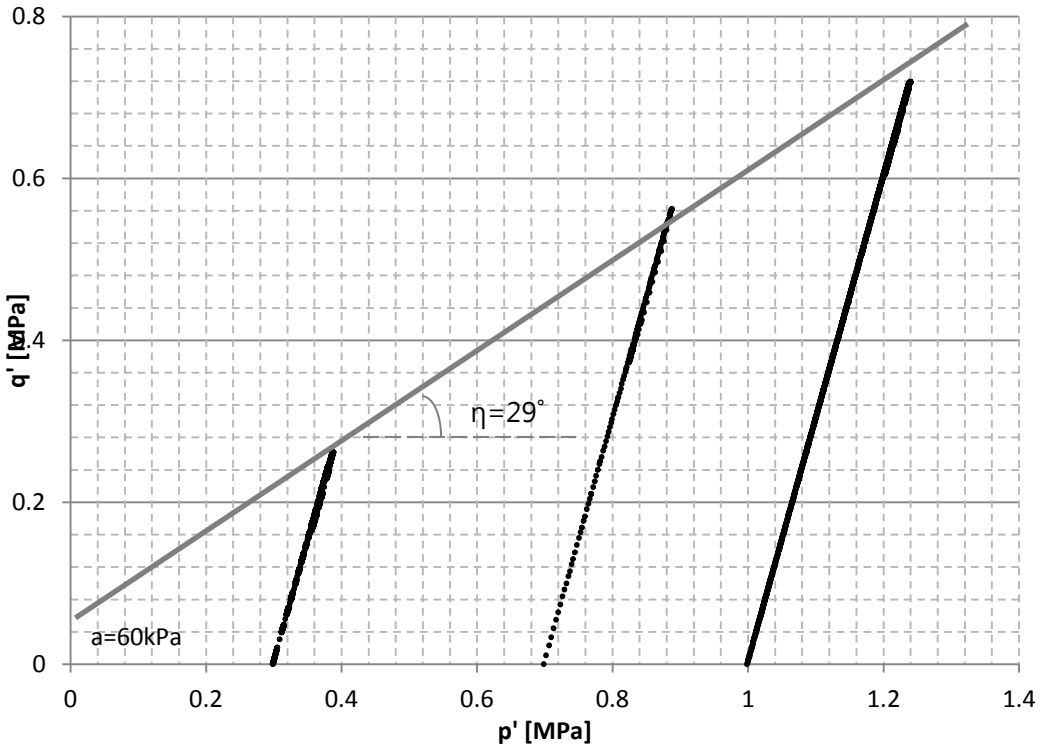

Figure B- 17 p'-q' plot for determine friction angle and cohesion.

Appendix C: Summary of First Overconsolidated Speswhite Kaolin Block Spinning with Lead Bars as Overburden

Three goals are achieved with the first good-quality overconsolidated Speswhite kaolin block. The first one is to see how the plane-strain box with Perspex glass performs at 100g since the vertical stress (1000kPa at 100g) at the base of the plane-strain box is beyond the limit recommended by Broadbent which is 500kPa. It turns out that the plane-strain box with Perspex glass works well at this stress level. The second one is to get the right setup for PIV tests (camera positions, lighting conditions, lens polarizer angle and etc.). During inflight consolidation, images were taken for subsequent PIV analysis of consolidation displacement. Finally, at 1g condition, an 11.5cm wide model footing was pushed by the X-Z actuator to create different displacement patterns from consolidation which will help get better understandings of how to conduct good PIV analysis. The PIV analysis results turn out to be reasonable, while improvements could be made for future tests.

Details will be covered in the next three sections.

C.1 100g consolidation

To mimic the influence of overburden, 89kg of closely packed lead bars were placed on top of the kaolin block. 89kg of lead bars at 100g spinning will generate equivalent vertical stress of 1/1000*100*(89kg*9.81m/s)/ (0.2m*0.7m) = 624kPa on top of the kaolin block. Before spinning, the thicknesses of the kaolin block and the lead bars were measured at 20cm and 7cm respectively. The water level was set just at the top of the lead bars. After 100g consolidation, the kaolin block thickness was immediately measured at 18cm. During spinning, there was significant water evaporation which could be prevented by adding a seal at the top of the plane-strain box for future tests.

In-flight consolidation was conducted in three stages: 50G, 70G and finally 100g. Each stage was kept running for 30min, 30min and 240min respectively.

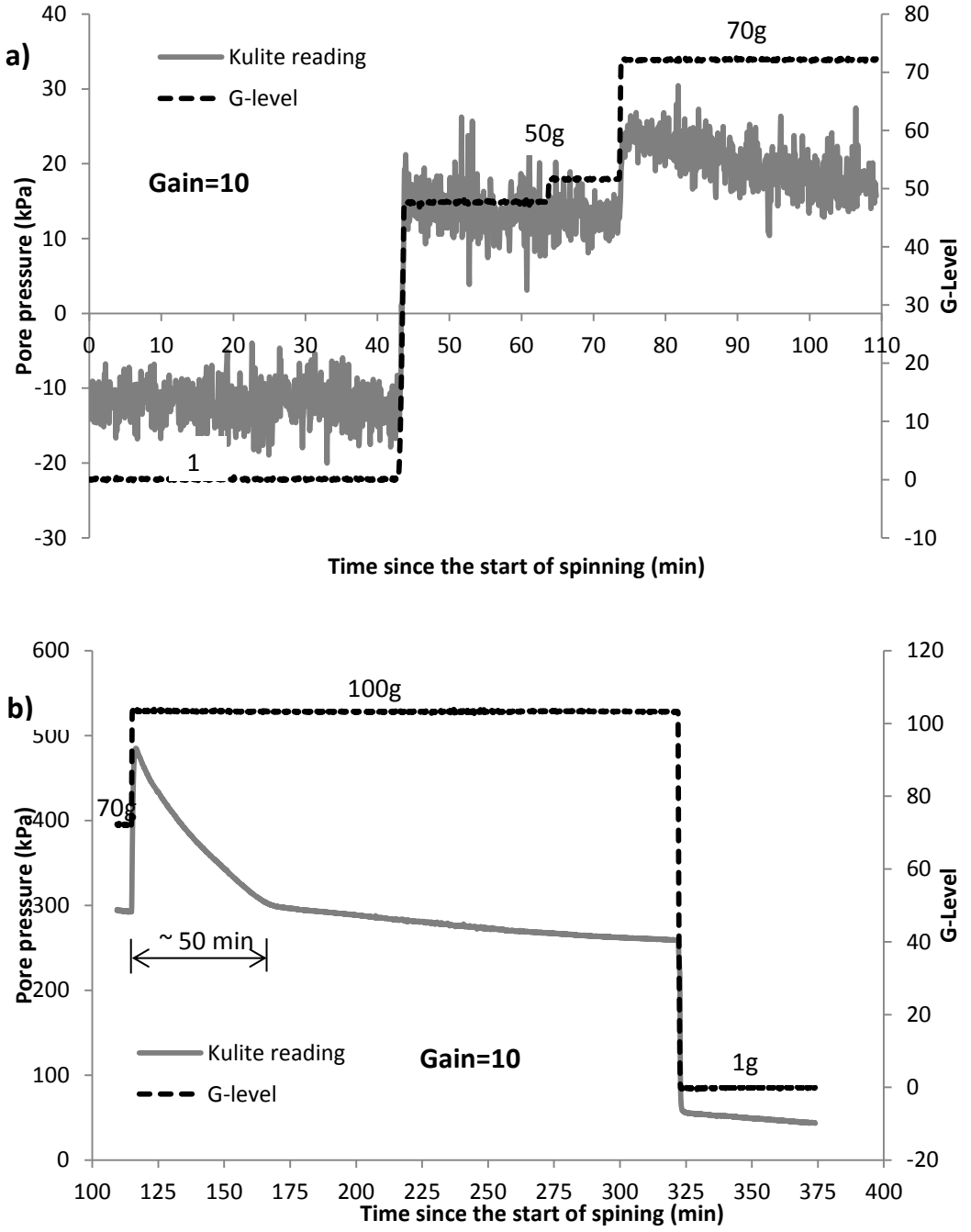

Figure C- 1 a) Kulite readings with gain set at 10 b) Kulite readings with gain set at 100.

Kulite Miniature Pore Pressure Transducer (PPT) worked well during inflight consolidation. However, the gain should be set at a right value. It is found that at low gain,

much signal noise is observed (Figure C-1a) and the Kulite PPT could not generate reasonable readings. It is recommended to set the gain at 100. As shown in Figure C-1b, the Kulite readings were significantly improved.

C.2 PIV analysis results of the inflight consolidation

As the lighting sources inside the centrifuge pit is not continuous, it is important to turn the pit light off during spinning which will help facilitate consistent lighting conditions. Also with the pit lights on, there will be some reflections of cradle in the Perspex glass which should be eliminated (Figure C-2a).

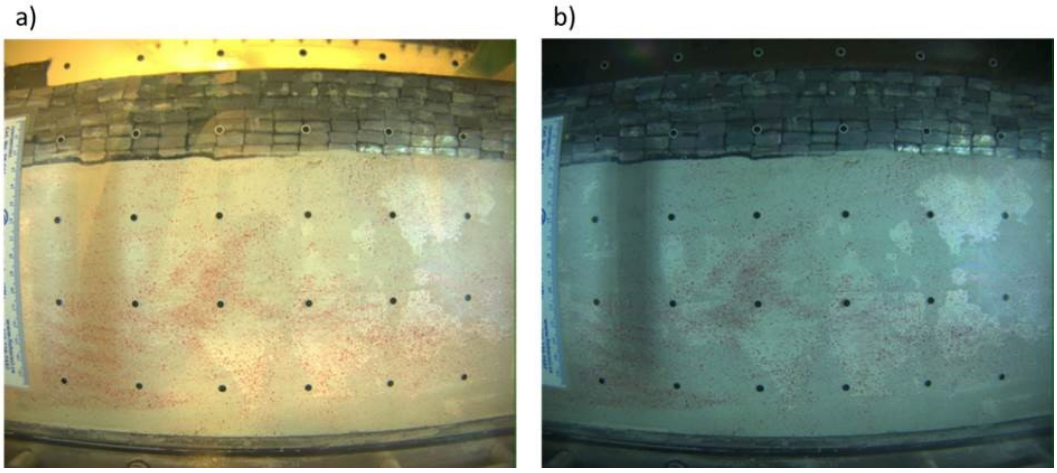

Figure C- 2 Comparison between the images taken a) with pit light on and b) with pit light off.

The plane-strain box has a width of 70cm and the lens was put at a position to cover 45cm of it. One favourable thing about this position choice is that the LED tower reflections on the Perspex glass could be automatically eliminated from the images. Even for the final test with the electromechanical device buried at the base of the plane-strain box, 45cm of view should be good enough as most of the displacement will happen in an area of 20 ~ 30cm. However, there might not be enough space in the vertical direction. The black dot of the control maker has a diameter of 4.5mm and the white edge has a

thickness of 2mm. The control markers are uniformly distributed in 60mm x 60mm spacing.

The PIV analysis of the consolidation displacement at 100g is presented here (Figure C-3). It is recommended that for the next test, a ruler could be attached between the Perspex glass and the transparency protecting the Perspex. By this method, the ruler is coplanar with the kaolin block and the ruler readings can accurately reflect the positions of the top of the kaolin block. However, how to prevent the blurring of the boundary of the lead bars and the top of kaolin block should be figured out.

C.3 PIV analysis of the model footing

After spinning, the lead bars are removed and an 11.5 cm wide model footing was pushed by the X-Z actuator into the kaolin. Due to limited capacity of the actuator, the footing was only pushed down for 10mm and the PIV analysis results of first 5mm displacement is presented here. As the footing is not firmly attached to the Perspex glass, the top part of the kaolin block was not deformed by 5mm. The displacement patterns generated by PIV analysis are reasonable.

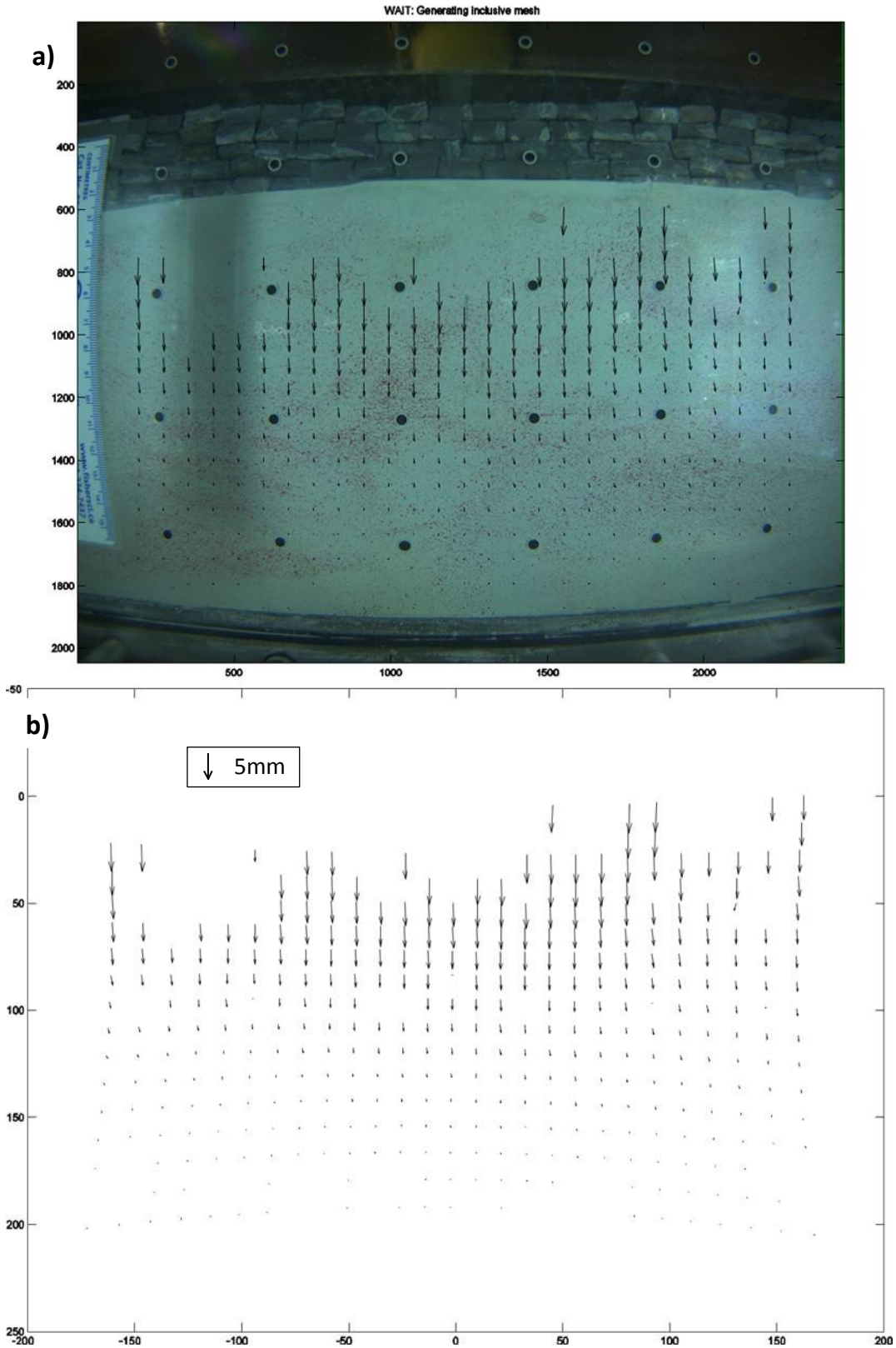

Figure C- 3 a) Image-space displacement vectors and b) object-space displacement vectors during 100g consolidation.

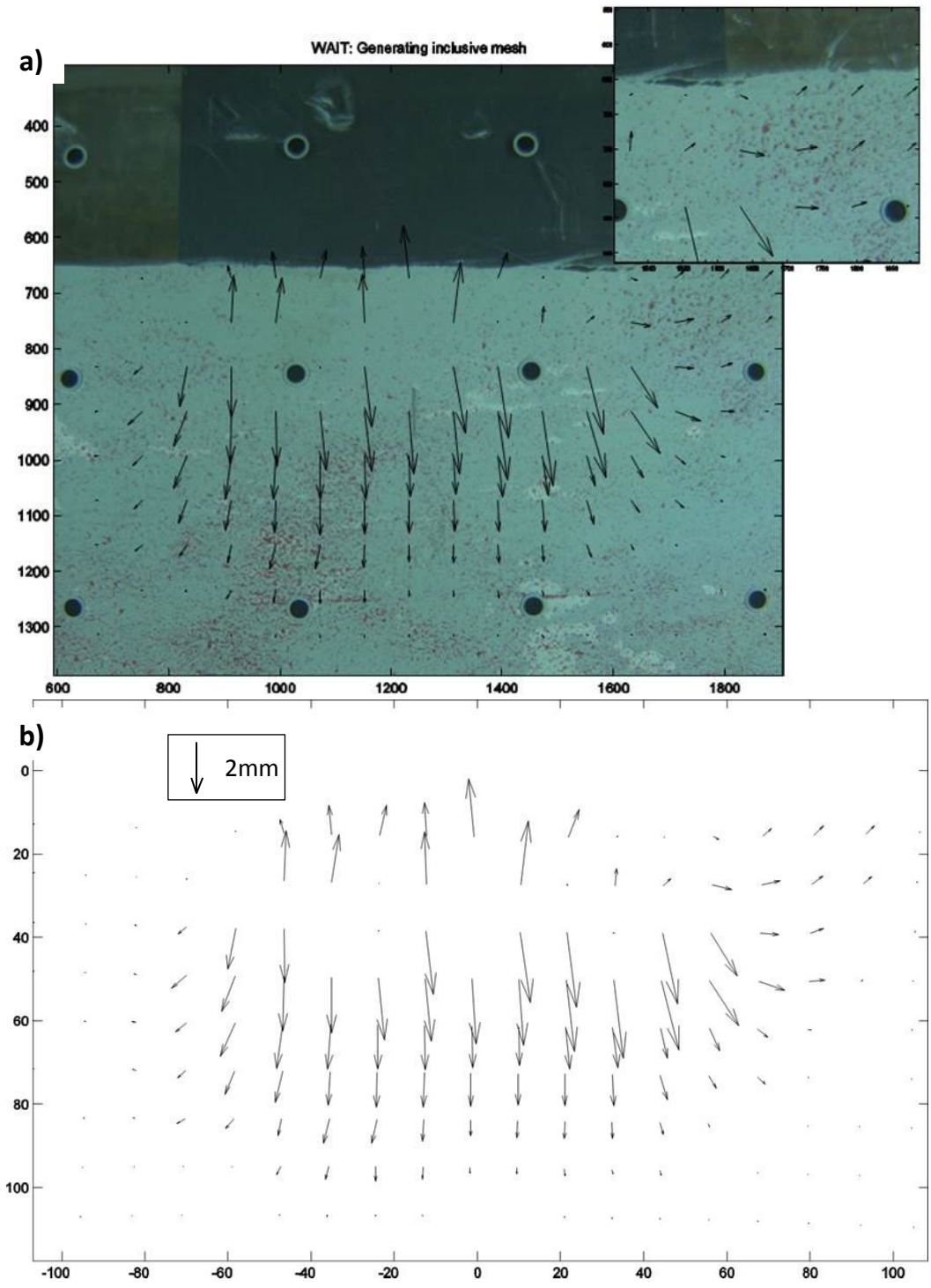

Figure C- 4 a) Image-space displacement vectors and b) Object-space displacement vectors of the model footing.

Appendix D: Preliminary Investigation of Boundary Effects of Plane-strain Box on Caprock Behavior in Centrifuge Modeling

As discussed in Chapter 4, the simplified vertical displacement (SVD) cannot fit into the plane-strain box because of its limited space. Thus, the plateau part of the simplified vertical displacement (SVD) has to be shortened to be accommodated into the plane-strain box, which makes the centrifuge simplified vertical displacement (cSVD). The simulations conducted in Section 4.4.2 have a length of 1000m. However, the plane-strain box only has a length of 70cm, which means at 100g centrifuge spinning, the prototype would have a length of 70m according to the scale law for centrifuge modeling. Consequently, 70m FLAC simulations should be run to study the boundary effects of the plane-strain box on caprock behavior during centrifuge modeling.

In section 4.4.2, the cSVD only considered the vertical displacement; while the horizontal displacement is not considered. It is also necessary to run the 70m FLAC simulation as well as the 1000m FLAC simulation with both the vertical displacements and horizontal displacement generated by the GeoCDM. The centrifuge simplified horizontal displacement (cSHD) and centrifuge simplified vertical displacements (cSVD) generated by GeoCDM are plotted in Figure D-1. With present setups, no horizontal displacements at the boundary of the plane strain box are allowed.

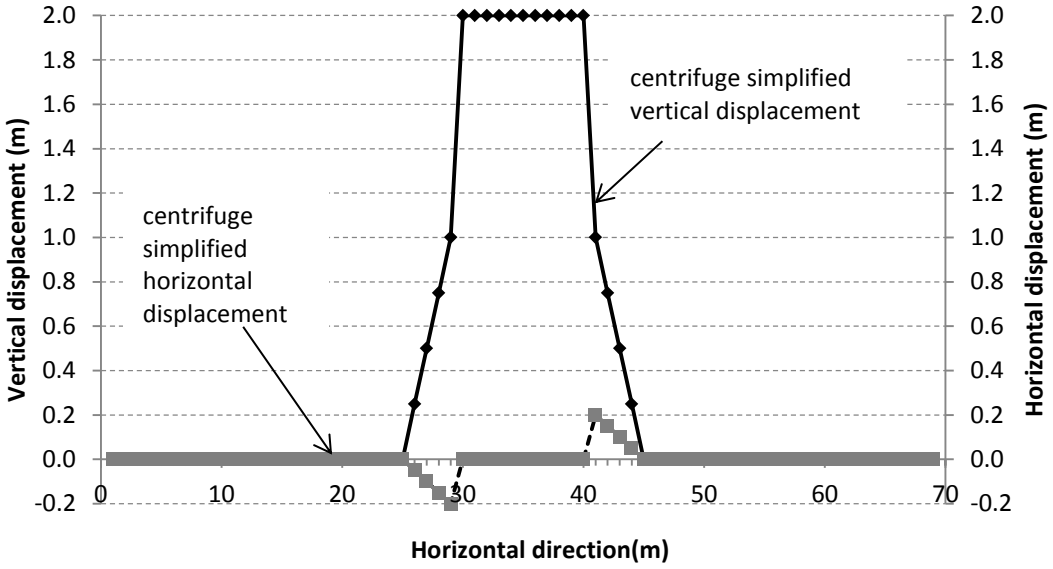

Figure D- 1 Centrifuge simplified vertical displacement and centrifuge simplified horizontal displacement generated by GeoCDM (negative horizontal displacement means displacement towards left and vice versa).

D. 1 Boundary effects of plane-strain box

Four scenarios are simulated to study the influences of GeoCDM generated horizontal displacement and boundary effects of the plane-strain box: 1) 1000m FLAC simulation with only centrifuge simplified vertical displacement (cSVD); 2) 70m FLAC simulation with only centrifuge simplified vertical displacement (cSVD); 3) 1000m FLAC simulation with both centrifuge simplified vertical displacement (cSVD) and centrifuge simplified horizontal displacement (cSHD) and 4) 70m FLAC simulation with both cSHD and cSVD. Displacement vectors and stress contours as well as the patterns of caprock shearing zones are compared for these four scenarios. For both 1000m and 70m FLAC simulations, the cSHD and cSVD are exerted at the center base of the model. For better comparison, stress contours and displacement vectors as well as shearing zones are plotted only for the areas from 465m and 535m (70m area) in the longitudinal direction in 1000m FLAC simulations.

1) Displacement vectors

a) Displacement vectors in **1000m** FLAC simulations with only cSVD

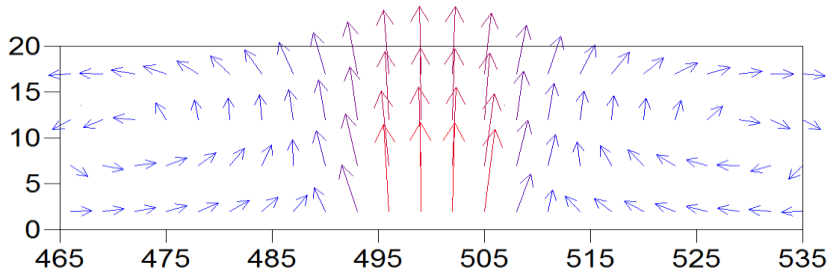

b) Displacement vectors in **70m** FLAC simulations with only cSVD

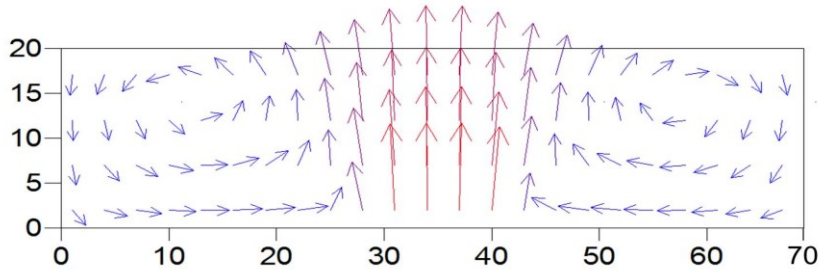

c) Displacement vectors in **1000m** FLAC simulation with both cSVD and cSHD

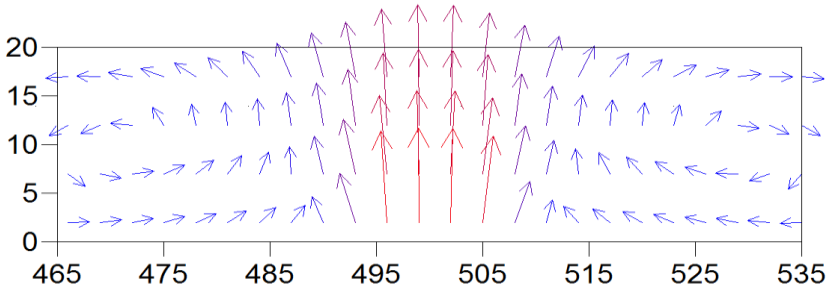

d) Displacement vectors in **70m** FLAC simulation with cSVD and cSHD

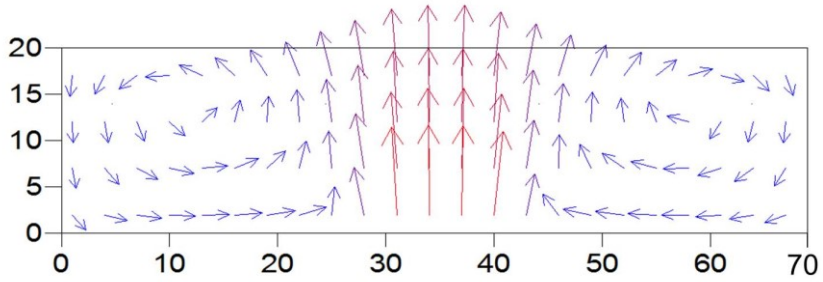

Figure D- 2 Displacement vectors in a) 1000m FLAC simulations with only cSVD; b) 70m FLAC simulations with only cSVD; c) 1000m FLAC simulation with both cSVD and cSHD; d) 70m FLAC simulation with cSVD and cSHD (unit in m).

2) Horizontal stress contours

a) Horizontal stress in **1000m** FLAC simulations with only cSVD (kPa)

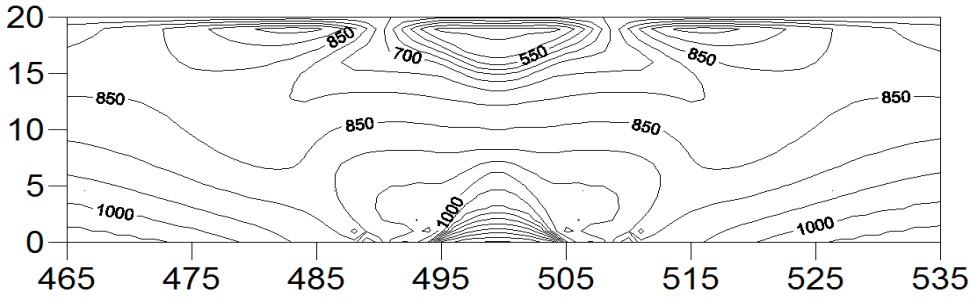

b) Horizontal stress in **70m** FLAC simulations with only cSVD (kPa)

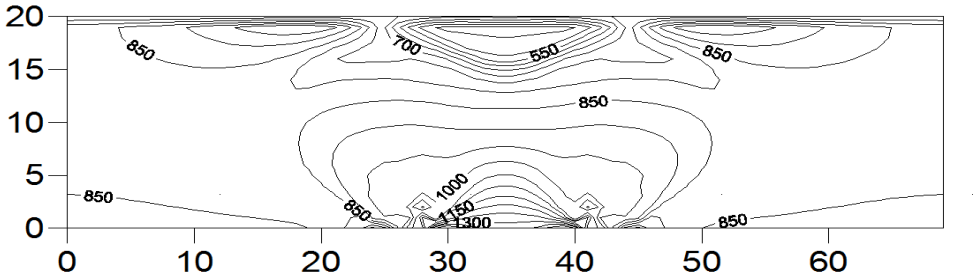

c) Horizontal stress in **1000m** FLAC simulation with both cSVD and cSHD (kPa)

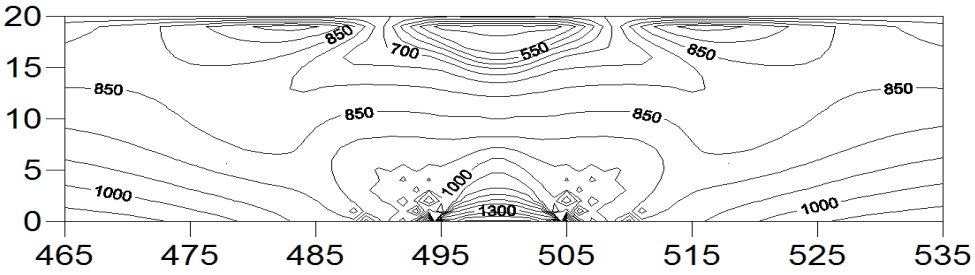

d) Horizontal stress in **70m** FLAC simulation with both cSVD and cSHD (kPa)

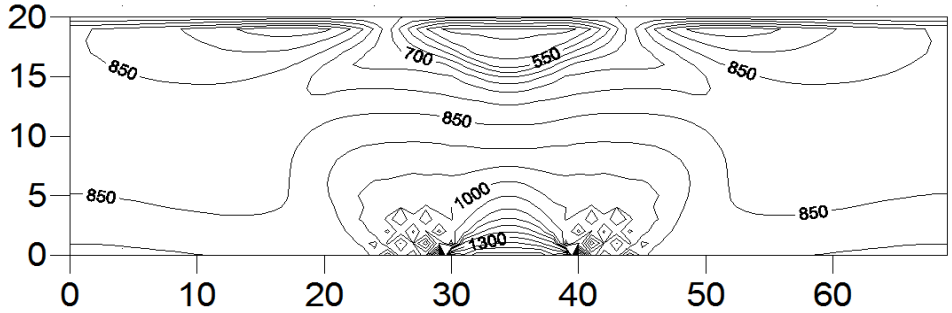

Figure D- 3 Horizontal stress in a) 1000m FLAC simulations with only cSVD; b) 70m FLAC simulations with only cSVD; c) 1000m FLAC simulation with both cSVD and cSHD; d) 70m FLAC simulation with cSVD and cSHD (unit in m).

3) Vertical stress contours

a) Vertical stress in **1000m** FLAC simulations with only cSVD (kPa)

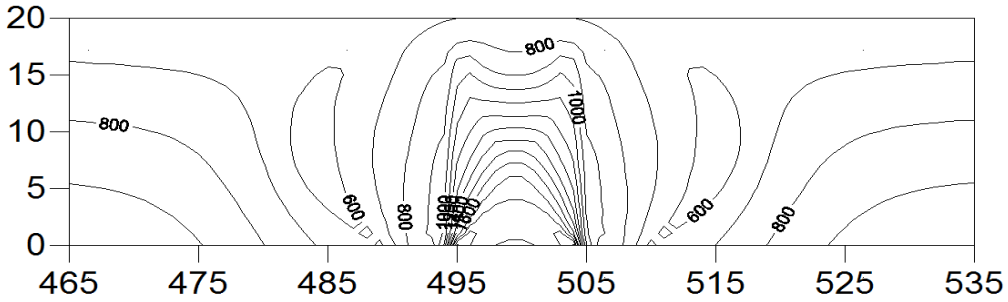

b) Vertical stress in **70m** FLAC simulations with only cSVD (kPa)

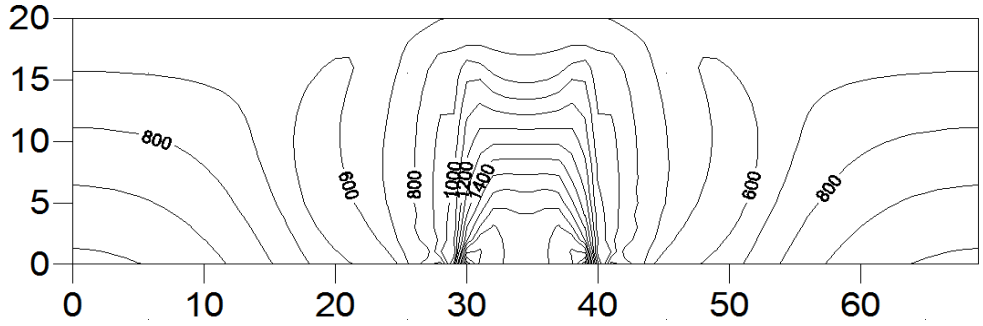

c) Vertical stress in **1000m** FLAC simulation with both cSVD and cSHD (kPa)

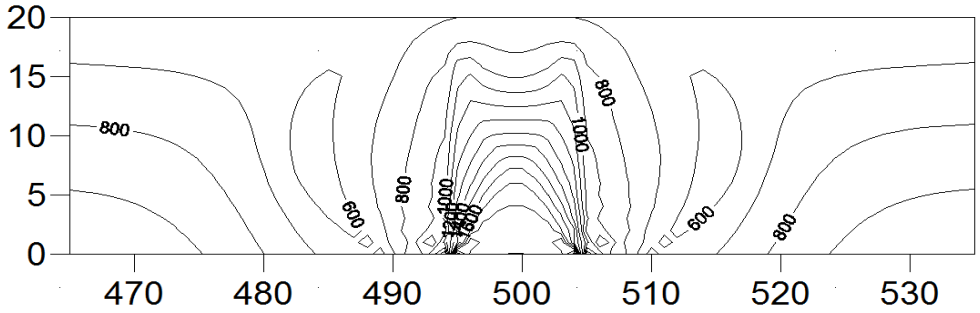

d) Vertical stress in **70m** FLAC simulation with both cSVD and cSHD (kPa)

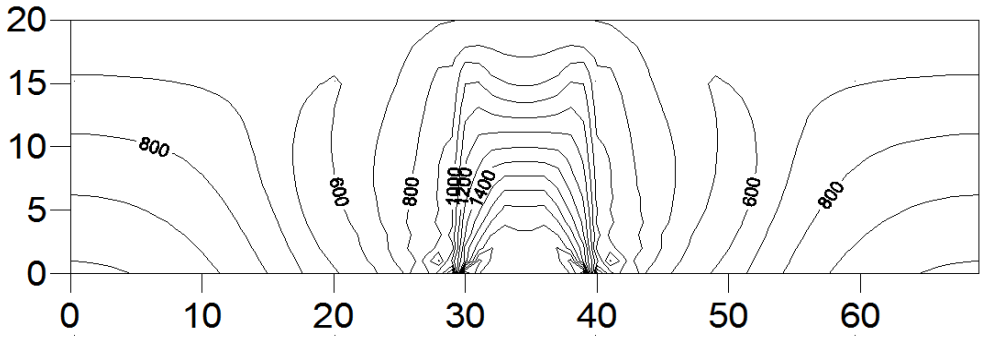

Figure D- 4 Vertical stress in a) 1000m FLAC simulations with only cSVD; b) 70m FLAC simulations with only cSVD; c) 1000m FLAC simulation with both cSVD and cSHD; d) 70m FLAC simulation with cSVD and cSHD (unit in m).

4) Shear stress contour

a) Shear stress in **1000m** FLAC simulations with only cSVD (kPa)

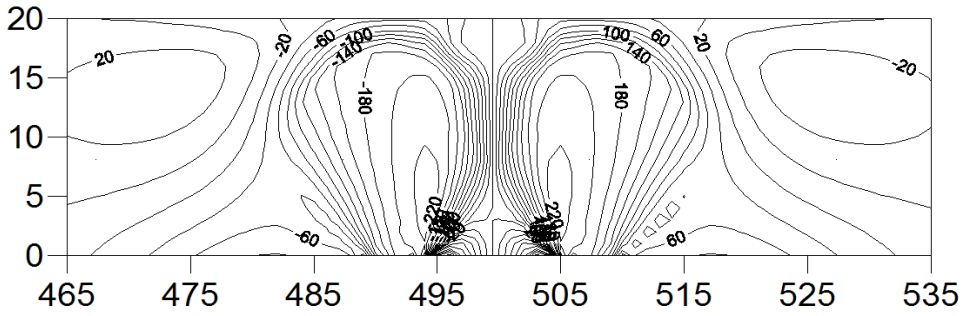

b) Shear stress in **70m** FLAC simulations with only cSVD (kPa)

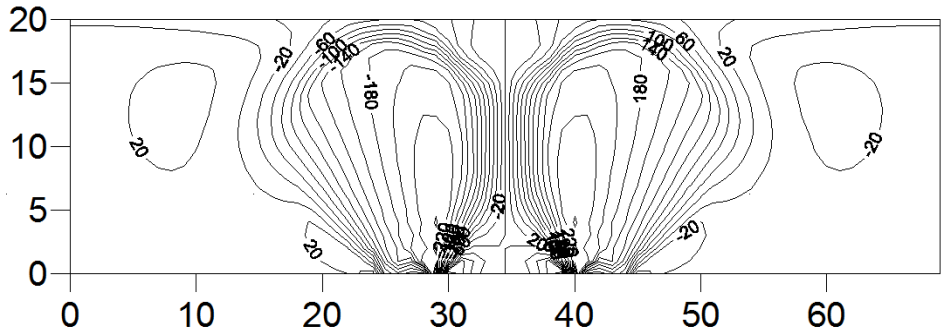

c) Shear stress in **1000m** FLAC simulation with both cSVD and cSHD (kPa)

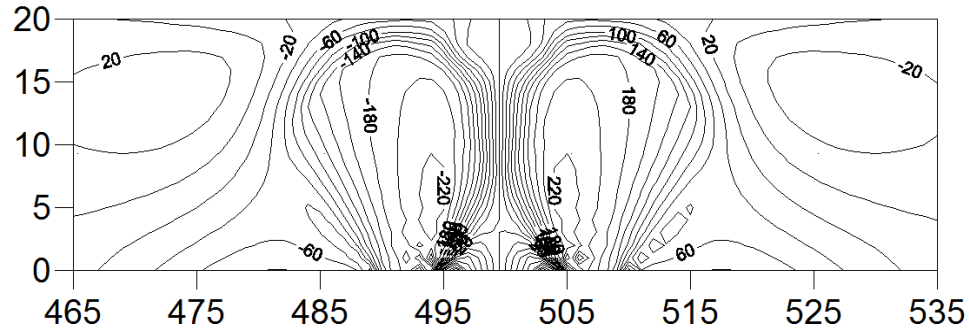

d) Shear stress in **70m** FLAC simulation with both cSVD and cSHD (kPa)

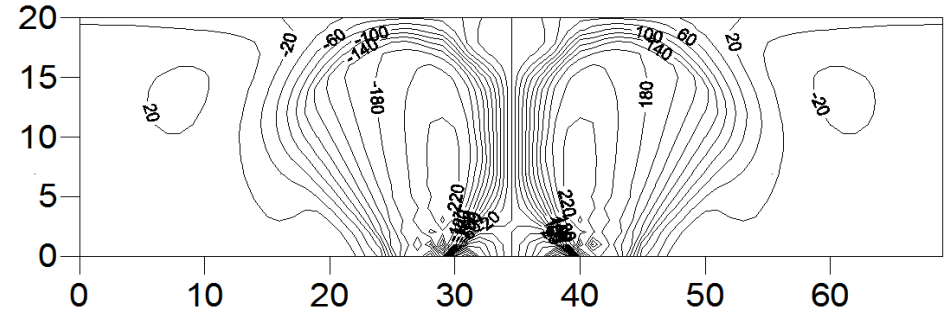

Figure D- 5 Shear stress in a) 1000m FLAC simulations with only cSVD; b) 70m FLAC simulations with only cSVD; c) 1000m FLAC simulation with both cSVD and cSHD; d) 70m FLAC simulation with cSVD and cSHD (unit in m).

5) Patterns of shearing zones

a) Patterns of shearing zones in **1000m** FLAC simulations with only cSVD

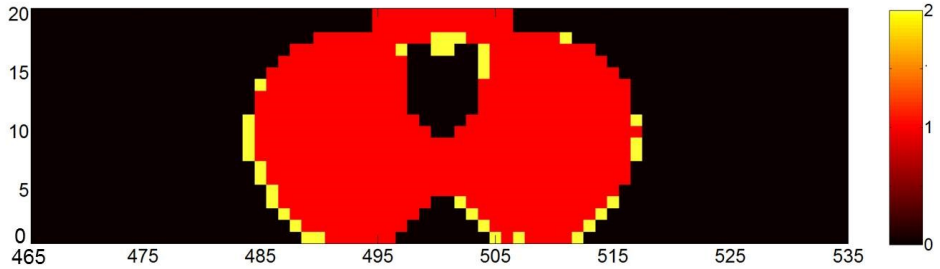

b) Patterns of shearing zones in **70m** FLAC simulations with only cSVD

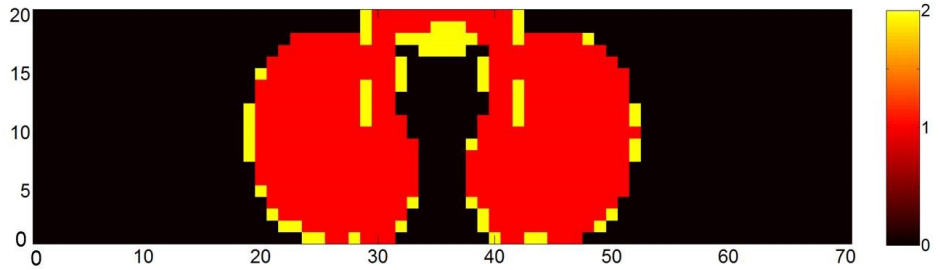

c) Patterns of shearing zones in **1000m** FLAC simulation with both cSVD and cSHD

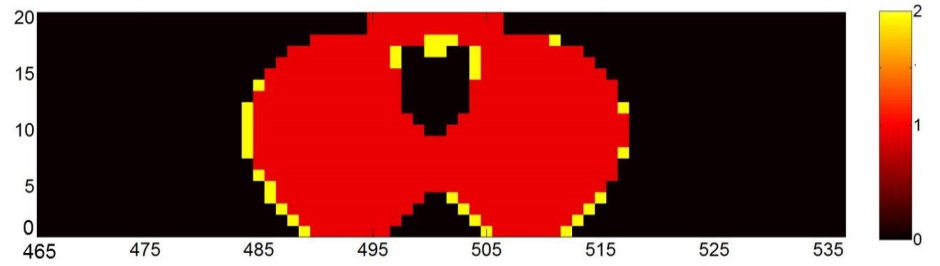

d) Patterns of shearing zones in **70m** FLAC simulation with both cSVD and cSHD

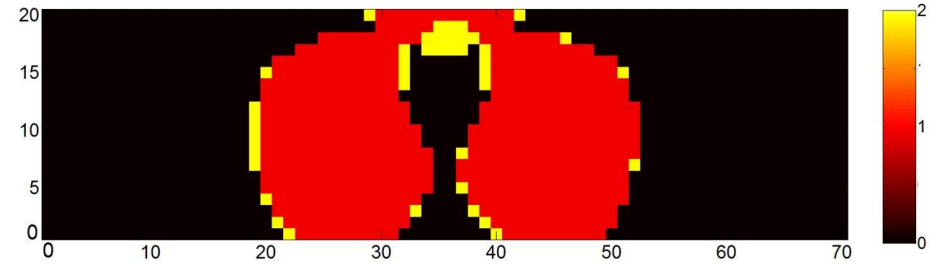

Figure D- 6 Patterns of shearing zones in a) 1000m FLAC simulations with only cSVD; b) 70m FLAC simulations with only cSVD; c) 1000m FLAC simulation with both cSVD and cSHD; d) 70m FLAC simulation with cSVD and cSHD (unit in).

There are a few conclusions by comparisons between these four scenarios.

1) The horizontal displacements generated by GeoCDM have minor influences on the caprock behavior (i.e. displacement, stress and shearing zones).

2) The boundary conditions of the plane-strain box have larger impacts on the horizontal stress distributions and the displacement field in the caprock.
3) Material rotations are both observed in both 70m and 1000m simulations, which means the boundary conditions are not the only factor causing such phenomena.

D.2 Future improvements

There are three major improvements which should be implemented in the next stage of this study. The first is to increase the size of the plane-strain box. The employment of the centrifuge simplified displacement at the base of caprock directly results from the limited space of the plane-strain box. Secondly, the technique of symmetry for centrifuge modeling has great potential to maximize the space usage of the plane-strain box considering that the caprock behavior is symmetric to the center of the well pairs. Last but not the least, to reduce the material rotation close to the boundary of the plane-strain box, a flexible boundary condition instead of a rigid one could be implemented in future studies.